SZKOŁA DOKTORSKA
BioMedChem
Uniwersytetu Łódzkiego
i Instytutów Polskiej
Akademii Nauk w Łodzi

INSTYTUT
ERCE BiolMed

Vivek

Praca doktorska:	**Pochodne antracenu podstawione grupami fosforoorganicznymi: synteza i ich właściwości optyczne**
Doctoral thesis:	**Anthracene derivatives substituted with organophosphorus groups: synthesis and their optical properties**

- Promotor/Supervisor
  Prof. dr hab. Piotr Bałczewski
  Division of Organic Chemistry, Centre of Molecular and Macromolecular Studies, Polish Academy of Sciences, Łódź, Poland

- Promotor pomocniczy/Assistant Supervisor
  Dr Ewa Różycka-Sokołowska
  Institute of Chemistry, Faculty of Science and Technology, Jan Długosz University in Częstochowa, Częstochowa, Poland

Łódź, 2025

DECLARATION

The presented work in this dissertation, entitled "Anthracene derivatives substituted with organophosphorus groups: synthesis and their optical properties," has been carried out by me under the guidance of Prof. Piotr Bałczewski at the Centre of Molecular and Macromolecular Studies of the Polish Academy of Sciences, Łódź, Poland. This work has not been submitted to any other university or institute of the Polish Academy of Sciences.

Date: 04.09.2025

Place: Łódź

Name and Signature

to my family

"You are what you believe in. You become that which you believe you can become".

- Bhagavad Gita

Acknowledgments

Abstract in English

The advancement of organic electronic materials relies heavily on the ability to design and synthesize new molecular frameworks with tunable optoelectronic properties. My research integrates synthetic organic chemistry with materials science, focusing on donor-acceptor (D-A) conjugated fluorophores belonging to the group of fused polycyclic aromatic and heteroaromatic hydrocarbons, which are multiply functionalized for light-emitting applications. Through my doctoral studies, I developed new synthetic strategies, explored fundamental structure property relationships. In addition to that, I also established versatile molecular design platforms that enable high-efficiency emission and controllable photophysical behavior. I also discovered various phenomena operating in these systems, like aggregation-caused quenching (ACQ), aggregation-induced emission (AIE), and twisted intramolecular charge transfer (TICT). The presented dissertation is part of a broad project aimed at the development of a new class of multi-substituted anthracene derivatives obtained *via* the *phospho*-Friedel-Crafts-Bradsher (F-C-B) cyclization. The main goal of this work was to develop novel synthetic routes for anthracene functionalization, primarily on peripheral rings, and to investigate photophysical, chemical, and electrochemical properties of the synthesized derivatives. Such compounds revealed high fluorescence quantum yields, significant photostability, and unique electronic properties.

The introduction part of this dissertation provides a general overview of a few classes of phosphorus substituted anthracene derivatives, which were obtained in the dissertation. Section 1.4, primarily concentrates on the synthesis and properties of phosphoryl (P=O) substituted anthracene derivatives, such as phosphine oxides, phosphine sulfides, phosphine selenides and phosphonates, the characteristic feature of which is multiply substitution by electronically diverse substituents. This section serves as a significant reference point for the achievements realized within this research area.

The results and discussion part of this dissertation focuses on the synthesis of multi-substituted anthracene derivatives containing diphenylphosphoryl, their thio- and seleno derivatives as well as diethoxyphosphoryl moieties, leading to several significant contributions. This part also helps to understand the electronic and optical properties of anthracenes and higher acenes through strategic incorporation of phosphorus substituents. Starting with section 3.1, which focuses on the one-pot three-step synthesis of 10-(diphenylphosphoryl)anthracenes, the C-O-P to C-P(=O) rearrangement is followed by the *phospho*-F-C-B cyclization. This strategy enabled the introduction of electron-withdrawing phosphorus moieties under mild conditions and provided access to anthracene derivatives with high photoluminescence quantum yields up to 95% yield in solution and > 95% in solid, and tunable emission properties. These findings were published in the *J. Org. Chem.* 2025, 90, 13, 4580-4590. In another project published in *Angewandte Chemie Int.Ed.* 2025, e202508168 (Section 3.3), I contributed to the synthesis and characterization of a phosphorus substituted (hetero)acene and corresponding substrates *via* the *phospho*-F-C-B cyclization. A brief overview of these findings is presented in sections 3.1 and 3.3, with comprehensive details available in the enclosed publications.

The obtained anthracene derivatives in section 3.1, substituted with bromine at the position 7 were utilized to further expand the synthesis of more π-conjugated anthracene derivatives. The Sonogashira cross-coupling was employed to introduce various electron-donating and electron-withdrawing substituents *via* phenylethynyl linkages at the 7-position of anthracene (Section 3.2). As a result of this work, a series of 10-(diphenylphosphoryl)-7-(phenylethynyl)anthracenes was obtained, which exhibited pronounced solvent-dependent photophysical properties, particularly twisted intramolecular charge transfer (TICT) in compounds bearing dimethylamino or dicyanovinyl groups. Detailed characterization of the resulted 10-(diphenylphosphoryl)-7-(phenylethynyl)anthracenes derivatives by spectroscopic (UV-Vis absorption, fluorescence emission, quantum yields) and electrochemical (cyclic voltammetry) methods was performed. The manuscript containing these results is being prepared for submission.

The last section in this dissertation concerns the *ortho*-positional isomers of anthracene and carbazole derivatives containing phosphonate ester groups (Section 3.4). These compounds were synthesized *via* a three-step strategy incorporating the key *phospho*-F-C-B cyclization, followed by post-functionalization through the Knoevenagel condensation and the Sonogashira coupling in order to introduce ethynyl and dicyanovinyl moieties in new sets of post-functionalized *ortho*-positional isomers (section 3.5). These studies showed that a small change in the substitution pattern could significantly change fluorescence behavior, quantum yields, and redox potentials. Interestingly, some isomers showed quantum yields exceeding 90% and offered precise control over HOMO-LUMO energy levels. The results of the first part of this study are currently undergoing a peer review process, while the manuscripts for the subsequent studies are in preparation for submission.

Abstract in Polish

Rozwój organicznych materiałów elektronicznych w dużym stopniu zależy od możliwości projektowania i syntezy nowych struktur molekularnych o regulowanych właściwościach optoelektronowych. Moje badania łączą syntetyczną chemię organiczną z chemią materiałową, koncentrując się na sprzężonych fluoroforach donorowo-akceptorowych (D-A) należących do grupy skondensowanych wielopierścieniowych węglowodorów aromatycznych i heteroaromatycznych, które są wielokrotnie funkcjonalizowane w celu zastosowań związanych z emisją światła. W trakcie studiów doktoranckich opracowałem nowe strategie syntezy, zbadałem podstawowe zależności między strukturą a właściwościami oraz stworzyłem platformy projektowania molekularnego, które umożliwiają wysoką wydajność emisji i kontrolowane zachowanie fotofizyczne. Odkryłem również różne zjawiska zachodzące w tych układach, takie jak wygaszanie spowodowane agregacją (ACQ), emisja indukowana agregacją (AIE) i transfer ładunku spowodowany skręconym wewnątrzcząsteczkowym transferem ładunku (TICT). Przedstawiona rozprawa jest częścią szeroko zakrojonego projektu mającego na celu opracowanie nowej klasy wielopodstawionych pochodnych antracenu otrzymanych w wyniku cyklizacji *fosfo*-Friedela-Craftsa-Bradshera (F-C-B). Głównym celem tej pracy było opracowanie nowych dróg syntezy funkcjonalizacji antracenu, przede wszystkim na peryferyjnych pierścieniach, oraz zbadanie właściwości fotofizycznych, chemicznych i elektrochemicznych syntetyzowanych pochodnych. Związki takie wykazały wysoką wydajność kwantową fluorescencji, znaczną fotostabilność i unikalne właściwości elektronowe.

Część niniejszej rozprawy poświęcona wynikom i dyskusji skupia się na syntezie wielopodstawionych pochodnych antracenu zawierających grupy difenylofosforylową, jej pochodne tio- i seleno, a także grupy dietoksyfosforylowe, co doprowadziło do kilku istotnych wniosków. Część ta pomaga również zrozumieć właściwości elektronowe i optyczne antracenów i wyższych acenów poprzez strategiczne włączenie podstawników fosforowych. Począwszy od sekcji 3.1, która skupia się na trzystopniowej syntezie 10-(difenylofosforylo)antracenów w jednym naczyniu reakcyjnym, poprzez przegrupowanie C-O-P do C-P(=O), a następnie cyklizację *fosfo*-F-C-B. Strategia ta umożliwiła wprowadzenie grup fosforowych wyciągających elektrony w łagodnych warunkach i zapewniła dostęp do pochodnych antracenu o wysokiej wydajności fotoluminescencji wynoszącej do 95% w roztworze i > 95% w stanie stałym oraz regulowanych właściwościach emisyjnych. Wyniki tych badań zostały opublikowane w *J. Org. Chem.* 2025, 90, 13, 4580–4590. W innym projekcie opublikowanym w *Angewandte Chemie Int.Ed.* 2025, e202508168, (sekcja 3.3), przyczyniłem się do syntezy i charakterystyki (hetero)acenu podstawionego fosforem i odpowiednich substratów poprzez cyklizację *fosfo*-F-C-B. Krótki przegląd tych wyników przedstawiono w sekcjach 3.1 i 3.3, a szczegółowe informacje można znaleźć w załączonych publikacjach.

Uzyskane w sekcji 3.1 pochodne antracenu, podstawione w pozycji 7 bromem, wykorzystano do dalszego rozszerzenia syntezy bardziej π-sprzężonych pochodnych antracenu. Zastosowano reakcję krzyżowego sprzęgania Sonogashiry w celu wprowadzenia różnych podstawników

oddających i pobierających elektrony poprzez wiązania fenyloetynylowe w pozycji 7 antracenu (sekcja 3.2). W wyniku tych prac uzyskano serię 10-(difenylofosforylo)-7-(fenyloetynylo)antracenów, które wykazywały właściwości fotofizyczne wyraźnie zależne od rozpuszczalnika, w szczególności zjawisko TICT w związkach zawierających grupy dimetyloaminową i dicyjanowinylową. Przeprowadzono szczegółową charakterystykę otrzymanych pochodnych 10-(difenylofosforylo)-7-(fenyloetynylo)antracenów metodami spektroskopowymi (absorpcja UV-Vis, emisja fluorescencji, wydajność kwantowa) i elektrochemicznymi (cykliczna woltamperometria). Manuskrypt zawierający te wyniki jest przygotowywany do publikacji.

Ostatnia część niniejszej rozprawy dotyczy izomerów *orto*-pozycyjnych, pochodnych antracenu i karbazolu zawierających estrowe grupy fosfonianowe (sekcja 3.4). Związki te zostały zsyntetyzowane w ramach trzyetapowej strategii obejmującej kluczową cyklizację *fosfo*-F-C-B, a następnie post-funkcjonalizację poprzez reakcje kondensacji Knoevenagela i sprzęgania Sonogashiry w celu wprowadzenia grup etynylowych i dicyjanowinylowej do nowych post-funkcjonalizowanych izomerów *orto*-pozycyjnych (sekcja 3.5). Badania te wykazały, w jaki sposób niewielkie zmiany w topologii podstawienia mogą radykalnie zmienić zachowanie fluorescencji, wydajność kwantową i potencjały redoks. Co ważne, niektóre izomery wykazywały wydajność kwantową przekraczającą 90% i umożliwiały precyzyjną kontrolę poziomów energii HOMO-LUMO. Wyniki pierwszej części badań są obecnie poddawane procesowi recenzji, natomiast manuskrypty kolejnych badań są w trakcie przygotowywania do złożenia.

Table of Contents

1. Introduction

1.1 Anthracene derivatives

Anthracene was first discovered in coal tar by French chemists Dumas and Laurent in 1832.[1]. The industrial production of anthracene began when Perkin developed a method for its purification. It is a solid with a melting point of 216°C. Its structure is planar, made up of three linearly fused benzene rings (Figure 1). Substituted anthracenes may undergo pronounced distortion of the planar structure, especially bending of the fused-ring plane, which disrupts the π-conjugation of the aromatic core. Due to the conjugated π-electron structure, anthracene and its derivatives may exhibit strong fluorescence properties, making them valuable in electroluminescent devices. Anthracene is a wide-band-gap organic semiconductor that strongly absorbs ultraviolet (UV) light, with a characteristic absorption peak around 350–400 nm.[3] Upon excitation, anthracene emits blue-violet light (around 400–450 nm) in 11 (chloroform) -36% (cyclohexane) fluorescence quantum yields.[4]
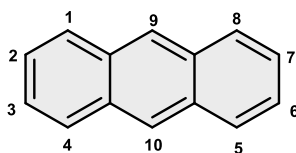
Figure 1. The structure of the anthracene molecule and its characteristic numbering.[1]

Although the use of anthracene itself as a fluorophore is limited to a few, such as UV tracers, substituted anthracenes greatly expand the range of applications, including organic light-emitting diodes (OLEDs),[5-8] organic field-effect transistors (OFETs),[9] semiconducting polymeric materials,[10] and various other types of materials.[11-12] Additionally, anthracene derivatives act as metal-free triplet photosensitizers,[13] absorbing light and transferring it to molecules that cannot absorb at the same wavelength. The triplet photosensitizing properties of anthracene derivatives come from the minimal energy gap between the singlet excited state (S_1) and the triplet excited state (T_1), which facilitates intersystem crossing (ISC) of up to 70%.[14] However, substituting anthracene with two phenyl groups at positions 9 and 10 separates the two excited states and inhibits both π-π stacking and intersystem crossing (ISC), thereby increasing the fluorescence quantum yield of anthracene derivatives (Figure 2).[15]

Previous studies have shown that substituents on the peripheral rings of anthracene also significantly influence its steric and optical properties, particularly its fluorescence intensity.[16,17] The fluorescence intensity depends on various factors, including the position of substituents, the dipole moment of the molecule, and the electron-donating or electron-withdrawing characteristics of the substituents. For example, a study of donor-acceptor 2,6-substituted anthracene derivatives with ester and oxazoline groups showed switchable emission properties and increased fluorescence intensity, which resulted from the donor-acceptor interplay.[18]

Matsika et al.,[19] in their computational research, suggested that in addition to the 9 and 10 positions, other positions in the anthracene structure can also affect the absorbance and emission characteristics. This study has demonstrated the effects of mono-, di-, and multi-substitution on anthracene derivatives, revealing that substitution of the anthracene core with either electron-donating groups (EDG) or electron-withdrawing groups (EWG) results in a red shift in nearly all cases. They have also predicted that the position of substitution has a significant impact on the excitation energies.

Substitution on the outer rings also affects the outcomes of chemical reactions by changing the distribution of anthracene's electronic density.[20] Similarly, Reiser and co-workers have shown that introducing electron-donating substituents on the outer rings can reverse the regioselectivity of the well-known Diels-Alder reactions, which usually occur on the central anthracene ring due to the relative aromatic stabilization energy of the two possible products, and the presence of the largest orbital coefficients of the highest occupied molecular orbital (HOMO) at the 9,10-positions.[21]
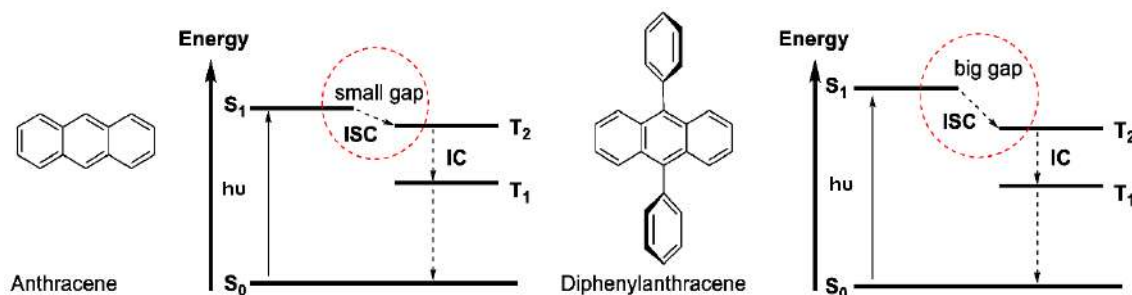
Figure 2. Effect of substitution on anthracene derivatives.[4]

Although previous research has proved that substituting the outer ring can significantly influence the photophysical properties and alter the reactivity pathway of the anthracene core, however, only a limited number of examples of anthracene derivatives exist where various functional groups, either electron-donating or electron-withdrawing, are substituted on the peripheral rings. This explanation highlights the significance of synthesizing new modified anthracene derivatives, particularly those incorporating functional groups at the peripheral rings.

1.2 Common reactions of anthracene derivatives

Anthracene is a highly reactive fused aromatic hydrocarbon because of its conjugated π-electron system. It mainly undergoes electrophilic substitution reactions, such as nitration, sulfonation, and halogenation, mainly at the 9- and 10-positions, where the electron density is highest (Scheme 1).[22-24] For example, the bromination of anthracene produces 9,10-dibromoanthracene **1**. The halogens located at these positions can be readily transformed into diverse substituents through cross-coupling reactions (the Suzuki or the Sonogashira cross-couplings).[25,26] These positions also make anthracene susceptible to oxidation, forming 1,4-anthraquinone **2**, an important industrial compound.[27] Carbonyl groups in 1,4-anthraquinone play an important role in the subsequent functionalization through nucleophilic addition, followed by reductive aromatization.[28]

Additionally, anthracene participates in the Diels-Alder [4+4] cycloaddition reactions to form a dimeric structure **4**, acting as a diene due to its electron-rich nature.[29] An interesting example of the Diels-Alder [4+2] cycloaddition of anthracene is the reaction with singlet oxygen, resulting in the formation of the peroxide **3**.[30] Cycloaddition reactions make anthracene a valuable substrate in organic synthesis, material science, and photochemistry.
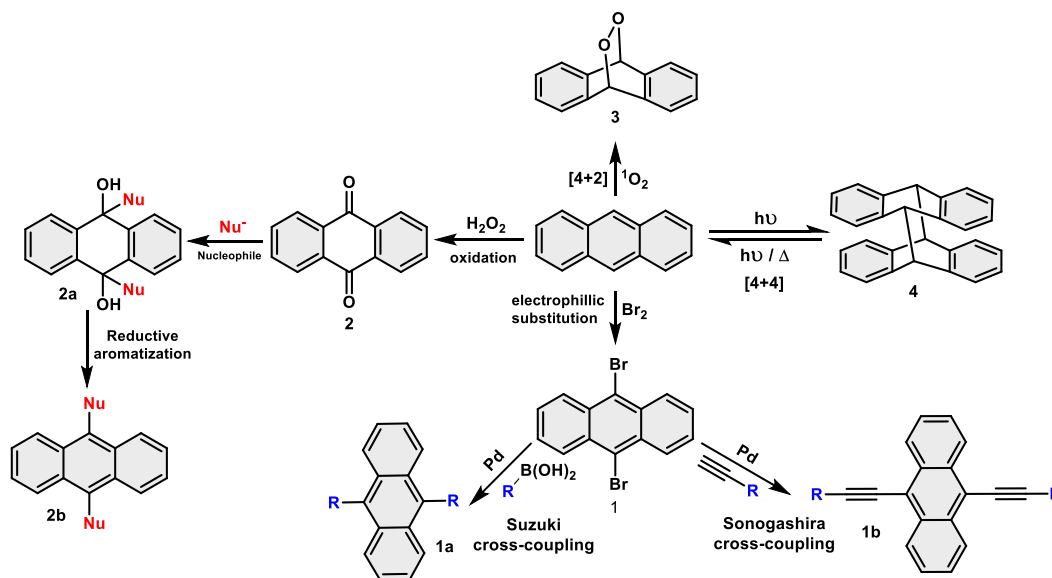
Scheme 1. The common reactions of anthracene and its derivatives.[4]

As illustrated in Scheme 1, anthracene reacts mainly at 9 and 10 positions because electrophilic substitution at these central positions allows the resulting intermediate to be stabilized by resonance over all three aromatic rings, preserving aromaticity in two of them. This stability makes substitution at the 9 and 10 positions both kinetically and thermodynamically favored, making it difficult to substitute the outer rings of anthracene.

1.3 An overview of phosphorus substituted anthracene derivatives

Over time, organic conjugated materials have been synthesized utilizing second-row elements, such as carbon, nitrogen, and oxygen.[31-33] However, to enhance the physical properties of novel compounds, heavier elements, including sulfur,[34] selenium,[35] boron,[36] silicon,[37] and, importantly, phosphorus, have been employed.[38] The phosphorus-based conjugated frameworks exhibit a unique reactivity through the transformation of the trivalent phosphorus center into tetra- and pentavalent ones, thereby imparting favorable nucleophilic and coordinating behavior. The modification of the electron characteristics of the phosphorus atom enhances the energy levels of the highest occupied and lowest unoccupied molecular orbitals (HOMO/LUMO), thereby directly influencing the optical properties of the conjugated compounds, predominantly in terms of absorption and emission.

The group of phosphinyl-substituted anthracenes is mainly used as precursors in the synthesis of other derivatives of phosphorus-based materials (phosphine oxides, phosphonium salts, etc.) by

modifications of the phosphorus center (Scheme 2). Compounds substituted with phosphinyl groups are most highly reactive, and their high reactivity can be mainly attributed to the electron-donating and electron-withdrawing behavior of the phosphinyl group, which behaves as both a Lewis base and a Lewis acid. Compounds of this nature typically display low luminescence due to efficient non-radiative relaxation pathways of the excited state, which occurs as a consequence of photoinduced electron transfer (PET).[39]
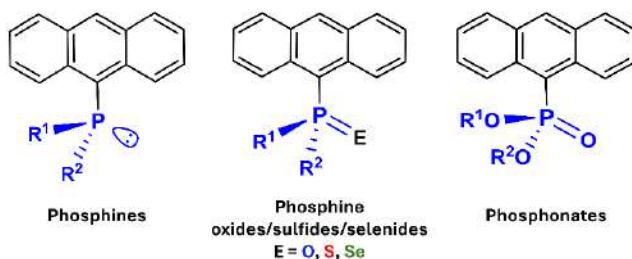
Scheme 2. Diversity of organophosphorus substituted anthracene derivatives.

Therefore, the inactivation of the electron pair through the formation of covalent bonds with chalcogens (O, S, and Se), metals, organic groups (alkyl/aryl), and Lewis acids (BR$_3$) *via* oxidation, quaternization, and coordination reactions changes the electron character of P-atom from donor (^{III}P) to acceptor (^{IV}P=X, ^{IV}P$^+$) and results in formation of phosphine oxide/sulfide/selenide, phosphonate and phosphonium salts, respectively, and a variety of photophysical behaviors (Figure 3).

The phosphoryl (phosphine oxides and phosphonates) substituted anthracene derivatives have gained significant attention due to their unique photophysical properties. Incorporating phosphoryl groups into the anthracene framework lowers the HOMO and LUMO energy levels of anthracene due to its electron-withdrawing property. Additionally, the phosphoryl groups can act as the Lewis basic site for metals, cations, and protons through different interactions. The tunable fluorescence of anthracene derivatives substituted with a phosphoryl group makes them valuable for organic light-emitting diodes (OLEDs) and sensing applications.[40-42] In addition, the phosphoryl functionalization can improve stability and charge transport properties, expanding their use in organic semiconductors.[43,44]
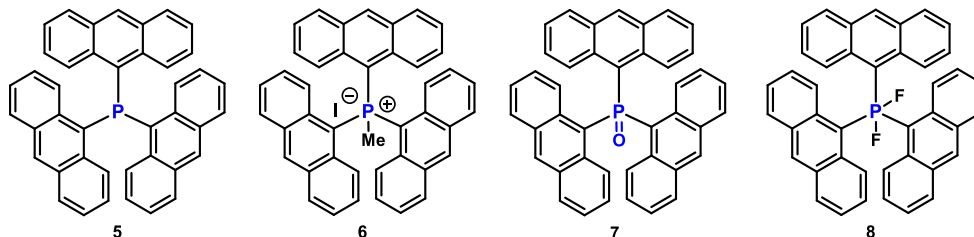
Scheme 3. Examples of phosphorus (P^{III} to P^{IV}) substituted anthracene derivative.[45]

The research conducted by Tamao and co-workers,[45] can serve as an example of changes in the photophysical properties of a series of differently P-substituted anthracene derivatives (Scheme 3). The investigation suggested that the fluorescence properties of triaryl phosphines were significantly influenced by the coordination number of the phosphorus atom. Consequently, while the P^{III} unsubstituted trianthryl phosphine Ant_3P, the P^{IV} salt Ant_3P^+, and the phosphine oxide $Ant_3P=O$ exhibited none or weak fluorescence (QY < 0.01), the P^V phosphorane Ant_3PF_2 with strongly electron-withdrawing fluorine substituents demonstrated more pronounced fluorescence (QY = 0.28), though still moderate. The absence of fluorescence in P^{III} species was attributed to the effective fluorescence quenching by the loosely bound lone electron pair on the phosphorus atom.

The phosphinyl (Ph_2P) group, when substituted at the anthracene moiety, facilitated transformations to phosphoryl (also called phosphinoyl, $Ph_2P=O$), thiophosphoryl (also called thiophosphinoyl, $Ph_2P=S$), and selenophosphoryl (also called selenophosphinoyl, $Ph_2P=Se$) substituted anthracenes. The oxidized compounds, such as $Ph_2P=O$, $Ph_2P=S$, and $Ph_2P=Se$, improved the optical properties of anthracene derivatives in both the solution and solid states, due to differences in polarizability, electronegativity, and spin-orbit coupling among the heteroatoms (O, S, Se). For example, the compound **9**, which contained the phosphoryl ($Ph_2P=O$) group at the 1-position, showed a quantum yield of 42.8% in solution (Scheme 4). However, the emission of the compound **10**, which contained $Ph_2P=S$, was completely quenched as a result of photoinduced electron transfer (PET) from the sulfur lone pair to the anthracene moiety.[46] In another study, the compound **11** with the $Ph_2P=O$ moiety was exposed to UV radiation at 366 nm, and a stronger emission was observed in common organic solvents, compared to compounds **12** and **13**, which contained $Ph_2P=S$ and $Ph_2P=Se$ groups, respectively,.[47] Interestingly, in the solid state, only the compound **12** emitted light in the UV region, which it lost after vacuum drying. In addition, a small amount of toluene restored the emission, a phenomenon not seen with other organic solvents. The results showed that the emission in the solid state for compound **12** was increased by the binding of toluene and its crystallization within the space group, which created a specific arrangement absent in compounds **11** and **13**. Consequently, anthracene compounds with the $Ph_2P=X$ (X = O, S, Se) groups play a significant role in tuning the photophysical properties, not only in solution but also in the solid state.
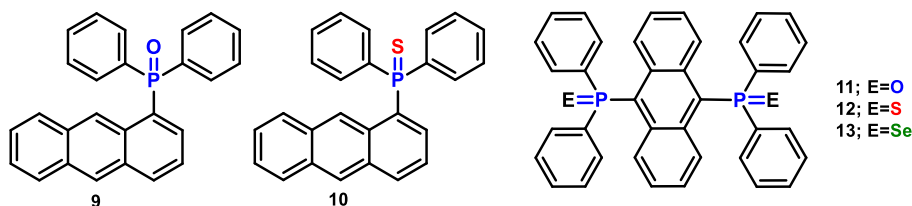
Scheme 4. Examples of phosphorus (P=O, P=S, and P=Se) substituted anthracene derivatives.[46,47]

Substitution of the anthracene core with dialkoxyphosphoryl group, $(RO)_2P=O$, another kind of phosphorus-containing group, with two P-O bonds, instead of two P-Ph bonds, as in $R_2P=O$ (R =

Ph), and one P=O bond, also significantly alters the photophysical properties of anthracene derivatives.[48,49] The $(RO)_2P=O$ group functions similarly to $R_2P=O$ as an electron-withdrawing moiety, enhancing π-conjugation through the P=O bond, provided that its position is coplanar with respect to the anthracene core. Electron-withdrawing character (EWG) of the $(RO)_2P=O$ group can be illustrated with the Hammett constant $\sigma_p = 0.56$, while σ_{ind} and σ_{res} components indicate that inductive (–I) and resonance (-M) effects are both responsible for the EWG character, with a slight predominance of the former ($\sigma_{ind}/\sigma_{res} = 0.32/0.24$).

The dialkoxyphosphoryl group also provides opportunities for tuning the properties of anthracene derivatives by replacing oxygen with sulfur atoms, as in dithioalkoxyphosphoryl $(RS)_2P=O$ and dihydroxyphosphoryl $(HO)_2P=O$ groups. French and co-workers have shown that 2-diethoxyphosphoryl substituted anthracene derivative **14** exhibited a fluorescence quantum yield of 33 % which was enhanced up to 40 % by transforming this group to 2-dihydroxyphosphoryl one in the anthracene **15** (Scheme 5).[50]
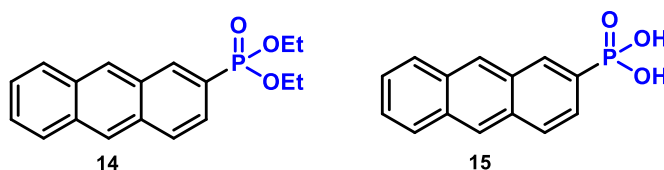
Scheme 5. Examples of 2-phosphryl substituted anthracene derivatives: the phosphonate **14** and the phosphonic acid **15**.[50]

The doctoral thesis presented here primarily concentrates on the synthesis and properties of phosphoryl (P=O) substituted anthracene derivatives, such as phosphine oxides, phosphine sulfides, phosphine selenides, and phosphonates, the characteristic feature of which is multiply substitution by electronically diverse substituents. This research area represents a new approach to the synthesis and properties of such compounds.

1.4 Synthesis of phosphorus substituted anthracene derivatives

Anthracene can be easily synthesized using established methods, such as the Elbs reaction discovered in 1884.[51] Over time, alternative reactions have emerged that offered access to unsubstituted and substituted anthracene, such as Friedel–Crafts reactions,[52] Bradsher-type reactions,[53] and metal-catalyzed reactions involving alkynes.[54] In 2021, Donate et al. presented a comprehensive review of the latest methodologies for the synthesis of substituted anthracene derivatives.[55] All of these reactions until today provided products substituted with thermally resistant groups, such as alkyl and methoxy, and suffered from the inability to introduce electron-diverse substituents, mainly due to the still high reaction temperatures. Also, it was rarely possible to achieve a high degree of substitution in anthracene derivatives. Most frequently modified were preferred positions 9 and 10.

Numerous examples in the literature demonstrate the use of 9,10-substituted anthracenes in various organic material applications.[4, 5-12] However, the synthesis of anthracene derivatives substituted at

the flanking (outer) rings still remains scarce. Only a limited number of examples show a selective substitution on the flanking rings of anthracene derivatives.[20] Moreover, problems related to regioselectivity of the anthracene substitution and synthetic complexity make selective substitution of both the central and lateral rings of anthracene particularly difficult and still remain a challenge.

The synthesis of the phosphorus-substituted anthracene derivatives was achieved through employing various methods for substituting halogen atoms with the phosphorus moiety. For example, $R_2P=O$ substituted anthracenes, described in the literature, can be mainly synthesized by following two methods. The first method involves the Br/Li exchange in 9-bromoanthracenes or 9,10-dibromoanthracenes, followed by a reaction with chlorodiphenylphosphine and subsequent oxidation with hydrogen peroxide.[45, 56-58] The alternative method required transition metal activation or cross-coupling reactions for the formation of the C-P bond, with several examples utilizing palladium and nickel-based catalysts.[59-62]

Similarly, effective approaches to synthesize dialkoxyphosphoryl, $(RO)_2P=O$ substituted anthracene derivatives, such as the Arbuzov reaction, were described in literature.[74,75] In the Arbuzov reaction, a halogen atom was substituted by a $(RO)_2P=O$ group through utilization of trialkylphosphite in the presence of $NiBr_2$, as a catalyst. Dialkoxyphosphite was also employed in the coupling reaction with anthrylhalides as an alternative source of the $(RO)_2P=O$ group.[76,77]

In this section, we have reviewed the existing literature on the synthesis of phosphorus-substituted anthracene derivatives. We have mainly focused on phosphine oxides, phosphine sulfides, and phosphine selenides. Later, several effective methods for synthesizing phosphonate-substituted anthracene derivatives were reviewed. However, the detailed synthesis and properties of phosphonate-substituted anthracenes have been addressed in a separate PhD thesis by a colleague.

1.4.1 Phosphoryl ($R_2P=O$, R=aryl, alkyl) substituted anthracene derivatives

This section provides a review of synthesized phosphoryl-substituted anthracene derivatives. The synthesis of these derivatives has been categorized into three sections based on information from existing literature. The initial two sections describe the fundamental methods for synthesizing the substituted anthracene derivatives. The remaining section of the three is dedicated to a miscellaneous method employed for the synthesis of phosphoryl-substituted anthracene derivatives.

1.4.1.1 The Br/Li exchange method

There are many methods for synthesizing diphenylphosphoryl-substituted anthracenes; however, the basic procedure was first carried out by Fujimoto and co-workers.[56] This procedure showed that 9-(diphenylphosphoryl)anthracene **17** could be efficiently prepared from 9-bromoanthracene **16** by replacing the chlorine in chlorodiphenylphosphine with 9-lithioanthracene, which was made from **16** via the Br/Li exchange. The process then involved oxidizing the resulting 9-(diphenylphosphoryl)anthracene with aqueous hydrogen peroxide (Scheme 6). This procedure resulted in the formation of the compound **17** in 90% yield.
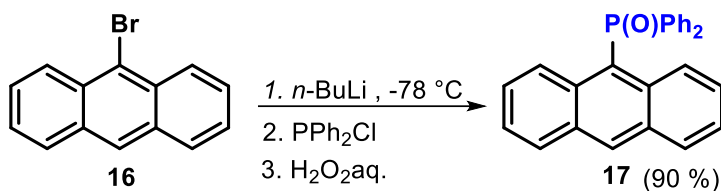
Scheme 6. Synthesis of 9-(diphenylphosphoryl)anthracene **17** from 9-bromoanthracene **16**.[56]

In the same study, the successful synthesis of the anthracene derivative **18** was performed using a similar methodology. This approach employed dichlorophenylphosphine (PPhCl₂), which enabled the introduction of two anthryl moieties in **18** starting from 9-bromoanthracene (Scheme 7).
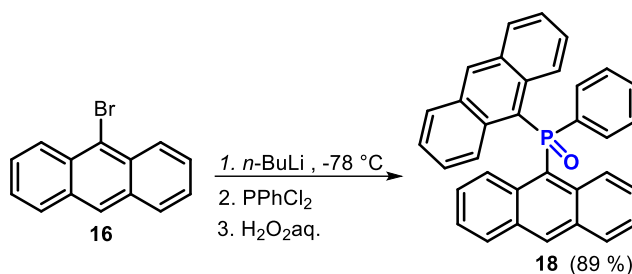
Scheme 7. Synthesis of the anthracene derivative **18** containing two anthryl moieties from 9-bromoanthracene **16**.[56]

This research also demonstrated that phosphine oxides substituted anthracene derivatives **17** and **18** do not undergo photodimerization in the solid state. But, in acetonitrile or chloroform under a nitrogen atmosphere, upon irradiation at a wavelength of 365 nm, the [4π + 4π] photodimerization of **17** was observed, giving the photoadduct **19** (Scheme 8).
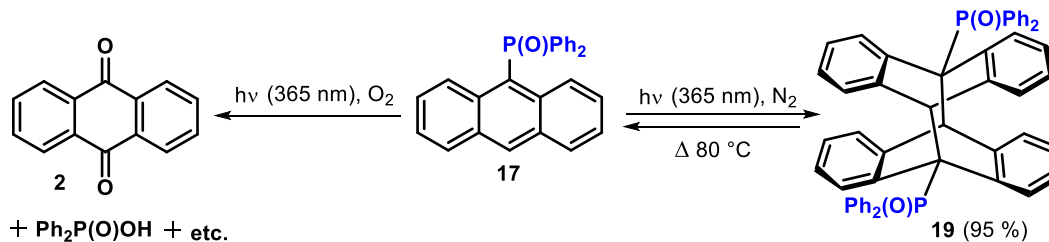
Scheme 8. Synthesis of the photodimer **19** and the anthraquinone **2** from 9-diphenylphosphorylanthracene **17**.[56]

In this process, the characteristic bands in the absorption and emission spectra associated with the anthryl moiety disappeared. However, it was possible to revert compound **19** to **17** by heating the sample to 80 °C. Interestingly, irradiation under an oxygen atmosphere resulted in the formation of anthraquinone **2** (Scheme 8).

Zhao and coworkers,[57] demonstrated that 9,10-bis(diphenylphosphoryl)anthracene **11** could be efficiently synthesized through substitution of chlorine in chlorodiphenylphosphine with 9,10-dilithioanthracene, obtained from 9,10-dibromoanthracene **1** *via* a double Br/Li exchange (Scheme 9). This step was followed by the oxidation of the resulting bis(diphenylphosphinyl)anthracene **20** using hydrogen peroxide to generate bis(diphenylphosphoryl)anthracene **11** in 47% yield. The

substrate **1**, was prepared by brominating anthracene in chloroform. The anthracene derivative **11**, substituted with two phosphoryl groups, was synthesized for an organic light-emitting diode (OLED) device using the exciplex method. The device made from the anthracene derivative **11** emitted a pure white light with Commission Internationale de l'Eclairage (CIE) coordinates of (0.33, 0.33). The interaction between **11** and aluminum (Al), which was investigated with X-ray photoelectron spectroscopy (XPS), suggested that the performance of device was facilitated without the necessity of injecting layer.
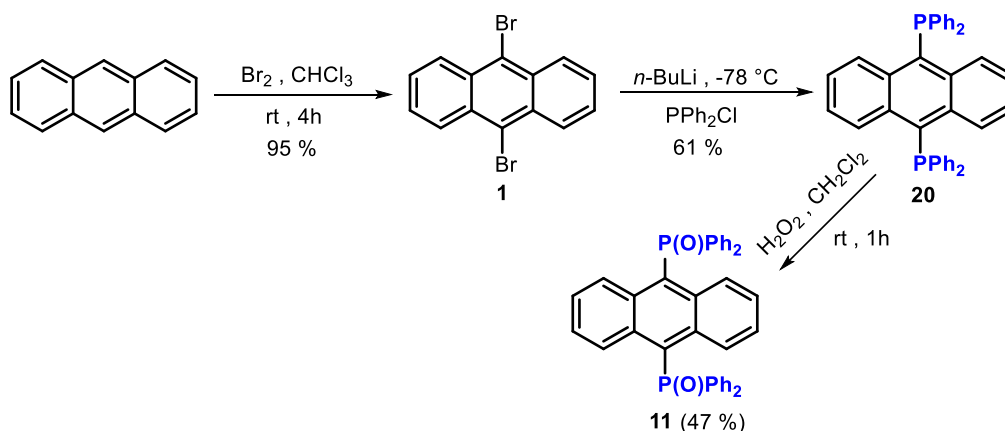
Scheme 9. Synthesis of 9,10-bis(diphenylphosphoryl)anthracene **11** from 9,10-dibromoanthracene **1**.[57]

Tamao and co-workers have successfully synthesized tri-(9-anthryl)phosphoryl **7** from tri-(9-anthryl)phosphinyl **5** (Scheme 10).[45] Additionally, they have investigated the photophysical properties of these compounds, including UV-vis absorption and fluorescence spectra. The findings indicated that the emission properties were significantly influenced by the coordination number of the phosphorus atom.
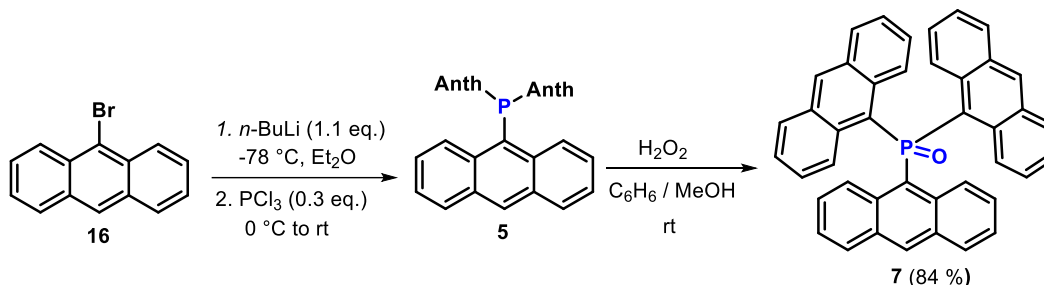
Scheme 10. Synthesis of tri-(9-anthryl)phosphoryl **7** from 9-bromoanthracene **16**.[45]

Su and co-workers have synthesized 9,10-diphenyl-2-diphenylphosphorylanthracene **22** from 2-bromo-9,10-diphenylanthracene **21** employing a previously developed method involving the Br/Li exchange using n-BuLi and subsequent reaction with chlorodiphenyl phosphine (PPh$_2$Cl) (Scheme 11).[58] Bulky substituents in **22** were intended to mitigate red-shift emission in the solid state and

to prevent spectral broadening. Nonetheless, the compound **22** exhibited excimer formation and red shift in solid, and thus turned out to be unsuitable for application in blue OLEDs.
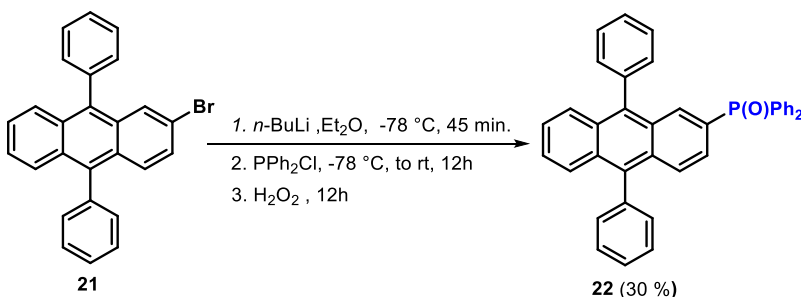
Scheme 11. Synthesis of 9,10-diphenyl-2-diphenylphosphorylanthracene **22** from 2-bromo-9.10-diphenylanthracene **21**.[58]

1.4.1.2 Transition-metal catalyzed reactions

Wang and co-workers have developed a methodology for synthesizing 2-(diphenylphosphoryl)anthracene **24** (Scheme 12).[59] This approach facilitates the formation of carbon-phosphorus (C-P) bonds through the nickel-catalyzed cross-coupling of organoammonium salts, such as the compound **23**, with phosphorus nucleophiles. This methodology also proved suitable for other substrates, including benzyl, aryl, pyridyl, and allyl ammonium triflates, which could function as electrophiles. The reaction gives substantial results with a wide range of functional groups, including cyano (CN), trifluoromethyl (CF$_3$), methoxy (OMe), fluoro (F), chloro (Cl), amido (C(O)NMe$_2$), and *tert*-butoxycarbonyl (^{t}BuCO).
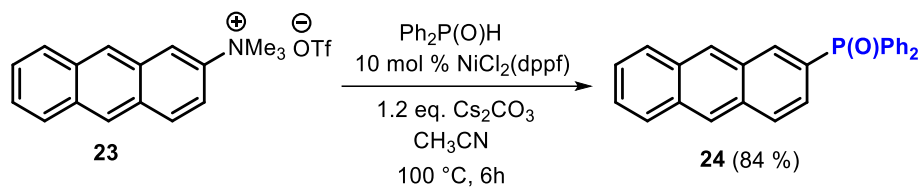
Scheme 12. Synthesis of 2-(diphenylphosphoryl)anthracene **24** from anthryl ammonium triflate **23**.[59]

Han and co-workers have employed an alternative approach for the synthesis of 2-(diphenylphosphoryl)anthracene **24** through the decarbonylative phosphorylation of 2-anthroic acid **25**, utilizing palladium as a catalyst (Scheme 13).[60] This methodology showed an alternative route to synthesize the P=O substituted anthracene derivatives directly from acids, bypassing the use of organoammonium salts. Despite the lower yield, the reaction conditions accommodated various P(O)H containing compounds and were applicable to different substrates. Furthermore, this approach introduced a strategy for the *in situ* activation of carboxylic acids with (Boc)$_2$O, which eliminated the need of their step-by-step pre-conversion into activated carboxylic derivatives.
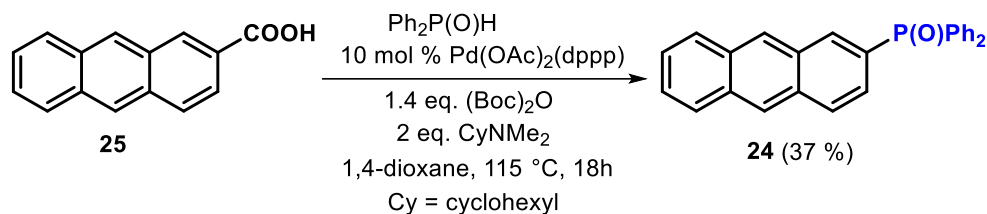
Scheme 13. Synthesis of 2-(diphenylphosphoryl)anthracene **24** from 2-anthroic acid **25.**[60]

In another approach developed by Wang and co-workers,[61] 9-(diphenylphosphoryl)anthracene **17** was synthesized by the decarbonylation of 9-(1-ketodiphenylphosphoryl)anthracene **26** in a good yield, using a palladium catalyst.[57] This method enabled the C-P bond activation without the anchoring effect that was typically observed in previous decarbonylation reactions employing, for example, nickel.[58]
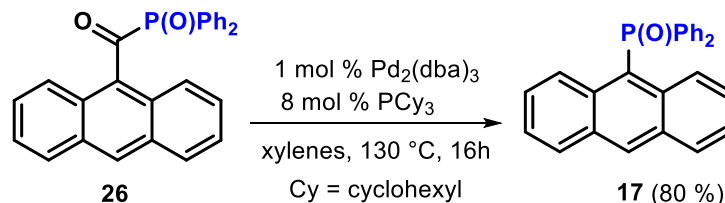
Scheme 14. Synthesis of 9-(diphenylphosphoryl)anthracene **17** from 9-(1-ketodiphenylphosphoryl)anthracene **26.**[61]

Drabowicz and co-workers have successfully synthesized optically active 9-[((t-butyl)(phenyl)phosphoryl)]anthracene **28** with a high yield through the Hirao cross-coupling reaction of 9-bromoanthracene **16** and optically active t-butylphenylphosphine oxide **27** using palladium catalyst (Scheme 15).[62] The C-P bond formation proceeded through retention of configuration, which was investigated by X-ray analysis.
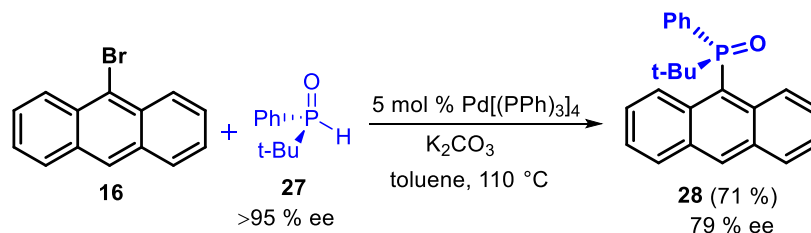
Scheme 15. Synthesis of 9-[((t-butyl)(phenyl)phosphoryl)]anthracene **28** from 9-bromoanthracene **16.**[62]

1.4.1.3 Other methods

Gates and co-workers attempted to synthesize a "masked" phosphaalkene by treating MgA·3THF (A = anthracenide) with MesPCl(CH$_2$Cl) (Scheme 16).[63] The term "mask" refers to a concept of stabilizing unusual species, such as phosphamethine cyanine cations and phosphinines, which are compounds containing a delocalized P=C bond, through the use of a ring system. The release of these species is accompanied by the formation of thermodynamically stable by-products, such as aromatic compounds.

In some cases, it is possible to isolate the species or to trap it. For example, Roark and Peddle, in 1972, successfully synthesized and isolated a "masked" disilene.[64] Although the compound **30** was not isolated in this project, it was successfully trapped using 1,3-cyclohexadiene, leading to the isolation of a rearrangement product **31**. The compound **32** was formed from **30** through a sequence of rearrangement and air oxidation.
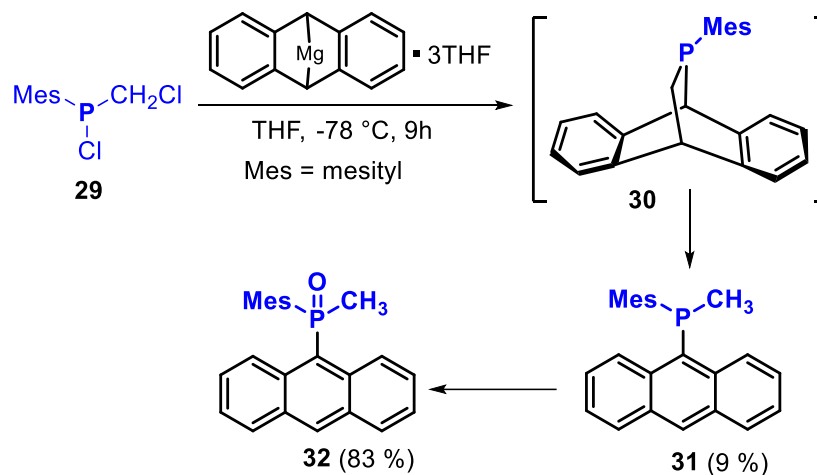
Scheme 16. Synthesis of 9-[(methyl)(mesityl)phosphinyl]anthracene **31** and the corresponding 9-[(methyl)(mesityl)phosphoryl]anthracene **32**.[63]

1.4.2 Phosphinyl (R₂P, aryl, alkyl) substituted anthracene derivatives

The phosphinyl substituted anthracene derivatives can be synthesized *via* halogen exchange and metal-catalyzed reactions (Scheme 17).[56-62] However, the phosphoryl P(IV) moieties present on the anthracene can also be a source of phosphinyl derivatives since they are readily reducible to phosphinyl derivatives P(III). A number of silanes, aluminum and boron-based reagents, are available for the reduction of secondary and tertiary phosphoryl to phosphinyl groups, as described by Buono and co-workers in 2015.[65] However, the most effective method for this reduction, particularly when these groups are present on anthracene, involves using the trichlorosilane in toluene under reflux conditions (Scheme 17).[20]
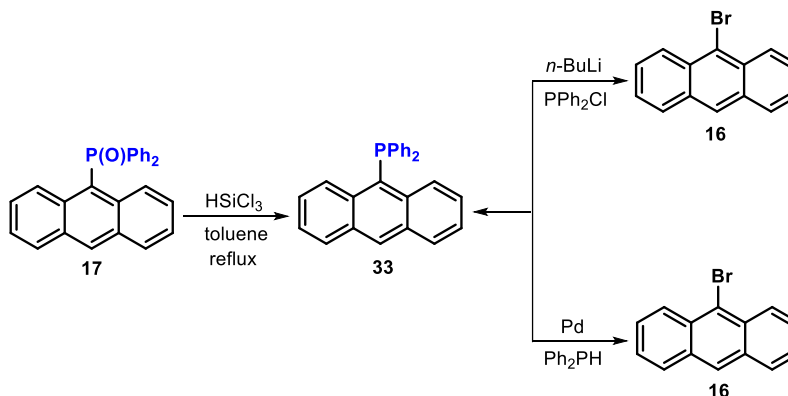
Scheme 17. Synthetic routes for 9-(diphenylphosphinyl)anthracene **33**.[65]

The phosphinyl group present on anthracene is not stable in air and can easily be oxidized to the phosphoryl group. Nevertheless, it serves as a precursor for transformations into other related functional groups, including thiophosphoryl (P=S) and selenophosphoryl (P=Se) ones. Furthermore, the phosphinyl group, possesses the capability to act as a ligand for metal complexes, such as those involving gold.[20]

1.4.3 Thiophosphoryl (R₂P=S, R=aryl, alkyl)) and selenophosphoryl (R₂P=Se, R=aryl, alkyl) substituted anthracene derivatives

The conversion of phosphoryl to thiophosphoryl and selenophosphoryl groups can be readily achieved by reduction of the P=O to (PIII) group followed by reactions with elemental sulfur (S₈) or selenium (Se). For example, Walensky and co-workers have successfully synthesized 9-(diphenylthiophosphoryl and diphenylselenophosphoryl) anthracenes **34** and **35**, from the diphenylphosphinyl substituted anthracene **33** (Scheme 18). In this study, they have investigated photophysical properties of these compounds and the ligand behavior towards Au(I) complex.[66]
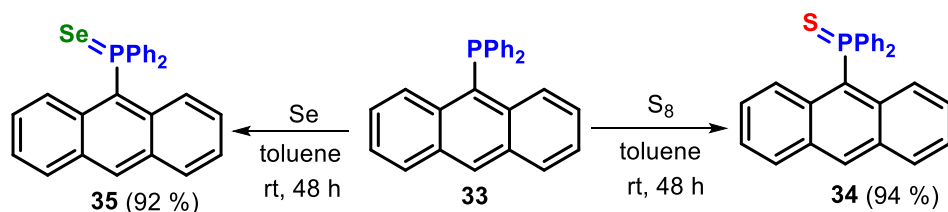
Scheme 18. Synthetic route to 9-(diphenylthiophosphoryl)anthracene **34** and 9-(diphenylselenophosphoryl)anthracene **35** from 9-(diphenylphosphinyl)anthracene **33**.[66]

Anthracenes **34** and **35** exhibited the upfield ³¹P-NMR chemical shifts compared to the corresponding phosphinyl substituted anthracene **33.** The peak deviation may be attributed to the non-planar geometry of the sulfur and selenium-containing compounds, which potentially results in stronger sigma than pi-bonding interactions between phosphorus and the 9-carbon of anthracene. This phenomenon was confirmed by X-ray analysis which indeed revealed the non-planarity of some substituted anthracene molecules and unusual bending of aromatic rings.

In another study, Stalke and co-workers have synthesized 9-bromo-10-diphenylphosphinylanthracene, along with its oxidized derivatives (P=O, P=S, and P=Se) (Scheme 19).[67] Interestingly, 10-diphenylthiophosphorylanthracene **38** acted as a solid-state chemosensor for toluene. The solid-state host/guest complex of **38** and toluene, with a mole ratio of 1:2, exhibited a green fluorescence at 508 nm.
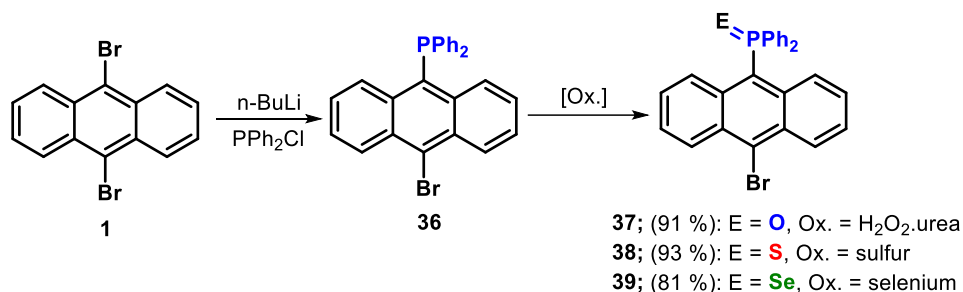
Scheme 19. Synthesis of 10-P=O, 10-P=S, and 10-P=Se substituted anthracenes **37**, **38**, and **39**.[67]

The X-ray analysis suggested that compounds **36** and **37** possessed an identical orientation of the lone pair and oxide groups with phenyl substituents positioned on either side of the anthracene plane. However, in compounds **38** and **39**, the phenyl groups were located on the same side of the anthracene plane. The orientation of these groups resulted in a non-planar anthracene structure, exhibiting a butterfly-like bend.

Later, the same research group have synthesized the symmetrical 9,10-disubstituted anthracene derivatives **11**, **12** and **13** by substituting both bromine atoms in **1** by diphenylphosphinyl groups (Scheme 20). They used hydrogen peroxide at 0 °C for oxidation of phosphorus atoms to give **11** and elemental sulfur and selenium in refluxing toluene to obtain **12** and **13** in 88 % and 84 % yields, respectively .[68]
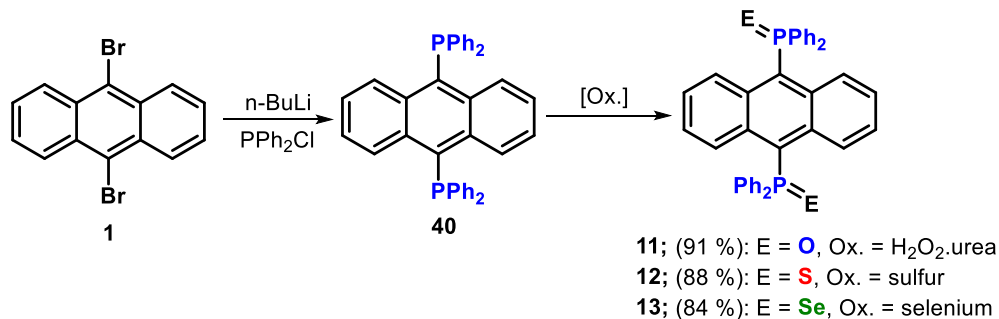
Scheme 20. Synthesis of P=O, P=S, and P=Se substituted anthracenes **11**, **12**, and **13**.[68]

Anthracene derivatives **11**, **12**, and **13** exhibited high solubility in common organic solvents compared to the P(III) compound **40**. The compound **11**, substituted with the Ph$_2$P=O moiety, showed stronger emission compared to compounds **12** and **13**, which were substituted with Ph$_2$P=S and Ph$_2$P=Se groups, respectively.

The X-ray analysis of these compounds revealed the same configuration, as previously reported for disubstituted anthracene **37-39**. The anthracene derivative **11** showed a planar geometry, whereas derivatives **12** and **13** exhibited an unusual bending within the anthracene plane. The emissive behavior of the anthracene derivative **12** in the solid state was attributed to the excimer formation, in which one excited molecule was associated with a ground-state molecule to form a fluorescent complex.

In another work from Stalke and co-workers, 9-diisopropylphosphinylanthracene **41** and 9-bromo-10-diisopropylphosphinylanthracene **42** were synthesized, and their interesting spectroscopic properties were studied in solution by low-temperature ^{1}H-NMR experiments (Scheme 21).[69]

41, R = H
42, R = Br

41a; (85 %), (R = H), **42a;** (85 %), (R = Br):
E = **O**, Ox. = H$_2$O$_2$.urea
41b; (72 %), (R = H), **42b;** (91 %), (R = Br):
E = **S**, Ox. = sulfur
41c; (75 %), (R = H), **42c;** (92 %), (R = Br):
E = **Se**, Ox. = selenium
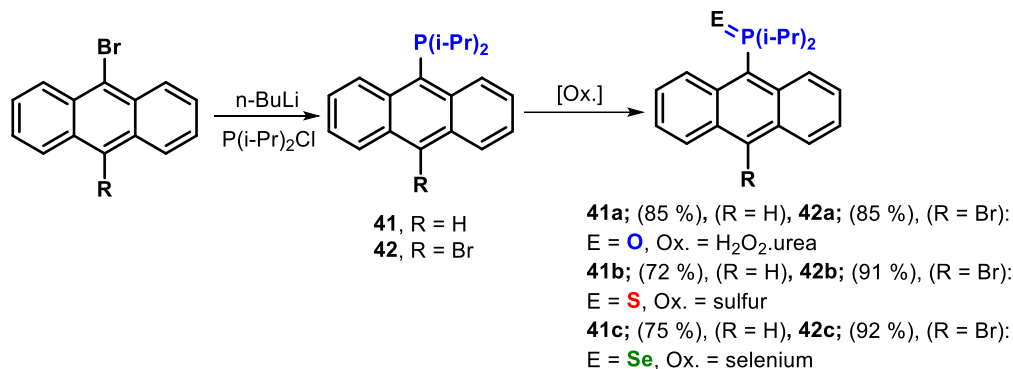
Scheme 21. Synthesis of compounds **41a-c** and **42a-c**.[69]

The investigated anthracene derivatives exhibited broadening of the aromatic signals, notably for C-1 and C-8 peaks, mainly because of the rotation of the phosphorus groups around the P-C bond. Under low temperature, the NMR spectra revealed split signals for C-1 and C-8 corresponding to staggered conformational isomers of the molecules. The rotational barrier around the P-C bond for the mono-substituted derivative **41** was determined to be 56 kJ mol^{-1} (ΔG_{298K}).

1

43

44; (87 %)
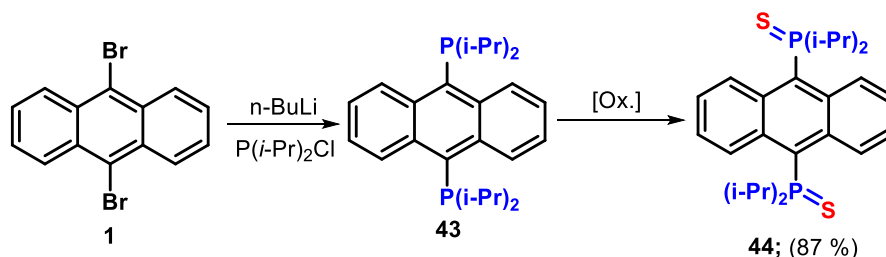
Scheme 22. Synthesis of 9,10-disubstituted anthracenes **43** and **44**.[69]

Likewise, the 9,10-disubstituted anthracene derivatives **43** and **44** were synthesized. The NMR studies at 183 K, for compound **40,** suggested the formation of cisoid and transoid forms. However, the transoid conformation was in a slightly higher amount than the cisoid form. The rotational conformers in solution at low temperatures were also analyzed through solid-state structural examinations.

In order to understand the effect of position of thiophosphoryl group (Ph$_2$P=S) on optical properties of substituted anthracenes, three positional isomers **10**, **45**, and **34**, were synthesized with the Ph$_2$P=S substituents at the 1, 2, and 9 positions of the anthracene (Scheme 23).[70] Interestingly, each isomer exhibited distinct colors in solid state ranging from blue and green to yellow.
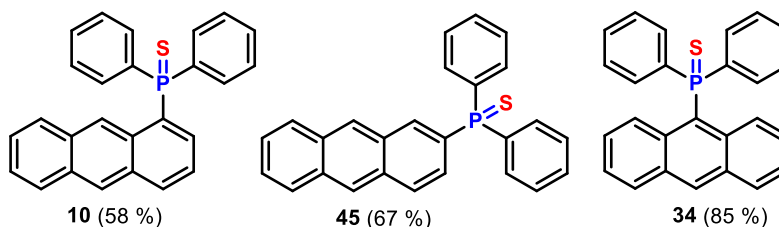
Scheme 23. Structures of Ph$_2$P=S substituted positional isomers **10**, **45,** and **34**.[70]

The optical properties showed that changing the position of substituents resulted in emission shifts of the anthracene derivatives by nearly 100 nm. Structural analysis indicated that the compounds **10** and **45** were more planar in contrast to the compound **34**, which exhibited a butterfly-bent configuration. The yellow emission observed in the solid state for the anthracene **10** substituted at the 1-position could be attributed to the formation of an excimer. In a separate study,[71] the formation of excimers and the influencing factors related to the structural and photophysical properties were thoroughly examined for the anthracene derivative **10**.

In another study, Matano and co-workers successfully synthesized a series of 9-(diphenylphosphoryl)-10-(phenylethynyl)anthracene derivatives (Scheme 24).[72] The compound **46** was synthesized from 9,10-dibromoanthracene **1** through replacement of the first bromine atom with PPh$_2$Cl followed by oxidation of the P(III) atom with hydrogen peroxide (H$_2$O$_2$). Then, the Sonogashira coupling reaction of the resulting 9-bromo-10-(diphenylphosphoryl)anthracene with 4-ethynyl-*N,N*-diphenylaniline was accomplished, utilizing the second bromine atom. Compound **47** was obtained through the reductive deoxygenation of **46** using trichlorosilane in toluene solution, and then it was transformed into the corresponding sulfides **48** and selenides **49** using elemental sulfur and selenium to the P(III) atom.
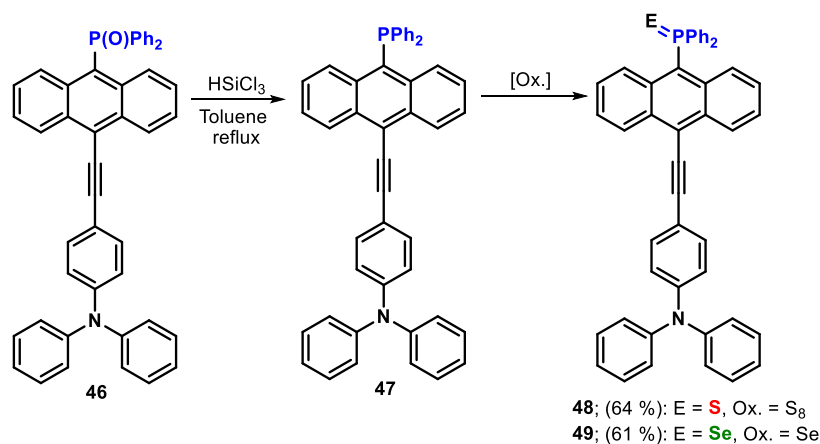
Scheme 24. Synthesis of phosphorus substituted anthracenes **47, 48,** and **49**.[72]

The excited states of these anthracene derivatives are solvent-dependent. The excited state S$_1$ was mainly dominated by the LE (locally excited) character in non-polar solvents, whereas charge transfer was observed in the polar solvents. In the case of the anthracene derivative **46**, the triplet-

triplet annihilation (TTA) phenomenon was observed, indicating the importance of anthracene derivatives for various optoelectronic applications.

1.4.4 Phosphoryl [(RO)$_2$P=O, R=alkyl] substituted anthracene derivatives

This section provides a basic overview of anthracene derivatives substituted with dialkoxyphosphoryl groups, containing one P-Csp^2 (Anth) bond, two P-O bonds, and one P=O bond.

Based on the previous literature, the substitution of bromine by dialkoxyphosphoryl group can be achieved through three main approaches. The first one is the halogen exchange using *t*-BuLi followed by a reaction of the resulting anthryllithium with chlorodialkylphosphate ClP(O)(OR)$_2$. Thus, Yazji and co-workers have synthesized anthracene derivatives **52** and **53** substituted with two diethoxyphosphoryl groups at anthracene positions 2 and 6 (Scheme 25).[73] In this method, they used *t*-BuLi for the double Br/Li exchange followed by the reaction with chlorodiethylphosphate.
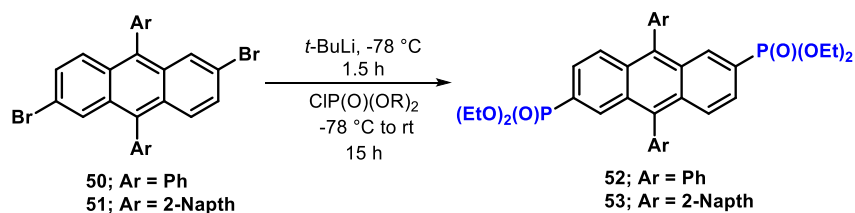
Scheme 25. Synthesis of 2,6-bis(diethoxyphosphoryl)anthracene **52** and **53**.[73]

The second and most important method is the Arbuzov reaction, facilitated by a catalyst, such as NiBr$_2$, wherein trialklyl phosphites react with an alkyl or aryl halide to form phosphonate esters. This approach was exemplified by French and co-workers who have synthesized the anthracene derivative **14**, substituted at position 2 with diethoxyphosphoryl group in the Arbuzov reaction of 2-bromoanthracence **54** with triethylphosphite, catalyzed by NiBr$_2$, in 60% yield (Scheme 26).[74]
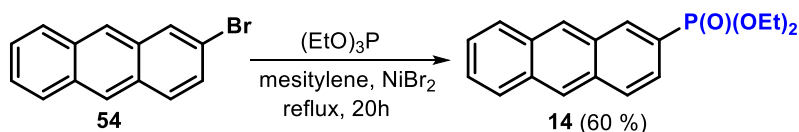
Scheme 26. Synthesis of 2-(diethoxyphosphoryl)anthracene **14**.[74]

In another example, 9,10-bis(diethoxyphosphoryl)anthracene **55** was synthesized using NiBr$_2$ catalyzed Arbuzov reaction (Scheme 27). In this synthesis, an excess of triethyl phosphite was used over 9,10-dibromoanthracene **1** in 1,3-diisopropylbenzene, as a solvent.[75]
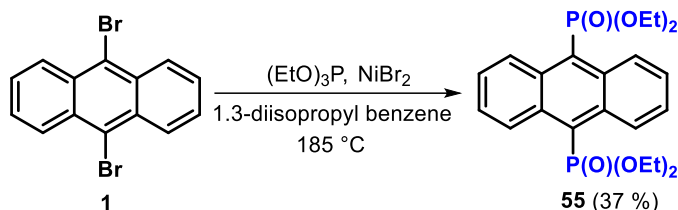
Scheme 27. Synthesis of 9,10-bis(diethoxyphosphoryl)anthracene **55**.[75]

Finally, the last method for synthesizing dialkoxyphosphoryl substituted anthracenes is the Hirao cross-coupling reaction. This is a palladium-catalyzed reaction of dialkyl phosphites and aryl bromides. For example, in a study conducted by Bessmertnykh and co-workers, 2-amino-9-(diethoxyphosphoryl)anthracene **57** was synthesized utilizing the Hirao reaction (Scheme 28).[76] In this reaction, 2-amino-9-bromoanthracene **56** was reacted with diethyl phosphite in the presence of *N,N*-dicyclohexylmethylamine in a methanol solution, using a catalytic amount of palladium acetate and triphenylphosphine.
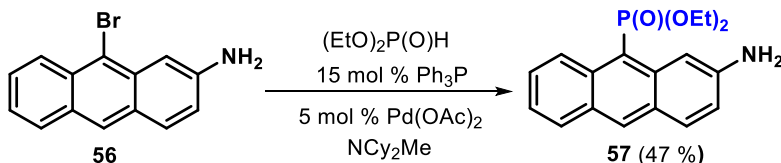
Scheme 28. Synthesis of 2-amino-9-(diethoxyphosphoryl)anthracene.[76]

In another example, 9,10-bis(dimethoxyphosphoryl)anthracene **58** was synthesized in 70% yield from 9,10-dibromoanthracene utilizing dimethyl phosphite (Scheme 29).[77] The reaction, catalyzed by palladium acetate/triphenylphosphine, was conducted under biphasic conditions within 30 hours at temperatures ranging from 70 to 80 °C in acetonitrile. Potassium carbonate, as a base and benzyltriethylammonium chloride (BTEAC), as a phase-transfer catalyst (PTC),were also used in this reaction.
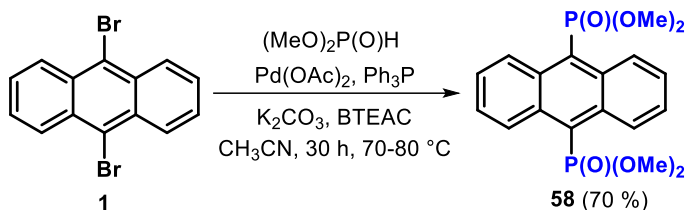
Scheme 29. Synthesis of 9,10-bis(dimethoxyphosphoryl)anthracene **58**.[77]

1.4.5 Phosphorus substituted anthracenes *via* the *phospho*-Friedel–Crafts/Bradsher reaction

The Bradsher reaction is an intramolecular electrophilic aromatic substitution (S_EAr) reaction and can be viewed as a cyclodehydrative modification of the classical Friedel-Crafts acylation. First described in 1940, it enables the synthesis of fused polycyclic aromatic hydrocarbons, such as anthracene derivatives, from *ortho*-substituted diarylmethanes.[78,79] In this reaction, typically *ortho*-formyl or *ortho*-acyl substituted diarylmethanes, were cyclized to acenes using strong Brønsted or Lewis acids (e.g., HBr, PPA, $FeCl_3$, TfOH, etc.) under harsh reaction conditions.[80,81]

However, utilizing a modified *oxo*-Friedel-Craft/Bradsher type intramolecular cyclization in 2012, our group have developed a novel synthetic strategy for the preparation of hexahydroxylated 10-RO-substituted anthracenes from *O*-protected *ortho*-acetal diarylmethanols.[82] We modified this reaction using very mild aqueous acidic conditions (1 *N* HCl in $MeOH/H_2O$ at room temperature). Interestingly, this method allowed us to functionalize both the central and flanking rings of the anthracene core, resulting in the synthesis of highly electron-rich anthracene derivatives that are rarely reported in the literature. Subsequently, this method was utilized in the synthesis of other multiply substituted anthracenes. For instance, in 2015, this approach facilitated the synthesis of pairs of anthracene-based positional isomers.[83]

Additionally, in a separate study conducted by our research group, RS-substituted (hetero)acenes were synthesized utilizing the *thio*-Friedel–Crafts/Bradsher modification.[84] In this work, unknown [*o*-(1,3-dithian-2-yl)aryl](aryl)methyl thioethers were used for this purpose employing the $FeCl_3/KI$ redox system in refluxing ethanol. The RS-products featured 1200-1900 fold greater photoresistance under aerobic and anaerobic conditions, both at 254 and 365 nm, than similar systems obtained so far. $RS(O)_n$ – Substituted anthracenes (n = 1, 2) were also obtained by oxidation of the corresponding RS-precursors.[85]

Later, both variants of the Friedel–Crafts/Bradsher reaction were also realized using the ultrasound assistance to significantly improve the cyclization process. In this work, the first sonocyclization of RO- and RS-substituted acene derivatives was achieved at lower temperatures in over 7500-fold and 2-fold reductions in reaction time, respectively.[86,87]

Therefore, the Friedel-Crafts/Bradsher cyclization reaction proves to be a suitable tool for synthesizing both multiply substituted anthracenes and higher acenes with various diverse functional groups on the outer and inner rings. Based upon this approach, we further modified the synthetic route to develop a strategy for the synthesis of 10-phosphorus-substituted anthracene derivatives using the *phospo*-Friedel–Crafts/Bradsher cyclization reaction.[20,88] This strategy retains the use and modification of readily available *ortho*-bromo aromatic aldehydes with a variety of electron-donating and electron-withdrawing groups (e.g., H, Br, F, CF_3, CN, CH_2–O–CH_2) to achieve diverse substitution on both the inner and outer rings of the anthracene framework which would allow for tuning of optical properties of these light emitters.

The synthetic sequence of the *phospo*-Friedel–Crafts/Bradsher reaction involves four key steps, as illustrated in Scheme 30:

1. **Protection of *ortho*-bromo aromatic aldehydes**: The *ortho*-bromo benzaldehydes **59** are protected using 1,3-propanediol in an acidic medium to achieve *O*-protected *ortho*-acetals.

2. **Formation of diarylmethanols**: A halogen-lithium exchange in **60** is carried out using *n*-BuLi, followed by the reaction with unprotected benzaldehydes containing electron-donating methoxy groups to afford diarylmethanols **61** . The presence of electron-donating groups on the benzaldehydes moiety facilitates cyclization in further steps to anthracenes according to the requirements of the S_EAr mechanism.

3. **Phosphorus functionalization**: The resulting diarylmethanols **61** are next converted into phosphorus-functionalized compounds such as dialkoxyphosphoryl **62** or diarylphosphoryl substituted derivatives **63** using a modified alcohol-based Michaelis-Arbuzov-type reaction with a suitable catalyst.

4. **The *phospho*-Friedel-Craft/Bradsher cyclization**: The final step involves cyclization of **62** or **63** to multiply substituted anthracenes **64** or **65** using aqueous solution of HCl at room temperature in a relevant solvent (mostly MeOH or CH_3CN).
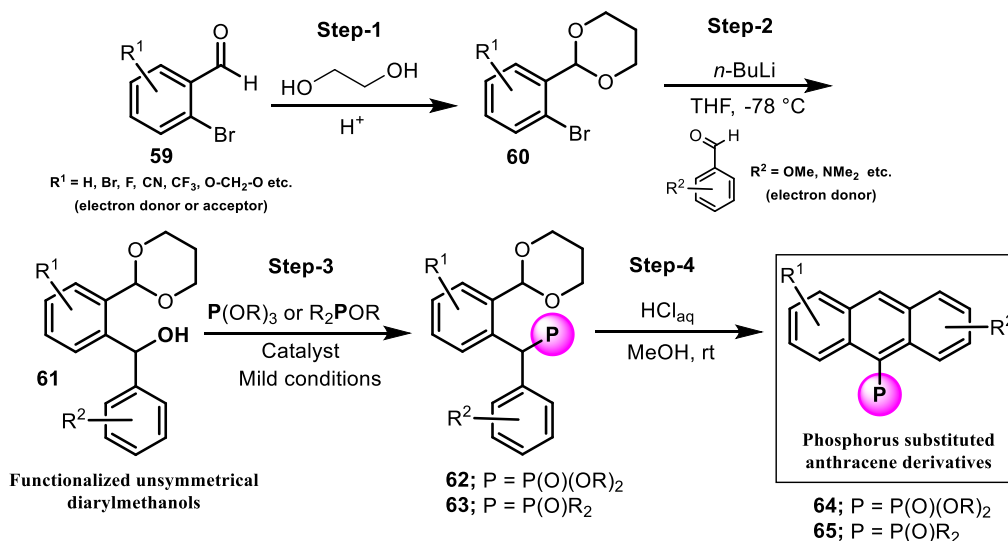
Scheme 30. A concept for the synthesis of phosphorus-substituted anthracenes.

This method makes it possible to incorporate phosphorous groups, such as phosphonates and phosphine oxide, into the anthracene core, while allowing for a variety of substitutions at different positions of the anthracene core. Hence, compared to other traditional synthetic methods, this approach offers greater flexibility and control in synthesizing structurally complex, multiply substituted phosphorus-based anthracene derivatives, which are important in materials science and organophosphorus chemistry.

1.5 References

1. M. Yoshizawa, J. K. Klosterman, *Chem. Soc. Rev.,* **2014**, *43*, 1885-1898.
2. (a) A. S. Travis, Lehigh University Press, Bethlehem, PA, **1993**; (b) W. H. Perkin, *Journal of the Society of Arts*, **1879**, *27*, 572-602.
3. R. Norman. Jones, Chemical Reviews **1947**, *41* (2), 353-37.
4. A. Kastrati, F. Oswald, A. Scalabre, K. M. Fromm, *Photochem* **2023**, *3*,227-273.
5. Y. Wang, W. Liu, S. Ye, Q. Zhang, Y. Duan, R. Guo, L. Wang, *J. Mater. Chem. C*, **2020**, *8*, 9678-9687.
6. Z. Wu, S. Song, X. Zhu, H. Chen, J. Chi, D. Ma, Z. Zhao, B. Z. Tang, *Mater. Chem. Front.,* **2021**, *5*, 6978-6986.
7. X. Zhu, Y. Li, Z. Wu, C. Lin, D. Ma, Z. Zhao, B. Z. Tang, *J. Mater. Chem. C*, **2021**, *9*, 5198-5205.
8. R. Guo, S. Ye, Y. Wang, Y. Duan, K. Di, L. Wang, *J. Mater. Chem. C*, **2021**, *9*, 13392-13401.
9. M. Chen, L. Yan, Y. Zhao, I. Murtaza, H. Meng, W. Huang, *J. Mater. Chem. C*, **2018**, *6*, 7416-7444.
10. J. V. Damme, F. D. Prez, *Prog. Polym. Sci*. **2018**, *82*, 92–119.
11. Y. Kim, M. Jung, R. Kumar, J. M. Choi, E. K. Lee, J. Lee, *ACS Appl. Mater. Interfaces* **2024**, *16*, 43774−43785.
12. K. Kondratenko, I. Carlescu, P.-E. Danjou, Y. Boussoualem, A. Simion, B. Duponchel, J. F. Blach, C. Legrand, N. Hurduc, A. Daoudia, *Phys. Chem. Chem. Phys*., **2021**, *23*, 13885–13894.
13. T. P. Fay, D. T. Limmer, *Chem. Sci*., **2024**, *15*, 6726–6737.
14. A. Yildiz, C. N. Reilley, Spectrosc. Lett **1968**, *1*, 335–343.
15. C. Coudret, V. Mazenc, *Tetrahedron Lett.,* **1997**, *38*, 5293–5296.
16. H. Becker, *Chem.Rev*. **1993**, *93*, 145−172.
17. R. Jones, *Chem. Rev*. **1947**, *41*, 353−371.
18. H. Ihmels, A. Meiswinkel, C. Mohrschladt, *Org. Lett*. **2000**, *2*, 2865−2867.
19. S. A. Hatab, V. A. Spata, S. Matsika, *J. Phys. Chem. A*, **2017**, *121*, 1213−1222.
20. V. Vivek, M. Koprowski, E. R. Sokołowska, M. Turek, B. Dudziński, K. Owsianik, Ł. Knopik, P. Bałczewski, *J. Org. Chem*. **2025**, *90*, 4580–4590.
21. V. N. Huynh, M. Leitner, A. Bhattacharyya, L. Uhlstein, P. Kreitmeier, P. Sakrausky, J. Rehbein, O. Reiser, *Commun Chem, 2020, 3*, 158.
22. O. L. Wright, L. E. Mura, *J. Chem. Educ*. **1966**, *43*, 3, 150.
23. C. E. Braun, C. D. Cook, C. Merritt, J. E. Rousseau, *Org. Synth*. **1951**, *31*, 77.
24. J. O. Morley, *J. Chem. Soc., Perkin Trans*. **1976**, *2*, 1554-1559.
25. K. J. Kim, J. Kim, J. T. Lim, J. Heo, B. J. Park, H. Nam, H. Choi, S. S. Yoon, W. Kim, S. Kang, T. Kim, *Mater. Horiz*., **2024**,*11*, 1484-1494.
26. M. Uejima, T. Sato, M. Detani, A. Wakamiya, F. Suzuki, H. Suzuki, T. Fukushima, K. Tanaka, Y. Murata, C. Adachi, H. Kaji, *Chemical Physics Letters*, **2014**, *602*, 80-83.

27. J. Jacob, J. H. Espenson, *Inorg. Chim. Acta*, **1998**, *270*, 55–59.

28. J. L. Marshall, D. Lehnherr, B. D. Lindner, R. R. Tykwinski, *ChemPlusChem*, **2017**, *82*, 967–1001.

29. G. W. Breton, X. Vang, *J. Chem. Educ*. **1998**, *75*, 81.

30. O. C. Musgrave, *Chem. Rev*. **1968**, *69*, 499–531.

31. E. Cho, S. M. Pratik, J. Pyun, V. Coropceanu, J. L. Brédas, *Adv. Optical Mater*. **2023**, *11*, 2300029.

32. P. H. Le, A. Liu, L. B. Zasada, J. Geary, A. A. Kamin, D. S. Rollins, H. A. Nguyen, A. M. Hill, Y. Liu, D. J. Xiao, *Angew. Chem. Int. Ed*. **2025**, *64*, e202421822.

33. G. Cheng, Y. Han, *New J. Chem.,* **2023**, *47*, 21600-21603.

34. J. Yuan, Z. Xu, M. O. Wolf , *Chem. Sci*., **2022**,*13*, 5447-5464.

35. B. Fan, F. Lin, X. Wu, Z. Zhu, A. K. Y. Jen, *Acc. Chem. Res*. **2021**, *54*, 20, 3906–3916.

36. F. Zhao, M. An, N. Wang, X. Yin, *Chem. Eur. J*. **2025**, *31*, e202403810.

37. M. Cornelius, F. Hoffmann, B. Ufer, P. Behrensc, M. Fröba, *J. Mater. Chem*., **2008**,*18*, 2587-2592.

38. T. Baumgartner, R. Reau, *Chem. Rev*. **2006**, *106*, 4681−4727.

39. N. Soh, O. Sakawaki, K. Makihara, Y. Odo, T. Fukaminato, T. Kawai, M. Iriea, T. Imato, *Bioorg. Med. Chem*., **2005**, *13*, 1131–1139.

40. I. Partanen, A. Belyaev, B. K. Su, Z. Y. Liu, J. J. Saarinen, I. I. Hashim, A. Steffen, P. T. Chou, C. R. Nieto, I. O. Koshevoy, *Chem. Eur. J.* **2023**, *29*, e202301073.

41. M. Koprowski, K. Owsianik, Ł. Knopik, V. Vivek, A. Romaniuk, E. R. Sokołowska, P. Bałczewski, *Molecules,* **2022**, *27*, 6611.

42. S. K. Bahadur, V. Thangaraji, N. Yadav, G. P. Nanda, S. Das, P. Gandeepan, E. Z. Colman, P. Rajamalli, *J. Mater. Chem. C*, **2021**, *9*, 15583.

43. M. Yoshizawa, J. K. Klosterman, *Chem. Soc. Rev*., **2014**, *43*, 1885-1898.

44. Y. Dienes, M. Eggenstein, T. Kμrpμti, T. C. Sutherland, L. Nyulμszi, T. Baumgartner, Chem. Eur. J. 2008, 14, 9878 – 9889.

45. S. Yamaguchi, S. Akiyama, K. Tamao, *Journal of Organometallic Chemistry*, **2002**, *646*, 277–281.

46. T. Schillmöller, R. Herbst-Irmer, D. Stalke, *Adv. Optical Mater*. **2021**, *9*, 2001814.

47. Z. Fei, N. Kocher, C. J. Mohrschladt, H. Ihmels, D. Stalke, *Angew. Chem. Int. Ed*. **2003**, *42*, 783-787.

48. M. Pramanik, N. Chatterjee, S. Das, K. D. Saha, A. Bhaumik, *Chem. Commun*., **2013**, *49*, 9461.

49. S. P. Hill, T. Banerjee, T. Dilbeck, K. Hanson, *J. Phys. Chem. Lett*. **2015**, *6*, 4510−4517.

50. D. N. French, J. G. Simmons, H. O. Everitt, S. H. Foulger, G. M. Gray, Synthesis and Characterization of Amphiphilic Arenephosphonates as Water-Soluble Micellular Radioluminescent Probes. *ChemRxiv* **2020.**

51. L. F. Fieser, *Org. React*. **2011**, 129–154.

52. G. K. S. Prakash, C. Panja, A. Shakhmin, E. Shah, T. Mathew, G.A. Olah, *J. Org. Chem.* **2009**, *74*, 8659–8668.

53. C. K. Bradsher, *J. Am. Chem. Soc.* **1940**, *62*, 486–488.

54. T. Yasukawa, T. Satoh, M. Miura, M. Nomura, *J. Am. Chem. Soc.* **2002**, *124*, 12680–12681.

55. G. S. Baviera, P. M. Donate, *Beilstein J. Org. Chem.* **2021**, *17*, 2028–2050.

56. K. Katagiri, Y. Yamamoto, Y. Takahata, R. Kishibe, N. Fujimoto, *Tetrahedron Letters*, **2019**, *60*, 2026–2029.

57. Y. Zhao, L. Duan, X. Zhang, D. Zhang, J. Qiao, G. Dong, L. Wang, Y. Qiu, *RSC Adv.*, **2013**, *3*, 21453–21460.

58. C. L. Wu, C. H. Chang, Y. T. Chang, C. T. Chen, C. T. Chen, C. J. Su, *J. Mater. Chem. C*, **2014**, *2*, 7188–7200.

59. B. Yang, Z. X. Wang, *J. Org. Chem.* **2019**, *84*, 1500−1509.

60. J. S. Zhang, T. Chen, L. B. Han, *Eur. J. Org. Chem.* **2020**, 1148–1153.

61. X. Chen, X. Liu, H. Zhu, Z. Wang, *Tetrahedron* **2021**, *81*, 131912.

62. J. Chrzanowski, D. Krasowska, M. Urbaniak, L. Sieroń, P. Pokora-Sobczak, O.M. Demchuk, J. Drabowicz, J. *Eur. J. Org. Chem.* **2018**, *2018*, 4614–4627.

63. L. Chen, S. Wang, P. Werz, Z. Han, D. P. Gates, *Heteroatom Chemistry*, **2018**, *29*, e21474.

64. D. N. Roark, G. J. D. Peddle, *J. Am. Chem. Soc.* **1972**, *94*, 16, 5837–5841.

65. D. Herault, D. H. Nguyen, D. Nuel, Gerard Buono, *Chem. Soc. Rev.*, **2015**, *44*, 2508-2528.

66. A. T. Breshears, A. C. Behrle, C. L. Barnes, C. H. Laber, G. A. Baker, J. R. Walensky, *Polyhedron*, **2015**, *100*, 333–343.

67. G. Schwab, D. Stern, D. Leusser, D. Stalke, *Zeitschrift für Naturforschung B*, **2007**, *62*, 5, 711-716.

68. Z. Fei, N. Kocher, C. J. Mohrschladt, H. Ihmels, D. Stalke, *Angew. Chem. Int. Ed.* **2003**, *42*, 783-787.

69. G. Schwab, D. Stern, D. Stalke, *J. Org. Chem.* **2008**, *73*, 14, 5242–5247.

70. T. Schillmoller, P. N. Ruth, R. H. Irmer, D. Stalke, *Chem. Commun.*, **2020**, *56*, 7479 –7482.

71. T. Schillmoller, R. H. Irmer, D. Stalke, *Adv. Optical Mater*. **2021**, *9*, 2001814.

72. N. Murayama, J. H. Jorolan, M. Minoura, H. Nakano, T. Ikoma, Y. Matano, *ChemPhotoChem*, **2022**, *6*, e202200100.

73. S. Yazji, C. Westermeier, D. Weinbrenner, M. Sachsenhauser, K.C. Liao, S. Noever, P. Postorino, J. Schwartz, G. Abstreiter, B. Nickel. *J. Raman Spectrosc.* **2017**, *48*, 235–242.

74. D. French, J. G. Simmons, H. Everitt, S. H. Foulger, G. M. Gray. *ChemRxiv* **2020**.

75. M. Pramanik, N. Chatterjee, S. Das, K. D. Saha, A. Bhaumik. *Chem. Commun.* **2013**, *49*, 9461–9463.

76. A. Bessmertnykh, C. M. Douaihy, R. Guilard. *Chem. Lett.* **2009**, *38*, 738–739.

77. M. Kabachnik, M. Solntseva, V. Izmer, Z. Novikova, I. Beletskaya. *Russ. J. Org. Chem.* **1998**, *34*, 93–97.

78. C. K. Bradsher. *J. Am. Chem. Soc*. **1940**, *62*, 486.

79. C. K. Bradsher. *Chem. Rev*. **1987**, *87*, 1277.

80. A. Bodzioch, E. Kowalska, J. Skalik, P. Bałczewski. *Chemistry of Heterocyclic Compounds* **2017**, *53*(1), 11–20.

81. J. Skalik, M. Koprowski, E. R. Sokołowska, P. Bałczewski. *Materials* **2020**, *13*(21), 4751.

82. A. Bodzioch, B. Marciniak, E. R. Sokołowska, J. K. Jeszka, P. Uznanski, S. Kania, J. Kulinski, P. Bałczewski. *Chem. Eur. J*. **2012**, *18*, 4866–4876.

83. P. Bałczewski, J. Skalik, P. Uznanski, D. Guziejewski, W. Ciesielskic. *RSC Adv*.,**2015**, *5*, 24700.

84. P. Bałczewski, E. Kowalska, E. R. Sokołowska, J. Skalik, K. Owsianik, M. Koprowski, B. Marciniak, D. Guziejewski, W. Ciesielski. *Chem. Eur. J*. **2019**, *25*,14148–14161.

85. P. Bałczewski, E. Kowalska, E. Różycka-Sokołowska, P. Uznański, J. Wilk, M. Koprowski, K. Owsianik, B. Marciniak, *Materials*, **2021**, *14*, 3506.

86. E. Kowalska, P. Bałczewski. *Ultrasonics Sonochemistry* **2017**, *34*, 743–753.

87. P. Bałczewski, E. Kowalska, J. Skalik, M. Koprowski, K. Owsianik, E. R. Sokołowska. *Ultrasonics Sonochemistry* **2019**, *58*, 104640.

88. M. Koprowski, Ł. Knopik, E. R. Sokołowska, B. Dudziński, V. Vivek, K. Owsianik, P. Bałczewski, *Angew. Chem. Int. Ed.* **2025**, e20250

2. Motivation and objectives of this dissertation

The presented dissertation is part of a broad project aimed at the development of a new class of multisubstituted anthracene derivatives *via* the *phospho*-Friedel–Crafts–Bradsher cyclization. The main goal of this work is to develop a novel synthetic route for anthracene functionalization (primarily on peripheral rings) and to investigate the photophysical, chemical, and electrochemical properties of the synthesized derivatives. Such compounds are expected to achieve high fluorescence quantum yields, significant photostability, and unique electronic properties. To achieve this goal, it was essential to develop a convenient synthetic method and conduct a detailed analysis of the structure-property relationships.

Previous results suggested that anthracene-based materials are significantly constrained by issues, such as strong intermolecular π–π stacking, limited substitution patterns (primarily at the 9,10-positions), and poor fluorescence quantum yields. To deal with these challenges and increase the use of highly substituted anthracene derivatives in optoelectronic applications, this research was motivated by the rational development of novel synthetic strategies that allow for:

i)   Multifunctional substitution patterns beyond conventional 9- and 10-positions
ii)   Fine-tuning of the HOMO-LUMO energy levels
iii)   Suppression of non-radiative decay pathways
iv)   Enhancement of fluorescence efficiencies both in solutions and in solid-state

A major inspiration came from the potential of phosphorus-containing substituents, particularly phosphine oxide and phosphonate ester groups, which offer electron-withdrawing capabilities, enable intramolecular charge transfer (ICT), based on the structural rigidity of the chromophores. In light of these motivations, this thesis explores synthetic strategies for structurally modifying anthracene cores *via* the *phospho*-Friedel–Crafts–Bradsher cyclization, Sonogashira coupling, and Knoevenagel condensations, aiming to generate a library of highly emissive, electronically tunable, and synthetically accessible anthracene derivatives.
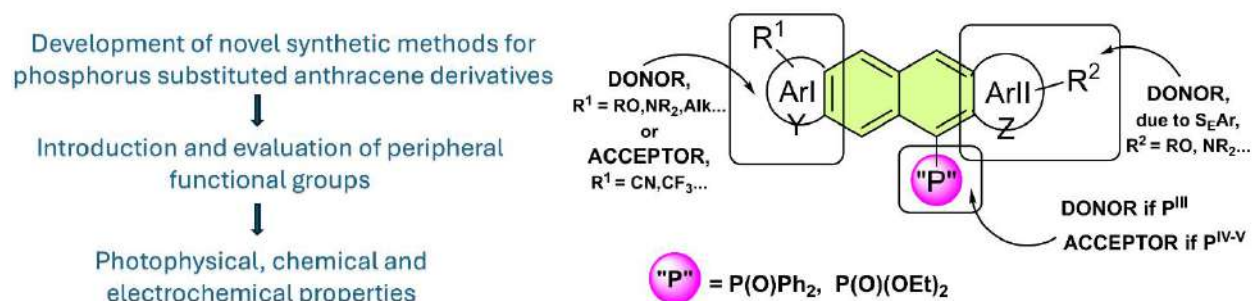
Figure 1. A graphical representation of the motivation and objective of this dissertation.

The main objectives of this thesis are as follows:

1. Development of synthetic methods for phosphorus-functionalized anthracene derivatives
   i) Modifications in the Arbuzov and Friedel–Crafts–Bradsher cyclization protocols to enable mild and selective substitution of phosphine oxide and phosphonate ester groups at the central core of anthracene and heteroacenes.
2. Introduction and evaluation of peripheral functional groups
   i) Synthesis of 10-(diphenylphosphoryl)-7-(phenylethynyl)anthracene derivatives through Sonogashira coupling to investigate the impact of electron-donating and electron-withdrawing substituents at the terminal positions.
   ii) Functionalization of *ortho*-positional isomers with dicyanovinyl (DCV) and phenylethynyl (PhE) moieties at the 6 and 7 positions of anthracene to assess their role in tuning emission wavelengths, quantum yields, and redox behavior.
3. Investigation of photophysical, chemical, and electrochemical properties
   i) Detailed analysis of UV-Vis absorption, photoluminescence (PL), and quantum yield measurements in various solvents.
   ii) Assessment of emission behavior affected by substituent topology and solvent polarity, emphasizing the appearance of Twisted Intramolecular Charge Transfer (TICT) states in polar environments.
   iii) Measurement of oxidation and reduction potentials using cyclic voltammetry to investigate the impact of substitution on HOMO-LUMO energy levels.
4. Theoretical and computational calculations
   i) Execution of DFT and TD-DFT calculations to support experimental findings such as position of orbital energy levels, charge transfer characters, and excited-state behaviour.
   ii) Visualization of how specific substituents affect the frontier molecular orbitals and overall electronic architecture.

By combining novel synthetic methods with a detailed investigation of optical properties, this thesis provides a comprehensive roadmap for designing multiply substituted anthracene-based emitters. The work not only broadens the structural and functional landscape of anthracene derivatives but also contributes knowledge that may bring benefits to the broadly understood field of organic optoelectronics.

3. Results and discussion

3.1 High-efficiency light emitters: 10-(diphenylphosphoryl)-anthracenes from one-pot synthesis including C–O–P to C–P(=O) rearrangement

The results of this work were described and published in the Journal of Organic Chemistry. My contribution to this work consisted of synthesizing all the final products, characterizing them, preparing the manuscript, and providing supporting information. A summary of the project's main objectives is presented in the introduction below. However, for details please refer to the attached publication: **V. Vivek**, M. Koprowski, E. Różycka-Sokołowska, M. Turek, B. Dudziński, K. Owsianik, Ł. Knopik, P. Bałczewski, *J. Org. Chem.* 2025, *90* (13), 4580-4590.

3.1.1 Introduction

Anthracene-based organic materials stand out due to their high fluorescence quantum yields and relative chemical stability. However, their practical use is often hindered by unfavorable intermolecular $\pi-\pi$ stacking, low substitution, and poor substituent diversity, except for the commonly functionalized 9,10-positions. These limitations reduce emission efficiency, especially in the solid state, necessitating structural modifications for their application in high-performance devices.

This work presents a novel, one-pot, three-step synthetic route for the preparation of a new class of multiply substituted 10-(diphenylphosphoryl) anthracenes. The methodology relies on the rearrangement of phosphinites to phosphine oxides catalyzed by trimethylsilyl triflate (TMSOTf), followed by the *phospho*-Friedel–Crafts–Bradsher cyclization, to give a series of structurally diverse D-A anthracene derivatives. This synthetic method enables access to a variety of highly substituted anthracene derivatives with electron-donating (OMe) and electron-withdrawing (CN, CF_3, halogens) groups, showing high photoluminescence quantum yields (up to 95%) in both solution and solid states. Introducing a suitable phosphorus group, such as diphenylphosphoryl ($Ph_2P=O$) at the 10-position, lowers the LUMO energy levels and allows for modifications at the phosphorus center.

In addition to novel synthetic methods, the synthesized anthracene derivatives showed tunable optical properties, high fluorescence efficiency, and distinct aggregation properties. These features make these compounds suitable candidates for different organic electronic applications. This work significantly expands the range of functionality of anthracene-based emitters and provides a basis for future development of high-efficiency, phosphorus-functionalized materials for optoelectronic technologies.

3.2 Synthesis and optical properties of 10-(diphenylphosphoryl)-7-(phenylethynyl) anthracene derivatives

In our previous study, we employed a novel one-pot synthesis of highly substituted anthracene derivatives featuring 10-diphenylphosphoryl and various functional groups on the anthracene flanking rings. This approach provides opportunity for substituting easily functionalizable groups, such as halogens. Halogen groups, particularly bromine, can be utilized in cross-coupling reactions to synthesize more π-extended anthracene derivatives. Inspired by the work of Matano and co-workers, in which they have synthesized 9-(diphenylphosphoryl)-10-(phenylethynyl)anthracene (DPPPEA) derivatives, in this study, we conducted the Sonogashira cross-coupling between a previously synthesized 7-bromo anthracene derivative and phenyl acetylene derivatives substituted at the *para* position with electron-withdrawing and electron-donating groups. These studies have not yet been published and further theoretical calculations are in progress. Nevertheless, the preliminary findings of photophysical and electrochemical properties, along with the results of density functional theory (DFT) calculations, are presented below. My contribution to this work consisted of the synthesis of all final products, their characterization, investigation of electrochemical properties, preparation of manuscript and supporting information.

3.2.1 Introduction

Anthracene derivatives are widely used in organic materials, especially in organic light-emitting diodes (OLEDs),[1–5] organic field-effect transistors (OFETs),[6,7] and in the triplet-triplet annihilation (TTA) process[8–10] due to their excellent photophysical properties, such as high fluorescence quantum yields and nanosecond lifetime. The substitution on the anthracene moiety with a suitable functional group on both the inner and outer rings may effectively inhibit π-π stacking and subsequently reduce the HOMO and LUMO energy levels. For instance, anthracene derivatives substituted with a phosphoryl group (P=O) have resulted in lower LUMO energy levels of the anthracene core because of its electron withdrawing property.[11,12] Furthermore, substituting the anthracene with phenylethynyl on one of outer rings significantly contributes to the enhancement of conjugation and the charge transport properties of anthracene core. For example, 2-(phenylethynyl)anthracene (2-pheA), exhibited a highest hole mobilities of 0.79 cm^2 V^{-1} s^{-1} compared to the other symmetrical anthracene derivatives.[13]
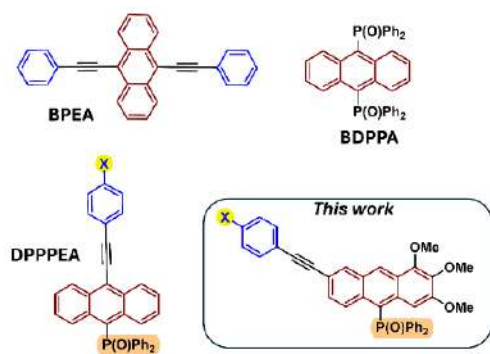

Figure 1. Structures of diphenylphosphoryl and/or ethynyl substituted anthracenes.

Initially, Matano and colleagues have introduced the diphenylphosphoryl and phenylethynyl groups at the anthracene 9 and 10-positions in 9-(diphenylphosphoryl)-10-(phenylethynyl)anthracene (DPPPEA) (Figure 1).[14] Their research was inspired by the idea of integrating bis(phenylethynyl)anthracene (BPEA)[15–17] with 9,10-bis(diphenylphosphoryl)anthracene (BDPPA)[18–20], extensively used emissive materials. Their studies have shown the dependence of the emissive excited state on various factors, including substituent, solvent, and temperature. Although the concept resulted in the synthesis of promising materials, there has been a lack of further research reported regarding multi-substituted anthracenes in addition to these two intriguing functional groups.

Our group previously reported the straightforward synthesis of anthracene derivatives containing various substituents on both the inner and flanking rings.[11] Halogen groups substituted on one of the outer ring can readily be replaced with various substituents *via* coupling reactions. Utilizing the previously obtained 7-bromo-1,2,3-trimethoxy-10-(diphenylphosphoryl)anthracene, we have synthesized a series of 7-(phenylethynyl)-10-(diphenylphosphoryl)anthracenes functionalized at the position 4 of phenyl group by electronically diverse substituents to investigate their influence on optical properties of the corresponding anthracenes. Furthermore, the *para* position of the phenylethynyl moiety was substituted with previously unexplored substituents, such as NMe_2 and dicyanovinyl (DCV). These groups showed distinct photophysical properties in different solvents due to their ability to rotate around a single bond and the formation of a distinct excited state known as the twisted intramolecular charge transfer state (TICT).[21] The objective of the molecular design in this work is to investigate the properties of peripherally substituted anthracenes, rather than limiting the focus to substitutions at the 9 and 10 positions of the inner ring.

3.2.2 Results and discussion

3.2.2.1 Synthesis

The 7-bromo anthracene derivative **1** was previously synthesized *via* a one-pot synthesis approach utilizing diaryl alcohols.[11] The anthracene derivatives **3a-f** were prepared using the Sonogashira cross-coupling reaction between the 7-bromo anthracene derivative **1** and arylacetylene derivatives **2a-f** (Scheme 1). The purification of all anthracene derivatives **3a-f** was achieved through the silica-gel column chromatography, resulting in their isolation as yellow or orange solids. Anthracene derivatives were fully characterized by NMR spectroscopy, high-resolution electrospray ionization (HR-ESI) mass spectroscopy and X-ray crystallography. The $^{31}P\{^{1}H\}$ NMR spectra of compounds **3a-f** revealed characteristic signals attributed to the phosphine oxide group (Figure S1-S23, Experimental Section-I).
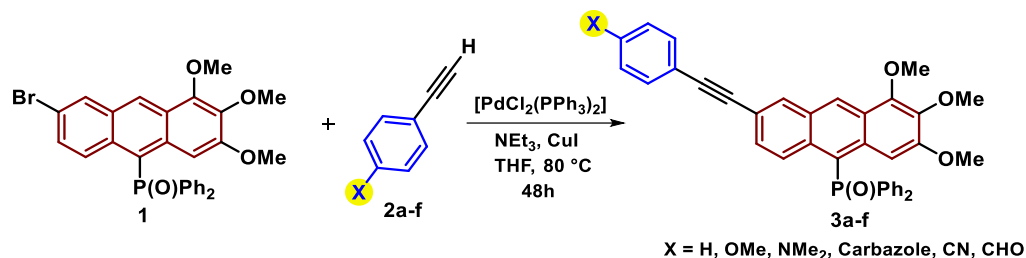
Scheme 1. Synthesis of anthracene derivatives **3a-f**.
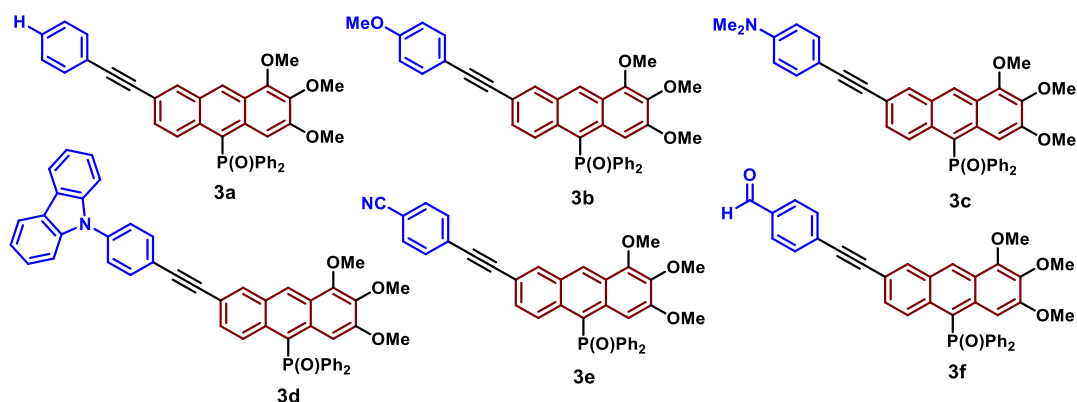
Scheme 2. Structures of synthesized anthracene derivatives **3a-f**.

The anthracene derivative **3g** was synthesized through the Knoevenagel condensation reaction involving the anthracene derivative **3f** and malononitrile [CH$_2$(CN)$_2$], utilizing piperidine and acetic acid as catalysts, in benzene solution (Scheme 3).
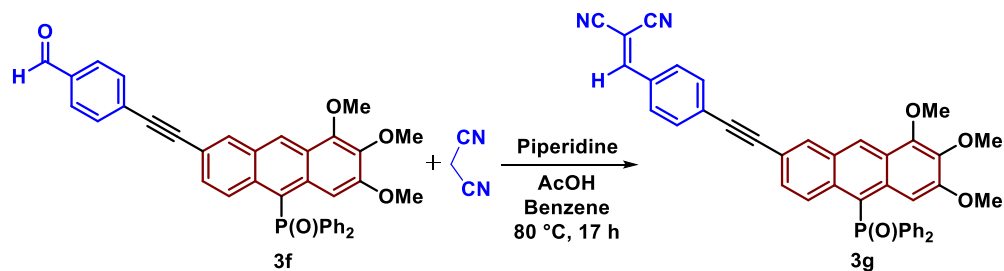
Scheme 3. Synthesis of the anthracene derivative **3g**.

3.2.2.2 Photophysical properties
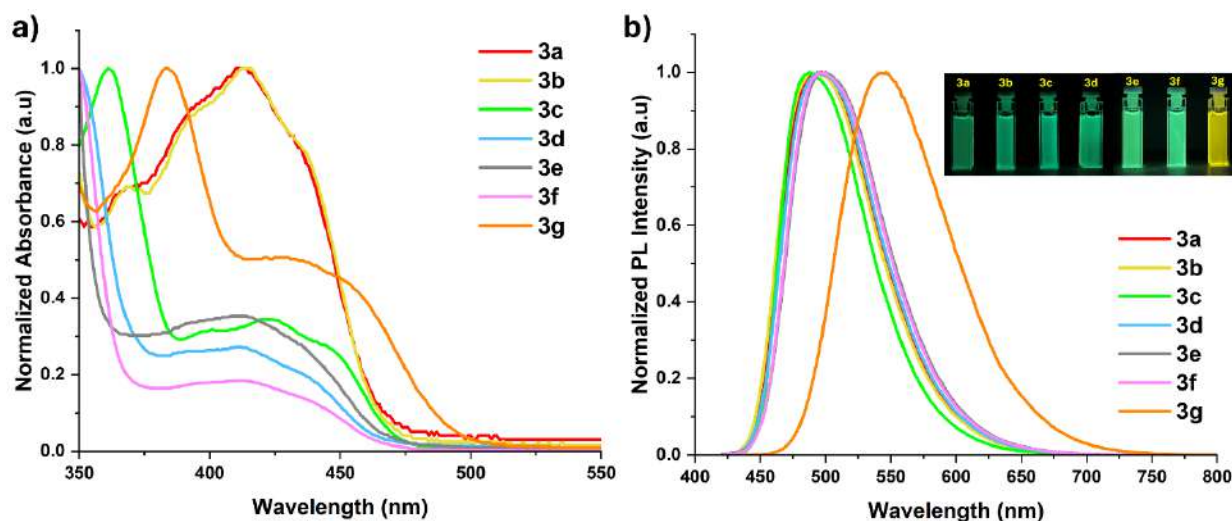
Figure 1. Normalized absorption (a) and emission spectra (b) of anthracene derivatives **3a-g** (10^{-5} mol/L, toluene).

UV and PL measurements: The ultraviolet−visible (UV−vis) absorption, photoluminescent emission (PL), and quantum yield data of anthracenes **3a-g** in four different solvents (toluene, DCM, MeOH, and MeCN) are given in Table 1 and S1 (ES-I). The results obtained are analyzed with respect to the electronic effects of substituents and the polarity of the solvents. As illustrated in Figure **1a**, the anthracene derivatives **3a-g** in toluene solution, exhibit the characteristic anthracene absorption band in the high energy range, while the broad absorption band observed in the low energy range is due to the n-π* charge transfer (CT) process.[22] Upon excitation in toluene solution, the anthracene derivative **3g**, which contains a dicyanovinyl (DCV) moiety at the *para* position, exhibited an emission band at a higher wavelength of 544 nm (Figure 1b). However, other anthracene derivatives **3a-f** did not exhibit significant differences in their wavelengths, showing emission bands in the range of 488-497 nm.

Table 1. Photophysical (in toluene) and electrochemical data for **3a-g** (in DCM).

Nr.	Photophysical data				Electrochemical data[e]	
	Abs.[a] (nm)	PL[b] (nm)	υ[c] (cm^{-1})	QY[d] (%)	$E_{Oxd.}$	$E_{Red(1)/(2)}$
3a	412	495	4070	74.09	1.18	-0.91 / -1.62
3b	415	491	3730	78.77	1.14	-0.91 / -1.64
3c	423	488	3148	61.74	0.77	-0.89 / -1.67
3d	411	495	4128	76.19	1.17	-0.95 / -1.65
3e	413	499	4173	74.87	1.22	-0.87 / -1.57
3f	412	497	4151	73.65	1.19	-0.90 / -1.59
3g	428	544	4982	77.17	1.24	-0.94 / -1.60

[a] Abs. – absorption maximum; [b] PL – emission maximum; [c] Stoke shift (υ) = $1/\lambda_{abs}$-$1/\lambda_{em}$; [d] The absolute photoluminescence quantum yield (QY); [e] Electrochemical analysis was estimated by DPV in 0.1 M solution of tetrabutylammonium hexafluorophosphate (TBAPF$_6$) in DCM at a 50 mVs^{-1} scan rate versus Ag/AgCl.

Upon increasing the polarity of solvents, no significant change is observed in the absorbance wavelengths of anthracene derivatives **3a-g**. In contrast, the emission wavelengths of **3a**, **3b**, **3d**, **3e**, and **3f** exhibit a red shift with the increased solvent polarity. The interesting features were observed for the emission of **3c** containing the dimethylamine and **3g** containing the DCV moieties. With the increase in polarity of solvents, a reduction in emission and fluorescence quantum yield was observed.

This phenomenon can be attributed to the twisted intramolecular charge transfer (TICT) state emissions, which are typically observed in arene compounds substituted with terminal dialkylamino and dicyanovinyl groups.[23–25] The D-A units involving these groups twist around the carbon-carbon and carbon-nitrogen bond to generate a relaxed perpendicular state. The existence of these states mainly depends on the solvent polarity, and in some solvents, they may achieve equilibrium with the locally excited (LE) states. In such cases, dual emission can be observed, with the LE state emitting in the higher-energy region and the TICT state emitting in the lower-energy region.[21]

In dichloromethane (DCM) solution, the anthracene derivative **3c** exhibited a significant red-shift with an emission wavelength at 561 nm, as compared to toluene, which exhibited an emission band at 488 nm (Figure S24, ES-I). In contrast, in acetonitrile (MeCN) and methanol (MeOH), the anthracene derivative **3c** showed emission bands at shorter wavelengths of 511 nm and 515 nm, respectively (Figure S25 and S26, ES-I). In acetonitrile, the compound **3c** exhibited dual emission bands at a higher wavelength, which is structureless and weaker in intensity relative to the main emission band and can be attributed to the TICT state emissions.

The anthracene derivative **3g**, which contains a DCV moiety, showed a blue shift in the emission wavelength as the polarity of the solvents increased. It exhibited a wavelength band at a higher wavelength of 544 nm in toluene and the lowest in DCM at 511 nm. The slight red shift in MeCN at 516 nm and MeOH at 519 nm may be attributed to the interaction of the solvent with the P=O group *via* hydrogen bonding. In the compound **3g**, a dual emission was observed in the DCM solution, and it once more exhibited a structureless band attributed to TICT in a lower energy region (Figure S24, ES-I).

QY measurements: The anthracene compound **3a**, unsubstituted at the 4-position of the phenyl moiety, showed the highest photoluminescence quantum yield (QY) of 85.07% in the DCM solution (Table 1). This QY is slightly higher compared to its parent compound, 7-bromoanthracene, which showed a QY of 80% in the same solvent. Anthracene compounds generally exhibited the highest quantum yield (QY) in a DCM solution; however, no observable trend in QY was observed based on the substitution at the *para* position with various functional groups. In contrast, the compound **3g** exhibited an exceptionally low quantum yield of 1.01% in the DCM solution. Similarly, in MeOH and MeCN, compounds **3c** and **3g** showed lower quantum yields. The reduced quantum yields of compounds **3c** and **3g** in polar solvents may be attributed to relaxation through a non-radiative pathway from the TICT state, resulting in lower emission.

3.2.2.3 Electrochemical properties
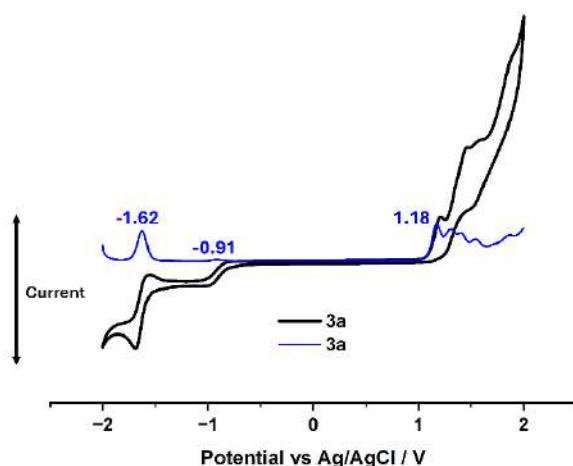
Figure 2. Cyclic voltammogram (black) and differential pulse voltammogram (blue) spectra of **3a;** measured in CH_2Cl_2 (DCM) solution, 20 °C, 50 mV s^{-1}, glassy carbon working electrode.

In order to understand electronic effects of various functional groups present at the 4-phenyl position, oxidation and reduction potentials of anthracene derivatives **3a-g** were determined through the cyclic voltammetry (CV) and differential pulse voltammetry (DPV) in the DCM solution with $Bu_4N^+PF_6^-$ (0.1 molL^{-1}) as a supporting electrolyte. The oxidation and reduction potentials of all anthracene derivatives **3a-g** are given in Table 1. The compound **3a**, which is unsubstituted at the 4-phenyl position, exhibited an oxidation potential of 1.18 V and two reduction potentials at -0.91 V and -1.62 V (Figure 2). The compound **3a**, showed a higher oxidation potential and a lower reduction potential in comparison to 9-(diphenylphosphoryl)-10-(phenylethynyl)anthracene, which was reported by Matano and co-workers to have an oxidation potential of 0.94 V and a reduction potential of -1.80 V. [14] This trend suggests that the position of the phenylethylene group can significantly affect the redox behavior of the anthracene core.

The oxidation and reduction potential values of anthracene derivatives **3a-g** showed a small variation, except for the compound **3c**, which had a significantly lower oxidation potential of 0.77 V, indicating its electron donating nature (Figure S27, SI). In addition, compounds substituted with electron donating groups such as **3b** (1.14 V) and **3d** (1.17 V) showed lower oxidation potentials compared to **3a** (1.18 V), which is unsubstituted at the 4-position of the phenyl moiety. The lower oxidation potential of these compounds suggested that they can be easily oxidized. However, compounds substituted with electron withdrawing groups, like **3e** (1.22 V) and **3g** (1.24 V), showed higher oxidation potentials, indicating stabilization of the HOMO and LUMO energy levels (Figure S27-S29, ES-I).

3.2.2.4 CIE studies
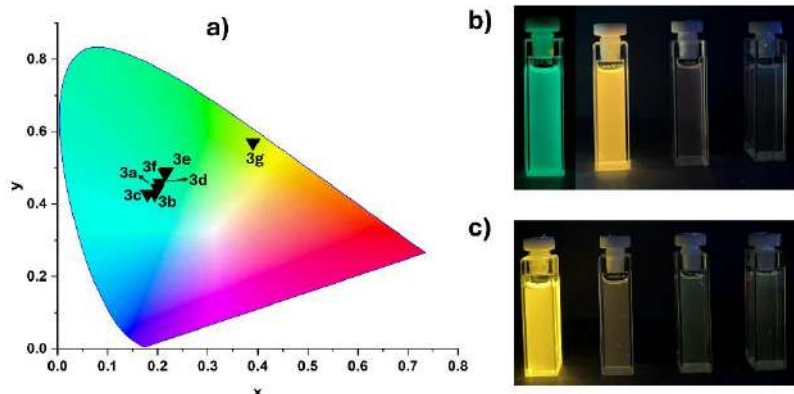
Figure 3. a) Commission Internationale de L'Eclairage (CIE) 1931 chromaticity coordinates for anthracene derivatives **3a-g;** b) a photograph of **3c-NMe₂** in four different solvents (toluene, DCM, MeCN, and MeOH) under 365 nm; c) a photograph of **3g-DCV** in four different solvents (toluene, DCM, MeCN, and MeOH) under 365 nm.

The anthracene compounds **3a-g** emitted green to yellow light in the 488-544 nm range in the toluene solution. In particular, anthracenes **3c** and **3g** emitted light of different colors in the different solvents (Figure 3b and 3c). The anthracene **3c** emitted green and yellow colors in less polar solvents, such as toluene and DCM, respectively, whereas **3g** emitted a yellow color in DCM. Nevertheless, emission was significantly quenched for both derivatives in highly polar solvents, including MeCN and MeOH. The CIE 1931 color space chromaticity coordinates of anthracene derivatives **3a-g** in toluene, DCM, toluene, MeCN, and MeOH are provided in Table S2 (ES-I).

3.2.3 Conclusions

In summary, a series of 10-(diphenylphosphoryl)-7-(phenylethynyl)anthracene derivatives were synthesized and fully characterized. The photophysical and electrochemical properties of synthesized anthracene derivatives revealed a significant influence of various electron-donating and electron-withdrawing substituents at the 4-phenyl position on emission, quantum yield, and redox potentials. Interestingly, derivatives substituted with dimethylamino and dicyanovinyl groups exhibited solvent-dependent twisted intramolecular charge transfer (TICT) behavior, displaying distinct emission and fluorescence quantum yields in various solvents. These results highlight the importance of flanking ring functionalization in tuning optoelectronic properties of anthracene-based materials.

3.2.4 References

1. Huang, J.; Su, J. H.; Tian, H. *J. Mater. Chem.,* **2012**, *22*, 10977-10989.

2. Slodek, A.; Filapek, M.; Schab-Balcerzak, E.; Grucela, M.; Kotowicz, S.; Janeczek, H.; Smolarek, K.; Mackowski, S.; Malecki, J. G.; Jedrzejowska, A.; Szafraniec-Gorol, G.; Chrobok, A.; Marcol, B.; Krompiec, S.; Matussek, M. *Eur. J. Org. Chem,* **2016***, 4020–4031.

3. Sharma, N.; Michael, A.; Wong, Y.; Hall, D.; Spuling, E.; Tenopala-Carmona, F.; Privitera, A.; Copley, G.; Cordes, D. B.; Slawin, A. M. Z.; Murawski, C.; Gather, M. C.; Beljonne, D.; Olivier, Y.; Samuel, I. D. W.; Zysman-Colman, E. *J. Mater. Chem. C,* **2020**, *8*, 3773-3783.

4. Sk, B.; Thangaraji, V.; Yadav, N.; Nanda, G. P.; Das, S.; Gandeepan, P.; Zysman-Colman, E.; Rajamalli, P. *J. Mater. Chem. C,* **2021**, *9* , 15583-15590.

5. Noda, T.; Sasabe, H.; Owada, T.; Sugiyama, R.; Arai, A.; Kumada, K.; Tsuneyama, H.; Saito, Y.; Kido, J. *Chempluschem,* **2022**, *87*, e202100517.

6. Chen, M.; Yan, L.; Zhao, Y.; Murtaza, I.; Meng, H.; Huang, W. *J. Mater. Chem. C,* **2018***, 6,* 7416-7444.

7. Qi, M.; Zhang, D.; Zhu, Y.; Zhao, C.; Li, A.; Huang, F.; He, Y.; Meng, H. *J. Mater. Chem. C,* **2024***, 12,* 6578-6587.

8. Lim, H.; Woo, S. J.; Ha, Y. H.; Kim, Y. H.; Kim, J. J. *Adv. Mater.* **2022***, 34,* 2100161.

9. Li, W.; Chasing, P.; Nalaoh, P.; Chawanpunyawat, T.; Chantanop, N.; Sukpattanacharoen, C.; Kungwan, N.; Wongkaew, P.; Sudyoadsuk, T.; Promarak, V. *J. Mater. Chem. C,* **2022***,10,* 9968-9979.

10. Bezvikonnyi, O.; Bucinskas, A.; Arsenyan, P.; Petrenko, A.; Wei, Z. Y.; Lee, J. H.; Volyniuk, D.; Rashid, E. U.; Chiu, T. L.; Grazulevicius, J. V. *ACS Appl. Electron. Mater.* **2024**, *6* , 4489-4503.

11. Vivek, V.; Koprowski, M.; Różycka-Sokołowska, E.; Turek, M.; Dudziński, B.; Owsianik, K.; Knopik, Ł.; Bałczewski, P. *J. Org. Chem.* **2025**, *90*, 4580-4590.

12. Koprowski, M.; Knopik, Ł.; Różycka-Sokołowska, E.; Dudziński, B.; Vivek, V.; Owsianik, K.; Bałczewski, P. *Angew. Chem. Int. Ed.* **2025**, e202508168.

13. Qiu, F.; Qiu, F.; Dong, Y.; Dong, Y.; Liu, J.; Sun, Y.; Geng, H.; Zhang, H.; Zhu, D.; Zhu, D.; Shi, X.; Shi, X.; Liu, J.; Zhang, J.; Zhang, J.; Ai, S.; Jiang, L. *J. Mater. Chem. C,* **2020**, *8* , 6006-6012.

14. Murayama, N.; Hao Jorolan, J.; Minoura, M.; Nakano, H.; Ikoma, T.; Matano, Y. *ChemPhotoChem,* **2022**, *6* , e202200100.

15. Demeter, A. First Steps in Photophysics. I. *J. Phys. Chem. A,* **2014**, 118, *43*, 9985-9993.

16. Bae, Y. J.; Kang, G.; Malliakas, C. D.; Nelson, J. N.; Zhou, J.; Young, R. M.; Wu, Y. L.; Van Duyne, R. P.; Schatz, G. C.; Wasielewski, M. R. *J. Am. Chem. Soc.* **2018**, 140, *45*, 15140-15144.

17. Zhang, W.; Wang, Q.; Feng, X.; Yang, L.; Wu, Y.; Wei, X. *Chem. Res. Chin. Univ*., **2017**, *33(4)*, 603-610.

18. Fei, Z.; Kocher, N.; Mohrschladt, C. J.; Ihmels, H.; Stalke, D. *Angew. Chem. Int. Ed.* **2003**, *42* (7), 783-787.

19. Jiang, Z.; Xu, M.; Li, F.; Yu, Y. *J. Am. Chem. Soc.* **2013***, 135, 44,* 16446-16453.

20. Xu, M.; Han, C.; Yang, Y.; Shen, Z.; Feng, W.; Li, F. *J. Mater. Chem. C.* **2016**, *4* (42), 9986-9992.

21. Sasaki, S.; Drummen, G. P. C.; Konishi, G. I. *J. Mater. Chem. C,* **2016***, 4,* 2731-2743.

22. Kastrati, A.; Oswald, F.; Scalabre, A.; Fromm, K. M. *Photochem.* **2023**, *3*, 227-273.

23. Dey, J.; Warner, I. M. *J. Phys. Chem. A,* **1997**, *101*, 27, 4872-4878.

24. Gupta, R. C.; Dwivedi, S. K.; Ali, R.; Razi, S. S.; Tiwari, R.; Krishnamoorthi, S.; Misra, A. *Spectrochimica Acta Part A: Molecular and Biomolecular Spectroscopy,* **2020**, *232*, 118153.

25. Chen, B.; Ding, Y.; Li, X.; Zhu, W.; Hill, J. P.; Ariga, K.; Xie, Y. *Chem. Commun.,* **2013**, *49*, 10136-10138.

3.3 Multiply substituted (hetero)acenes containing phosphonate group at the central unit as high-efficiency light emitters

The results of this work were described and published in the Angewandte Chemie. My contribution to this work was to synthesize and characterize the starting materials, as well as synthesize two of the final products, as a member of the project research team. Additionally, I have contributed to the revision of the manuscript. A summary of the main assumptions for this project is presented in the introduction below. However, for details, please refer to the attached publication: M. Koprowski, Ł. Knopik, E. Różycka-Sokołowska, B. Dudziński, **V. Vivek**, K. Owsianik, P. Bałczewski, *Angew. Chem. Int. Ed.* 2025, e202508168.

3.3.1 Introduction

Acenes and their heteroatom-containing analogues represent a class of polycyclic aromatic hydrocarbons that are especially attractive for applications in organic electronics and photonics due to their high charge-carrier mobility and tunable fluorescence characteristics. In this context, the introduction of functional groups that modulate both electronic structure and photophysical performance is of critical importance.

In this work, we introduced a novel synthetic method for the synthesis of multiply substituted (hetero)acenes through a modified Friedel-Crafts-Bradsher (F-C-B) cyclization reaction. A dialkoxyphosphoryl $[(RO)_2P(O)]$ phosphorus moiety was introduced by using this approach at the central position of tri- and tetracyclic acenes under mild conditions. The synthesized compounds exhibit high chemical stability and photoluminescence (PL) quantum yields (QYs) up to 87.7%. In addition to high PLQY, these class of compounds also have a significantly large Stokes shift (up to 7943 cm^{-1}), making them promising candidates for light-emitting applications.

Introducing an electron-withdrawing phosphonate group not only enhanced the PL efficiency but also enabled modification of electronic properties. Theoretical calculations, such as DFT and TD-DFT indicate that the emission in these compounds arises from a hybrid local excitation (LE) and charge transfer (CT) mechanism, with optimal QYs observed when CT contributes approximately 30% to the excited-state. Furthermore, the study reveals that the quantum yield is highly dependent on the solvent polarity, the position of substituents, and the presence of intramolecular interactions. These results indicate a complex interplay between molecular structure and photophysical behavior of the compounds. This work provides a strong foundation for the rational design of acene-based fluorophores and also highlights the importance of phosphonate functional groups in enhancing emission efficiency.

3.4 *ortho*-Positional isomers of anthracenes and carbazole derivatives containing phosphonate ester group and their optical properties

The results of this work are under peer review in the Organic Letters. My contribution in this work was to synthesize and characterize the starting materials and most of the final products (except **2a** and **2d**). Additionally, I have performed the cyclic voltammetry experiments and contributed to the preparation of the manuscript and supporting information data. A brief report of the background and details of this work is provided in the introduction section. However, for details, please refer to the attached submitted file and Section II of the experimental section.

3.4.1 Introduction

Based on our previous studies using the *phospho*-Friedel–Crafts–Bradsher cyclization for the synthesis of highly substituted anthracene derivatives featuring a phosphonate ester group, we propose extending this methodology to the *ortho*-positional isomers of anthracene derivatives, which are poorly recognized in the literature. Hence, in this work, we presented a systematic study of four pairs of *ortho*-positional isomers of anthracene and carbazole derivatives, each bearing a phosphonate ester group and various *ortho*-substituents (formyl and bromo groups). A three-step synthetic strategy, featuring a key *phospho*-Friedel–Crafts–Bradsher cyclization, yielded these compounds.

Detailed photophysical and electrochemical properties, along with DFT calculations, indicated that small structural changes in substituent topology significantly change the emissive properties and position of molecular orbitals. These compounds exhibited a significantly high fluorescence quantum yield, with one of the isomers showing a yield of 93.3%. These findings highlighted the importance of functionally rich organic emitters, positional isomerism, and phosphorus-based functionalization in the development of organic materials.

3.5 Post-synthetic functionalization of *ortho*-positional isomers

In our previous study (Section 3.4), we synthesized *ortho*-positional isomers containing readily functionalizable groups, such as formyl and bromine. These functional groups may not only influence the properties of anthracene derivatives but also may be post-synthetically transformed to other conjugated groups, thus providing more π-extended systems. Consequently, in this research, we have utilized these groups to transform them to dicyanovinyl (DCV) and phenylethynyl (PhE) moieties and have investigated electronic and optical properties of the resulting fluorophores. These studies have not yet been published, and further theoretical calculations are ongoing. Nevertheless, the preliminary findings of photophysical and electrochemical properties, along with the results of density functional theory (DFT) calculations, are presented below. My contribution in this work consisted of synthesizing all final products (except **2ab**), a contribution to their characterization, investigating electrochemical properties, preparing the manuscript, and supporting information.

3.5.1 Introduction

Anthracene and its derivatives have played an important role in the study and application of organic chromophores due to their high fluorescence quantum yields and the relative simplicity of their synthesis. Consequently, in recent years, anthracene derivatives have been widely investigated in the field of organic light-emitting diodes (OLEDs)[1–6], fluorescent probes[7–10], and in photon-upconversion *via* the triplet-triplet annihilation.[11–13]

Aromatic compounds substituted with dicyanovinyl (DCV) moiety are widely studied due to their push-pull architecture, and these materials exhibited interesting optoelectronic properties.[14–19] Xie et al.[20] investigated anthracene derivatives functionalized with a DCV moiety at the 2 and 9 positions which served as fluorescent probes for the detection of cyanide anions. The study suggested that introduction of the DCV unit into the outer rings of anthracene maintained a planar geometry with the anthryl plane while being introduced at sterically demanding 9-position caused intramolecular rotation, leading to a twisted intramolecular charge transfer (TICT) state. The different structural characteristics of the DCV unit, present on inner or outer rings of anthracene, makes it an important functional group that modulates the fluorescent properties of anthracene derivatives. Additionally, phenylethynyl (PhE) substituted aromatic compounds have been known to enhance the photophysical and charge transport properties by extending π-conjugation and reducing the HOMO-LUMO energy gap.[21–24] Functionalization of anthracene and higher acenes with triple bond also prevents them from photo-oxidation and decomposition.[25] Jing et al.[26] conducted an investigation of the charge transport properties of 2-(phenylethynyl)anthracene and indicated that it exhibited the highest hole mobility at the level of 0.79 cm² V⁻¹ s⁻¹ when compared to other anthracene derivatives, such as (*E*)-2-styrylanthracene and 2-phenylanthracene. In an another study, Xianfu et al.[27] demonstrated that the HOMO-LUMO gap was reduced to 2.99 eV for 9,10-bis(phenylethynyl)anthracene in comparison to 9-(phenylethynyl)anthracene, which exhibited a gap of 3.29 eV, attributable to enhanced conjugation. Previous studies indicated that both functional groups DCV and PhE are essential for the photophysical properties of anthracene

derivatives. In contrast, the structural integration of DCV and PhE, and *ortho*-positional Isomeric structures of anthracenes are poorly recognized in the literature.
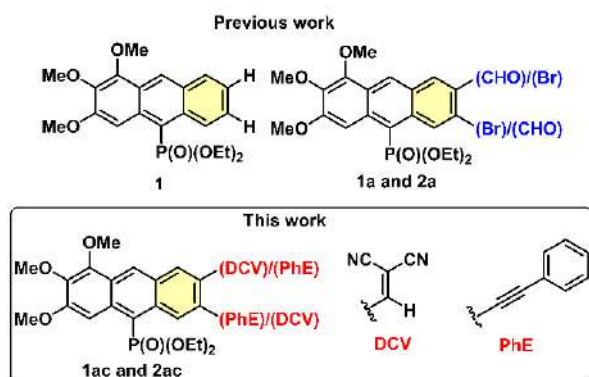

Figure 1. Background and structures of highly substituted anthracene based *ortho*-positional isomers.

In this work, we have synthesized three pair of *ortho*-positional isomers containing PhE and DCV units at 6 and 7 position of anthracene. Anthracenes **1ac** and **2ac**, each containing DCV and PhE moieties at the 6 or 7 positions, respectively, and incorporating a 10-diethylphosphonate ester moiety were synthesized from **1a** and **2a**. To understand the impact of individual functional groups, such as DCV and PhE at the peripheral rings of **1a** and **2a**, we have synthesized pairs of *ortho*-positional isomers containing only DCV (**1aa** and **2aa**) and only PhE (**1ab** and **2ab**) groups. This investigation extends our previous work wherein we have synthesized the anthracene **1,** unsubstituted at 6- and 7-positions as well as *ortho*-positional isomers **1a** and **2a** substituted with formyl or bromine at 6 or 7 positions, using a novel *phospho*-Friedel-Crafts-Bradsher cyclization (Figure 1).[28,29] Subsequently, a systematic study was conducted to assess the influence of the functionalization by DCV and PhE groups at the 6 and 7 positions of anthracene derivatives **1a** and **2a**.

3.5.2 Results and discussion

3.5.2.1 Synthesis
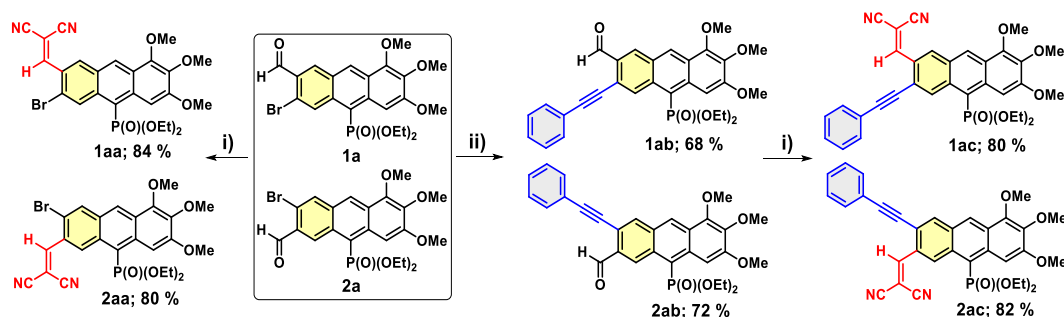
Scheme 1. Synthetic routes for *ortho*-positional Isomers **1aa, 2aa, 1ab, 2ab, 1ac** and **2ac**. Reaction conditions: (i) phenylacetylene (1.3 eq.), Pd(PPh$_3$)$_2$Cl$_2$ (0.05 eq.), CuI (0.1 eq.), Et$_3$N (3 eq.), THF, 80 °C, 48h. (ii) malononitrile (1.2 eq.), piperidine (0.2 eq.), AcOH (1 eq.), benzene, 80 °C, 17h.

Scheme 1, illustrates the synthesis of functionalized *ortho*-positional isomers **1aa-ac** and **2aa-ac.** Characterization data are given in Figure S1-S18, Experimental Section-III. The starting substrates **1a** and **2a** were synthesized according to the following literature,[29] using a three-step procedure and a novel *phospho*-Friedel-Crafts-Bradsher cyclization. Compounds **1aa** and **2aa** were prepared from the starting material **1a** and **2a** using the Knoevenagel condensation with malononitrile. Compounds **1ac** and **2ac** were synthesized utilizing the Sonogashira cross-coupling reaction between substrates **1a**/**2a** and phenylacetylene to give **1ab**/**2ab**, which subsequently underwent the Knoevenagel condensation leading to the synthesis of **1ac**/**2ac**. The *ortho*-positional isomers crystallized as yellow solids (**1ab**/**2ab**) and red solids (**1aa**, **1ac**, **2aa**, **2ac**), all of which exhibited solubility in common organic solvents.
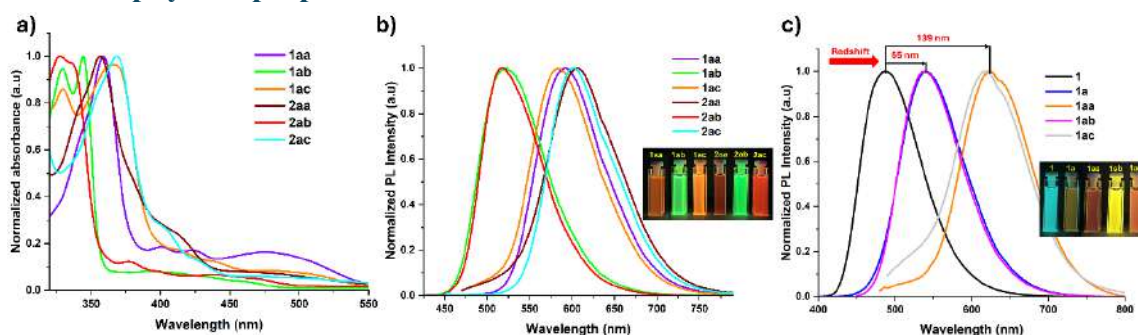
3.5.2.2 Photophysical properties

Figure 2. (a) Normalized absorbance, (b) normalized emission of **1aa-ac** and **2aa-ac** (10^{-5} mol/L, toluene)**,** (c) normalized emission of **1**, **1a**, and **1aa-ac** (10^{-5} mol/L, DCM).

Table 1. Photophysical properties of compounds 1a-c and 2a-c in different solvents.											
	Toluene				**DCM**				**MeOH**		
Nr.	**Abs.[a]** $\lambda_{max.}$ **(nm)**	**PL[b]** $\lambda_{max.}$ **(nm)**	**υ[c]** **(cm^{-1})**	**QY[d]** **(%)**	**Abs.[a]** $\lambda_{max.}$ **(nm)**	**PL[b]** $\lambda_{max.}$ **(nm)**	**υ[c]** **(cm^{-1})**	**QY[d]** **(%)**	**Abs.[a]** $\lambda_{max.}$ **(nm)**	**PL[b]** $\lambda_{max.}$ **(nm)**	**υ[c]** **(cm^{-1})**	**QY[d]** **(%)**
1aa	483	591	3783	15.13	486	625	4576	15.98	463	520	2367	7.07
1ab	462	522	2487	59.11	463	539	3045	66.43	435	519	3720	30.92
1ac	503	585	2786	42.54	503	618	3699	16.98	490	523	1287	4.92
2aa	481	607	4315	9.66	482	619	4592	17.35	472	520	1956	1.45
2ab	470	519	2009	56.80	467	538	2825	61.25	434	510	3433	34.80
2ac	493	601	3645	25.09	498	627	4131	5.14	490	515	990	9.90

[a] Abs. ($\lambda_{max.}$) - absorption maximum; [b] PL ($\lambda_{max.}$) - emission maximum; [c] Stokes shift, (υ) = $1/\lambda_{abs}$-$1/\lambda_{em}$; [d] the absolute photoluminescence quantum yield (QY).

UV-Vis and PL measurements: Absorption (UV-Vis) and photoluminescence (PL) spectra, as well as photoluminescence quantum yields (QY) of **1aa-1ac** and **2aa-ac**, were recorded in DCM, toluene and methanol solutions (Table 1). In toluene, compounds **1a-c** and **2a-c** exhibited high-

intensity absorption peaks within the 300-375 nm wavelength region, with one or more peaks of lower intensity in the 375-480 nm wavelength region (Figure 2a). The absorption band in the lower wavelength range was attributed to the $S_0 \rightarrow S_1$ transition, however the absorption bands at higher wavelengths were assigned to the $\pi \rightarrow \pi^*$ transitions, known for many anthracene derivatives.[30,31] The observed broad peaks in the higher wavelength region derive from intramolecular charge transfer (ICT) between the anthracene and DCV moieties, a phenomenon also evidenced in the 9-DCV substituted anthracene derivative.[19,32] Furthermore, these peaks are clearly absent in **1ab** and **2ab**, which do not contain the DCV moiety (Figure 2a). Compounds **1aa-ac** and **2aa-ac** exhibit photoluminescence, from yellow (**1ab** and **2ab**) to red (**1aa**, **1ac**, **2aa**, and **2ac**) within the wavelength range of 519-607 nm in the toluene solution (Figure 2b).

In toluene, compounds **1aa-ac** and **2aa-ac** exhibit higher absorption wavelengths compared to **1a** (433 nm) and **2a** (438 nm) (Figure 2a). As expected, compounds **1ac** (503 nm) and **2ac** (493 nm) exhibit higher absorption, which may be attributed to the most extensive conjugation arising from the presence of DCV and PhE moieties. A similar trend was observed in the emission wavelengths of **1ac** (585 nm) and **2ac** (601 nm), both of which exhibit emissions at higher wavelengths compared to **1a** (522 nm) and **2a** (524 nm) (Figure 2a). In contrast, the introduction of the PhE group did not exhibit any redshift in the emission wavelengths of compounds **1ab** and **2ab**. Specifically, the compound **1ab** emitted at 522 nm, equivalent to **1a**, while the compound **2ab** emitted at 519 nm, which was even lower than for **2a**. The same pattern was observed for compounds **1ab** and **2ab** across the three solvents investigated (Table 1).

In order to fully understand the impact of DCV and PhE functionalization at the 6 and 7 positions of *ortho*-positional isomers **1a** and **2a**, we have compared the absorbance and emission spectra of anthracenes **1**, **1a**, and **1aa-ac** in the DCM solution. All these anthracene derivatives exhibited lower wavelengths which were characteristic bands attributed to the $S_0 \rightarrow S_1$ transition (Figure S21, ES-III). The compound **1a**, which was substituted with 6-Br and 7-CHO, exhibited a high-intensity redshifted band at 433 nm, in comparison to the 6,7-unsubstituted anthracene **1**, which exhibited an absorbance band at 396 nm. In contrast, anthracenes **1aa-ac** exhibited a low-intensity charge transfer bands in a higher wavelength region compared to **1** and **1a** with the 6-PhE and 7-DCV substituted anthracene **1ac** which showed the highest wavelength at 503 nm (Figure S21, ES-III).

Additionally, anthracenes **1aa-ac** emitted light ranging from yellow to deep red in the DCM solution (Figure 2c). All the 6,7-functionalized **1a**, **1aa-ac** and **2aa-ac** anthracene derivatives showed a redshift compared to the 6,7-unsubstituted anthracene derivative **1**, which emitted blue light at 486 nm. Compounds **1a** and **1ab** emitted yellow light at nearly identical wavelengths of 540 nm and exhibited a redshift of approximately 55 nm in comparison to **1**. Interestingly, anthracene derivatives **1aa** and **1ac**, substituted with the DCV moiety, emitted red light at the highest wavelengths of 625 nm and 618 nm, with **1aa** exhibiting a significant redshift of 139 nm compared to **1** and 84 nm compared to **1a** (Figure 2c).

Compounds **1aa-ac** and **2aa-ac** showed almost similar absorption wavelengths in the DCM solution in the range of 463-503 nm and in the toluene solution (Figure S19a, ES-III). However, **1aa-ac** and **2aa-ac** showed lower absorption wavelengths in the methanol solution in the range of 434-490 nm compared to the toluene and DCM solutions (Figure S20a, ES-III). The similar pattern for their absorbance wavelength in methanol solution was observed for the anthracenes **1a** and **2a**.[29] Compounds **1aa-ac** and **2aa-ac** showed highest emission wavelengths in DCM solution in the range from 538 (**2b**) to 627 (**2c**) nm (Figure S19b, ES-III), and the lowest emission wavelengths in the methanol solution in the range from 510 (**2ab**) to 523 (**1ac**) nm (Figure S20b, ES-III).

QY measurements : Compounds **1a-c** and **2a-c** exhibited significant fluorescence quantum yields in DCM and toluene solutions upto 66.43 %, with the exception of methanol, where the compounds exhibited low quantum yields of 30.92 % (Table 1 and Figure S22, ES-III). Furthermore, the compounds with 6/7-DCV moiety exhibited lower quantum yields in comparison to those substituted with 6/7-PhE group **1ab** and **2ab**, as well as when compared to compounds **1a** (93.3 % in toluene) and **2a** (67.9 % in toluene).[29] The low fluorescence quantum yield observed in DCV substituted anthracenes is most likely a consequence of molecular twisting towards non-planar configurations, which facilitates intramolecular rotation and non-radiative relaxation of the excited state.[20,33] Additionally, the presence of heavy atom (bromine) and interaction with the solvent could be the reason for reduction in the quantum yield.[34]

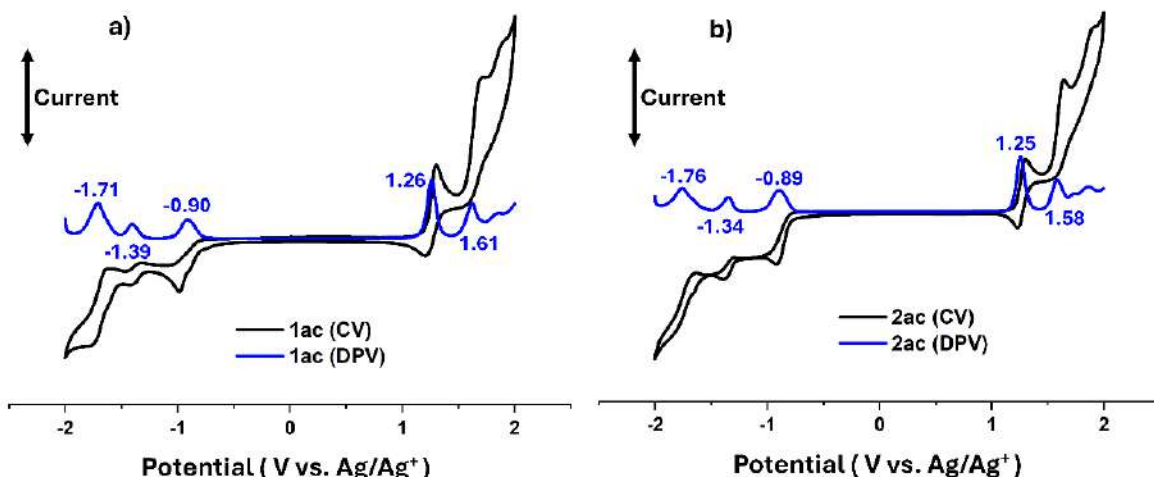### 3.5.2.3 Electrochemical properties

Figure 2. (a) cyclic voltammogram (black) and (b) differential pulse voltammogram (blue) spectra of **1ac** and **2ac**; measured in CH_2Cl_2 solution, 20 °C, 50 mV s^{-1}, glassy carbon working electrode.

The cyclic voltammetry (CV) and differential pulse voltammetry (DPV) were carried out in the DCM solution with $Bu_4N^+PF_6^-$ (0.1 molL^{-1}) as a supporting electrolyte to explore the redox behavior of isomers **1aa-ac** and **2aa-ac**. The oxidation and reduction potentials are given in the Figure S23-S24, Tabel S1, ES-III. Compounds **1aa-ac** and **2aa-ac** exhibited two oxidation potentials in a narrow range of 1.21-1.26 V and 1.53-1.61 V. Anthracene derivatives functionalized

with 6/7-PhE group **1ab**/**2ab** showed the oxidation potentials in a lower range of 1.21/1.23 V indicating the electron donating nature of these compounds compared to the compounds functionalized with 6/7-DCV moieties (**1aa**, **2aa**, **1ac**, and **2ac**) (Figure S24, ES-III).

Compounds substituted with the DCV moieties mostly exhibited the reduction potentials on more positive side, for example compounds **1ac** and **2ac** showed the first reduction value at -0.90 V and -0.89 V, respectively (Figure 3a and 3b) . However, compounds substituted with 6/7-PhE group, i.e. **1ab** (-0.95 V) and **2ab** (-0.98 V), as well as the parent compounds **1a** (-1.08 V) and **2a** (-0.93 V), exhibited reduction potentials that were more negative in comparison to **1ac** and **2ac**.[29] These results suggest that compounds substituted with 6/7-DCV groups at the outer rings significantly stabilized the energy levels (HOMO and LUMO) of the anthracene derivatives. The findings obtained through cyclic voltammetry are in agreement with the theoretical calculations performed using Density Functional Theory (DFT).
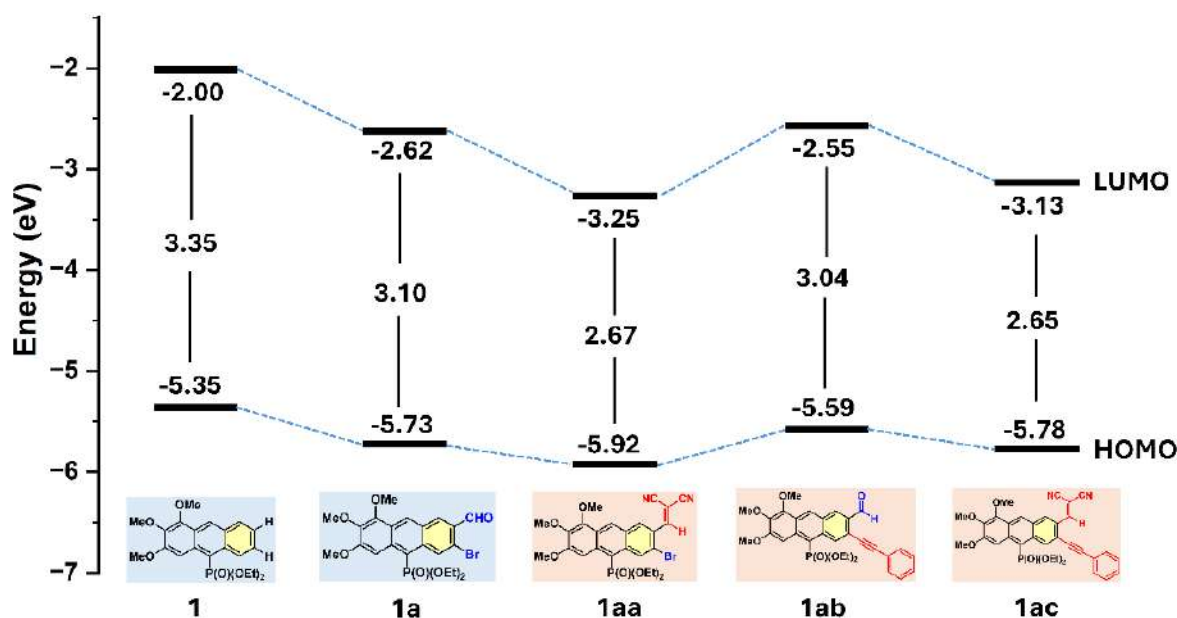
3.5.2.4 DFT calculations

Figure 3. Molecular orbitals calculated for *ortho*-positional isomers **1**, **1a**, and **1aa-ac** at DFT B3LYP/6-311++G(d,p).

The electronic structures of all functionalized anthracene derivatives **1aa-ac** and **2aa-ac** were optimized by DFT calculations and given in Table S2 and Figure S25, ES-III. The effect of functionalization on the HOMO and LUMO energy levels of compounds **1, 1a**, and **2a** as well as on the difference between the energy levels was observed depending on electron character of substituents (Figure 4). For example, anthracene derivatives **1ab** and **2ab** substituted with 6-PhE and 7-PhE group exhibited higher HOMO levels at -5.59 eV and -5.48 eV compared to its parent compounds **1a** and **2a** which exhibited the HOMO levels at -5.73 eV and -5.68 eV.[29] In contrast, anthracene derivatives substituted with the DCV moiety exhibited slightly lower HOMO levels,

with **1aa** showing the lowest value at -5.92 eV in comparison to parent compounds **1a** and **2a.** Additionally, both pairs **1a/2a** and **1aa-ac/2aa-ac** of *ortho*-positional isomers, substituted with different functional groups, exhibited lower HOMO levels compared to the 6 and 7-unsubstituted anthracene derivative **1,** which exhibited the HOMO level at -5.35 eV (Figure S25, ES-III).[28]

The LUMO energy levels exhibited more notable differences (Figure 4). Functionalization, especially with electron-withdrawing groups such as CHO and DCV, significantly lowered the LUMO energy and also reduced the band gaps. Likewise, as compared to **1,** which revealed the LUMO level at -2.00 eV, all functionalized *ortho*-positional isomers **1a/2a** and **1aa-ac/2aa-ac** showed lower LUMO levels. Compounds **1aa** and **2aa**, substituted with 7-DCV and 6-DCV groups, exhibited the lowest LUMO levels at -3.25 eV and -3.27 eV. Compounds **1ab** (3.04 eV) and **2ab** (2.93 eV) exhibited energy gap ΔEg levels that were mostly similar to those of compounds **1a** (3.11 eV) and **2a** (2.95 eV). All isomers functionalized with the DCV moieties, including **1aa** (2.67 eV), **1ac** (2.65 eV), and **2aa** (2.59 eV), exhibited lower energy gaps, with **2ac** (2.47 eV) possessing the lowest gap observed (Table S2, ES-III).

These findings suggested that the functionalization of *ortho*-positional isomers **1a** and **2a** is important for tuning the energy levels of these compounds. For example, substitution with the PhE group can elevate the position of HOMO and LUMO levels, while introducing the DCV group has the potential to lower the LUMO levels and to reduce the energy gap, due to its strong electron-withdrawing character.
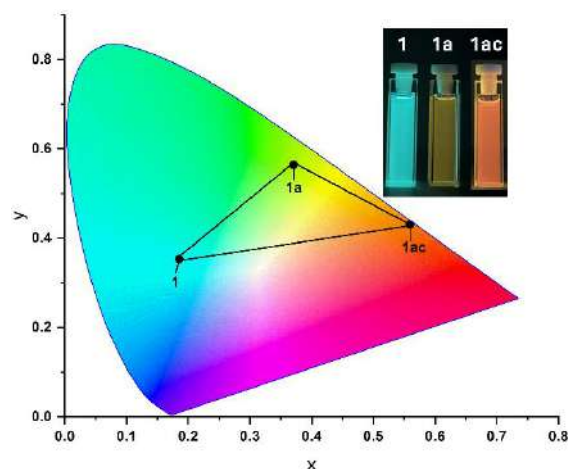
3.5.2.5 CIE studies

Figure 5. Commission Internationale de L'Eclairage (CIE) 1931 chromaticity coordinates for **1**, **1a**, and **1ac** in DCM solution.

Anthracene derivatives **1aa-ac** and **2aa-ac** emitted green to deep red light in the 538-627 nm range in DCM solution. The functionalization of compounds **1** and **1a**, with the DCV moiety, significantly influenced their photoluminescent properties. For example, the 6,7-unsubstituted

anthracene **1** emitter exhibited blue luminescence, whereas the 6-Br and 7-CHO substituted anthracene **1a** displayed yellow luminescence, and the **1ac** with 6-PhE and 7-DCV substitutions emitted red luminescence. The luminescence properties of *ortho*-positional isomers **1aa-ac** and **2aa-ac** also depended upon the polarity of solvents. Interestingly, the positional isomers **1aa**, **1ac**, **2aa**, and **2ac**, which were functionalized with the DCV moiety, emitted green light in polar solvents, such as methanol, whereas they emitted orange to deep red emission in less polar solvents, such as toluene and DCM. The CIE 1931 color space chromaticity coordinates [35] of **1aa-1ac** and **2aa-ac** in DCM, toluene, and MeOH are provided in Figure S44 and Table S13 (ES-III).

3.5.3 Conclusions

In summary, we have successfully synthesized three pairs of novel anthracene-based *ortho*-positional isomers functionalized with phenylethynyl (PhE) and dicyanovinyl (DCV) groups, also substituted with a 10-diethylphosphonate ester moiety. Detailed photophysical, electrochemical, and computational studies revealed that these functional groups can tune the optical and electronic properties of the anthracene core. The DCV substitution significantly decreased the HOMO-LUMO energy gaps, while the PhE functionalization resulted in higher fluorescence quantum yields and increased HOMO energy levels due to extended conjugation. These findings emphasize the strategic importance of ortho-functionalization in fine-tuning the optoelectronic features of anthracenes, with promising applications in OLEDs and sensors.

3.5.4 References

1.   J. Huang, J. H. Su, H. Tian, *J. Mater. Chem*., **2012**, *22*, 10977.

2.   N. Sharma, A. Michael, Y. Wong, D. Hall, E. Spuling, F. Tenopala-Carmona, A. Privitera, G. Copley, D. B. Cordes, A. M. Z. Slawin, C. Murawski, M. C. Gather, D. Beljonne, Y. Olivier, I. D. W. Samuel, E. Zysman-Colman, *J. Mater. Chem. C*, **2020**, *8*, 3773-3783.

3.   Y. Wang, W. Liu, S. Ye, Q. Zhang, Y. Duan, R. Guo, L. Wang, *J. Mater. Chem. C,* **2020***, 8,* 9678-9687.

4.   P. Ludwig, J. Mayer, L. Ahrens, F. Rominger, G. Ligorio, F. Hermerschmidt, E. J. W. List-Kratochvil, J. Freudenberg, U. H. F. Bunz, *Chem.Eur.J.* **2024***, 30,* e202303037.

5.   T. Noda, H. Sasabe, T. Owada, R. Sugiyama, A. Arai, K. Kumada, H. Tsuneyama, Y. Saito, J. Kido, *ChemPlusChem* **2022***, 87,* e202100517.

6.   J. S. Huh, Y. H. Ha, S. K. Kwon, Y. H. Kim, J. J. Kim, *ACS Appl. Mater. Interfaces,* **2020***, 12,*15422−15429.

7.   Z. Fei, D. R. Zhu, X. Yang, L. Meng, Q. Lu, W. H. Ang, R. Scopelliti, C. G. Hartinger, P. J. Dyson, *Chem. Eur. J.* **2010***, 16,* 6473–6481.

8.   P. Chinna Ayya Swamy, J. Shanmugapriya, S. Singaravadivel, G. Sivaraman, D. Chellappa, *ACS Omega,* **2018***, 3,* 12341-12348.

9. X. Liu, Z. Liu, Y. Li, Y. Wang, W. Zhang, *Org. Biomol. Chem.,* **2025***, 23,*1708-1713.

10. K. Duraimurugan, M. Harikrishnan, J. Madhavan, A. Siva, S. J. Lee, J. Theerthagiri, M. Y. Choi, *Environmental Research,* **2021***, 194*, 110741.

11. A. Olesund, V. Gray, J. Mårtensson, B. Albinsson, *J. Am. Chem. Soc.***2021***, 143*, 5745−5754.

12. C. H. Mulyadi, M. Uji, B. Parmar, K. Orihashi, N. Yanai, *Precis. Chem*. **2024**, *2*, 539-544.

13. K. Higashi, T. Okamoto, N. Iwaya, E. Sakuda, C. W. M. Kay, T. Ikoma, M. Higashi, Y. Kobori, *Angew. Chem. Int. Ed*. **2025**, e202503846.

14. S. Haid, A. Mishra, M. Weil, C. Uhrich, M. Pfeiffer, P. Bäuerle, *Adv. Funct. Mater*. **2012**, *22*, 4322-4333.

15. B. Zou, A. Liang, P. Ding, J. Yao, X. Zeng, H. Li, R. Ma, C. Li, W. Wu, D. Chen, M. Qammar, H. Yu, J. Yi, L. Guo, S. H. Pun, J. E. Halpert, G. Li, Z. Kan, H. Yan, *Angew. Chem. Int. Ed.* **2025**, *64*, e202415332.

16. S. Biswas, R. Manikandan, N. Shauloff, S. K. Bhaumik, R. Jelinek, *RSC Appl. Interfaces,* **2024**, *1*, 920-927.

17. S. Bhuin, S. Halder, S. K. Saha, M. Chakravarty, *RSC Adv*, **2021**, *11*, 1679-1693.

18. J. Orrego-Hernández, J. Portilla, *J. Org. Chem*. **2017**, *82*, 13376-13385.

19. S. Kotowicz, D. Sęk, S. Kula, A. Fabiańczyk, J. G. Małecki, P. Gnida, S. Maćkowski, M. Siwy, E. Schab-Balcerzak, *Dyes and Pigments*, **2020**, *180*, 108432.

20. B. Chen, Y. Ding, X. Li, W. Zhu, J. P. Hill, K. Ariga, Y. Xie, *Chem. Commun*., **2013**, *49*, 10136-10138.

21. N. Murayama, J. Hao Jorolan, M. Minoura, H. Nakano, T. Ikoma, Y. Matano, ChemPhotoChem, **2022**, *6*, e202200100.

22. M. Yoosuf, S. C. Pradhan, S. Soman, K. R. Gopidas, *Solar Energy*, **2019**, *188*, 55-65.

23. B. Angelov, A. Angelova, R. Ionov, *J. Phys. Chem. B*, **2000**, *104*, 9140-9148.

24. J. A. Hur, S. Y. Bae, K. H. Kim, T. W. Lee, M. J. Cho, D. H. Choi, *Org. Lett*, **2011**, *13*, 1948-1951.

25. W. Fudickar, T. Linker, *J. Am. Chem. Soc*. **2012**, *134*, 15071-15082.

26. F. Qiu, F. Qiu, Y. Dong, Y. Dong, J. Liu, Y. Sun, H. Geng, H. Zhang, D. Zhu, D. Zhu, X. Shi, X. Shi, J. Liu, J. Zhang, J. Zhang, S. Ai, L. Jiang, *J. Mater. Chem. C*, **2020**, *8*, 6006-6012.

27. W. Zhang, Q. Wang, X. Feng, L. Yang, Y. Wu, X. Wei, *Chem. Res. Chin. Univ*., **2017**, *33*(4), 603-610.

28. M. Koprowski, Ł. Knopik, E. Różycka-Sokołowska, B. Dudziński, V. Vivek, K. Owsianik, P. Bałczewski, *Angew. Chem. Int. Ed*. **2025**, e202508168.

29. V. Vivek, M. Koprowski, E. Różycka-Sokołowska, Ł. Knopik, B. Dudziński, K. Owsianik, P. Bałczewski, *Org Lett*. **2025** (submitted)

30. R. N. Jones, *Chem. Rev.* **1947**, *41*, 2, 353-371.

31. A. Kastrati, F. Oswald, A. Scalabre, K. M. Fromm, *Photochem*, **2023**, *3*, 227–273.

32. A. R. Katritzky, D.-W. Zhu and K. S. Schanze, *J. Phys. Chem.* **1991**, *95*, 5737-5742.

33. V. Gray, D. Dzebo, A. Lundin, J. Alborzpour, M. Abrahamsson, B. Albinsson and K. Moth-Poulsen, *J. Mater. Chem. C*, **2015**, *3*, 11111-11121.

34. J. R. Lakowicz, **2006**, *Principles of Fluorescence Spectroscopy Third Edition*.

35. "The C.I.E. colorimetric standards and their use". T. Smith, J Guild, Trans. Opt. Soc. 1931, 33, 73- 134. The Measurement of Colour, W. D. Wright, 1969, Van Nostrand Reinhold Company. Commission Internationale de L'éclairage (CIE), Colorimetry, Publication Report No. 15.2, 1986.

3.6 Summary

My doctoral dissertation has focused on the design and synthesis of novel donor-acceptor fluorophores, belonging to the group of polycyclic aromatic and heteroaromatic hydrocarbons, with tailored optoelectronic properties. The main feature of the fluorophores, so far unknown, is a multiply substitution by electronically diverse functional groups and phosphorus P^{III} and P^{IV} moieties, usually critical for these properties. Through my doctoral studies, I have also developed new synthetic methodologies and structure-property insights that advance the field of organic electronic materials. Key achievements include:

- **First one-pot, three-step synthesis of 10-(diphenylphosphoryl)anthracenes** through the C–O–P to C–P(=O) rearrangement coupled with the *phospho*-Friedel–Crafts–Bradsher (F–C–B) cyclization. The new fluorophores featured a rare multi-substitution on flanking rings with a variety of donor−acceptor groups (F, Br, CN, CF_3, MeO, OCH_2O) and provided outstanding photoluminescence quantum yields up to 95% in solution and tunable emission. Two phenomena were observed for this group of compounds in the solid state: aggregation-caused quenching (ACQ) and aggregation-induced emission (AIE), the latter being responsible for very high emissions in the solid state >95 %. This research, was published in *J. Org. Chem. 2025*.

- **Post-synthetic functionalization at the 7-position of the 7-bromoanthracene derivative with donor-acceptor phenylethynyl linkages**, showing solvent-dependent twisted intramolecular charge transfer (TICT) behavior in compounds substituted with dimethylamino or dicyanovinyl groups. These findings (manuscript in preparation) highlight the potential of peripheral ring substitution in tuning the optoelectronic properties of anthracene-based materials.

- **First synthesis of *ortho*-positional isomers of anthracene and carbazole derivatives with phosphonate esters at the central position,** enabling precise control over HOMO–LUMO energy levels and again showing outstanding quantum yields up to 93% in solution. These findings (under review in *Org. Lett.*) demonstrate how small topological changes profoundly influence optical and redox behavior.

- **Post-synthetic functionalization of Br and CHO groups in 6/7-*ortho*-positional anthracene isomers by phenylethynyl (PhE) and dicyanovinyl (DCV) groups** to obtain more conjugated *ortho*-positional systems. Both functional groups effectively tune the optical and electronic properties of the anthracene core. The strong electron-withdrawing nature of the DCV substitution reduces the HOMO-LUMO energy gaps, while substitution with PhE increases fluorescence quantum yields and HOMO energy levels through extended conjugation. These findings (manuscript in preparation) highlight the strategic value of *ortho*-functionalization in fine-tuning the optoelectronic characteristics of anthracene-based emitters.

My research is unique in integrating phosphorus chemistry with acene functionalization strategies to achieve record breaking-high emission efficiencies and tunable optoelectronic properties. Among my main general achievements, I would like to mention the following:

- Introduction of P^{III} and P^{IV} phosphorus groups into multiply substituted acenes under mild, room temperature conditions.

- Establish a platform for systematically controlling emission properties through positional isomerism and charge-transfer tuning.

- Demonstration of how subtle structural modifications in acene systems translate into major functional advances in light-emitting materials.

- Achievement of quantum yields approaching unity both in solution and solid state in rationally designed multiply substituted anthracene derivatives.

Through rational synthetic design, my work bridges fundamental organic chemistry with applied materials science, providing new molecular tools for the next generation of organic electronic devices.

3.7 Experimental section-I for synthesis and optical properties of 10-(diphenylphosphoryl)-7-(phenylethynyl) anthracene derivatives

3.7.1 General information

Tetrahydrofuran and toluene were dried using Solvent Purification System (MBraun SPS-800). Glassware equipment was oven-dried and flushed with dry argon. For flash chromatography, Chromatography System – Büchi Pure C-850 FlashPrep was used. The melting points were measured with an Electrothermal Model IA9100 apparatus and were uncorrected. Mass spectra were obtained using a SYNAPT G2-Si HDMS (Waters) instrument. NMR spectra were recorded with a Bruker AV 200 MHz, Bruker AVANCE Neo 400 MHz or Bruker AVANCE III 500 MHz using $CDCl_3$, C_6D_6, CD_2Cl_2, CD_3CN, as internal standards. The UV-Vis absorption spectra were recorded in 1 cm cuvettes on a Shimadzu spectrophotometer UV-2700. Emission spectra were obtained with the Horiba Jobin Yvon, Fluoromax 4 Plus spectrofluorometer. The fluorescence quantum yields Φ of the obtained compounds were determined in four different solvents (toluene, CH_2Cl_2, MeCN, and MeOH) on excitation at their absorption maximum using an integrating sphere (Horiba, Jobin Yvon, Quanta-φ F-3029 Integrating sphere). Electrochemical characterization were conducted using a Metrohm Autolab PGSTAT128N potentiostat/galvanostat instrument.

Starting Materials: Phenylacetylene derivatives **2a-f** (except **2d)** and 9-(4-bromophenyl)-9*H*-carbazole **1d** were commercially available from Merck; the compound **1** was prepared according to the reported procedure.[1]

3.7.2 Synthesis and characterization

Synthesis of 2d: Following the modified literature procedure,[2] 9-(4-bromophenyl)-9*H*-carbazole (500 mg, 1.5 mmol), trimethylsilylacetylene (0.28 mL, 2.01 mmol), triethylamine (0.65 mL), and THF (5 mL) were added to a Schlenk flask, and the mixture was degassed for 10 min. Subsequently, $Pd(PPh_3)_2Cl_2$ (55 mg, 0.07 mmol) and CuI (30 mg, 0.15 mmol) were added to the mixture, and the sealed flask was heated for 16 h at 75 °C. The volatiles were then evaporated under reduced pressure, and a residue was extracted with CH_2Cl_2. The combined organic extracts were washed with saturated aqueous solution of NH_4Cl, dried over Na_2SO_4, and evaporated under reduced pressure to afford the Me_3Si-protected product, which was then stirred in DCM/MeOH with an excess amount of K_2CO_3 to give the product **2d** in quantitative yield which was used for the next Sonogashira reaction.
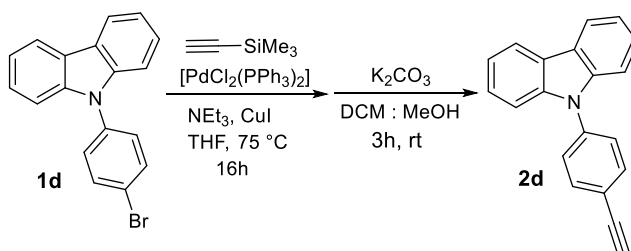

Scheme S1. Synthesis of the carbazole substrate **2d**.

51

Synthesis of 3a-f: Following the literature procedure,[3] a mixture of bromoanthracene (**1**) (1 eq.), phenylacetylene derivatives (**2-f**) (1.2 eq.), [Pd(PPh$_3$)$_2$Cl$_2$] (0.05 eq.) and CuI (0.1 eq.) was dissolved in THF under argon followed by addition of triethylamine (3 eq.) *via* syringe. The mixture was stirred for 48 h at 70 °C and left to cool to room temperature and for the precipitate to form. The resulting precipitate was collected by filtration and was successively washed with ethyl acetate and water. The product was then further purified by column chromatography with hexane-EtOAc to give **3a-f**.
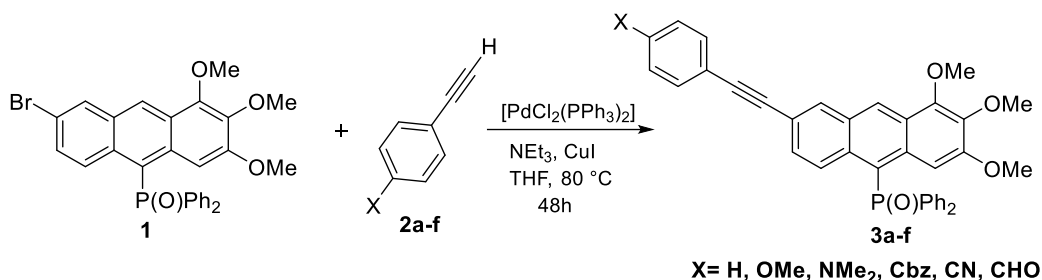
Scheme S2. Synthesis of the anthracene derivatives **3a-f**.

Synthesis of 3g: Following a modified literature procedure,[4] to a solution of the anthracene (**3f**) (200 mg, 1.0 eq.) in benzene (10 mL) were successively added malononitrile (1.1 eq.), piperidine (0.2 eq.), and AcOH (1.0 eq.) at room temperature and then the resulting mixture was heated at 80 °C for 17 h. Then, the crude product as concentrated in vacuo, and the residue was purified by column chromatography over silica gel eluting with hexane-EtOAc to give **3g**.
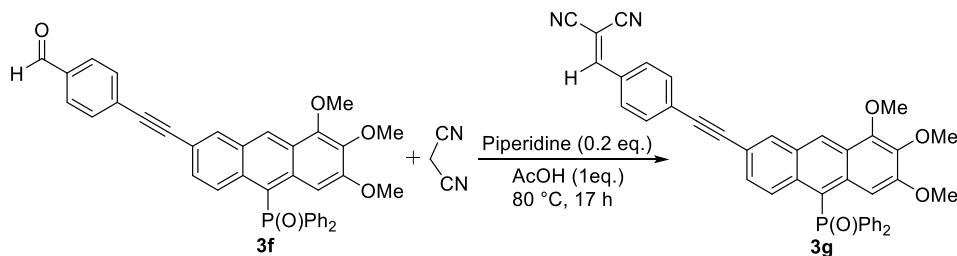
**Scheme S3.** Synthesis of the anthracene derivative **3g**.

Diphenyl(2,3,4-trimethoxy-6-(phenylethynyl)anthr-9-yl)phosphine oxide (3a):
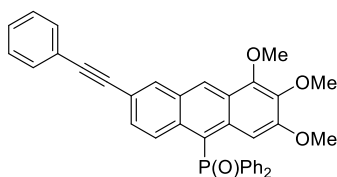
R$_f$ = 0.48 (EtOAc/hexane 2:1), Yellow solid, m.p. 201-203 °C, 80 % yield: **^{31}P NMR** (162 MHz, C$_6$D$_6$) δ 28.40; **^{1}H NMR** (400 MHz, C$_6$D$_6$) δ 8.99 (s, 1H), 8.81 (d, *J* = 9.3 Hz, 1H), 8.59 (s, 1H), 8.08 (d, *J* = 1.9 Hz, 1H), 7.83 (ddd, *J* = 12.0, 8.1, 1.5 Hz, 4H), 7.55 (dd, *J* = 7.9, 1.7 Hz, 2H), 7.26 (dd, *J* = 9.3, 1.9 Hz, 1H), 7.07 − 7.00 (m, 3H), 7.00 − 6.91 (m, 6H), 3.89 (s, 3H), 3.75 (s, 3H), 3.31(s, 3H); **^{13}C{^{1}H} NMR** (101 MHz, C$_6$D$_6$) δ 155.09 (s), 147.58 (s), 140.81 (s), 137.55 (d, *J$_{PC}$*

= 102.1 Hz), 135.12 (d, J_{PC} = 8.6 Hz), 134.51 (d, J_{PC} = 8.9 Hz), 133.66 (s), 133.99 (s), 131.89 (d, J_{PC} = 9.6 Hz), 131.28 (d, J_{PC} = 2.8 Hz), 130.16 (d, J_{PC} = 10.5 Hz), 128.92 (s), 128.80 (s), 128.71 (s), 128.55 (s), 128.52 (s), 125.87 (d, J_{PC} = 10.6 Hz), 124.00 (s), 120.18 (d, J_{PC} = 98.5 Hz), 119.44 (s), 103.02 (d, J_{PC} = 6.7 Hz), 91.16 (s), 90.34 (s), 61.33 (s), 60.84 (s), 55.53 (s); **HRMS** (TOF MS ES+): Calc. for $C_{37}H_{30}O_4P$ [M+H$^+$]: 569.1882; Found: 569.1870.

Diphenyl(2,3,4-trimethoxy-6-((4-methoxyphenyl)ethynyl)anthr-9-yl)phosphine oxide (3b):
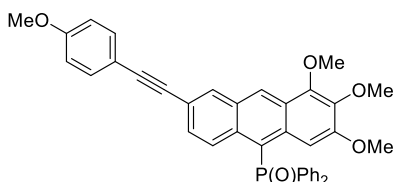
R_f = 0.50 (EtOAc/hexane 2:1), Yellow solid, m.p. 194-196 °C, 86 % yield: **^{31}P NMR** (162 MHz, C$_6$D$_6$) δ 28.50; **^{1}H NMR** (400 MHz, C$_6$D$_6$) δ 9.00 (s, 1H), 8.82 (d, J = 9.3 Hz, 1H), 8.58 (s, 1H), 8.13 (s, 1H), 7.86 – 7.80 (m, 4H), 7.52 – 7.50 (m, 2H), 7.31 (dd, J = 9.3, 1.8 Hz, 1H), 7.02 – 6.90 (m, 6H), 6.68 – 6.60 (m, 2H), 3.89 (s, 3H), 3.75 (s, 3H), 3.31 (s, 3H), 3.20 (s, 3H); **^{13}C{^{1}H} NMR** (101 MHz, C$_6$D$_6$) δ 160.24 (s), 154.99 (s), 147.58 (s), 140.79 (s), 137.55 (d, J_{PC} = 102.2 Hz), 135.01 (d, J_{PC} = 8.5 Hz),134.43 (d, J_{PC} = 8.8 Hz), 133.50 (s), 133.25 (s), 131.89 (d, J_{PC} = 9.8 Hz), 131.27 (d, J_{PC} = 2.8 Hz), 130.27 (d, J_{PC} = 10.7 Hz), 128.92 (s), 128.81 (s), 125.86 (d, J_{PC} = 10.7 Hz), 120.14 (d, J_{PC} = 98.7 Hz), 119.92 (s), 116.01 (s), 114.50 (s), 103.01 (d, J_{PC} = 6.7 Hz), 91.42 (s), 89.04 (s), 61.33 (s), 60.84 (s), 55.52 (s), 54.80 (s); **HRMS** (TOF MS ES+): Calc. for $C_{38}H_{32}O_5P$ [M+H$^+$]: 599.1987; Found: 599.1983.

(6-((4-(Dimethylamino)phenyl)ethynyl)-2,3,4-trimethoxyanthr-9-yl)diphenylphosphine oxide (3c):
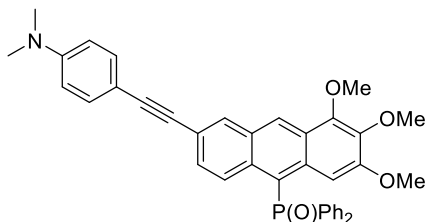
R_f = 0.48 (EtOAc/hexane 2:1), Yellow solid, m.p. 234-236 °C, 64 % yield: **^{31}P NMR** (162 MHz, C$_6$D$_6$) δ 28.53; **^{1}H NMR** (400 MHz, C$_6$D$_6$) δ 8.99 (s, 1H), 8.74 (d, J = 9.3 Hz, 1H), 8.66 (s, 1H), 8.15 (s, 1H), 7.88 – 7.77 (m, 4H), 7.65 – 7.60 (m, 2H), 7.34 (dd, J = 9.3, 1.9 Hz, 1H), 7.04 – 6.86 (m, 6H), 6.49 – 6.34 (m, 2H), 3.89 (s, 3H), 3.76 (s, 3H), 3.33 (s, 3H), 2.39 (s, 6H); **^{13}C{^{1}H} NMR** (101 MHz, C$_6$D$_6$) δ 154.87 (s), 150.39 (s), 147.58 (s), 140.81 (s), 137.64 (d, J_{PC} = 102.1 Hz), 135.00 (d, J_{PC} = 8.4 Hz), 134.24 (d, J_{PC} = 8.8 Hz), 133.24 (s), 132.76 (s), 131.91 (d, J_{PC} = 9.8 Hz), 131.21 (d, J_{PC} = 2.8 Hz), 130.43 (d, J_{PC} = 10.7 Hz), 129.02 (s), 128.83 (d, J_{PC} = 11.9 Hz), 128.55 (s), 125.86 (d, J_{PC} = 10.8 Hz), 120.61 (s), 120.03 (d, J_{PC} = 98.7 Hz), 112.32 (s), 110.96 (s), 103.06

(d, J_{PC} = 6.7 Hz), 92.97 (s), 88.50 (s), 61.32 (s), 60.84 (s), 55.52 (s), 39.67 (s); **HRMS** (TOF MS ES+): Calc. for $C_{39}H_{35}O_4PN$ [M+H$^+$]: 612.2304; Found: 612.2303.

(6-((4-(9*H*-Carbazol-9-yl)phenyl)ethynyl)-2,3,4-trimethoxyanthr-9-yl)diphenylphosphine oxide (3d):
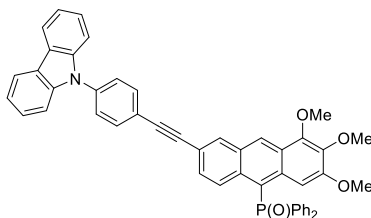
R_f = 0.56 (EtOAc/hexane 2:1), Yellow solid, m.p. 220-222 °C, 78 % yield: **^{31}P NMR** (162 MHz, CD$_2$Cl$_2$) δ 29.49; **^{1}H NMR** (400 MHz, CD$_2$Cl$_2$) δ 8.98 (s, 1H)J, 8.72 (d, *J* = 8.3 Hz, 1H), 8.33 (d, *J* = 2.0 Hz, 1H), 8.16 (dd, *J* = 7.7, 1.0 Hz, 2H), 7.82 (dd, *J* = 8.6, 1.8 Hz, 2H), 7.74 - 7.68 (m, 4H), 7.62 (dd, *J* = 8.4, 1.6 Hz, 2H), 7.57 - 7.54 (m, 2H), 7.53 (d, *J* = 1.5 Hz, 1H), 7.50 -7.48 (m, 4H), 7.47- 7.46 (m, 2H), 7.45 - 7.42 (m, 2H), 7.38 (dd, *J* = 9.3, 1.9 Hz, 1H), 7.31 (ddd, *J* = 8.0, 6.8, 1.3 Hz, 2H), 4.16 (s, 3H), 3.94 (s, 3H), 3.38 (s, 3H); **^{13}C {^{1}H} NMR** (101 MHz, CD$_2$Cl$_2$) δ 154.75 (s), 147.36 (s), 140.93 (s), 140.31 (s), 138.06 (s), 136.62 (d, J_{PC} = 102.8 Hz), 134.87 (d, J_{PC} = 8.5 Hz), 133.99 (d, J_{PC} = 8.8 Hz), 133.54 (s), 131.98 (d, J_{PC} = 2.9 Hz), 131.71 (d, J_{PC} = 9.9 Hz), 130.06 (d, J_{PC} = 10.7 Hz), 129.26 (d, J_{PC} = 12.0 Hz), 128.56 (d, J_{PC} = 3.4 Hz), 127.53 (d, J_{PC} = 6.8 Hz), 127.26 (s), 126.47 (s), 125.48 (d, J_{PC} = 10.7 Hz), 123.89 (s), 122.45 (s), 120.66 (s), 120.61 (s), 119.53 (d, J_{PC} = 99.4 Hz), 118.97 (s), 110.16 (s), 102.43 (d, J_{PC} = 7.6 Hz), 90.58 (s), 90.12 (s), 62.03 (s), 61.36 (s), 55.91 (s). **HRMS** (TOF MS ES+): Calc. for $C_{49}H_{37}O_4PN$ [M+H$^+$]: 734.2460; Found: 734.2433.

4-((10-(Diphenylphosphoryl)-6,7,8-trimethoxyanthr-2-yl)ethynyl)benzonitrile (3e):
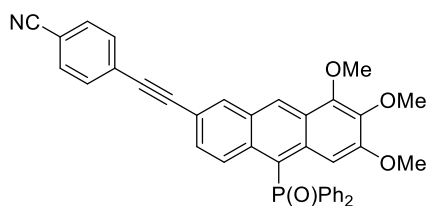
R_f = 0.50 (EtOAc/hexane 2:1), Yellow solid, m.p. 264-266 °C, 74 % yield: **^{31}P NMR** (162 MHz, C$_6$D$_6$) δ 28.33; **^{1}H NMR** (400 MHz, C$_6$D$_6$) δ 9.06 (s, 1H), 9.03 (d, *J* = 3.1 Hz, 1H), 8.39 (s, 1H), 8.07 (d, *J* = 1.9 Hz, 1H), 7.89 – 7.75 (m, 4H), 7.25 (dd, *J* = 9.2, 1.9 Hz, 1H), 7.06 – 7.01 (m, 2H), 7.00 – 6.91 (m, 6H), 6.85 – 6.80 (m, 2H), 3.90 (s, 3H), 3.74 (s, 3H), 3.24 (s, 3H); **^{13}C{^{1}H} NMR** (101 MHz, CD$_2$Cl$_2$) δ 154.87 (s), 147.33 (s), 140.29 (s), 136.47 (d, J_{PC} = 102.9 Hz), 135.03 (d, J_{PC} = 8.4 Hz), 134.10 (s), 134.07 (d, J_{PC} = 8.4 Hz), 132.52 (s), 132.42 (s), 131.99 (d, J_{PC} = 3.0 Hz), 131.66 (d, J_{PC} = 9.9 Hz), 129.87 (d, J_{PC} = 10.7 Hz), 129.25 (d, J_{PC} = 12.1 Hz), 128.74 (d, J_{PC} = 3.2 Hz), 128.34 (s), 128.27 (s), 127.60 (d, J_{PC} = 6.7 Hz), 125.46 (d, J_{PC} = 10.8 Hz), 119.55 (d, J_{PC} = 99.3 Hz), 118.85 (s), 118.15 (s), 111.92 (s), 102.38 (d, J_{PC} = 7.5 Hz), 93.93 (s), 89.11 (s), 62.00

(s), 61.34 (s), 55.89 (s); **HRMS** (TOF MS ES+): Calc. for $C_{38}H_{29}O_4PN$ [M+H⁺]: 594.1834; Found: 594.1817.

4-((10-(Diphenylphosphoryl)-6,7,8-trimethoxyanthr-2-yl)ethynyl)benzaldehyde (3f):
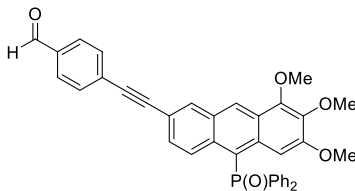

R_f = 0.42 (EtOAc/hexane 2:1), Yellow solid, m.p. 226-228 °C, 70 % yield: **³¹P NMR** (162 MHz, C_6D_6) δ 29.60; **¹H NMR** (400 MHz, CD_2Cl_2) δ 10.02 (s, 1H), 8.97 (s, 1H), 8.74 (d, J = 9.3 Hz, 1H), 8.32 (s, 1H), 7.93 – 7.85 (m, 2H), 7.76 – 7.66 (m, 6H), 7.57 – 7.49 (m, 3H), 7.45 (m, 4H), 7.36 (dd, J = 9.4, 1.9 Hz, 1H), 4.16 (s, 3H), 3.94 (s, 3H), 3.37 (s, 3H); **¹³C{¹H} NMR** (101 MHz, CD_2Cl_2) δ 191.67 (s), 154.86 (s), 147.36 (s), 140.30 (s), 136.51 (d, J_{PC} = 103.0 Hz), 135.99 (s), 135.00 (d, J_{PC} = 8.6 Hz), 134.07 (d, J_{PC} = 10.1 Hz), 134.02 (s), 132.48 (s), 132.00 (d, J_{PC} = 2.8 Hz), 131.68 (d, J_{PC} = 9.9 Hz), 129.93 (d, J_{PC} = 10.1 Hz) , 129.89 (s), 129.65 (s), 129.26 (d, J_{PC} = 12.1 Hz), 128.73 (d, J_{PC} = 3.1 Hz), 128.38 (s), 128.15 (s), 127.91 (s), 127.59 (d, J_{PC} = 6.7 Hz), 125.48 (d, J_{PC} = 10.8 Hz), 119.54 (d, J_{PC} = 99.6 Hz), 118.42 (s), 102.41 (d, J_{PC} = 7.5 Hz), 93.63 (s), 89.90 (s), 62.02 (s), 61.35 (s), 55.90 (s); **HRMS** (TOF MS ES+): Calc. for $C_{38}H_{30}O_5P$ [M+H⁺]: 597.1831; Found: 597.1846.

2-(4-((10-(Diphenylphosphoryl)-6,7,8-trimethoxyanthr-2-yl) ethynyl)benzylidene) malononitrile (3g):
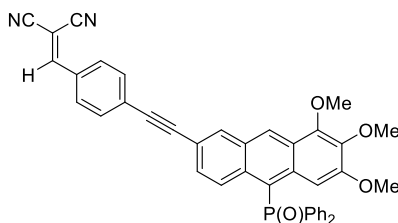
R_f = 0.50 (EtOAc/hexane 2:1), Yellow solid, m.p. 258-260 °C, 80 % yield: **³¹P NMR** (162 MHz, C_6D_6) δ 29.50; **¹H NMR** (400 MHz, CD_2Cl_2) δ 8.96 (s, 1H), 8.75 (d, J = 9.3 Hz, 1H), 8.32 (s, 1H), 7.92 (m, 2H), 7.80 (s, 1H), 7.73 – 7.65 (m, 6H), 7.54 (m, 2H), 7.49 – 7.41 (m, 5H), 7.34 (dd, J = 9.3, 1.8 Hz, 1H), 4.15 (s, 3H), 3.93 (s, 3H), 3.35 (s, 3H); **¹³C{¹H} NMR** (101 MHz, CD_2Cl_2) δ 159.12 (s), 154.93 (s), 147.36 (s), 140.30 (s), 136.49 (d, J_{PC} = 102.7 Hz), 135.08 (d, J_{PC} = 8.4 Hz), 134.31 (s), 134.10 (d, J_{PC} = 8.9 Hz), 132.74 (s), 132.00 (d, J_{PC} = 2.5 Hz), 131.67 (d, J_{PC} = 9.9 Hz), 131.11 (s), 130.84 (s), 129.93 (s), 129.88 (d, J_{PC} = 10.5 Hz), 129.26 (d, J_{PC} = 12.1 Hz), 128.81 (s), 128.28 (s), 127.63 (d, J_{PC} = 6.7 Hz), 125.48 (d, J_{PC} = 10.7 Hz), 119.61 (d, J_{PC} = 99.6 Hz), 118.15 (s), 114.27 (s), 113.14 (s), 102.41 (d, J_{PC} = 7.5 Hz), 95.15 (s), 89.87 (s), 83.03 (s), 62.02 (s), 61.35 (s), 55.90 (s); **HRMS** (TOF MS ES+): Calc. for $C_{41}H_{30}O_4PN_2$ [M+H⁺]: 645.1943; Found: 645.1940.

3.7.3 NMR spectra of anthracene derivatives
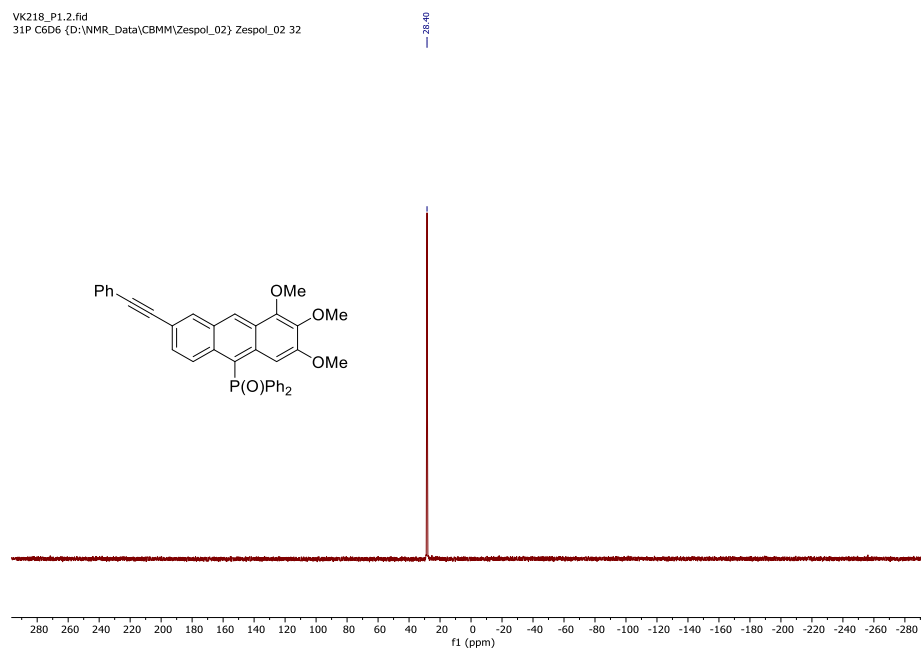
Figure S1. ^{31}P-NMR (162 MHz, C$_6$D$_6$) spectrum of **3a**.
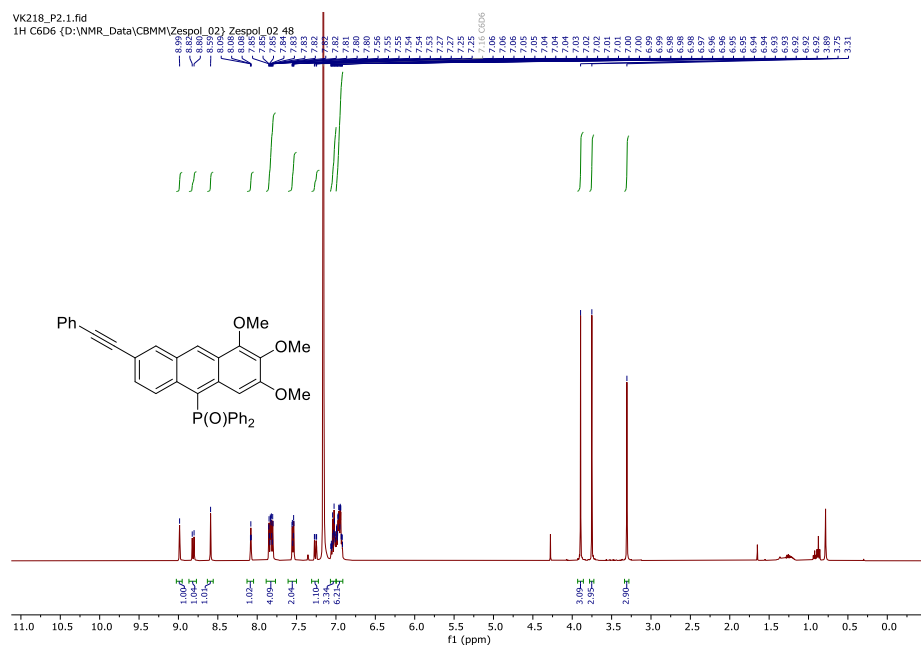
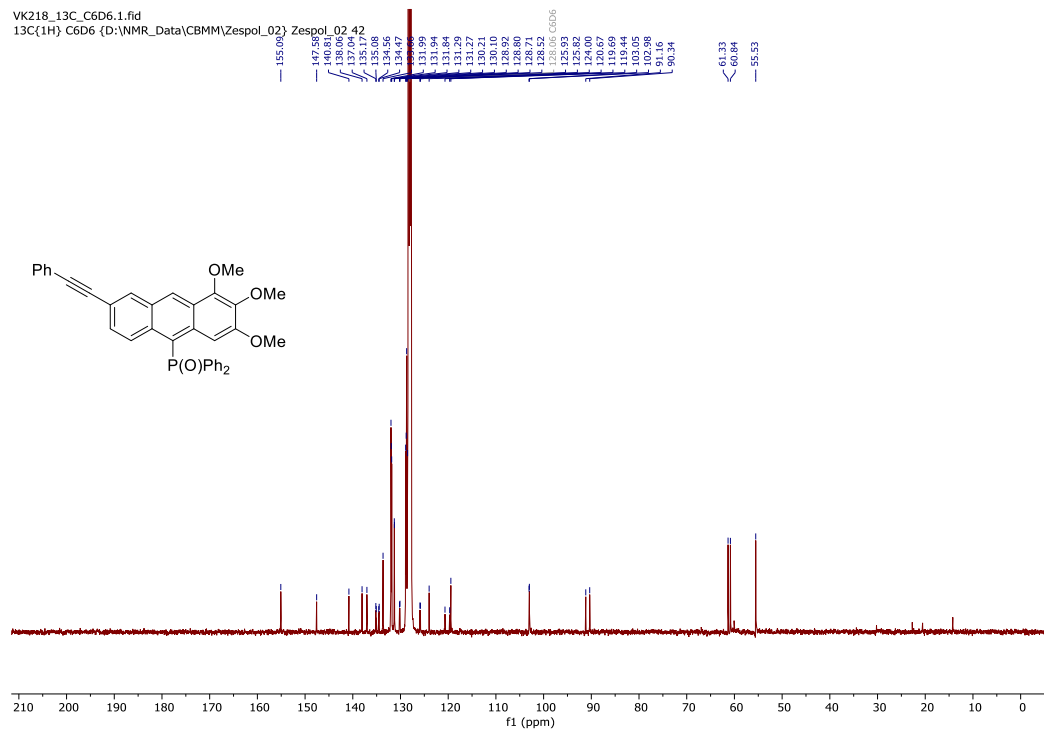**Figure S2**. ^{1}H-NMR (400 MHz, C$_6$D$_6$) spectrum of **3a**.

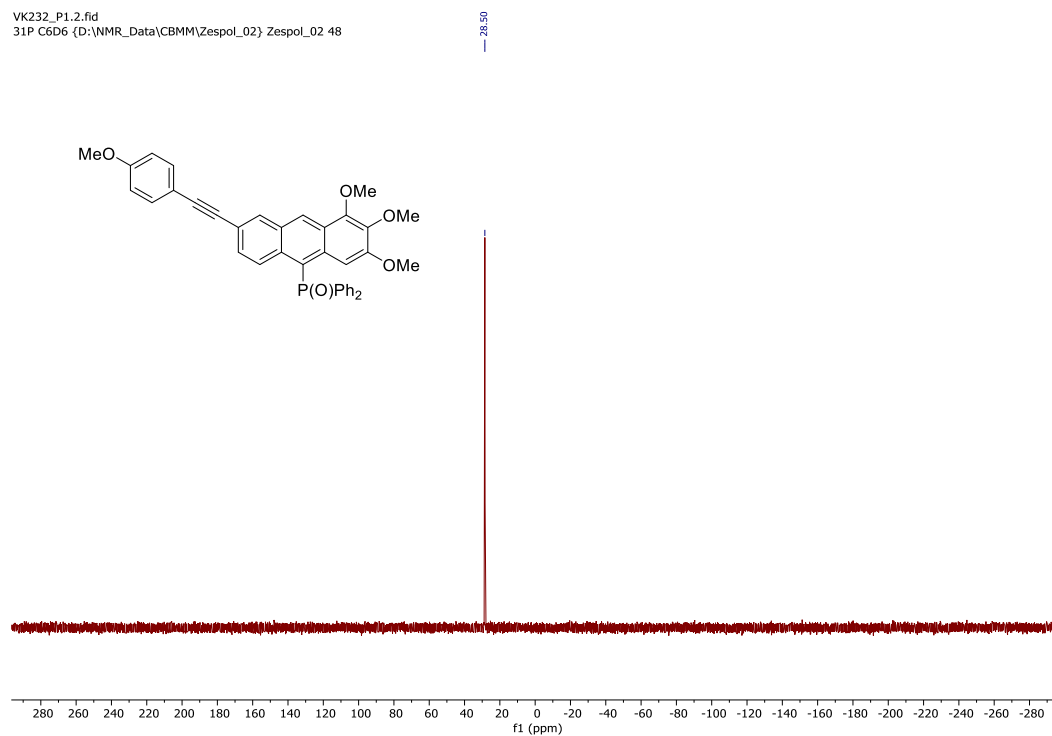**Figure S3**. $^{13}C\{^1H\}$-NMR (101 MHz, C_6D_6) spectrum of the compound **3a**.

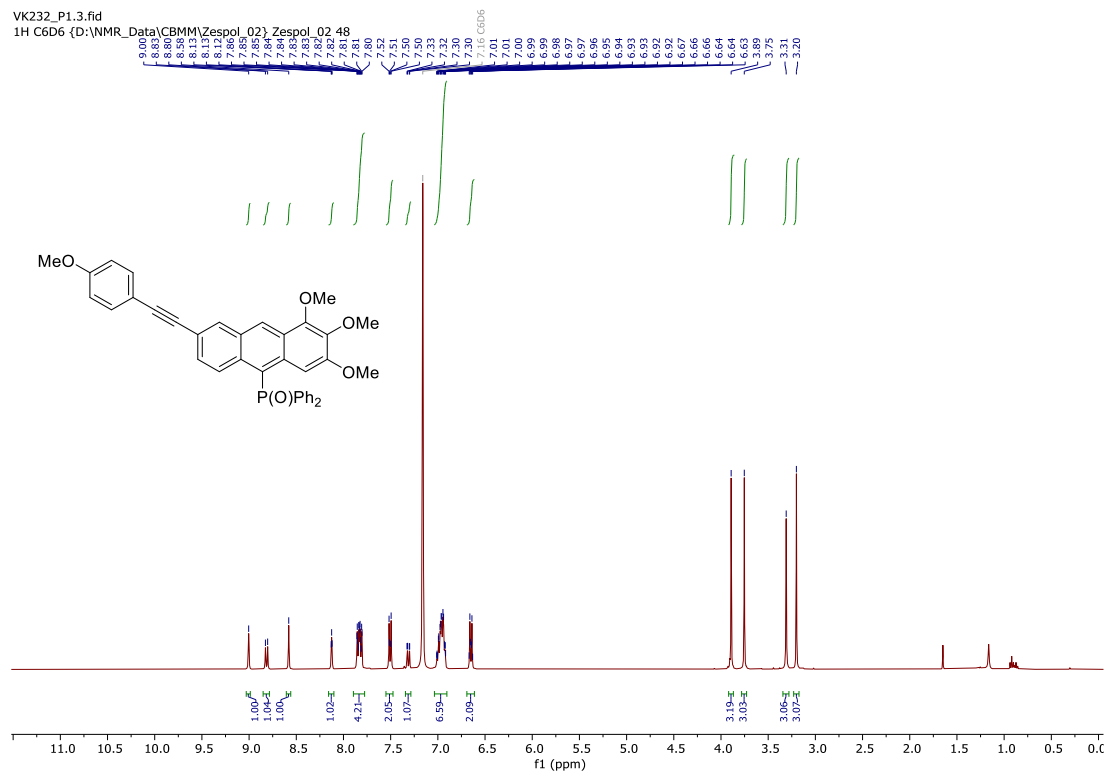**Figure S4**. ^{31}P-NMR (162 MHz, C_6D_6) spectrum of **3b**.

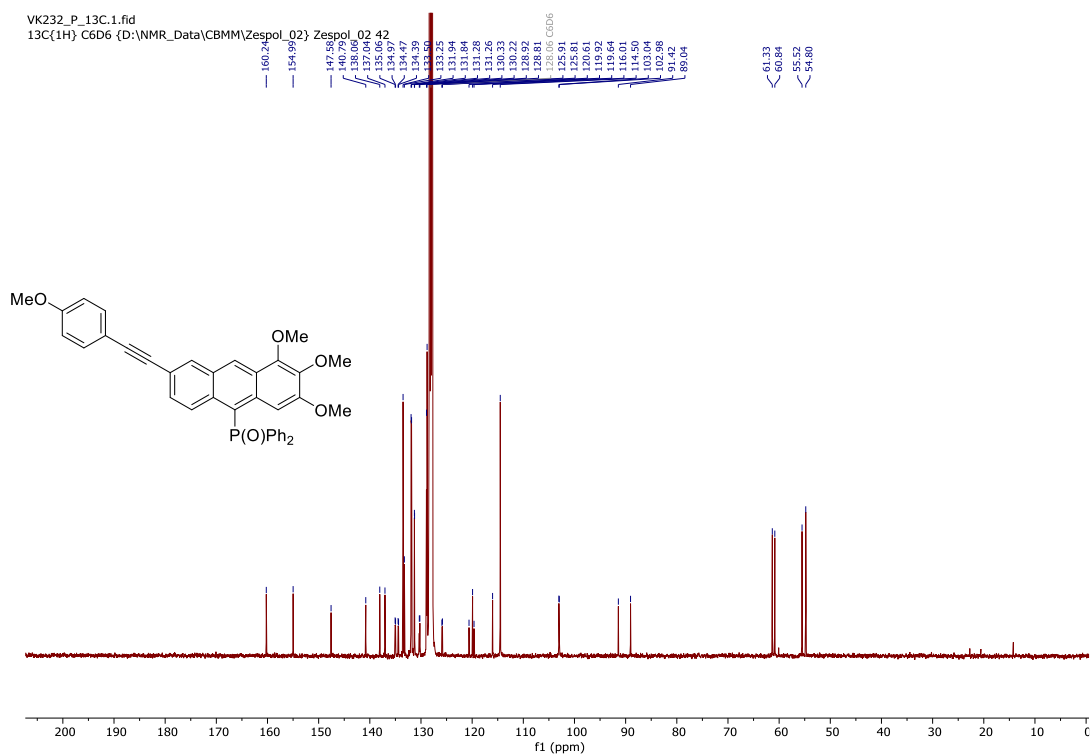**Figure S5**. ^{1}H-NMR (400 MHz, C$_6$D$_6$) spectrum of **3b**.

Figure S6. ^{13}C{^{1}H}-NMR (101 MHz, C$_6$D$_6$) spectrum of **3b**.

VK235R_P1.1.fid
31P{1H} C6D6 {D:\NMR_Data\CBMM\Zespol_02} Zespol_02 42

— 28.53

f1 (ppm)
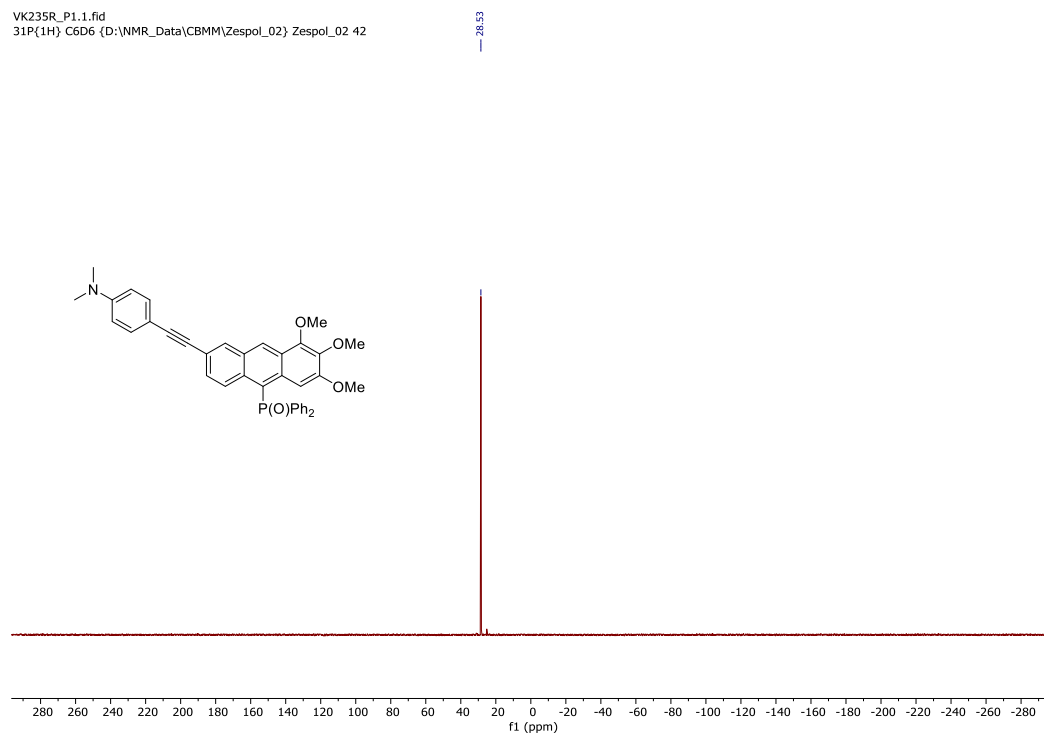
Figure S7. ^{31}P-NMR (162 MHz, C$_6$D$_6$) spectrum of **3c**.

VK235R_P1.3.fid
1H C6D6 {D:\NMR_Data\CBMM\Zespol_02} Zespol_02 42

f1 (ppm)
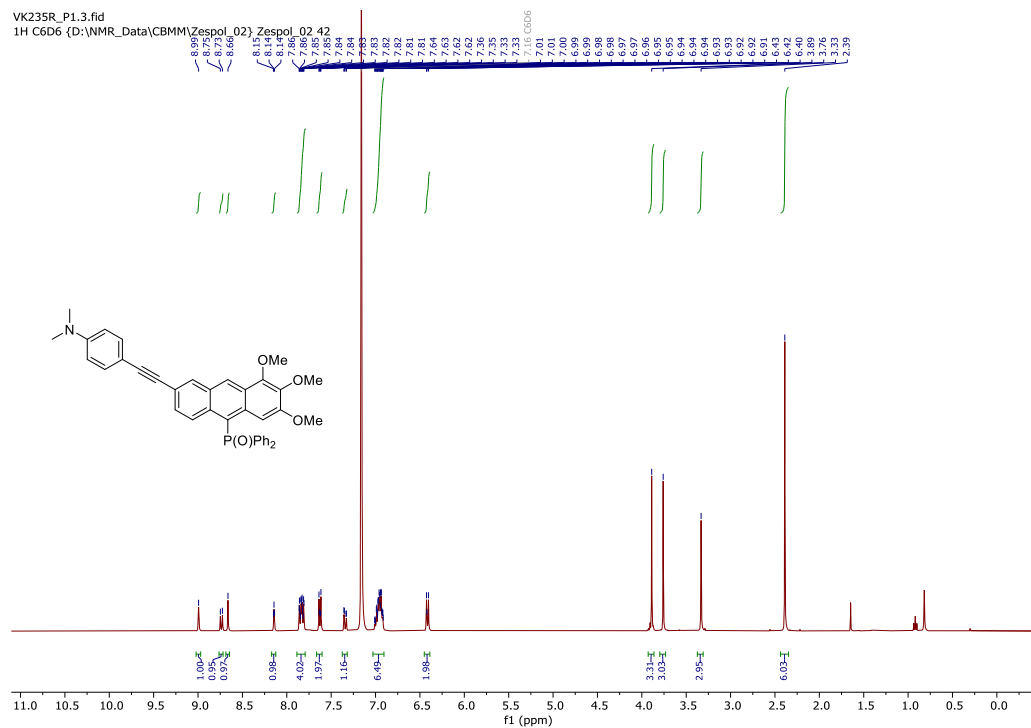
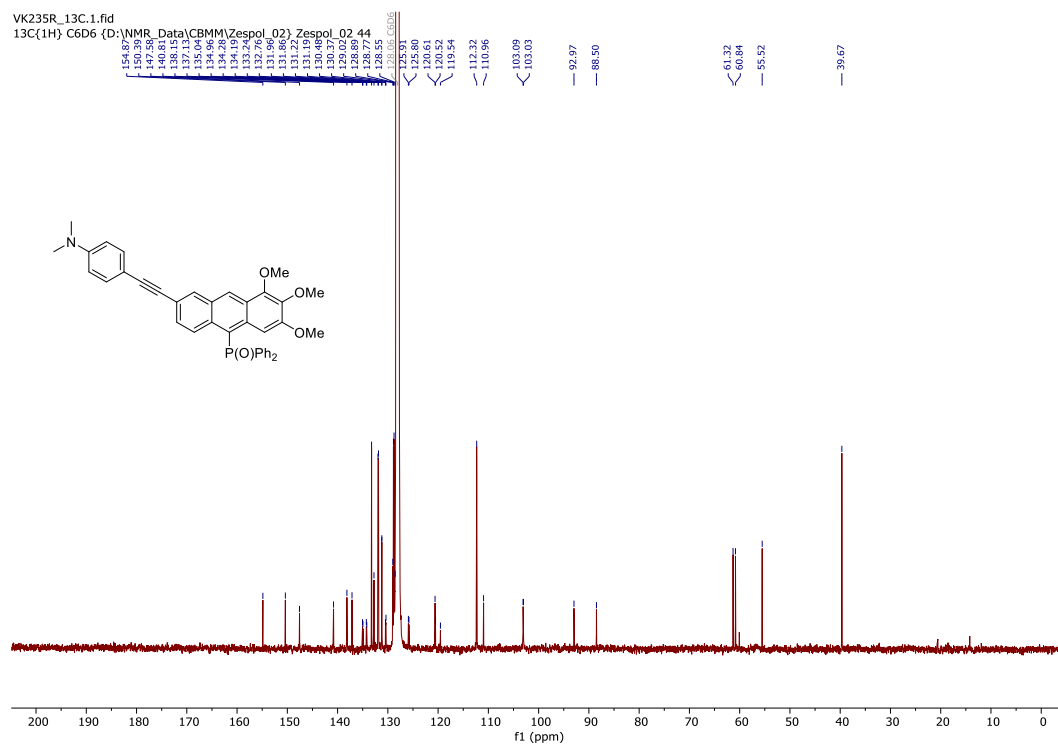**Figure S8**. ^{1}H-NMR (400 MHz, C$_6$D$_6$) spectrum of **3c**.

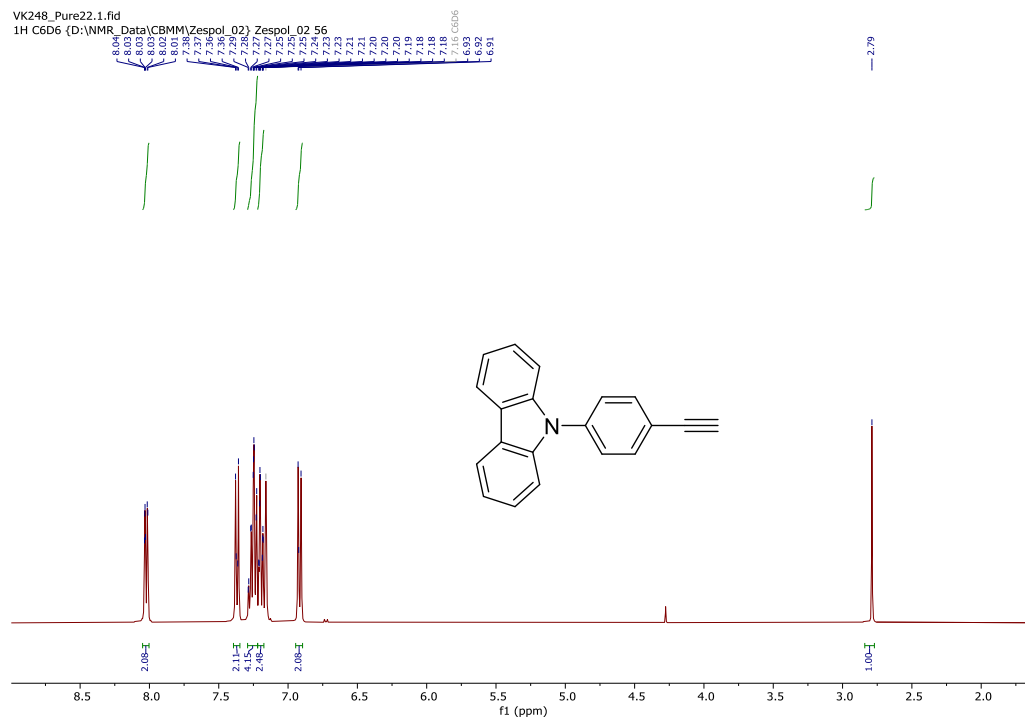**Figure S9**. $^{13}C\{^1H\}$-NMR (101 MHz, C_6D_6) spectrum of **3c**.

Figure S10. ^1H-NMR (400 MHz, C_6D_6) spectrum of **2d**.
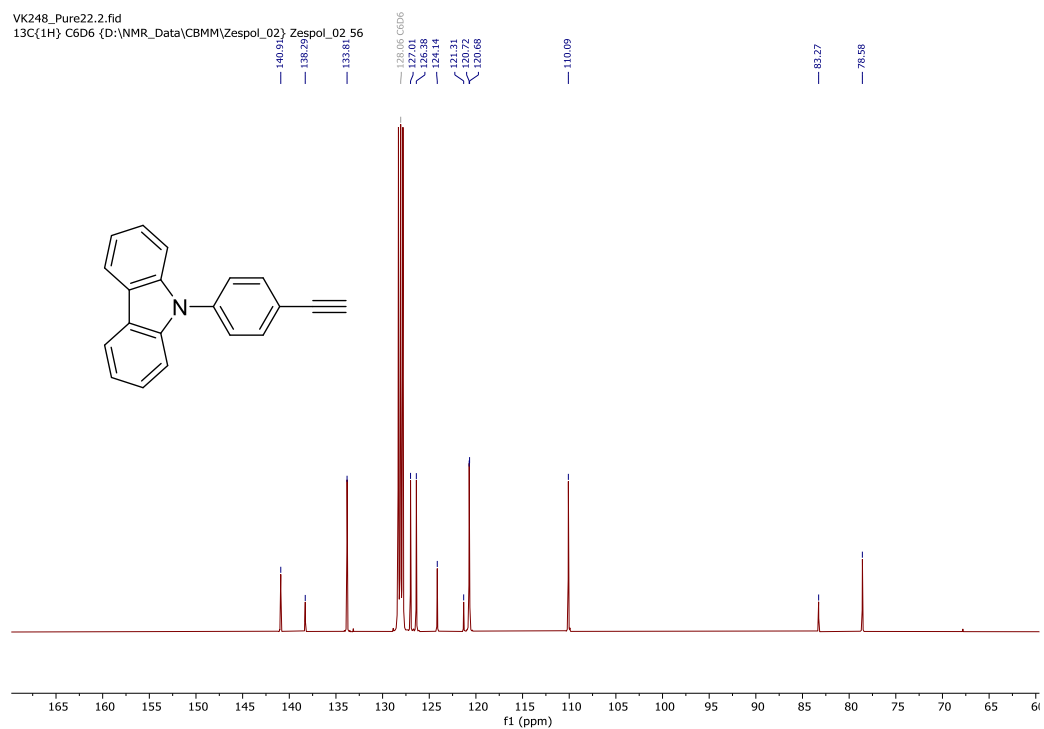
VK248_Pure22.2.fid
13C{1H} C6D6 {D:\NMR_Data\CBMM\Zespol_02} Zespol_02_56

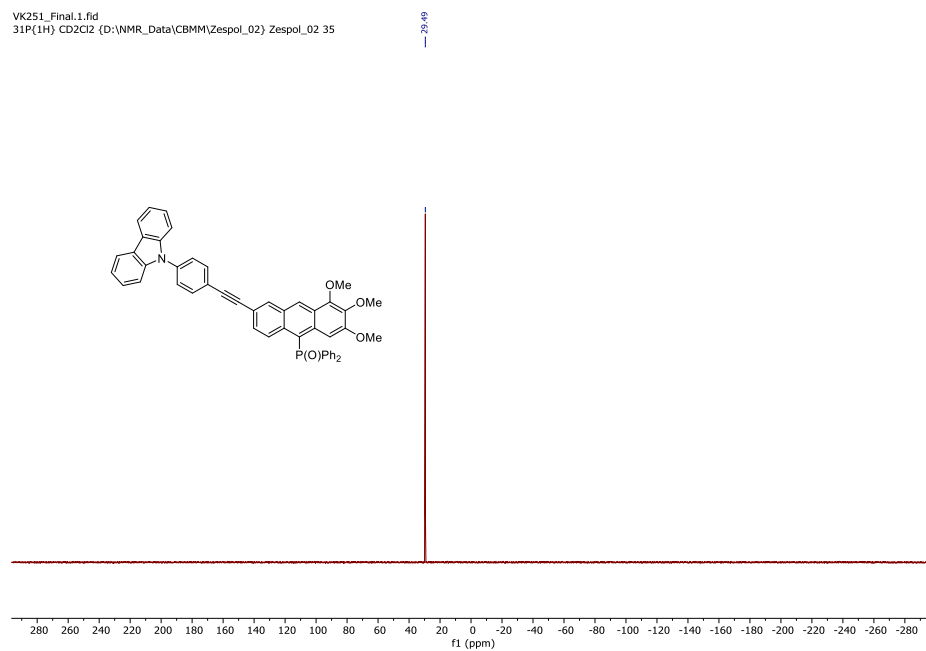**Figure S11**. $^{13}C\{^{1}H\}$-NMR (101 MHz, C_6D_6) spectrum of **2d**.

VK251_Final.1.fid
31P{1H} CD2Cl2 {D:\NMR_Data\CBMM\Zespol_02} Zespol_02 35

Figure S12. $^{31}P\{^{1}H\}$-NMR (162 MHz, C_6D_6) spectrum of **3d**.

Figure S13. ^{1}H-NMR (400 MHz, CD₂Cl₂) spectrum of **3d**.

Figure S14. ^{13}C{^{1}H}-NMR (101 MHz, CD₂Cl₂) spectrum of **3d**.

VK234_22.2.fid
31P{1H} C6D6 {D:\NMR_Data\CBMM\Zespol_02} Zespol_02 35

— 28.33
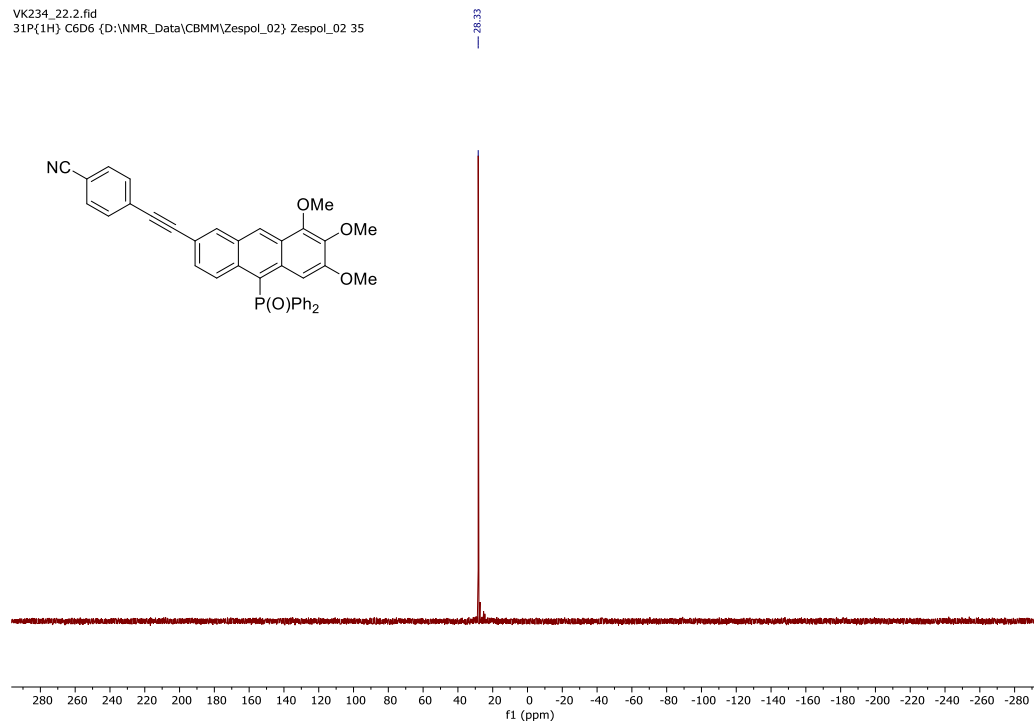
Figure S15. ^{31}P{^{1}H}-NMR (162 MHz, C$_6$D$_6$) spectrum of **3e**.

VK234_22.1.fid
1H C6D6 {D:\NMR_Data\CBMM\Zespol_02} Zespol_02 35
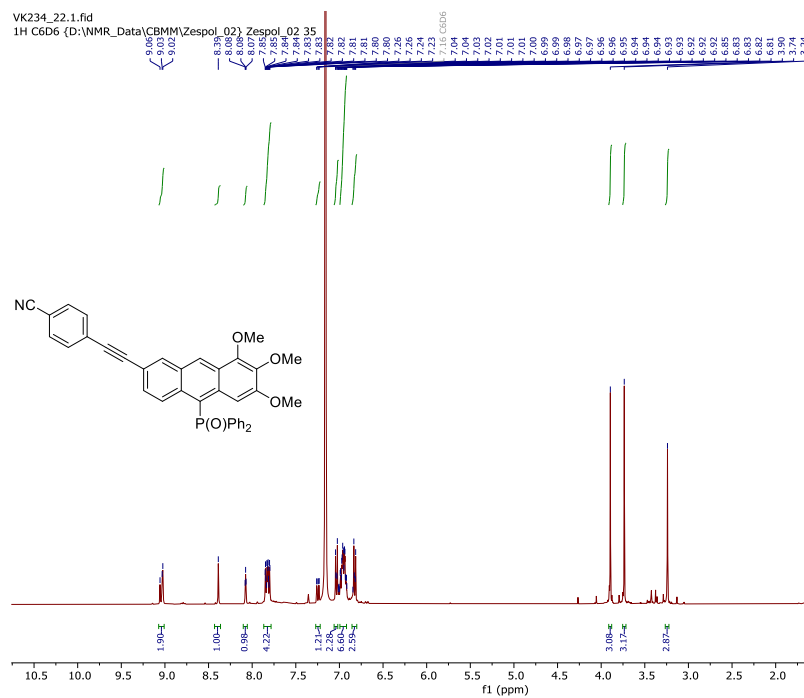
Figure S16. ^{1}H-NMR (400 MHz, C$_6$D$_6$) spectrum of **3e**.

VK234.5.fid
13C{1H} CD2Cl2 {D:\NMR_Data\CBMM\Zespol_02} Zespol_02 34
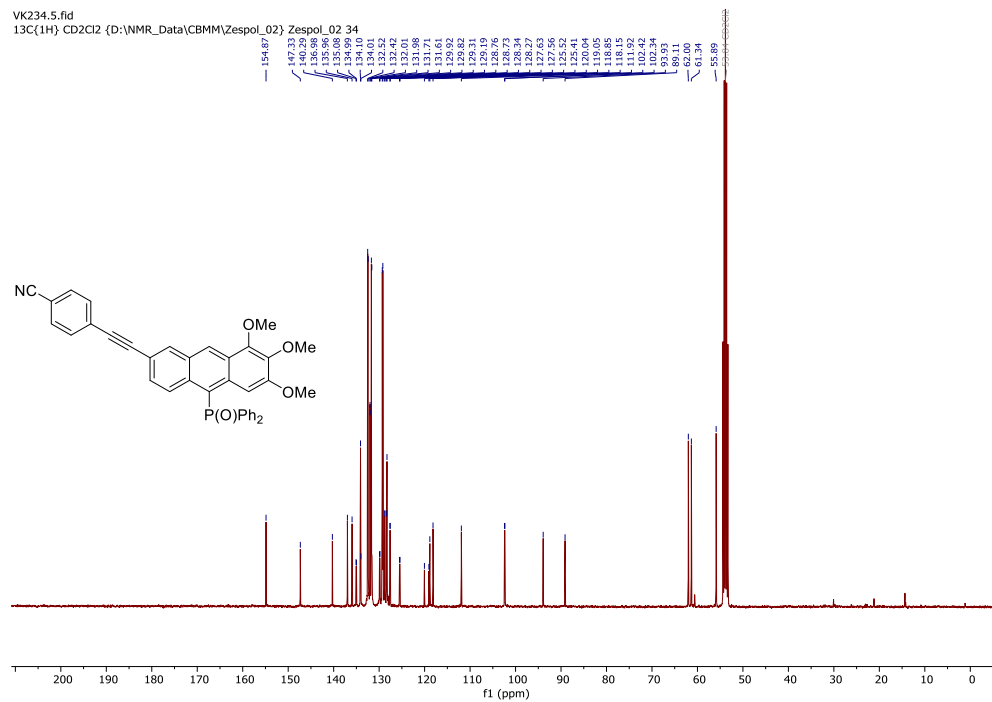
Figure S17. $^{13}C\{^1H\}$-NMR (101 MHz, CD_2Cl_2) spectrum of **3e**.

VK241_P2_CHO.1.fid
31P{1H} CD2Cl2 {D:\NMR_Data\CBMM\Zespol_02} Zespol_02 42
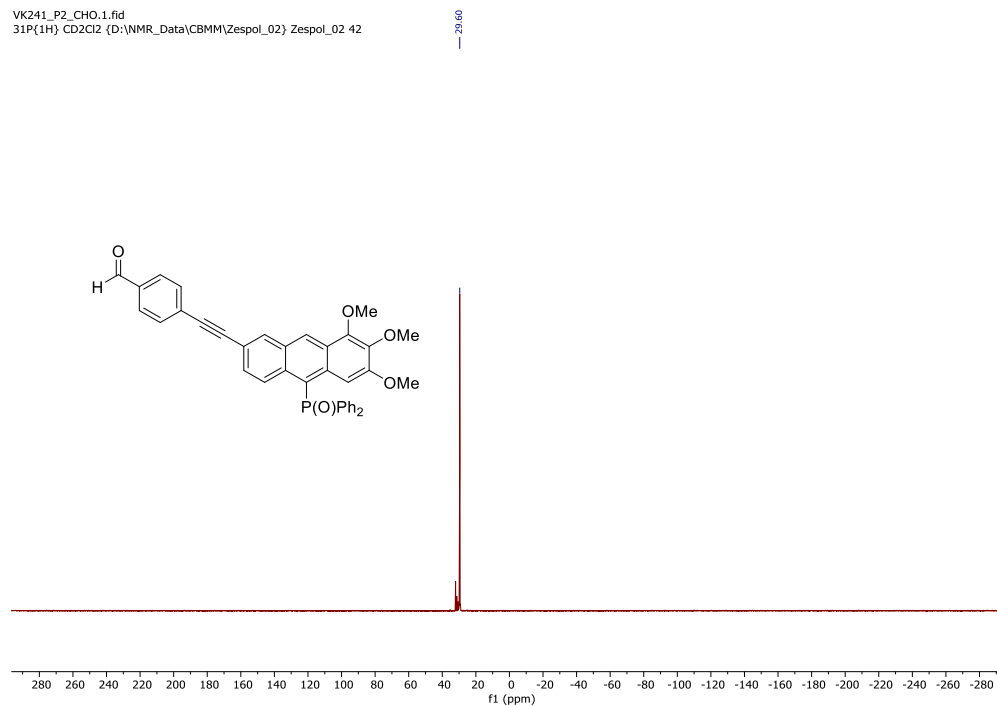
Figure S18. $^{31}P\{^1H\}$-NMR (162 MHz, CD_2Cl_2) spectrum of **3f**.
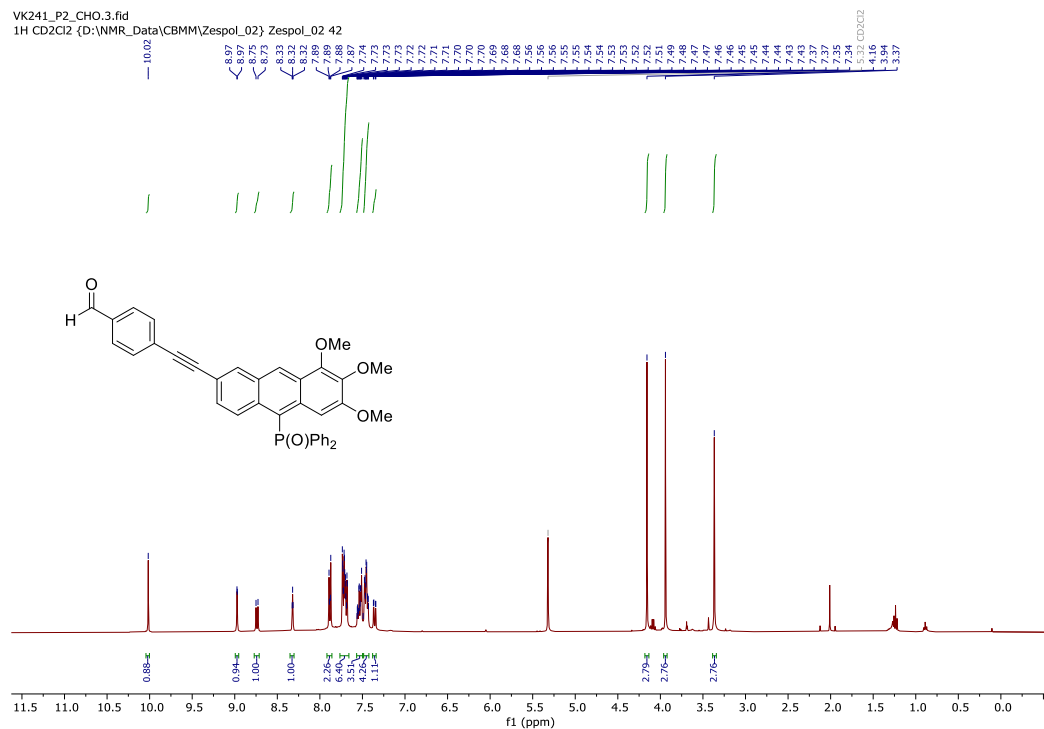
Figure S19. ^{1}H-NMR (400 MHz, CD$_2$Cl$_2$) spectrum of **3f**.
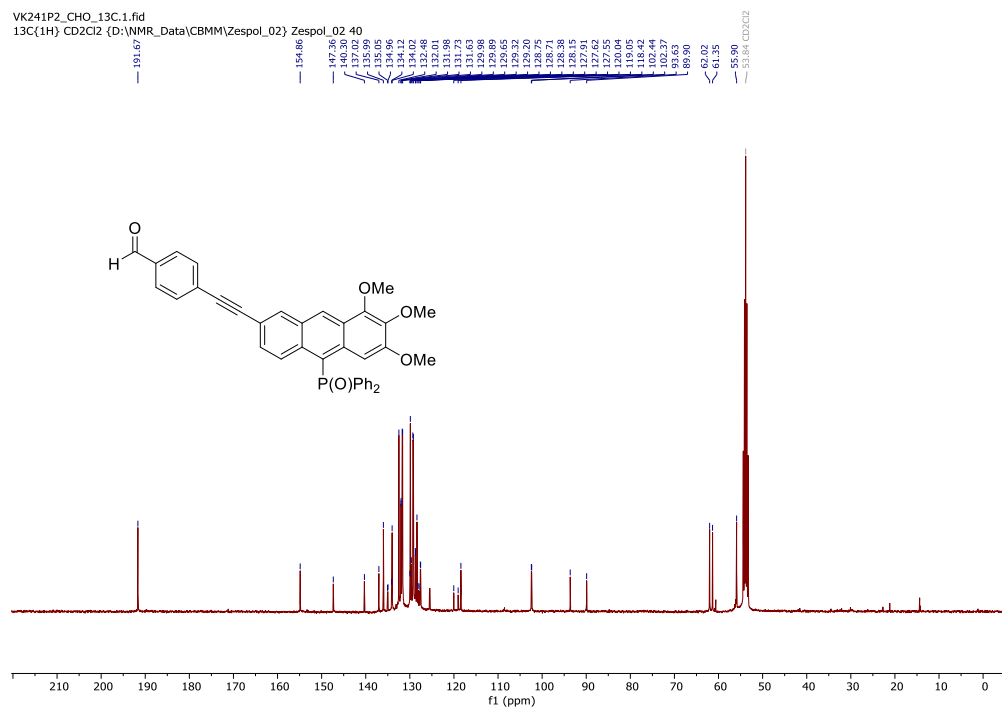
Figure S20. ^{13}C{^{1}H}-NMR (101 MHz, CD$_2$Cl$_2$) spectrum of **3f**.

VK242_Pure_CD2Cl2.1.fid
31P{1H} CD2Cl2 {D:\NMR_Data\CBMM\Zespol_02} Zespol_02 51

—29.50
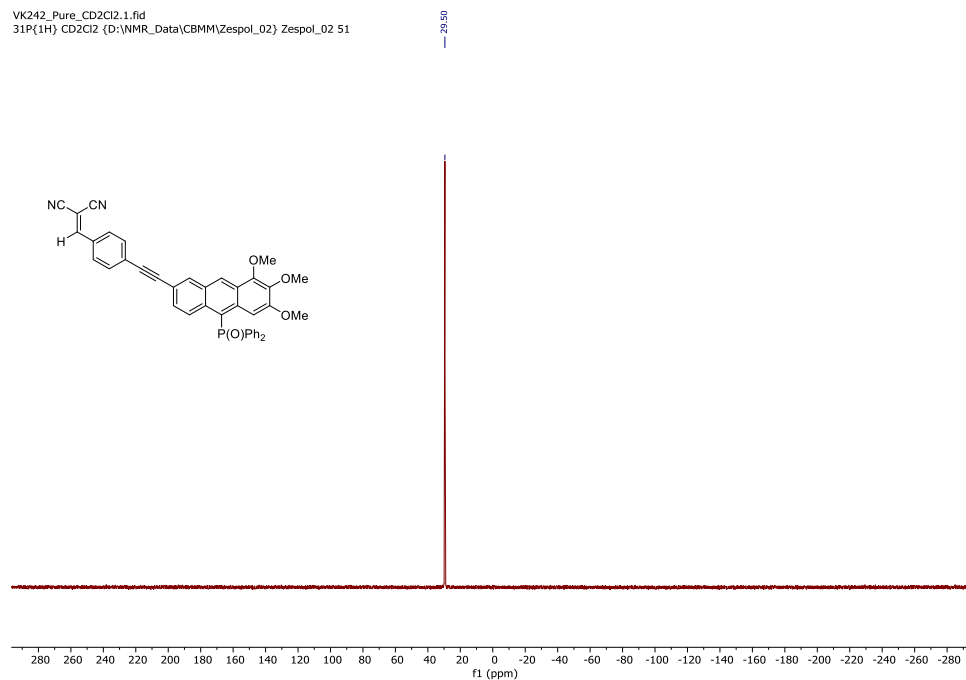
Figure S21. $^{31}P\{^1H\}$-NMR (162 MHz, CD$_2$Cl$_2$) spectrum of **3g**.

VK242_Pure_CD2Cl2.3.fid
1H CD2Cl2 {D:\NMR_Data\CBMM\Zespol_02} Zespol_02 51
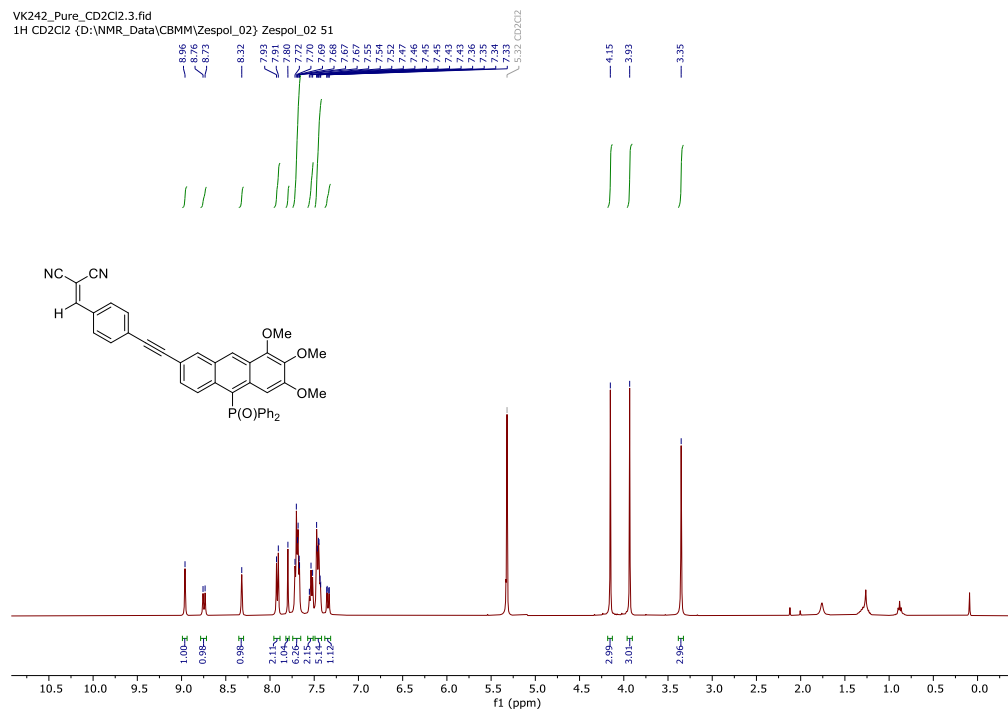
Figure S22. ^1H-NMR (400 MHz, CD$_2$Cl$_2$) spectrum of **3g**.

VK242_Pure_CD2Cl2.5.fid
13C{1H} CD2Cl2 {D:\NMR_Data\CBMM\Zespol_02} Zespol_02 51
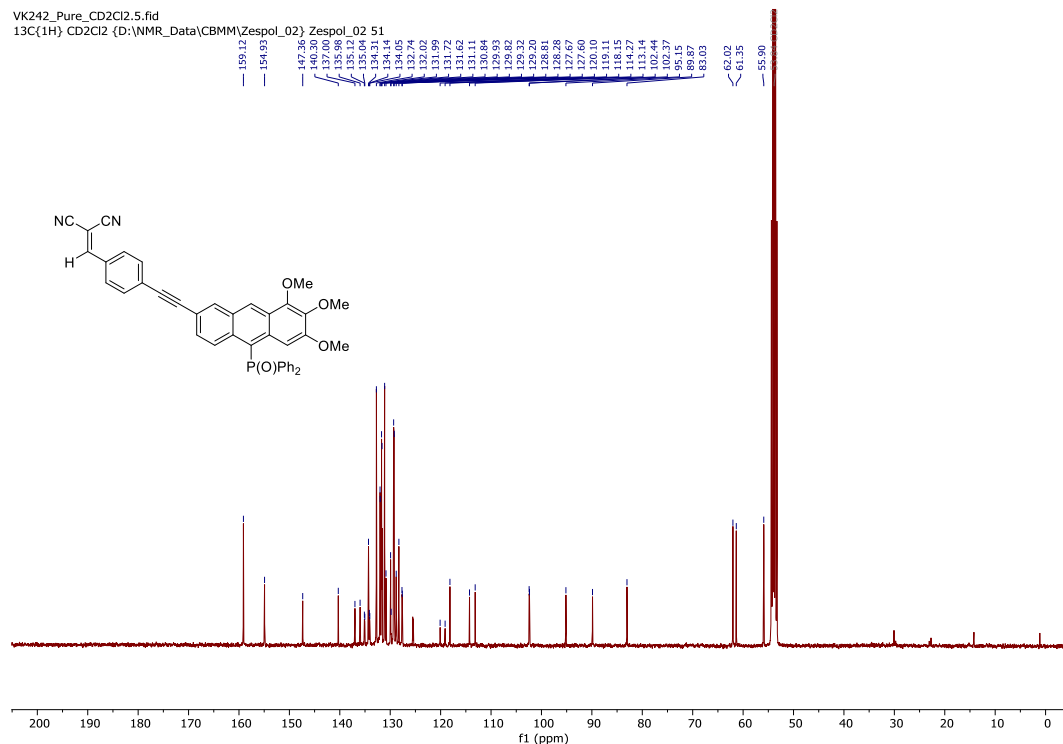
Figure S23. $^{13}C\{^1H\}$-NMR (101 MHz, CD$_2$Cl$_2$) spectrum of **3g**.

3.7.4 Photophysical Properties
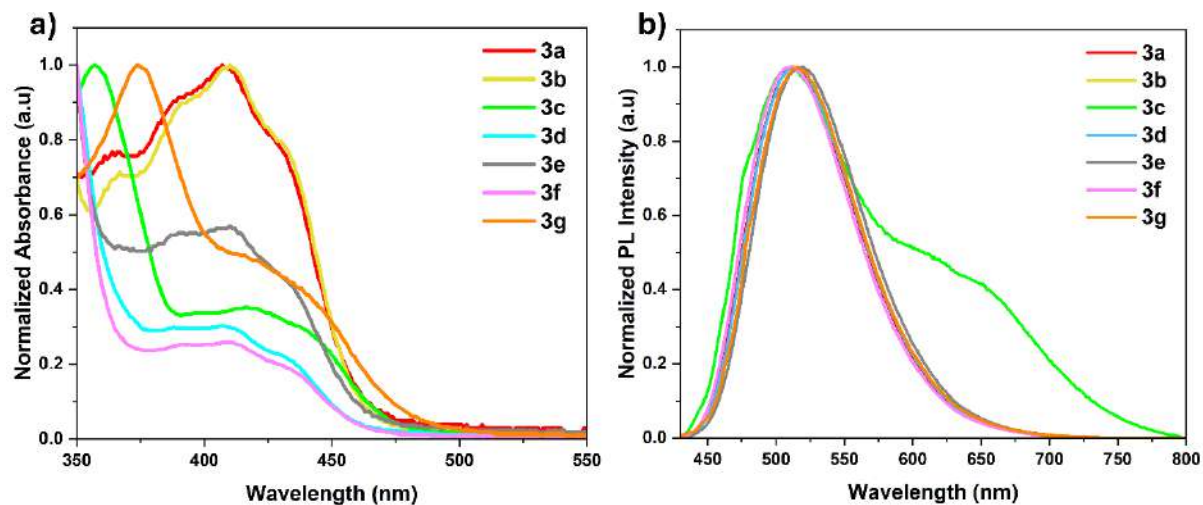
**Figure S24**. (a) Normalized absorption and (b) emission spectra of anthracene derivatives **3a-g** (10^{-5} mol/L, DCM).

Figure S25. (a) Normalized absorption and(b) emission spectra of anthracene derivatives **3a-g** (10^{-5} mol/L, acetonitrile).

Figure S26. (a) Normalized absorption and (b) emission spectra of anthracene derivatives **3a-g** (10^{-5} mol/L, MeOH).

Table S1. Photophysical data of **3a-g** in three different solvents (DCM, MeCN, and MeOH).

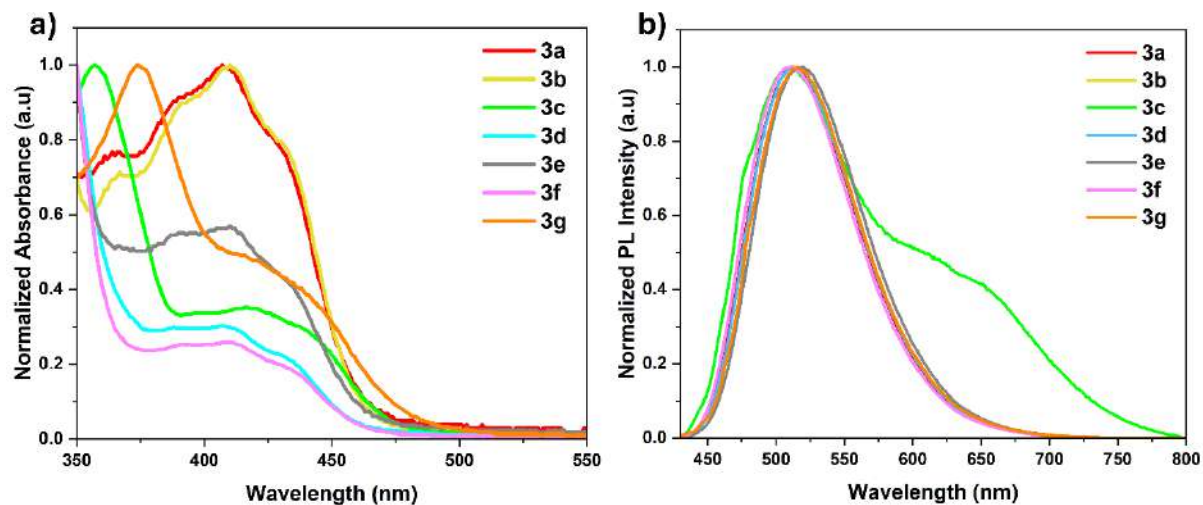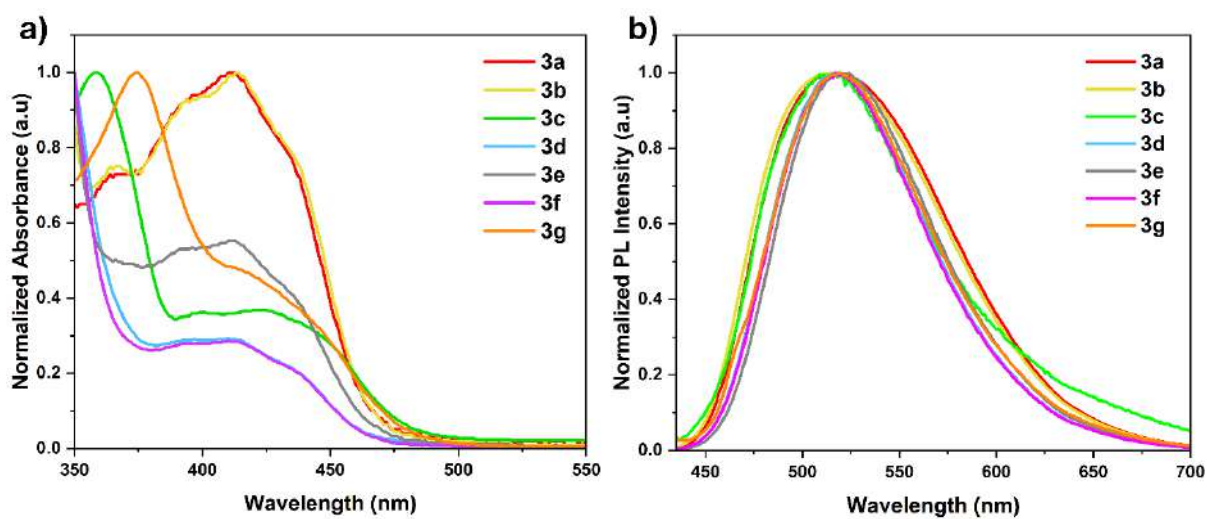| Nr.	DCM			MeOH			MeCN		
	Abs.[a] $\lambda_{max.}$ (nm)	PL[b] $\lambda_{max.}$ (nm)	QY[c] (%)	Abs.[a] $\lambda_{max.}$ (nm)	PL[b] $\lambda_{max.}$ (nm)	QY[c] (%)	Abs.[a] $\lambda_{max.}$ (nm)	PL[b] $\lambda_{max.}$ (nm)	QY[c] (%)
3a	411	505	85.07	412	517	76.51	408	513	62.38
3b	412	503	80.06	413	514	70.83	410	510	63.19
3c	422	561	61.33	423	515	2.34	420	511	1.37
3d	410	505	80.20	410	518	67.39	410	515	71.07
3e	411	509	71.91	412	521	60.01	409	517	56.76
3f	412	510	73.29	412	517	11.37	410	510	36.00
3g	425	511	1.01	422	519	2.33	428	516	3.47

[a] Abs. – absorption maximum; [b] PL – emission maximum; [c] The absolute photoluminescence quantum yield (QY)

3.7.5 Electrochemical properties

Electrochemical characterization of anthracene derivatives **3a-g** were conducted using a Metrohm Autolab PGSTAT128N potentiostat/galvanostat instrument. All anthracene deriavtives were dissolved in dry CH_2Cl_2 of spectroscopic grade (concentration 0.5 mM) in the presence of [n-Bu$_4$N]$^+$[PF$_6$] $^-$ as an electrolyte (concentration 100 mM), and the resulting solution was degassed by purging with Ar gas for 20 minutes. A three-electrode electrochemical cell was used with a glassy carbon disk as the working electrode, Pt wire as the counter electrode, and Ag/AgCl wire as the reference electrode. Cyclic voltammetry (CV) and differential pulse voltammetry (DPV) plots are shown in Figures S27–S29.
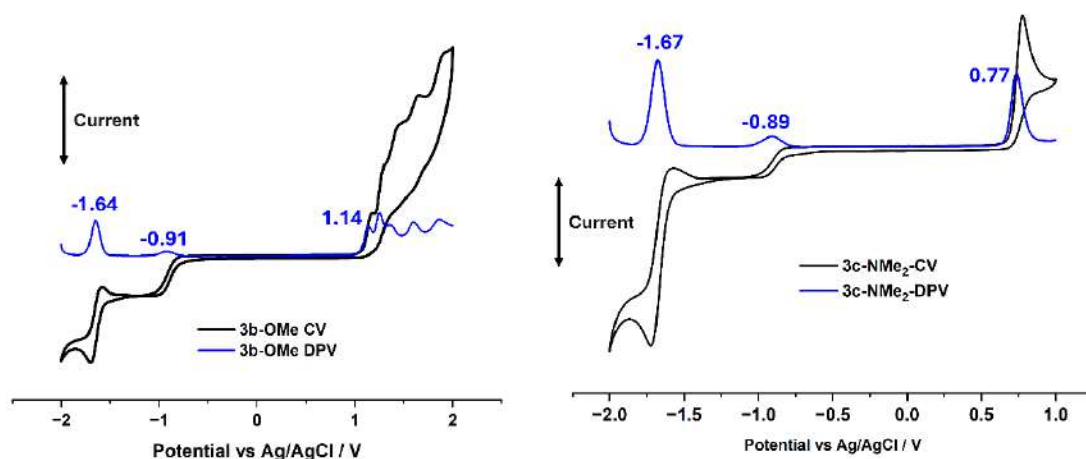
Figure S27. Cyclic voltammogram (black) and differential pulse voltammogram (blue) spectra of **3b** and **3c;** measured in the CH_2Cl_2 solution, 20 °C, 50 mV s^{-1}, glassy carbon working electrode.

Figure S28. Cyclic voltammogram (black) and differential pulse voltammogram (blue) spectra of **3d** and **3e;** measured in the CH$_2$Cl$_2$ solution, 20 °C, 50 mV s^{-1}, glassy carbon working electrode.

Figure S29. Cyclic voltammogram (black) and differential pulse voltammogram (blue) spectra of **3f** and **3g;** measured in the CH$_2$Cl$_2$ solution, 20 °C, 50 mV s^{-1}, glassy carbon working electrode.
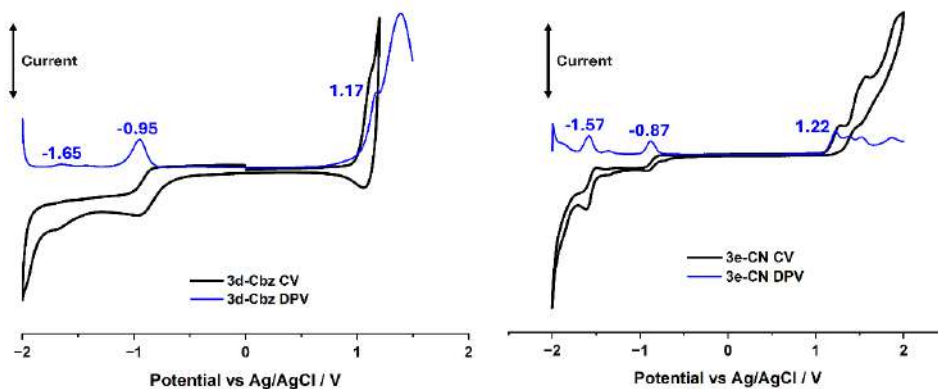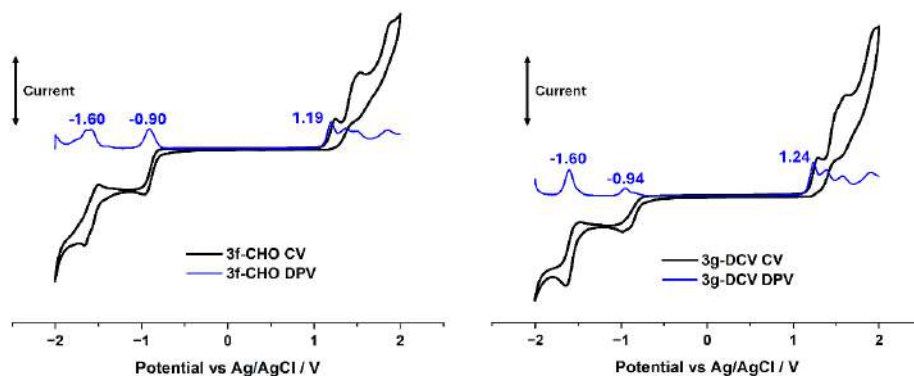
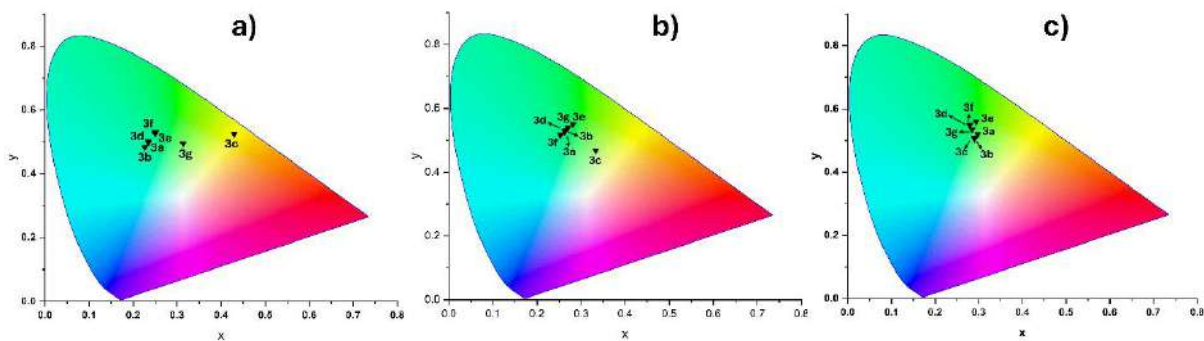### 3.7.6 CIE 1931 chromaticity studies

Figure S30. Commission Internationale de L'Eclairage (CIE) 1931 chromaticity coordinates for anthracene derivatives **3a-g** in three solvents (a) DCM (b) MeCN and (c) MeOH.

Table S2. Chromaticity coordinates for anthracene derivatives **3a-g** in four different solvents.

	Toluene		DCM		MeCN		MeOH	
	X	**Y**	**X**	**Y**	**X**	**Y**	**X**	**Y**
3a	0.245	0.482	0.278	0.526	0.317	0.538	0.338	0.549
3b	0.234	0.470	0.269	0.517	0.302	0.536	0.326	0.548
3c	0.215	0.473	0.487	0.495	0.487	0.446	0.488	0.458
3d	0.241	0.493	0.288	0.524	0.319	0.539	0.333	0.550
3e	0.259	0.521	0.298	0.546	0.332	0.554	0.345	0.556
3f	0.259	0.515	0.300	0.547	0.338	0.555	0.332	0.562
3g	0.439	0.537	0.528	0.458	0.457	0.475	0.452	0.510

3.7.7 References

1. Vivek, V.; Koprowski, M.; Różycka-Sokołowska, E.; Turek, M.; Dudziński, B.; Owsianik, K.; Knopik, Ł.; Bałczewski, P. High-Efficiency Light Emitters: 10-(Diphenylphosphoryl)-Anthracenes from One-Pot Synthesis Including C-O-P to C-P(═O) Rearrangement. *J. Org. Chem*. **2025**, *90*, 13, 4580–4590.
2. Murayama, N.; Hao Jorolan, J.; Minoura, M.; Nakano, H.; Ikoma, T.; Matano, Y. 9-(Diphenylphosphoryl)-10-(Phenylethynyl)Anthracene Derivatives: Synthesis and Implications for the Substituent and Solvent Effects on the Light-Emitting Properties. *ChemPhotoChem* **2022**, *6*, e202200100.
3. Qiu, F.; Qiu, F.; Dong, Y.; Dong, Y.; Liu, J.; Sun, Y.; Geng, H.; Zhang, H.; Zhu, D.; Zhu, D.; Shi, X.; Shi, X.; Liu, J.; Zhang, J.; Zhang, J.; Ai, S.; Jiang, L. Asymmetric Organic Semiconductors for High Performance Single Crystalline Field-Effect Transistors with Low Activation Energy. *J. Mater. Chem.* **2020**, *8* (18), 6006–6012.
4. S. Yamazaki, K. Katayama, Z. Wang, Y. Mikata, T. Morimoto, A. Ogawa, *ACS Omega* **2021**, *6*, 42, 28441–28454.

3.8 Experimental Section II for *ortho*-positional isomers of anthracenes and carbazole derivatives containing phosphonate ester group and their optical properties

3.8.1 General information

Tetrahydrofuran and toluene were dried using Solvent Purification System (MBraun SPS-800). Glassware equipment was oven-dried and flushed with dry argon. For flash chromatography, Chromatography System – Büchi Pure C-850 FlashPrep was used. The melting points were measured with an Electrothermal Model IA9100 apparatus and were uncorrected. Mass spectra were obtained using a SYNAPT G2-Si HDMS (Waters) instrument. NMR spectra were recorded with a Bruker AV 200 MHz, Bruker AVANCE Neo 400 MHz or Bruker AVANCE III 500 MHz using $CDCl_3$, C_6D_6, CD_2Cl_2, as internal standards. The UV-Vis absorption spectra were recorded in 1 cm cuvettes on a Shimadzu spectrophotometer UV-2700. Emission spectra were obtained with the Horiba Jobin Yvon, Fluoromax 4 Plus spectrofluorometer. The fluorescence quantum yields Φ of the obtained compounds were determined in three different solvents (DCM, $CHCl_3$, CCl_4, MeOH, MeCN, THF, and toluene) on excitation at their absorption maximum using an integrating sphere (Horiba, Jobin Yvon, Quanta-φ F-3029 Integrating sphere).

Starting Materials: *m*-xylene, *p*-xylene, and aromatic aldehydes were commercially available from Merck; compounds **7** and **8** were prepared according to a reported procedure.[1]

3.8.2 Synthesis and characterization
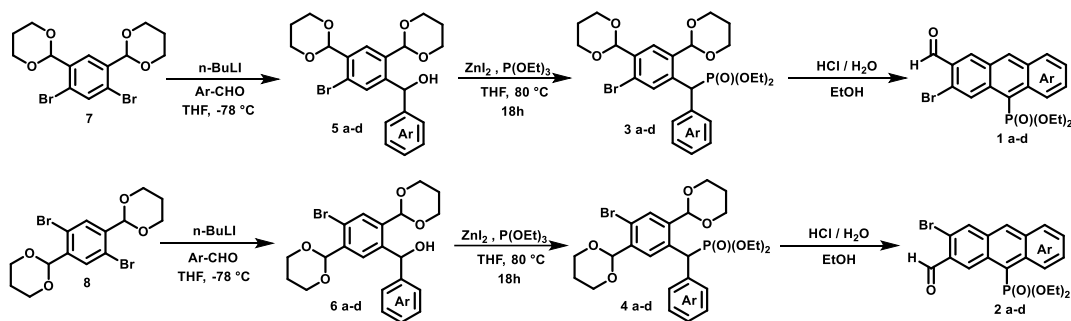
Scheme S1. Synthesis of **5a-d**, **6a-d**, **3a-d**, **4a-d**, **1a-d**, and **2a-d**.

General procedure for the synthesis of diarylmethanols 5a-d and 6a-d:

Following a literature procedure,[2] the 1,4-dibomo-2,5-bis(1,3-dioxan-2-yl)-benzene (**7**) or 1,5-dibromo-2,4-bis(1,3- dioxan-2-yl)-benzene (**8**) (1 mmol) was dissolved in dry THF (50 mL), cooled to -78 °C and then *n*-BuLi in heptane (2.6 M, 1.2 mmol) was added. The resulting mixture was stirred for 40 min under argon atmosphere. The corresponding (hetero)aromatic aldehydes (1.1 mmol) in dry THF (3 mL), was added at -78 °C and stirring was continued for 1.5 h from -78 °C to room temperature. Then saturated aqueous solution of NH_4Cl was added and the organic layer was evaporated. The residue was diluted with ethyl acetate (50 mL) and washed with water (3×20 mL). The organic layer was dried ($MgSO_4$) and then filtrated. The solvent was removed in

vacuum and the residue purified by column chromatography (mixtures n-hexane/acetone) to give the corresponding diarymethanols (**5a-d**) and (**6a-d**).

General procedure for the synthesis of phosphonates 3a-d and 4a-d:

Diarylmethanol derivatives **5a-d** and **6a-d** (1.0 mmol), ZnI_2 (1.1 equiv.) and triethyl phosphite (1.5 mmol) were placed in the Schlenk tube (20 mL) and dissolved in dry THF (3 mL). Then, the mixture was heated at reflux under argon atmosphere for 18 h. Next, the solvent and the excess of $(EtO)_3P$ were evaporated under vacuum. The residue was dissolved in ethyl acetate (20 mL), washed with water (5 mL) and dried over anhydrous $MgSO_4$. After filtration, ethyl acetate was removed in vacuum and the crude products **3a-d** and **4a-d** were purified by flash column chromatography over silica gel with a mixture of n-hexane/EtOAc.

General procedure for the synthesis of acenes 1a-d and 2a-d:

Phosphonates **3a-d** or **4a-d** (1.0 mmol) were dissolved in EtOH (4 mL) and then aqueous HCl (6N, 4 mL) was added. The mixture was stirred at ambient temperature for 2 h, then solid $NaHCO_3$ was added and extracted with ethyl acetate (3×10 mL). The organic layer was washed with water (2×5 mL) and dried ($MgSO_4$). The solvent was removed and the crude product was purified by flash chromatography (n-hexane/EtOAc) to give pure acenes **1a-d** or **2a-d**.

Diethyl ((5-bromo-2,4-di(1,3-dioxan-2-yl)phenyl)(3,4,5-trimethoxyphenyl)methyl) phosphonate (3a):
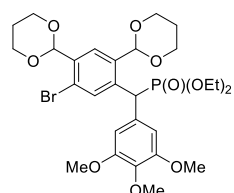
R_f = 0.42 (EtOAc), white solid, 46 % yield; **^{1}H NMR** (400 MHz, C_6D_6) δ 8.69 (d, J = 2.2 Hz, 1H), 8.57 (d, J = 1.1 Hz, 1H), 7.22 (d, J = 1.5 Hz, 2H), 5.72 (d, J = 8.2 Hz, 2H), 5.32 (d, J = 25.1 Hz, 1H), 3.99 – 3.90 (m, 2H), 3.89 – 3.80 (m, 4H), 3.79 (s, 3H), 3.75 – 3.61 (m, 2H), 3.54 – 3.45 (m, 3H), 3.51 (s, 6H), 3.38 – 3.31 (m, 1H), 1.85 – 1.75 (m, 2H), 0.94 (t, J = 7.1 Hz, 3H), 0.82 (t, J = 7.0 Hz, 3H), 0.62 (dd, J = 13.4, 1.5 Hz, 2H); **^{31}P NMR** (162 MHz, C_6D_6) δ 25.47; **^{13}C{^{1}H} NMR** (101 MHz, C_6D_6) δ 154.10 (s), 138.71 (s), 138.43 (d, J_{PC} = 4.4 Hz), 137.41 (d, J_{PC} = 2.3 Hz), 137.11 (d, J_{PC} = 9.4 Hz), 134.73 (d, J_{PC} = 5.1 Hz), 132.70 (d, J_{PC} = 4.7 Hz), 123.17 (d, J_{PC} = 2.7 Hz), 108.08 (d, J_{PC} = 8.7 Hz), 101.00 (s), 99.94 (s), 67.28 (s), 67.08 (s), 63.05 (d, J_{PC} = 6.8 Hz), 62.57 (d, J = 6.7 Hz), 60.48 (s), 55.89 (s), 45.37 (d, $[1]J_{PC}$ = 138.9 Hz), 25.76 (d, J = 10.0 Hz), 16.47 (d, J_{PC} = 5.4 Hz), 16.34 (d, J_{PC} = 5.5 Hz); **HRMS** (TOF MS ES+): Calc. for $C_{28}H_{39}O_{10}PBr$ [M+H^{+}]: 645.1464; Found: 645.1470.

6-Bromo-10-(diethoxyphosphoryl)-7-formyl-1,2,3-trimethoxyanthracene (1a):
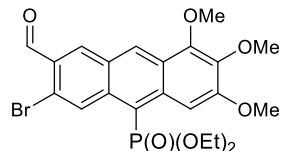
R_f = 0.65 (EtOAc), orange solid, m.p. = 191-193 °C, 88 % yield; **^{1}H NMR** (400 MHz, C_6D_6) δ 10.45 (s, 1H), 9.93 (s, 1H), 9.26 (s, 1H), 8.90 – 8.88 (m, 1H), 8.45 (d, J = 2.3 Hz, 1H), 4.12 – 4.06 (m, 2H), 3.89 – 3.86 (m, 2H), 3.84 (s, 3H), 3.76 (s, 6H), 0.99 (t, J = 7.0 Hz, 6H); **^{31}P NMR** (162 MHz, C_6D_6) δ 18.85; **^{13}C{^{1}H} NMR** (101 MHz, C_6D_6) δ 190.13 (s), 156.94 (s), 147.32 (d, J_{PC} = 2.3 Hz), 140.73 (s), 136.81 (d, J_{PC} = 9.9 Hz), 136.18 (d, J_{PC} = 12.8 Hz), 134.13 (s), 132.12 (d, J_{PC} = 4.0 Hz), 131.33 (d, J_{PC} = 3.5 Hz), 129.22 (s), 125.61 (d, J_{PC} = 15.4 Hz), 121.67 (s), 116.52 (d, J_{PC} = 177.8 Hz), 102.04 (d, J_{PC} = 3.8 Hz), 61.83 (d, J_{PC} = 5.0 Hz), 61.15 (s), 60.64 (s), 54.35 (d, J_{PC} = 246.5 Hz), 16.13 (d, J_{PC} = 6.3 Hz); **HRMS** (TOF MS ES+): Calc. for $C_{22}H_{24}O_7PBr$ [M+]: 511.0522; Found: 511.0521.
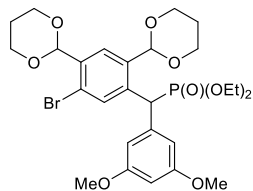
Diethyl ((5-bromo-2,4-di(1,3-dioxan-2-yl)phenyl)(3,5-dimethoxyphenyl)methyl) phosphonate (3b):

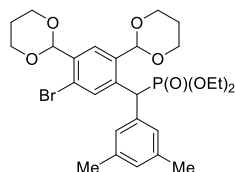R_f = 0.50 (EtOAc), white solid, m.p. = 131-133 °C, 42 % yield; **^{1}H NMR** (400 MHz, C_6D_6) δ 8.76 (d, J = 2.1 Hz, 1H), 8.59 (d, J = 1.1 Hz, 1H), 7.23 (d, J = 1.9 Hz, 2H), 6.46 (t, J = 1.7 Hz, 1H), 5.71 (d, J = 4.3 Hz, 2H), 5.38 (d, J = 25.1 Hz, 1H), 3.99-3.90 (m, 2H), 3.89-3.78 (m, 4H), 3.73-3.66 (m, 2H), 3.52-3.41 (m, 4H), 3.55 (s, 6H), 1.84-1.71 (m, 2H), 0.93 (t, J = 7.0 Hz, 3H), 0.83 (t, J = 7.0 Hz, 3H), 0.61-0.54 (m, 2H); **^{31}P NMR** (162 MHz, C_6D_6) δ 25.28; **^{13}C{^{1}H} NMR** (101 MHz, C_6D_6) δ 161.14 (s), 139.30 (d, J_{PC} = 4.7 Hz), 137.81 (d, J_{PC} = 4.7 Hz), 137.06 (d, J_{PC} = 1.8 Hz), 136.94 (d, J_{PC} = 9.4 Hz), 134.43 (d, J_{PC} = 5.4 Hz), 122.84 (s), 108.23 (d, J_{PC} =8.3 Hz), 100.68 (s), 99.39 (s), 66.85 (s), 66.61 (s), 62.63 (d, J_{PC} = 6.7 Hz), 62.25 (d, J_{PC} = 6.6 Hz), 54.47 (s), 45.35 (d, J_{PC} = 138.7 Hz), 25.37 (d, J_{PC} = 12.6 Hz), 16.01 (dd, J_{PC} = 12.1, 6.0 Hz); **HRMS** (TOF MS ES+): Calc. for $C_{27}H_{37}O_9PBr$ [M+H+]: 615.1357; Found: 615.1359.

6-Bromo-10-(diethoxyphosphoryl)-7-formyl-1,3-dimethoxyanthracene (1b):
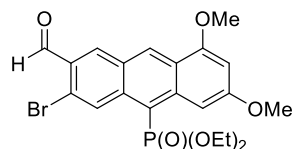
R_f = 0.68 (EtOAc), orange solid, m.p. = 196-198 °C, 94 % yield; **^{1}H NMR** (400 MHz, C_6D_6) δ 10.42 (s, 1H), 10.00 (s, 1H), 8.90 (d, J = 7.2 Hz, 1H), 8.38 (d, J = 2.2 Hz, 1H), 6.35 (d, J = 2.0 Hz, 1H), 4.11 (ddd, J = 10.3, 8.5, 7.5 Hz, 2H), 3.87 (ddd, J = 10.9, 8.6, 7.1 Hz, 2H), 3.81 (s, 3H), 3.34

(s, 3H), 1.01 (t, J = 7.0 Hz, 6H); **31P NMR** (162 MHz, C$_6$D$_6$) δ 18.97; **13C{1H} NMR** (101 MHz, C$_6$D$_6$) δ 190.02 (s), 161.74 (s), 157.01 (d, J_{PC} = 2.4 Hz), 139.94 (d, J_{PC} = 12.7 Hz), 137.89 (d, J_{PC} = 10.4 Hz), 134.17 (s), 132.15 (d, J_{PC} = 3.2 Hz), 131.92 (d, J_{PC} = 3.6 Hz), 128.89 (s), 127.06 (d, J_{PC} = 14.4 Hz), 122.82 (d, J_{PC} = 15.5 Hz), 122.45 (s), 115.34 (d, J_{PC} = 178.5 Hz), 98.03 (s), 97.54 (d, J_{PC} = 3.8 Hz), 61.76 (d, J_{PC} = 5.0 Hz), 55.29 (s), 55.06 (s), 16.15 (d, J_{PC} = 6.3 Hz); **HRMS** (TOF MS ES+): Calc. for C$_{21}$H$_{23}$O$_6$PBr [M+H$^+$]: 481.0416; Found: 481.0416.

Diethyl ((5-bromo-2,4-di(1,3-dioxan-2-yl)phenyl)(3,5-dimethylphenyl)methyl) phosphonate (3c):


R$_f$ = 0.64 (EtOAc), white solid, m.p. = 160-162 °C, 42 % yield; **1H NMR** (400 MHz, CD$_2$Cl$_2$) δ 8.07 (d, J = 2.0 Hz, 1H), 7.80 (d, J = 1.2 Hz, 1H), 7.03 (s, 1H), 6.89 (s, 1H), 5.69 (s, 1H), 5.56 (s, 1H), 4.91 (d, J = 25.5 Hz, 1H), 4.40-4.19 (m, 4H), 4.03-3.93 (m, 4H), 3.92-3.81 (m, 4H), 2.28 (s, 6H), 2.26-2.16 (m, 2H), 1.48-1.41 (m, 2H), 1.15 (t, J = 7.0 Hz, 6H). **31P NMR** (162 MHz, CD$_2$Cl$_2$) δ 24.74. **13C{1H} NMR** (101 MHz, CD$_2$Cl$_2$) δ 138.36 (d, J_{PC} = 1.7 Hz), 137.84 (d, J_{PC} = 4.1 Hz), 136.89 (d, J_{PC} = 10.4 Hz), 136.71 (d, J_{PC} = 1.9 Hz), 136.14 (d, J_{PC} = 5.9 Hz), 134.32 (d, J_{PC} = 5.5 Hz), 129.18 (d, J_{PC} = 2.4 Hz), 127.82 (d, J_{PC} = 7.5 Hz), 126.83 (s), 122.64 (d, J_{PC} = 2.4 Hz), 100.18 (d, J_{PC} = 145.6 Hz), 67.91 (d, J_{PC} = 2.7 Hz), 67.75 (s), 63.04 (d, J_{PC} = 6.7 Hz), 45.03 (d, J_{PC} = 138.2 Hz), 26.09 (s), 21.48 (s), 16.45 (d, J_{PC} = 5.8 Hz); **HRMS** (TOF MS ES+): Calc. for C$_{27}$H$_{37}$O$_4$PBr [M+H$^+$]: 583.1382; Found: 583.1292.

6-Bromo-10-(diethoxyphosphoryl)-7-formyl-1,3-dimethylanthracene (1c):
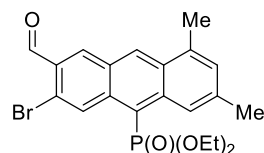
R$_f$ = 0.78 (EtOAc), yellow solid, m.p. = 186-188 °C, 92 % yield; **1H NMR** (400 MHz, CD$_2$Cl$_2$) δ 10.56 (s, 1H), 9.87 (s, 1H), 8.97 (d, J = 2.0 Hz, 1H), 8.85 (s, 1H), 8.64 (d, J = 2.4 Hz, 1H), 7.30 (s, 1H), 4.31-4.22 (m, 2H), 4.10-4.00 (m, 2H), 2.82 (s, 3H), 2.57 (s, 3H), 1.29 (t, J = 7.0 Hz, 6H); **31P NMR** (162 MHz, CD$_2$Cl$_2$) δ 18.04; **13C{1H} NMR** (101 MHz, CD$_2$Cl$_2$) δ 191.81 (s), 140.14 (s), 138.05 (d, J_{PC} = 10.8 Hz), 137.14 (d, J_{PC} = 11.6 Hz), 135.79 (s), 134.42 (s), 134.08 (d, J_{PC} = 3.9 Hz), 132.45 (d, J_{PC} = 3.7 Hz), 130.63 (d, J_{PC} = 14.1 Hz), 129.79 (s), 129.64 (s), 128.52 (d, J_{PC} = 15.3 Hz), 124.82 (d, J_{PC} = 4.7 Hz), 121.53 (s), 118.76 (d, J_{PC} = 177.9 Hz), 62.54 (d, J_{PC} = 5.2 Hz), 23.07 (s), 20.10 (s), 16.53 (d, J_{PC} = 6.4 Hz); **HRMS** (TOF MS ES+): Calc. for C$_{21}$H$_{23}$O$_4$PBr [M+H$^+$]: 449.0526; Found: 449.0517.

75

Diethyl ((5-bromo-2,4-di(1,3-dioxan-2-yl)phenyl)(1-methyl-1*H*-indol-2yl)methyl) phosphonate (3d):
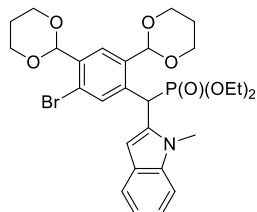
R_f = 0.55 (EtOAc), white solid, m.p. = 171-173 °C, 30 % yield; **¹H NMR** (400 MHz, CD₂Cl₂) δ 7.90 (s, 1H), 7.61–7.57 (m, 2H), 7.24 (d, J = 8.2 Hz, 1H), 7.17 (ddd, J = 8.0 Hz, J = 6.9 Hz, J = 1.2 Hz, 1H), 7.17 (ddd, J = 8.2 Hz, J = 6.9 Hz, J = 1.2 Hz, 1H), 6.96 (s, 1H), 5.98 (s, 1H), 5.66 (s, 1H), 5.21 (d, J = 25.5 Hz, 1H), 4.37– 4.33 (m, 1H), 4.29 –4.18 (m, 3H), 4.13–3.96 (m, 8H), 3.53 (s, 3H), 2.29– 2.17 (m, 2H), 1.47 (dd, J = 29.1, 13.5 Hz, 2H), 1.23–1.16 (m, 6H); **³¹P NMR** (162 MHz, CD₂Cl₂) δ 22.49; **¹³C{¹H} NMR** (101 MHz, CD₂Cl₂) δ 137.83 (s), 137.21 (d, J_{PC} = 3.3 Hz), 136.83 (d, J_{PC} = 6.7 Hz), 135.40 (d, J_{PC} = 6.8 Hz), 134.55 (d, J_{PC} = 4.7 Hz), 134.31 (s), 127.77 (s), 126.83 (d, J_{PC} = 2.6 Hz), 122.88 (d, J_{PC} = 3.7 Hz), 121.89 (s), 120.78 (s), 119.78 (s), 109.56 (s), 104.11 (d, J_{PC} = 4.0 Hz), 100.83 (s), 99.35 (s), 67.96–67.90 (m), 63.53 (dd, J = 26.5, 7.1 Hz), 38.52 (d, J_{PC} = 141.1 Hz), 30.02 (s), 26.09 (s), 16.50 (dd, J_{PC} = 13.0, 5.9 Hz); **HRMS** (TOF MS ES+): Calc. for $C_{28}H_{36}O_7NPBr$ [M+H⁺]: 608.1413; Found: 608.1434.

8-Bromo-6-(diethoxyphosphoryl)-9-formyl-5*N*-methylbenzo[b]carbazole (1d):
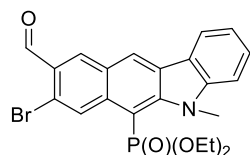

R_f = 0.59 (EtOAc), yellow solid, m.p. = 198-200 °C, 92 % yield; **¹H NMR** (400 MHz, CD₂Cl₂) δ 10.46 (s, 1H), 9.10 (s, 1H), 8.76 (d, J = 1.9 Hz, 1H), 8.59 (d, J = 2.0 Hz, 1H), 8.19 (d, J = 7.6 Hz, 1H),7.63 (ddd, J = 8.1 Hz, J = 6.8 Hz, J = 1.1 Hz, 1H), 7.37 (ddd, J = 8.2 Hz, J = 7.2 Hz, J = 1.2 Hz, 1H), 7.47 (d, J = 8.1 Hz, 1H), 4.17 (dd, J = 10.1, 7.2 Hz, 2H), 4.10, 4.05 (dd, J = 10.2, 7.4 Hz, 2 H), 1.33 (t, J = 7.1 Hz, 6H); **³¹P NMR** (162 MHz, CD₂Cl₂) δ 16.43; **¹³C{¹H} NMR** (101 MHz, CD₂Cl₂) δ 191.75 (s), 148.86 (d, J_{PC} = 4.4 Hz), 146.24 (s), 138.27 (d, J_{PC} = 8.8 Hz), 132.71 (s), 131.78 (d, J_{PC} = 4.6 Hz), 129.25 (s), 128.97 (d, J_{PC} = 10.9 Hz), 128.19 (s), 126.53 (d, J_{PC} = 3.3 Hz), 126.32 (d, J_{PC} = 11.6 Hz), 122.24 (s), 121.64 (s), 121.41 (s), 121.00 (s), 110.58 (s), 100.69 (d, J_{PC} = 190.0 Hz), 62.76 (d, J_{PC} = 5.9 Hz), 37.09 (s), 16.40 (d, J_{PC} = 6.7 Hz); **HRMS** (TOF MS ES+): Calc. for $C_{22}H_{22}O_4NPBr$ [M+H⁺]: 474.0470; Found: 474.0475.

Diethyl ((4-bromo-2,5-di(1,3-dioxan-2-yl)phenyl)(3,4,5-trimethoxyphenyl)methyl) phosphonate (4a):
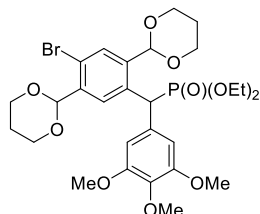
R_f = 0.23 (CH$_2$Cl$_2$:EtOAc 1:1 v/v), white crystals, m.p. = 151 – 152 °C, 52% yield; **^{1}H NMR** (400 MHz, C$_6$D$_6$) δ 8.88 (d, J = 2.0 Hz, 1H), 8.28 (d, J = 0.9 Hz, 1H), 7.23 (d, J = 1.6 Hz, 2H), 5.69 (s, 1H), 5.68 (s, 1H), 5.29 (d, J = 25.6 Hz, 1H), 3.77 – 4.00 (m, 6H), 3.79 (s, 3H), 3.65 – 3.76 (m, 2H), 3.57 (s, 6H), 3.41 – 3.51 (m, 2H), 3.40 (ddd, J = 12.3 Hz, J = 12.5 Hz, J = 2.4 Hz, 1H), 3.29 (ddd, J = 12.3 Hz, J = 12.5 Hz, J = 2.4 Hz, 1H), 1.71 – 1.84 (m, 2H), 0.96 (t, J = 7.1 Hz, 3H), 0.88 (t, J = 7.1 Hz, 3H), 0.54 – 0.60 (m, 1H), 0.51 – 0.56 (m, 1H); **^{31}P NMR** (162 MHz, C$_6$D$_6$) δ 25.36; **^{13}C{^{1}H} NMR** (101 MHz, CDCl$_3$) δ 153.06 (d, J_{PC} = 1.2 Hz); 138.75 (d, J_{PC} = 9.6 Hz), 137.83 (d, J_{PC} = 2.3 Hz), 137.08 (d, J_{PC} = 2.4 Hz), 134.37 (d, J_{PC} = 4.9 Hz), 131.98 (d, J_{PC} = 5.3 Hz), 130.81 (d, J_{PC} = 1.0Hz), 129.87 (d, J_{PC} = 5.1 Hz), 120.80 (d, J_{PC} = 2.8 Hz), 106.92 (d, J_{PC} = 8.2 Hz), 100.46 (s), 98.84 (s), 67.56 (s), 67.53 (s), 67.43 (s), 62.79 (d, J_{PC} = 6.9 Hz), 62.63 (d, J_{PC} = 7.1 Hz), 60.38 (d, J_{PC} = 1.2 Hz), 55.88 (s), 44.69 (d, J_{PC} = 138.8 Hz), 25.71 (s), 25.66 (s), 16.18 (d, J_{PC} = 5.8 Hz), 16.04 (d, J_{PC} = 6.1 Hz); **HRMS** (TOF MS ES): calc. for C$_{28}$H$_{38}$BrO$_{10}$P+H 645.1464/647.1444 found 645.1475/647.1456; calc. for C$_{28}$H$_{38}$BrO$_{10}$P [M+H$^+$+Et$_3$N] 746.2669/748.2648 found 746.2673/748.2652.

7-Bromo-10-(diethoxyphosphoryl)-6-formyl-1,2,3-trimethoxyanthracene (2a):
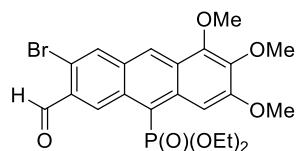
R_f = 0.42 (*n*-hexane/EtOAc 1:2 v/v), yellow crystals, m.p. = 114 - 116 °C, Yield 93% (6N HCl and CH$_3$CN, 1h, rt); **^{1}H NMR** (CDCl$_3$): 10 54 (s, 1H); 9.73 (s, 1H), 8.88 (s, 1H), 8.85 (s, 1H), 8.34 (d, J = 2.2 Hz, 1H), 4.31 – 4.41 (m, 2H), 4.15 (s, 3H), 4.12 (s, 3H), 4.09 – 4.18 (m, 2H), 4.08 (s, 3H), 1.35 (t, J = 7.1 Hz, 6H); **^{31}P NMR** (162 MHz, C$_6$D$_6$) δ 18.46; **^{13}C{^{1}H} NMR** (101 MHz, CDCl$_3$) δ 191.90 (s), 155.29 (d, J_{PC} = 1.4 Hz), 146.28 (d, J_{PC} = 2.2 Hz), 141.38 (s), 134.48 (d, $^3J_{PC}$ = 12.5 Hz), 133.75 (d, $^4J_{PC}$ = 1.0 Hz, =CH), 133.45 (d, $^3J_{PC}$ = 4.1 Hz, =CH), 132.19 (d, J_{PC} = 14.3 Hz, >C<),131.68 (d, J_{PC} = 9.8 Hz), 130.71 (d, J_{PC} = 1.2 Hz), 127.01 (d, J_{PC} = 15.7 Hz), 126.62 (d, J_{PC} = 3.6 Hz), 119.76 (d, J_{PC} = 180.1 Hz), 117.45 (s), 101.42 (d, J_{PC} = 4.1 Hz), 62.35 (d, J_{PC} = 5.5 Hz), 61.65 (s), 61.28 (s), 56.13 (s), 16.36 (d, J_{PC} = 6.5 Hz); **HRMS** (TOF MS ES+): calc. for C$_{22}$H$_{25}$BrO$_7$P [M+H$^+$] 511.0521/513.0501 found 511.0524/513.0502; calc. for C$_{22}$H$_{24}$BrO$_7$PNa [M+Na$^+$]533.0341/535.0320 found 533.0342/535.0322; calc. for C$_{22}$H$_{24}$BrO$_7$PK [M+K$^+$]549.0080/551.0060 found 549.0081/551.0063.

Diethyl ((4-bromo-2,5-di(1,3-dioxan-2-yl)phenyl)(3,5-dimethoxyphenyl)methyl) phosphonate (4b):
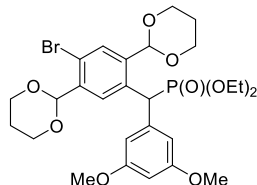
R_f = 0.46 (EtOAc), colourless liquid, 38 % yield; **¹H NMR** (400 MHz, CD$_2$Cl$_2$) δ 8.20 (d, J = 2.1 Hz, 1H), 7.76 (d, J = 1.2 Hz, 1H), 6.63 (d, J = 2.0 Hz, 2H), 6.34 (dd, J = 2.4, 1.4 Hz, 1H), 5.67 (s, 1H), 5.59 (s, 1H), 4.90 (d, J = 25.5 Hz, 1H), 4.28-4.19 (m, 4H), 4.05-3.93 (m, 8H), 3.75 (s, 6H), 2.24-2.16 (m, 2H), 1.48-1.41 (m, 2H), 1.21 (t, J = 7.1 Hz, 3H), 1.15 (t, J = 7.0 Hz, 3H); **³¹P NMR** (162 MHz, CD$_2$Cl$_2$) δ 24.23; **¹³C{¹H} NMR** (101 MHz, CD$_2$Cl$_2$) δ 161.05 (s), 139.28 (d, J_{PC} = 9.9 Hz), 138.98 (d, J_{PC} = 5.4 Hz), 138.15 (d, J_{PC} = 2.4 Hz), 134.54 (d, J_{PC} = 4.8 Hz), 131.18 (s), 130.19 (d, J_{PC} = 5.3 Hz), 121.31 (d, J_{PC} = 2.6 Hz), 108.28 (d, J_{PC} = 7.9 Hz), 100.93 (s), 99.03 (s), 99.15 (d, J_{PC} = 2.1 Hz), 67.13 (s), 67.78 (s), 63.26 (d, J_{PC} = 10.8 Hz), 55.58 (s), 45.26 (d, J_{PC} = 138.25 Hz), 25.68 (d, J_{PC} = 4.5 Hz), 21.39 (s), 16.40 (d, J_{PC} = 5.5 Hz); **HRMS** (TOF MS ES+): Calc. for C$_{33}$H$_{52}$O$_9$PBrN [M+H$^+$+NEt$_3$]: 716.2563; Found: 716.2544.

7-Bromo-10-(diethoxyphosphoryl)-6-formyl-1,3-dimethoxyanthracene (2b):
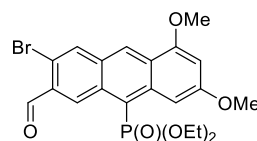
R_f = 0.68 (EtOAc), orange solid, m.p. = 188-190 °C, 90 % yield; **¹H NMR** (400 MHz, C$_6$D$_6$) δ 10.51 (s, 1H), 10.06 (s, 1H), 9.34 (s, 1H), 8.78 (s, 1H), 7.80 (d, J = 2.2 Hz, 1H), 6.43 (d, J = 2.1 Hz, 1H), 4.18 (ddd, J = 10.2, 8.4, 7.0 Hz, 2H), 3.93 (ddd, J = 10.2, 8.5, 7.0 Hz, 2H), 3.84 (s, 3H), 3.33 (s, 3H), 1.03 (t, J = 7.1 Hz, 6H); **³¹P NMR** (162 MHz, C$_6$D$_6$) δ 18.46; **¹³C{¹H} NMR** (101 MHz, C$_6$D$_6$) δ 191.06 (s), 160.63 (s), 156.62 (d, J_{PC} = 2.6 Hz), 139.09 (d, J_{PC} = 13.4 Hz), 134.18 (s), 133.25 (d, J_{PC} = 4.2 Hz), 133.14 (s), 132.11 (d, J_{PC} = 13.7 Hz), 131.63 (s), 124.70 (d, J_{PC} = 16.3 Hz), 120.47 (d, J_{PC} = 16.3 Hz), 120.47 (d, J_{PC} = 179.1 Hz), 117.82 (s), 99.36 (s), 97.58 (d, J_{PC} = 3.7 Hz), 62.18 (d, J_{PC} = 5.4 Hz), 55.59 (s), 55.28 (s), 16.39 (d, J_{PC} = 6.2 Hz); **HRMS** (TOF MS ES+): Calc. for C$_{21}$H$_{23}$O$_6$PBr [M+H$^+$]: 481.0416; Found: 481.0425.

Diethyl ((4-bromo-2,5-di(1,3-dioxan-2-yl)phenyl)(3,5-dimethylphenyl)methyl) phosphonate (4c):
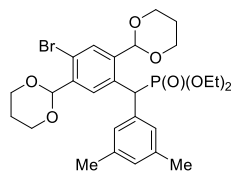
R_f = 0.47 (EtOAc), white solid, m.p. = 158-160 °C, 42 % yield; **^{1}H NMR** (400 MHz, C6D6) δ 8.99 (d, *J* = 2.0 Hz, 1H), 8.30 (d, *J* = 1.2 Hz, 1H), 7.54 (s, 1H), 6.68 (s, 1H), 5.73 (s, 1H), 5.69 (s, 1H), 5.34 (d, *J* = 26.0 Hz, 1H), 4.04 - 3.90 (m, 3H), 3.89 – 3.80 (m, 4H), 3.73 – 3.68 (m, 1H), 3.52 – 3.43 (m, 3H), 3.31 – 3.25 (m, 1H), 2.09 (s, 6H), 1.86 – 1.72 (m, 2H), 0.94 (dt, *J* = 12.0, 7.1 Hz, 6H), 059 – 0.53 (m, 2H); **^{31}P NMR** (162 MHz, C6D6) δ 25.66; **^{13}C{^{1}H} NMR** (101 MHz, C_6D_6) δ 139.86 (d, J_{PC} =10.6 Hz), 138.72 (s), 137.97 (s), 137.19 (d, J_{PC} = 5.6 Hz), 135.48 (d, J_{PC} = 4.1 Hz), 131.47 (s), 131.21 (d, J_{PC} = 5.5 Hz), 129.11 (d, J_{PC} = 2.4 Hz), 121.74 (d, J_{PC} = 2.3 Hz), 101.21 (s), 98.83 (s), 67.37 (d, J_{PC} = 4.2 Hz), 67.15 (d, J_{PC} = 28.8 Hz), 62.92 (d, J_{PC} = 6.8 Hz), 62.40 (d, J_{PC} = 6.7 Hz), 46.01 (d, J_{PC} = 138.4 Hz), 25.68 (d, J_{PC} = 4.5 Hz), 21.39 (s), 16.40 (d, J_{PC} = 5.5 Hz); **HRMS** (TOF MS ES+): Calc. for $C_{27}H_{37}O_4PBr$ [M+H^{+}]: 583.1460; Found: 583.1464.
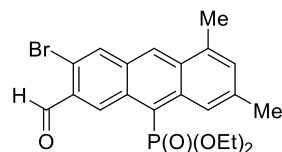
7-Bromo-10-(diethoxyphosphoryl)-6-formyl-1,3-dimethylanthracene (2c):

R_f = 0.75 (EtOAc), yellow solid, m.p. = 180-182 °C, 94 % yield; **^{1}H NMR** (400 MHz, C_6D_6) δ 10.51 (s, 1H), 10.30 (s, 1H), 9.86 (s, 1H), 8.15 (d, *J* = 2.0 Hz, 1H), 7.80 (d, *J* = 2.3 Hz, 1H), 6.90 (s, 1H), 4.20 - 4.12 (m, 2H), 3.97 - 3.87 (m, 2H), 2.40 (s, 3H), 2.33 (s, 3H), 1.01 (t, *J* = 7.1 Hz, 6H); **^{31}P NMR** (162 MHz, C_6D_6) δ 17.54; **^{13}C{^{1}H} NMR** (101 MHz, C_6D_6) δ 190.87 (s), 138.15 (s), 137.25 (d, J_{PC} = 12.1 Hz), 134.37 (d, J_{PC} = 4.0 Hz), 133.91 (s), 132.98 (d, J_{PC} = 14.5 Hz), 132.23 (d, J_{PC} = 9.9 Hz), 131.96 (d, J_{PC} = 15.1 Hz), 131.38 (s), 130.52 (s), 129 (d, J_{PC} = 3.9 Hz), 128.35 (s), 125.49 (d, J_{PC} = 4.4 Hz), 123.93 (d, J_{PC} = 177.1 Hz), 118.32 (s), 62.30 (d, J_{PC} = 5.4 Hz), 22.69 (s), 19.91 (s), 16.39 (d, J_{PC} = 6.2 Hz); **HRMS** (TOF MS ES+): Calc. for $C_{21}H_{23}O_4PBr$ [M+H^{+}]: 449.0517; Found: 449.0519.
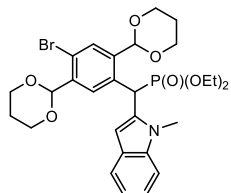
Diethyl ((4-bromo-2,5-di(1,3-dioxan-2-yl)phenyl)(1-methyl-1*H*-indol-2-yl)methyl) phosphonate (4d):

R_f = 0.52 (EtOAc), white solid, m.p. = 176-178 °C, 38 % yield; **^{1}H NMR** (400 MHz, CD$_2$Cl$_2$) δ 7.91 (s, 1H), 7.80 (d, J = 2.6 Hz, 1H), 7.65 (d, J = 7.9 Hz, 1H), 7.30 (d, J = 8.2 Hz, 1H), 7.22 (dd, J = 8.2 Hz, J = 6.9 Hz, J = 1.2 Hz, 1H), 7.12 (ddd, J = 7.9 Hz, J = 6.9 Hz, J = 1.2 Hz, 1H), 6.98 (s, 1H), 5.99 (s, 1H), 5.65 (s, 1H), 5.21 (d, J = 25.7 Hz, 1H), 3.80 – 4.42 (m, 12H), 3.60 (s, 3H), 2.13 - 2.35 (m, 2H), 1.49 - 1.59 (m, 1H), 1.37 - 1.45 (m, 1H), 1.27 (t, J = 7.1 Hz, 3H), 1.23 (t, J = 7.1 Hz, 3H); **^{31}P NMR** (162 MHz, CD$_2$Cl$_2$) δ 22.53; **^{13}C{^{1}H} NMR** (101 MHz, CD$_2$Cl$_2$) δ 139.41 (d, J_{PC} = 7.0 Hz), 138.46 (d, J_{PC} = 3.1 Hz), 137.90 (s), 134.62 (s), 132.58 (d, J_{PC} = 6.7 Hz), 131.48 (d, J_{PC} = 2.4 Hz), 130.38 (d, J_{PC} =4.7 Hz), 127.97 (s), 122.02 (s), 121.98 (s), 120.97 (s), 119.92 (s), 109.73 (s), 104.22 (d, J_{PC} = 4.1 Hz), 101.08 (s), 99.04 (s), 68.13 (s), 68.07 (s), 67.10 (s), 63.51 (d, J_{PC} = 7.0 Hz), 63.05 (d, J_{PC} = 7.0 Hz), 38.74 (d, J_{PC} = 141.5 Hz), 30.21 (s), 26.13 (d, J_{PC} = 4.3 Hz), 16.70 (d, J_{PC} = 5.8 Hz), 16.53 (d, J_{PC} = 6.4 Hz); **HRMS** (TOF MS ES+): *m/z* Calc. for C$_{28}$H$_{36}$BrNO$_7$P [M+H$^+$]: 608.1413, Found: 608.1422.

9-Bromo-6-(diethoxyphosphoryl)-8-formyl-5*N*-methylbenzo[b]carbazole (2d):
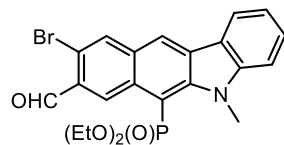
R_f = 0.54 (EtOAc), yellow solid, m.p. = 194-196 °C, 90 % yield; **^{1}H NMR** (400 MHz, CD$_2$Cl$_2$) δ 10.49 (s, 1H), 9.41 (s, 1H), 8.58 (d, J = 2.1 Hz, 1H), 8.28 (d, J = 2.1 Hz, 1H), 8.18 (d, J = 7.5 Hz, 1H), 7.64 (ddd, J = 8.2, J = 7.5, J = 1.2 Hz, 1H), 7.45 (d, J = 8.2 Hz, 1H), 7.35 (ddd, J = 8.2 Hz, J = 7.5 Hz, J = 1.1 Hz, 1H), 4.19 (dd, J = 10.3 Hz, J = 7.2 Hz, 2H), 4.09 (s, 3H), 4.00 - 4.12 (m, 2H), 1.31 (t, J = 7.1 Hz, 6H); **^{31}P NMR** (162 MHz, CD$_2$Cl$_2$) δ 16.22; **^{13}C{^{1}H} NMR** (101 MHz, CD$_2$Cl$_2$) δ 192.36 (s), 147.74 (d, J_{PC} = 4.2 Hz), 147.02 (s), 133.38 (s), 132.60 (d, J_{PC} = 8.9), 132.17 (d, J_{PC} = 4.5 Hz), 131.98 (d, J_{PC} = 11.7 Hz), 131.08 (d, J_{PC} = 11.4 Hz), 130.24 (s), 129.95 (s), 123.11 (d, J_{PC} = 3.4 Hz), 122.23 (s), 121.44 (s), 117.38 (s), 110.72 (s), 103.69 (d, J_{PC} = 189.4 Hz), 63.04 (s), 62.99 (s), 37.30 (s), 16.54 (d, J_{PC} = 6.6 Hz); **HRMS** (TOF MS ES+): *m/z* Calc. for C$_{22}$H$_{22}$BrNO$_4$P [M+H$^+$]: 474.0470, Found: 474.0465.

3.8.3 NMR spectra of anthracene derivatives
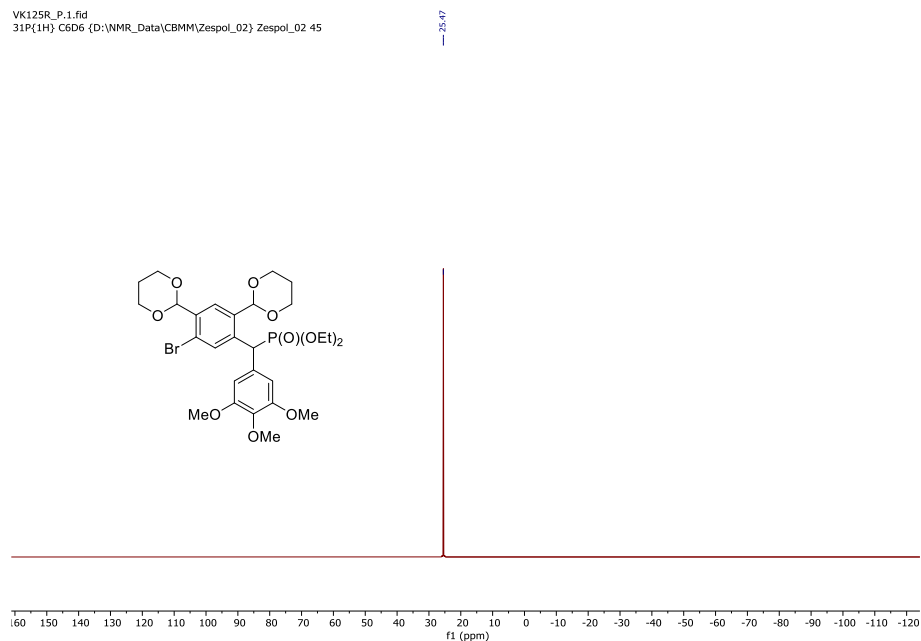
Figure S1. ^{31}P (162 MHz, C$_6$D$_6$) NMR spectrum of **3a**.
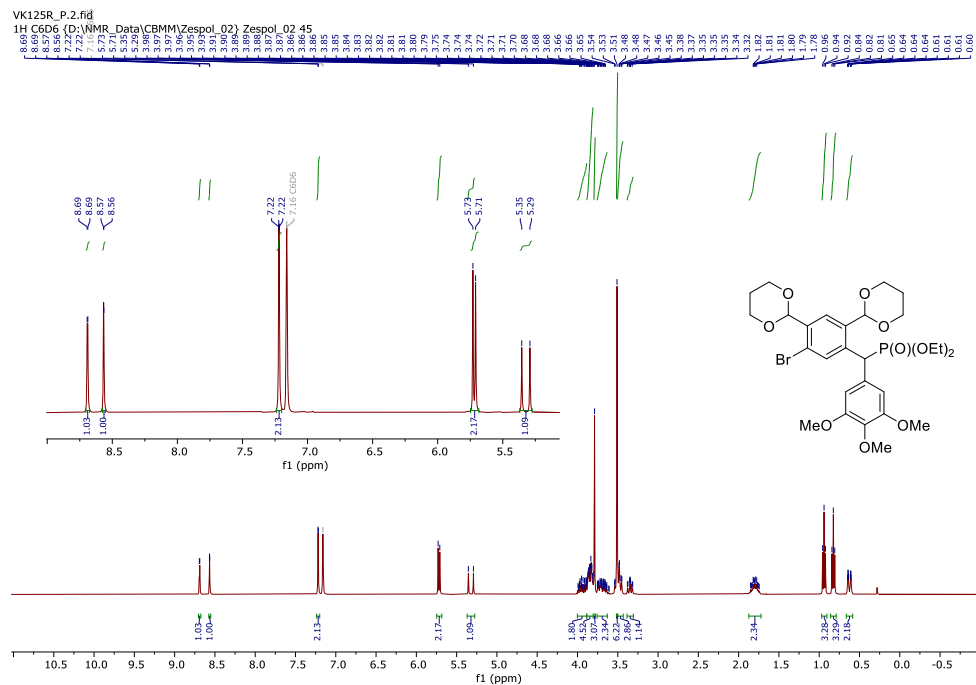
Figure S2. ^{1}H (400 MHz, C$_6$D$_6$) NMR spectrum of **3a**.
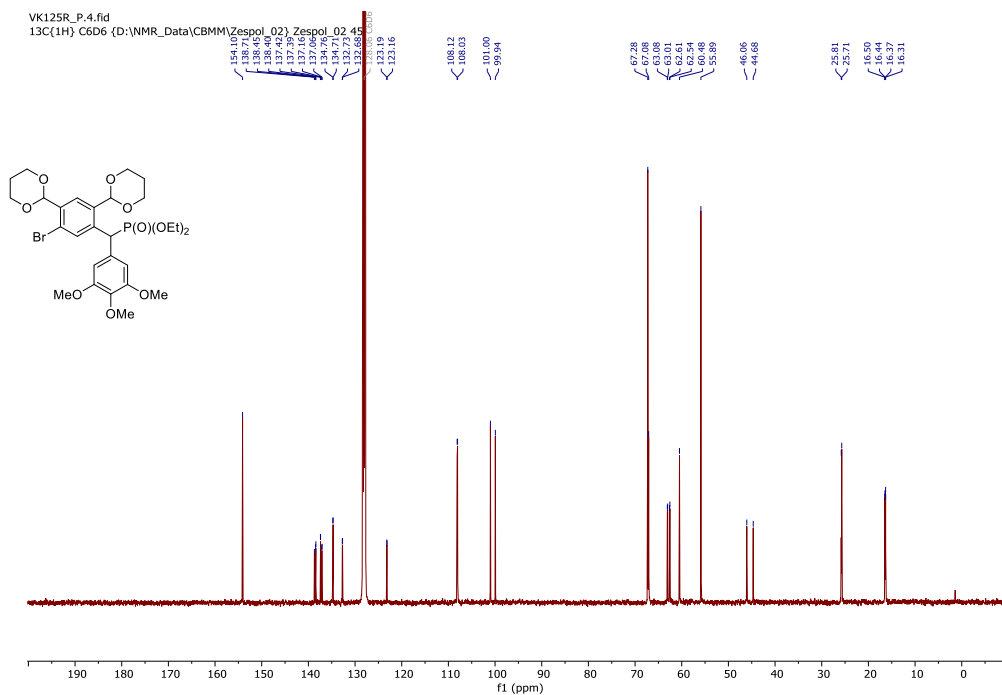
Figure S3. $^{13}C\{^1H\}$ (101 MHz, C_6D_6) NMR spectrum of **3a**.
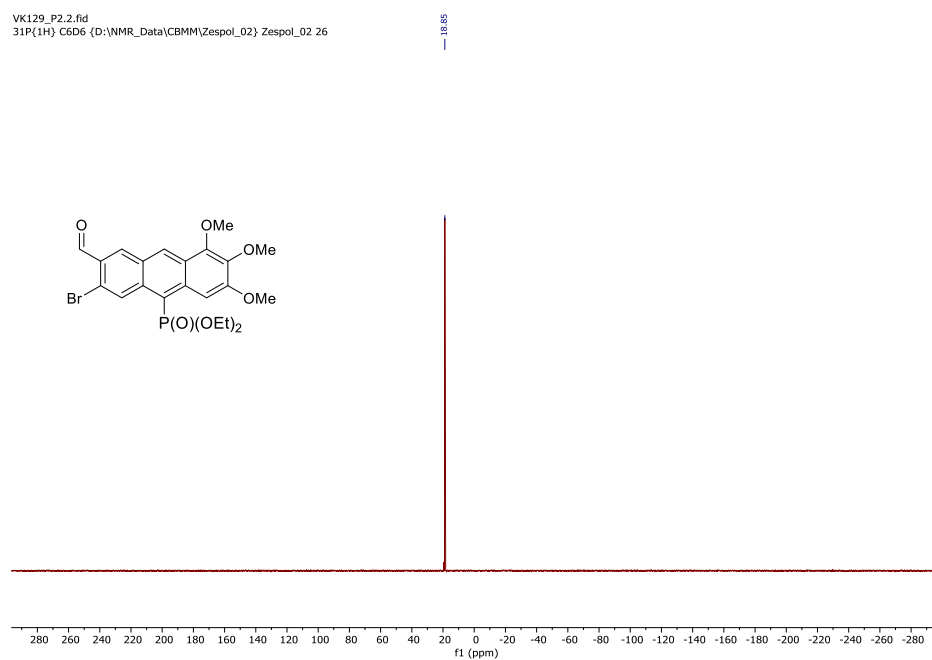
Figure S4. ^{31}P (162 MHz, C_6D_6) NMR spectrum of **1a**.
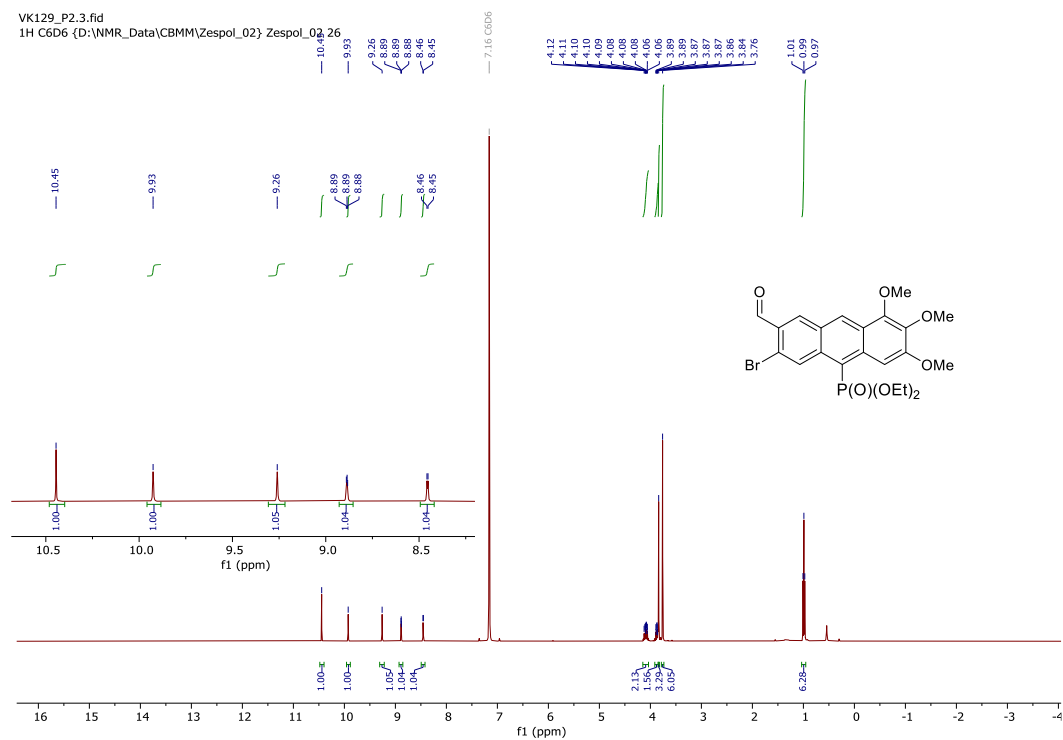
Figure S5. ^{1}H (400 MHz, C$_6$D$_6$) NMR spectrum of **1a**.
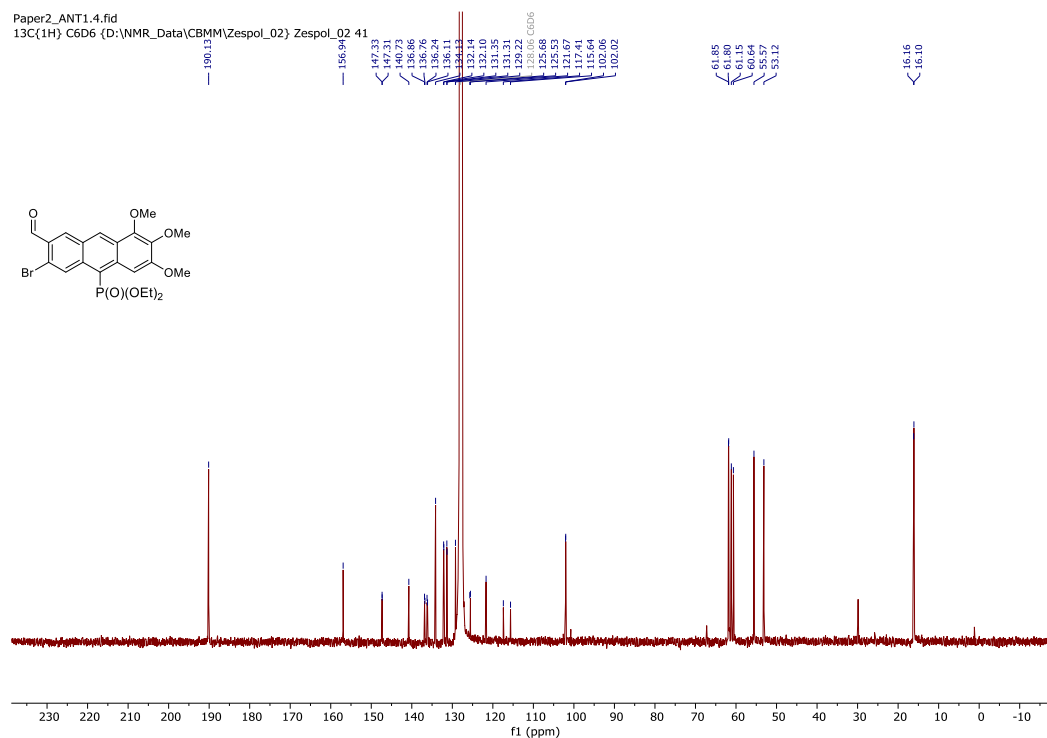
Figure S6. ^{13}C{^{1}H} (101 MHz, C$_6$D$_6$) NMR spectrum of **1a**.

VK139_P2.2.fid
31P{1H} C6D6 {D:\NMR_Data\CBMM\Zespol_02} Zespol_02 59

— 25.28

Figure S7. ^{31}P (162 MHz, C$_6$D$_6$) NMR spectrum of **3b**.

VK139_P2.3.fid
1H C6D6 {D:\NMR_Data\CBMM\Zespol_02} Zespol_02 59

Figure S8. ^{1}H (400 MHz, C$_6$D$_6$) NMR spectrum of **3b**.

84
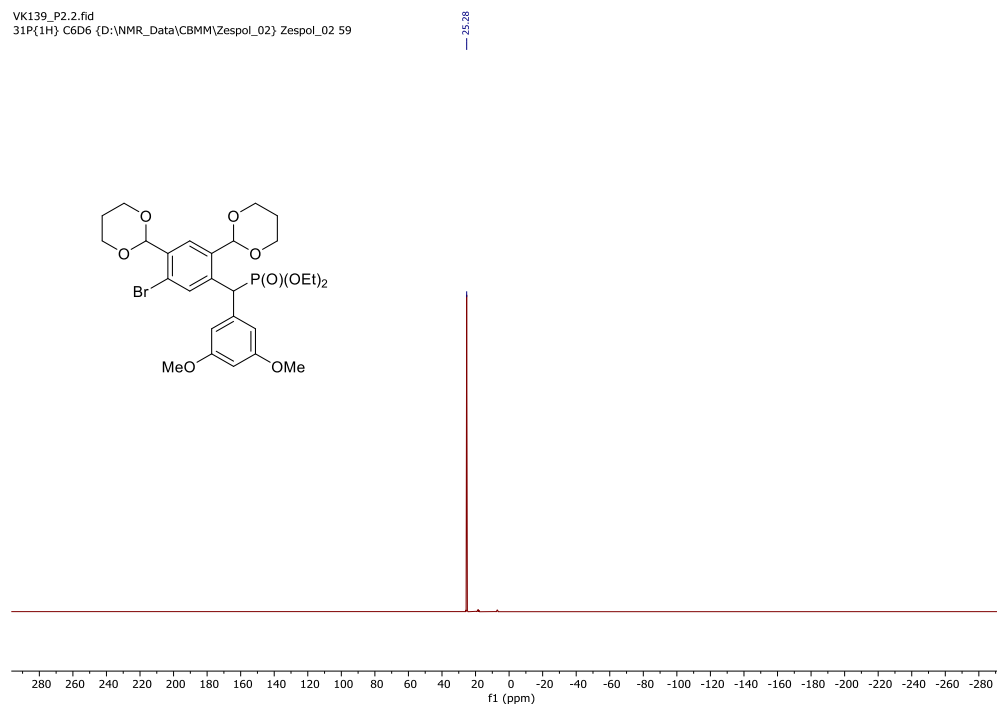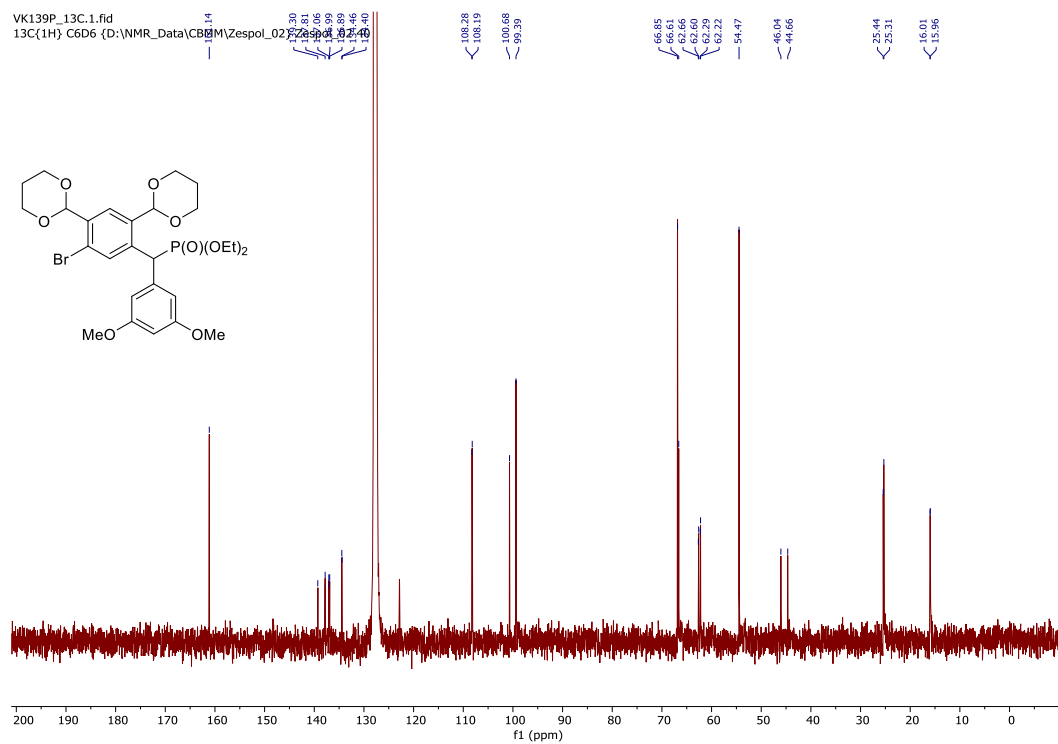
Figure S9. $^{13}C\{^1H\}$ (101 MHz, C_6D_6) NMR spectrum of **3b**.
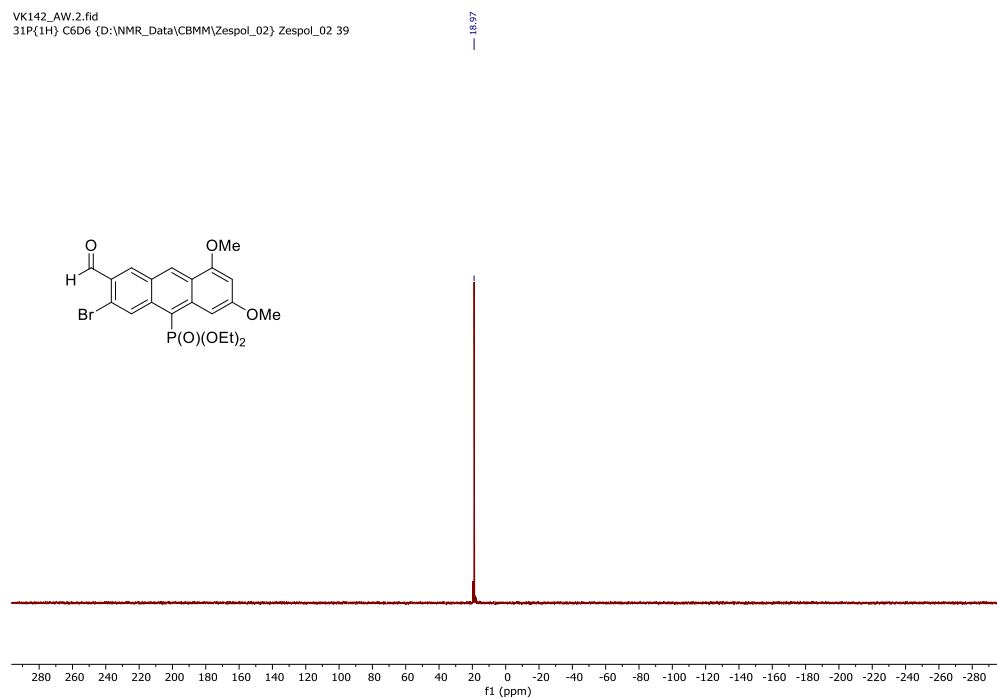
Figure S10. ^{31}P (162 MHz, C_6D_6) NMR spectrum of **1b**.
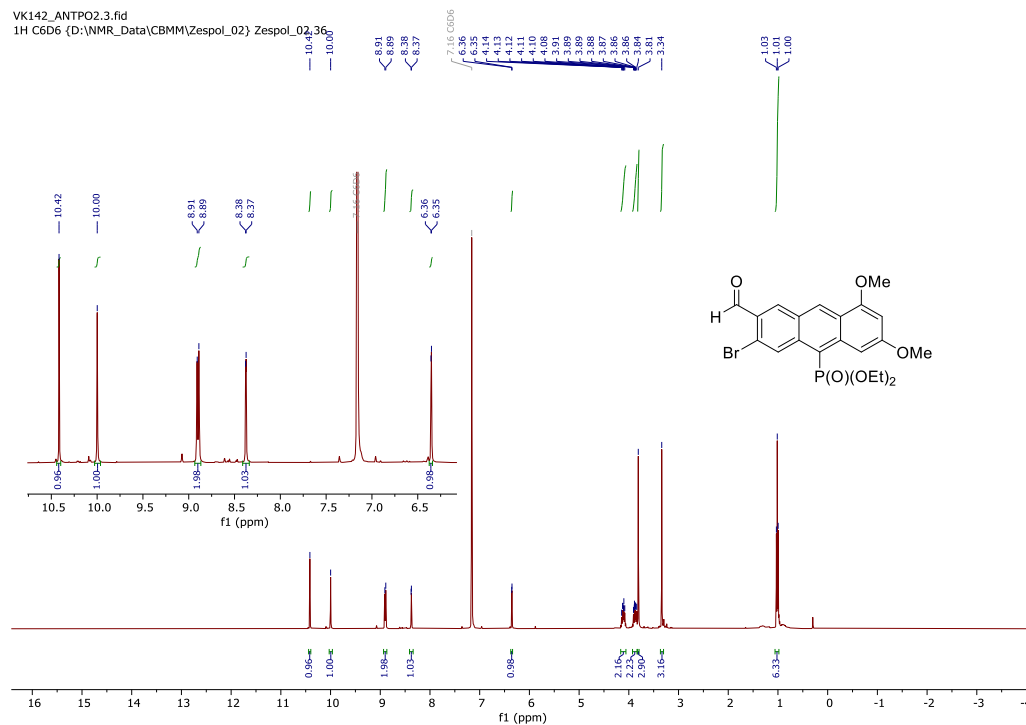
Figure S11. ^{1}H (400 MHz, C$_6$D$_6$) NMR spectrum of **1b**.
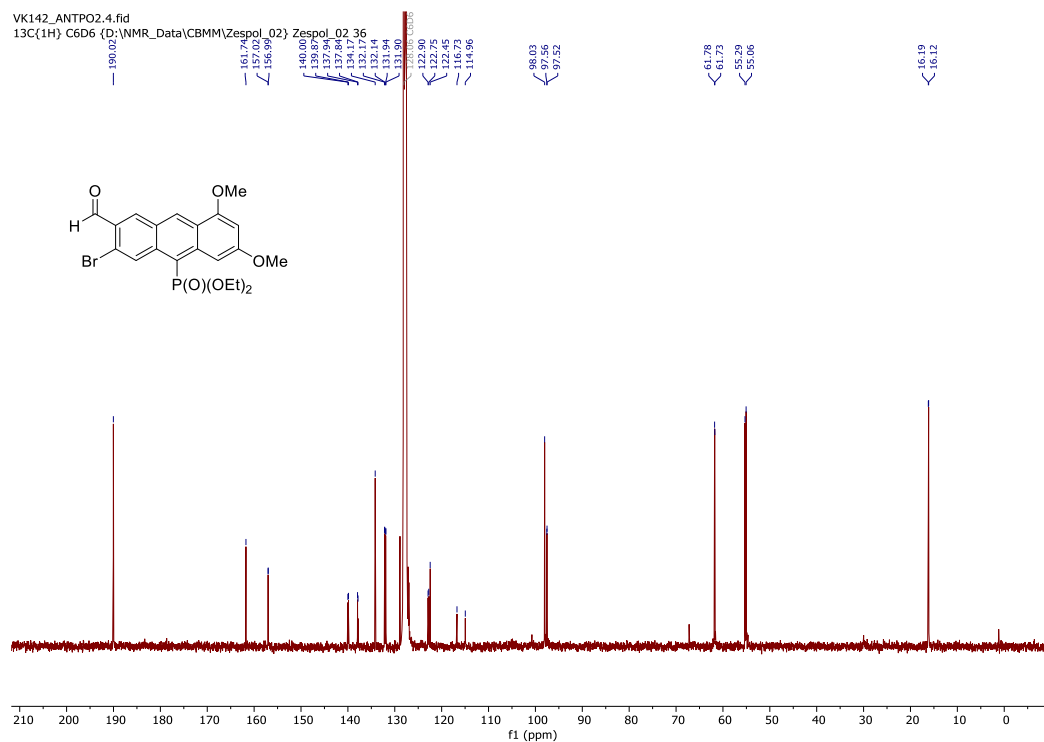
Figure S12. ^{13}C{^{1}H} (101 MHz, C$_6$D$_6$) NMR spectrum of **1b**.

VK167F_DCM.2.fid
31P{1H} CD2Cl2 {D:\NMR_Data\CBMM\Zespol_02} Zespol_02 50

— 24.74
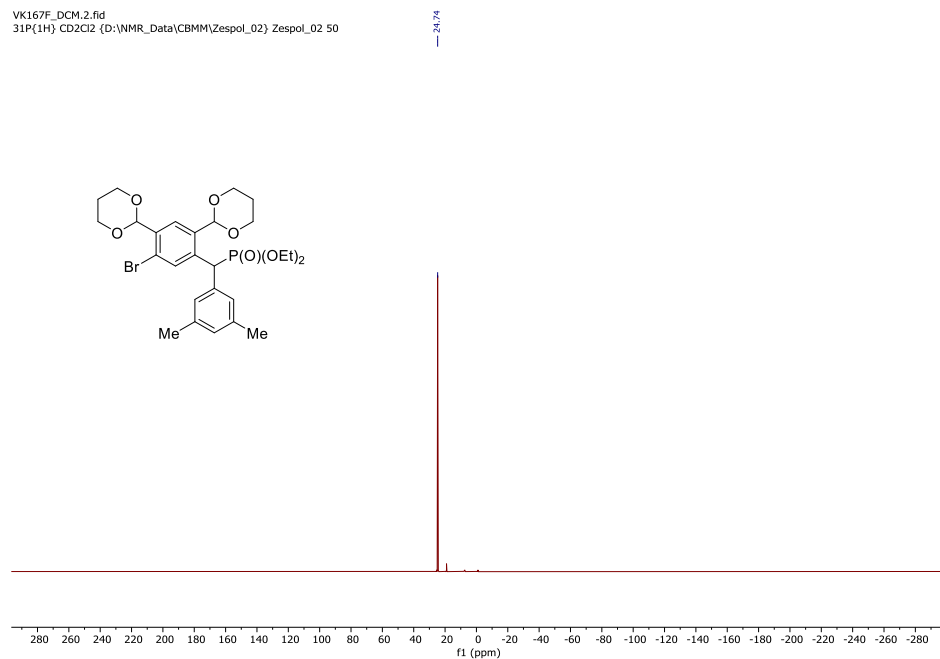
Figure S13. ^{31}P (162 MHz, CD$_2$Cl$_2$) NMR spectrum of **3c**.

VK167F_DCM.3.fid
1H CD2Cl2 {D:\NMR_Data\CBMM\Zespol_02} Zespol_02 50
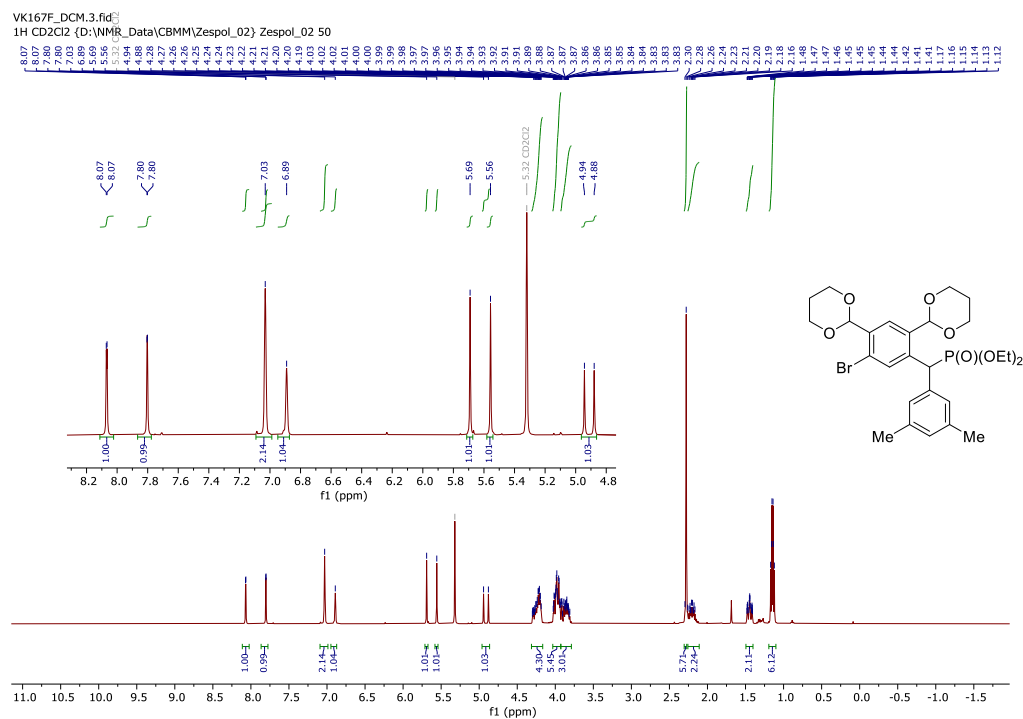
Figure S14. ^{1}H (400 MHz, CD$_2$Cl$_2$) NMR spectrum of **3c**.

VK167F_DCM.5.fid
13C{1H} CD2Cl2 {D:\NMR_Data\CBMM\Zespol_02} Zespol_02 50

Figure S15. $^{13}C\{^{1}H\}$ (101 MHz, CD$_2$Cl$_2$) NMR spectrum of **3c**.

VK172_P.2.fid
31P{1H} CD2Cl2 {D:\NMR_Data\CBMM\Zespol_02} Zespol_02 42
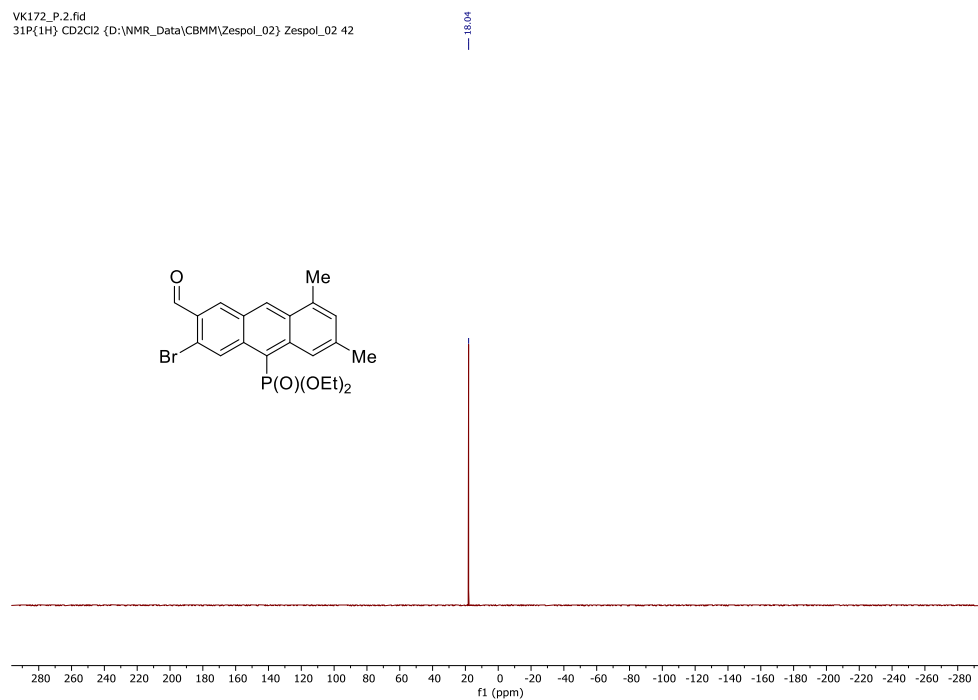
Figure S16. ^{31}P (162 MHz, CD$_2$Cl$_2$) NMR spectrum of **1c**.
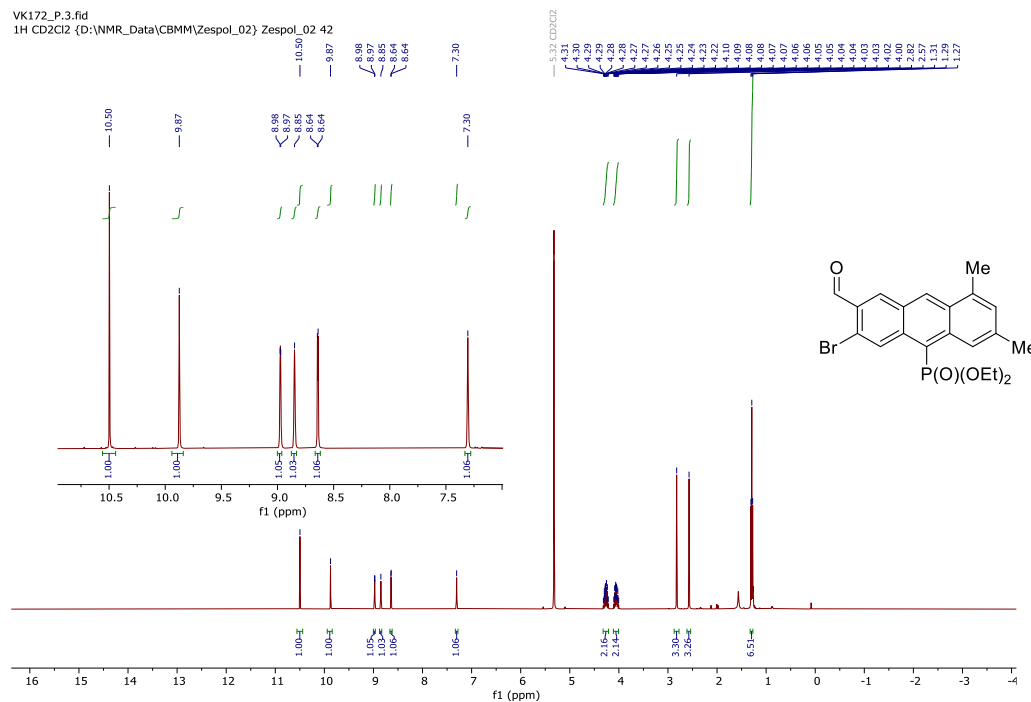
Figure S17. ^{1}H (400 MHz, CD$_2$Cl$_2$) NMR spectrum of **1c**.
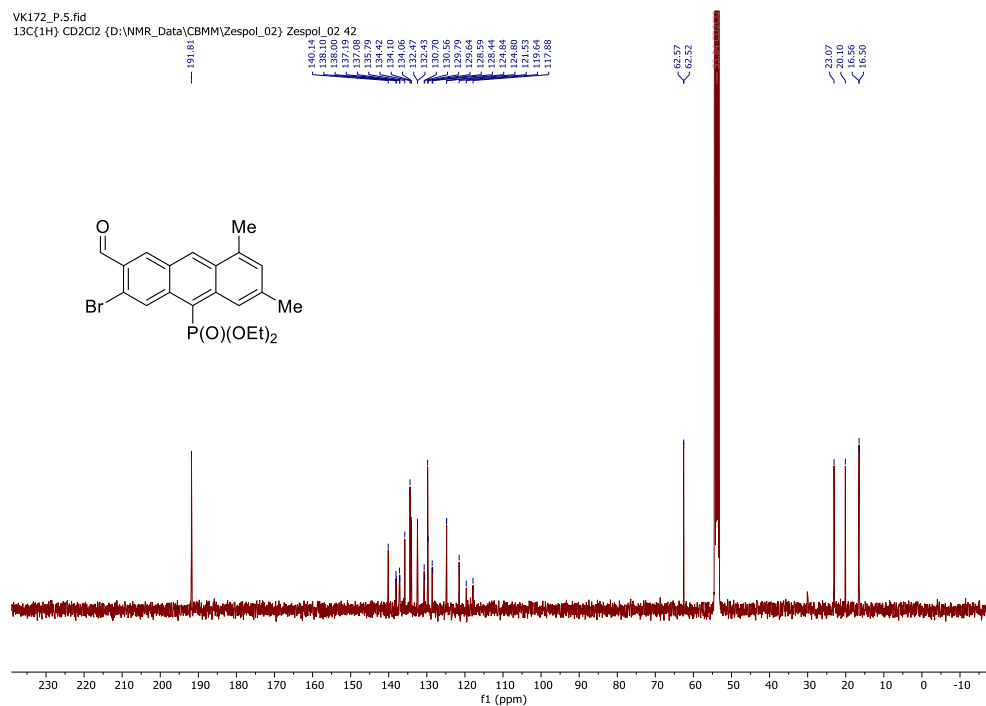
Figure S18. ^{13}C{^{1}H} (101 MHz, CD$_2$Cl$_2$) NMR spectrum of **1c**.

VK147_P2R2.2.fid
31P{1H} CD2Cl2 {D:\NMR_Data\CBMM\Zespol_02} Zespol_02 48

22.49

Figure S19. ^{31}P (162 MHz, CD$_2$Cl$_2$) NMR spectrum of **3d**.

VK147_Final.3.fid
1H CD2Cl2 {D:\NMR_Data\CBMM\Zespol_02} Zespol_02 48

Figure S20. ^{1}H (400 MHz, CD$_2$Cl$_2$) NMR spectrum of **3d**.

VK147_Final.4.fid
13C{1H} CD2Cl2 {D:\NMR_Data\CBMM\Zespol_02} Zespol_02 48

Figure S21. $^{13}C\{^1H\}$ (101 MHz, CD$_2$Cl$_2$) NMR spectrum of **3d**.

VKANT3_Paper 2.2.fid
31P{1H} CD2Cl2 {D:\NMR_Data\CBMM\Zespol_02} Zespol_02 30

Figure S22. ^{31}P (162 MHz, CD$_2$Cl$_2$) NMR spectrum of **1d**.

VKANTPO_3_P.3.fid
1H CD2Cl2 {D:\NMR_Data\CBMM\Zespol_02} Zespol_02 28

Figure S23. ^{1}H (400 MHz, CD$_2$Cl$_2$) NMR spectrum of **1d**.

VKANT3_Paper 2.5.fid
13C{1H} CD2Cl2 {D:\NMR_Data\CBMM\Zespol_02} Zespol_02 30
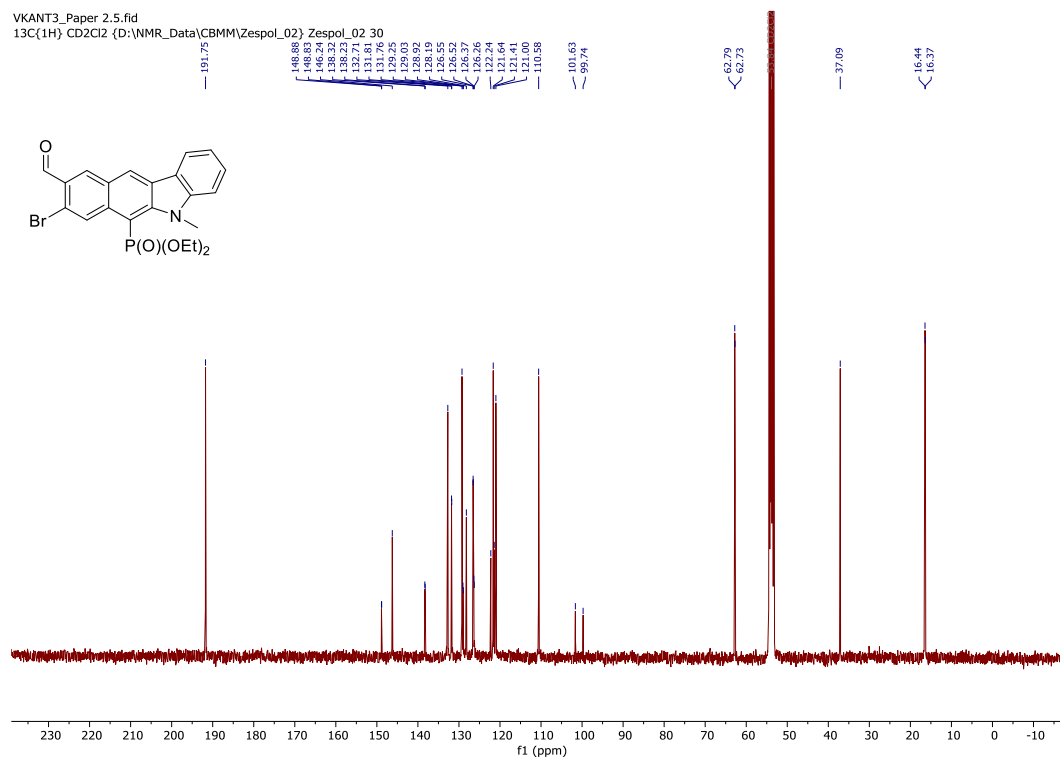
Figure S24. ^{13}C{^{1}H} (101 MHz, CD$_2$Cl$_2$) NMR spectrum of **1d**.
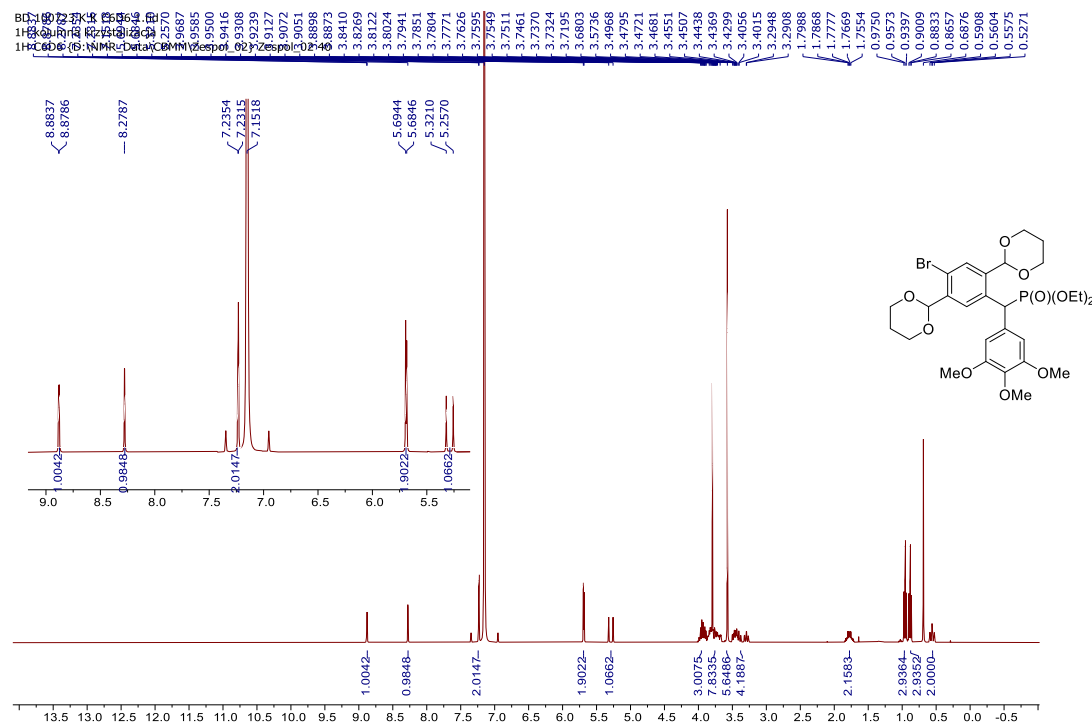
Figure S25. ^{1}H (400 MHz, C$_6$D$_6$) NMR spectrum of **4a**.
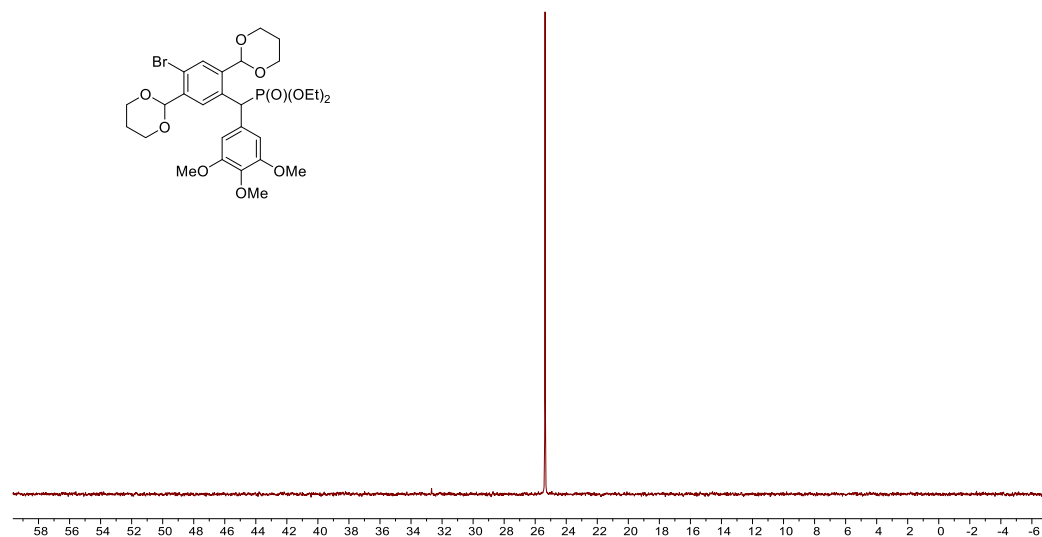
Figure S26. ^{31}P (162 MHz, C$_6$D$_6$) NMR spectrum of **4a**.

Figure S27. $^{13}C\{^1H\}$ (101 MHz, CDCl$_3$) NMR spectrum of **4a**.

Figure S28. ^1H (400 MHz, CDCl$_3$) NMR spectrum of **2a**.

MK 1490 H plus CDCl3.4.fid
31P{1H} kolumna
31P{1H} CDCl3 {D:\NMR_Data\CBMM\Zespol_02} Zespol_02 28

—18.4689
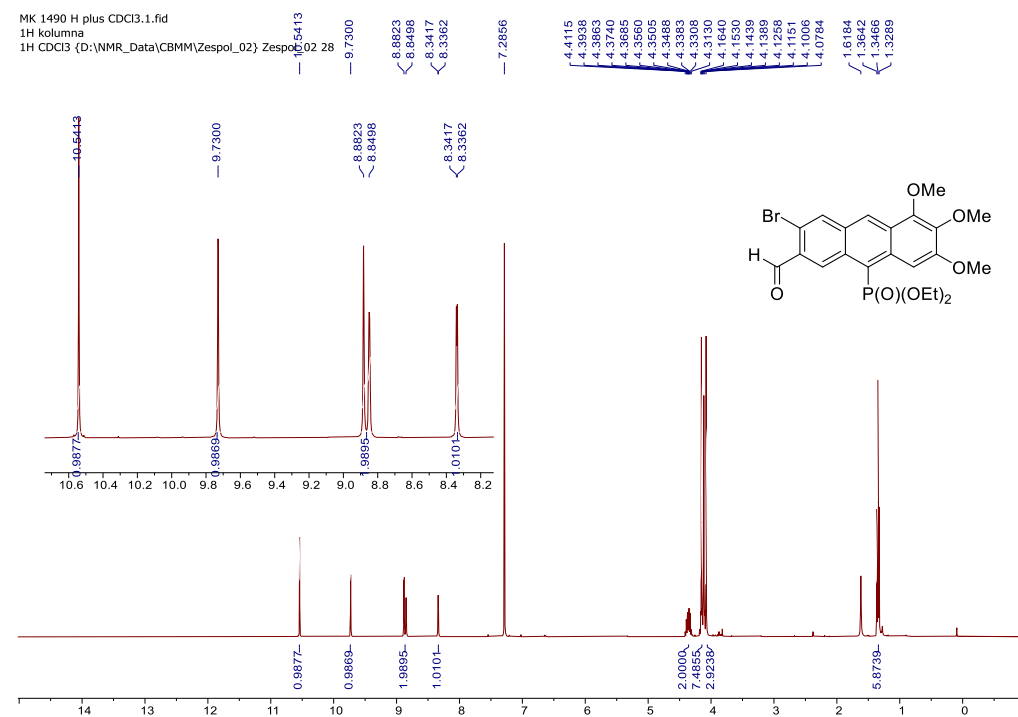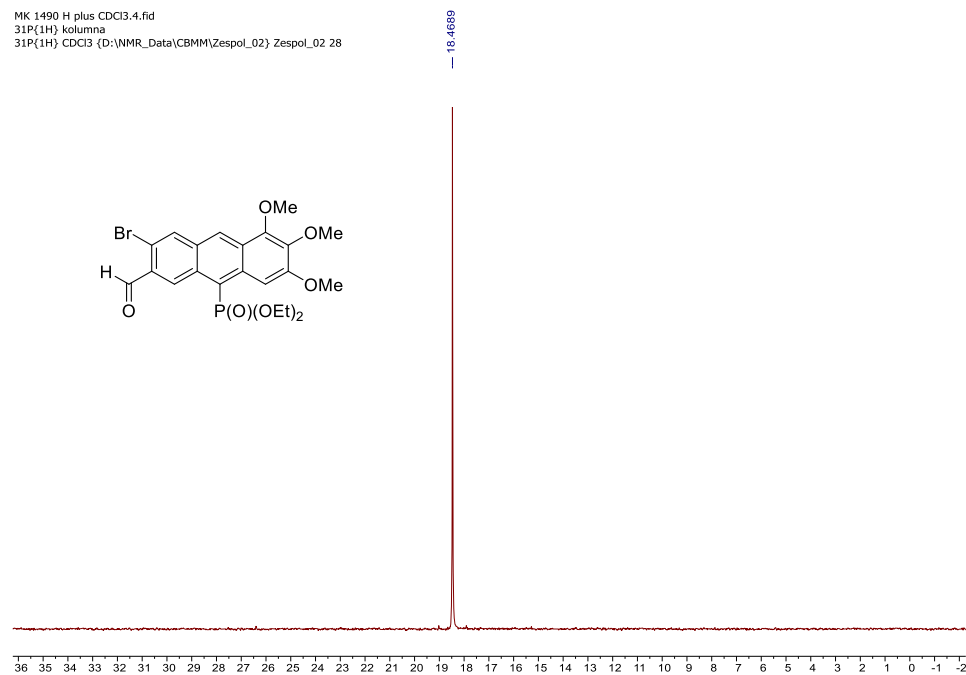
Figure S29. ^{31}P (162 MHz, CDCl$_3$) NMR spectrum of **2a**.

MK 1490 H 13C CDCl3.1.fid
13C kolumna
13C{1H} CDCl3 {D:\NMR_Data\CBMM\Zespol_02} Zespol_02
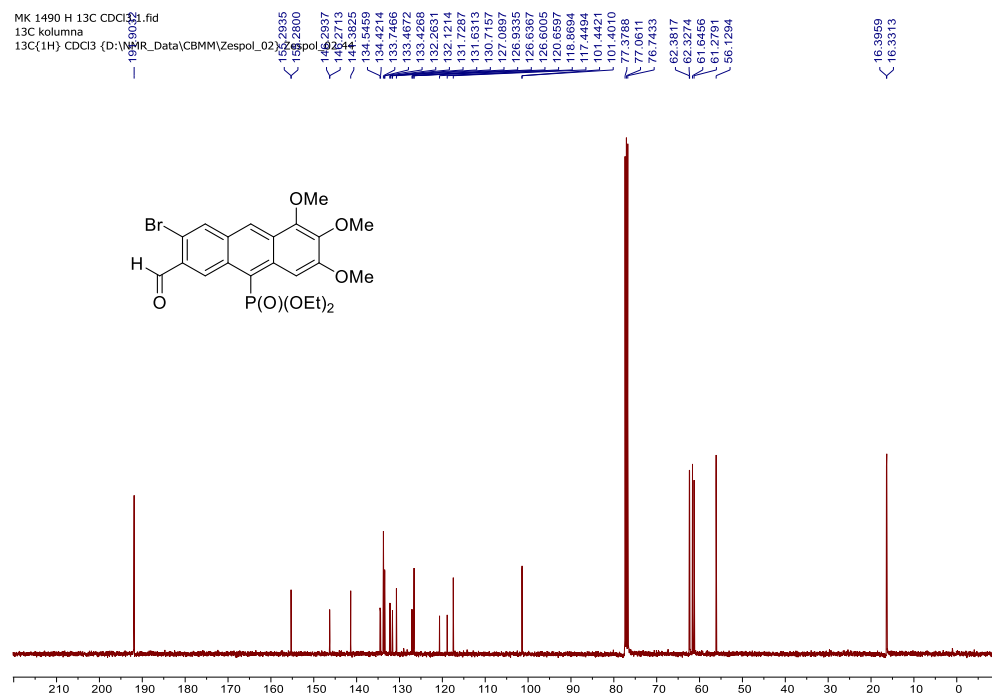
Figure S30. ^{13}C{^{1}H} (101 MHz, CDCl$_3$) NMR spectrum of **2a**.

VK192_Pentwash1.2.fid
31P{1H} CD2Cl2 {D:\NMR_Data\CBMM\Zespol_02} Zespol_02 56
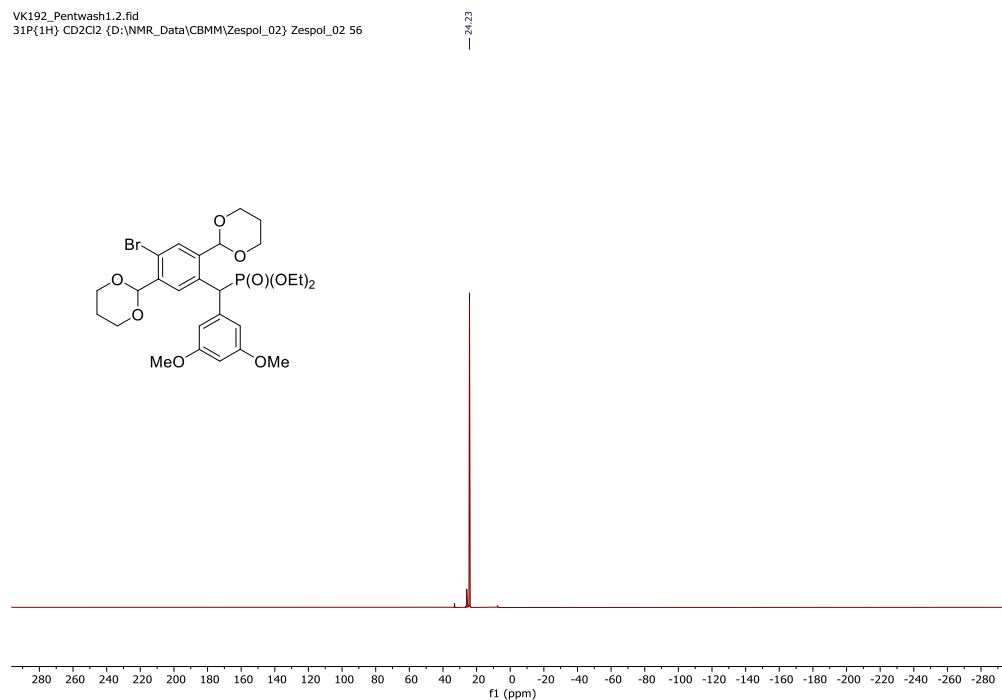
Figure S31. ^{31}P (162 MHz, CD$_2$Cl$_2$) NMR spectrum of **4b**.

VK192_Pentwash1.3.fid
1H CD2Cl2 {D:\NMR_Data\CBMM\Zespol_02} Zespol_02 56
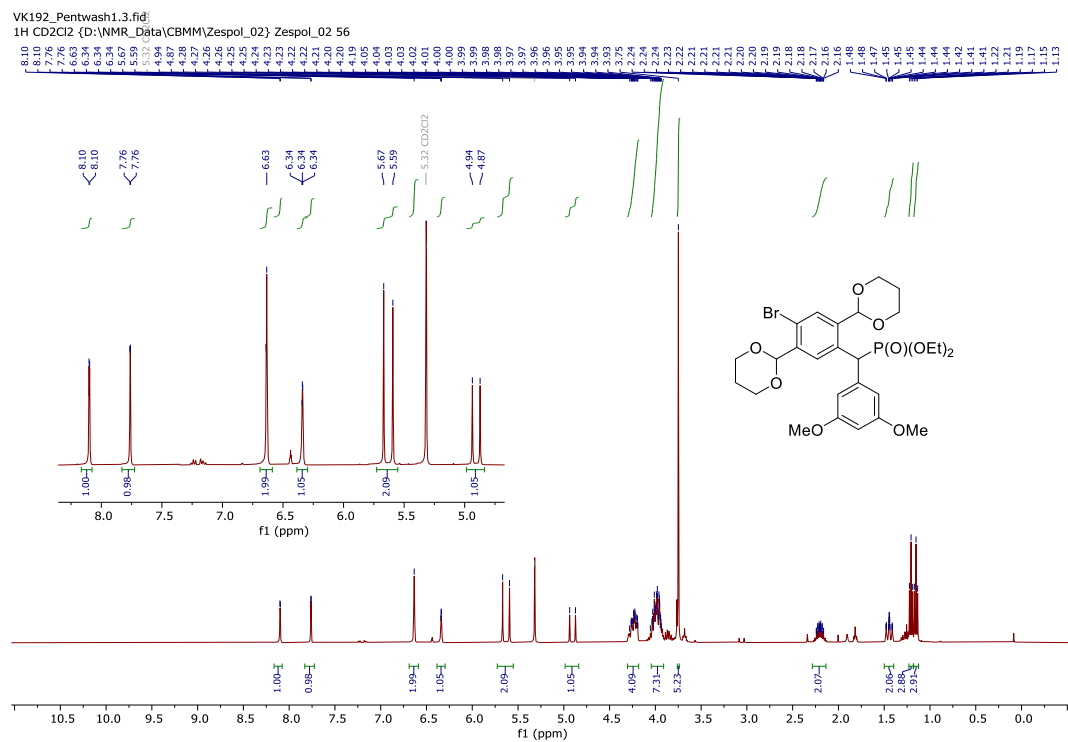
Figure S32. ^{1}H (400 MHz, CD$_2$Cl$_2$) NMR spectrum of **4b**.

VK192_PW_13C.1.fid
13C{1H} CD2Cl2 {D:\NMR_Data\CBMM\Zespol_02} Zespol_02 48
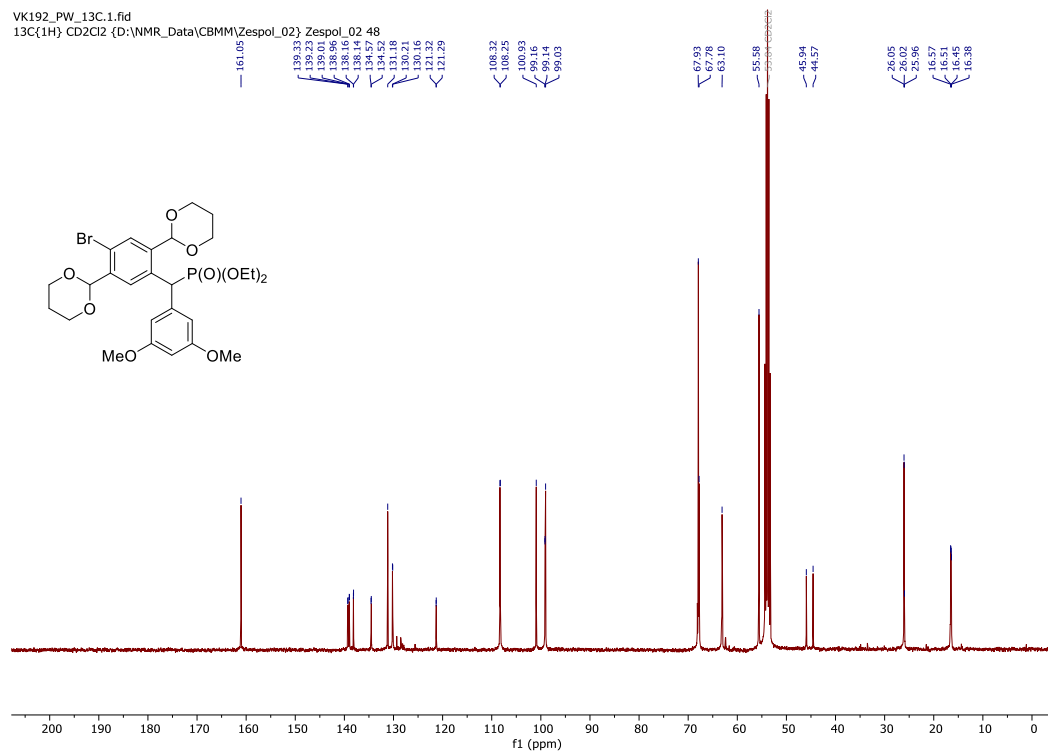
Figure S33. $^{13}C\{^1H\}$ (101 MHz, CD$_2$Cl$_2$) NMR spectrum of **4b**.

VK184_P2.2.fid
31P{1H} C6D6 {D:\NMR_Data\CBMM\Zespol_02} Zespol_02 36
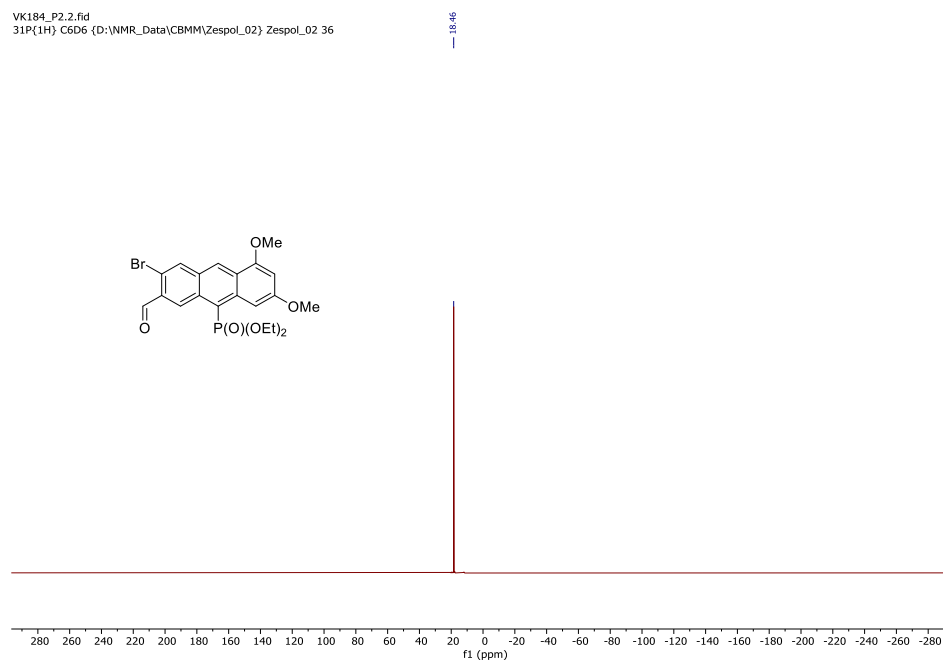
Figure S34. ^{31}P (162 MHz, C$_6$D$_6$) NMR spectrum of **2b**.
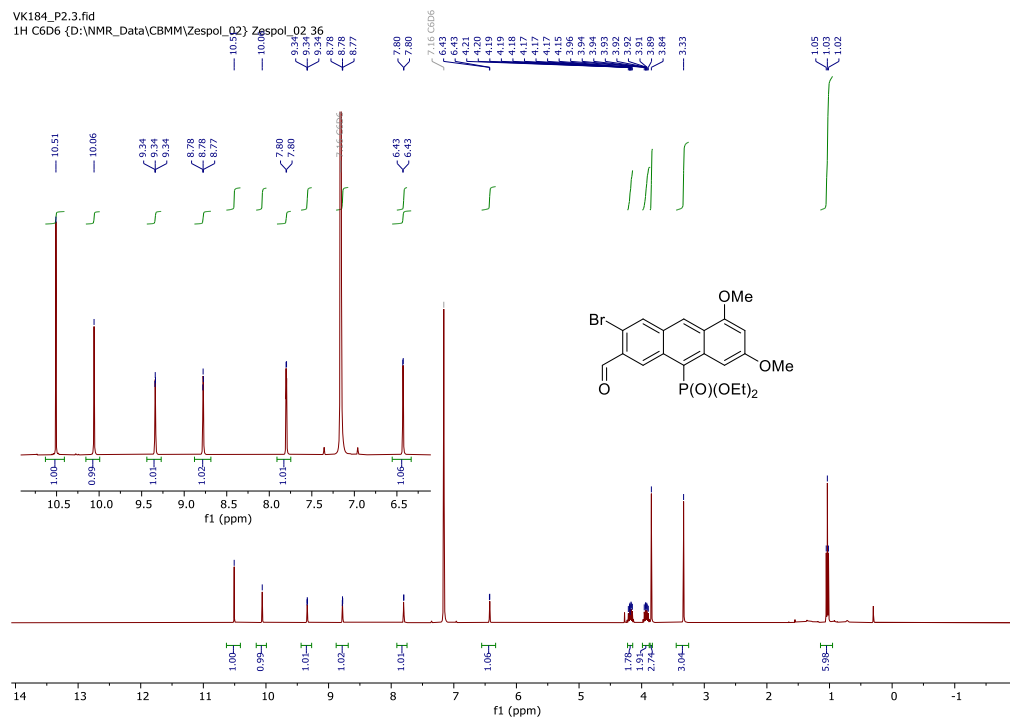
Figure S35. ^{1}H (400 MHz, C$_6$D$_6$) NMR spectrum of **2b**.
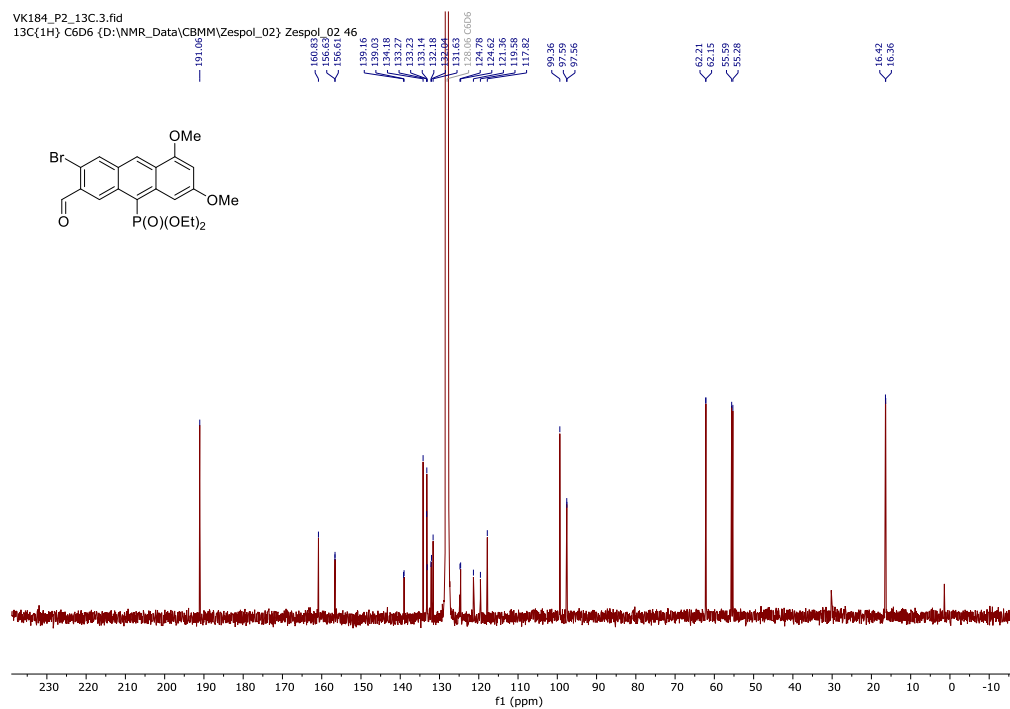
Figure S36. ^{13}C{^{1}H} (101 MHz, C$_6$D$_6$) NMR spectrum of **2b**.

VK203_P2.2.fid
31P{1H} C6D6 {D:\NMR_Data\CBMM\Zespol_02} Zespol_02 36

— 25.66
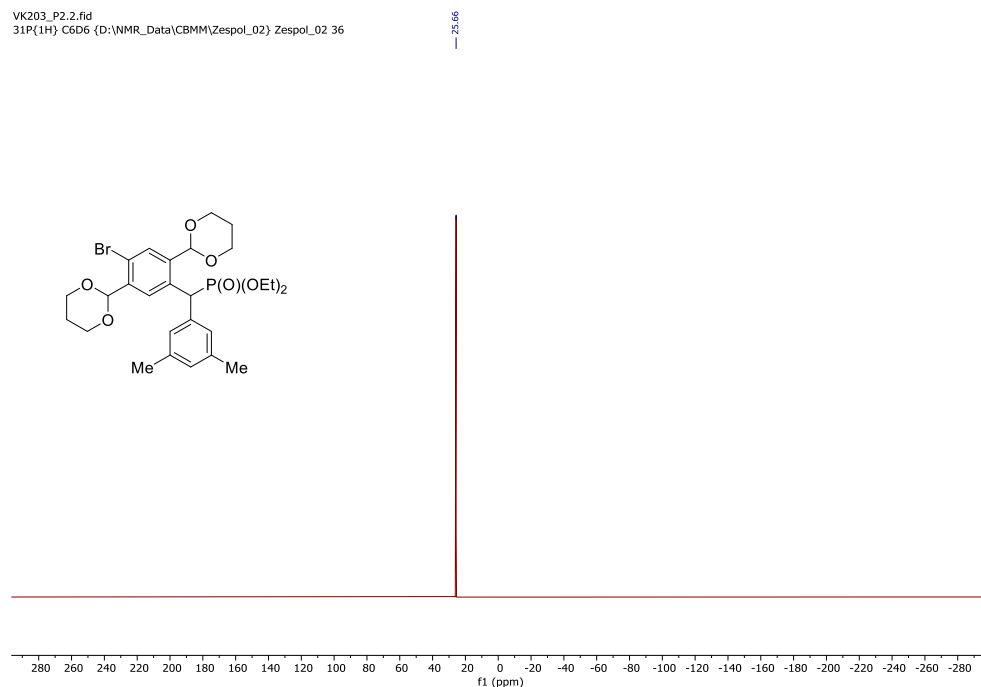
Figure S37. ^{31}P (162 MHz, C$_6$D$_6$) NMR spectrum of **4c**.

VK203_P2.3.fid
1H C6D6 {D:\NMR_Data\CBMM\Zespol_02} Zespol_02 36
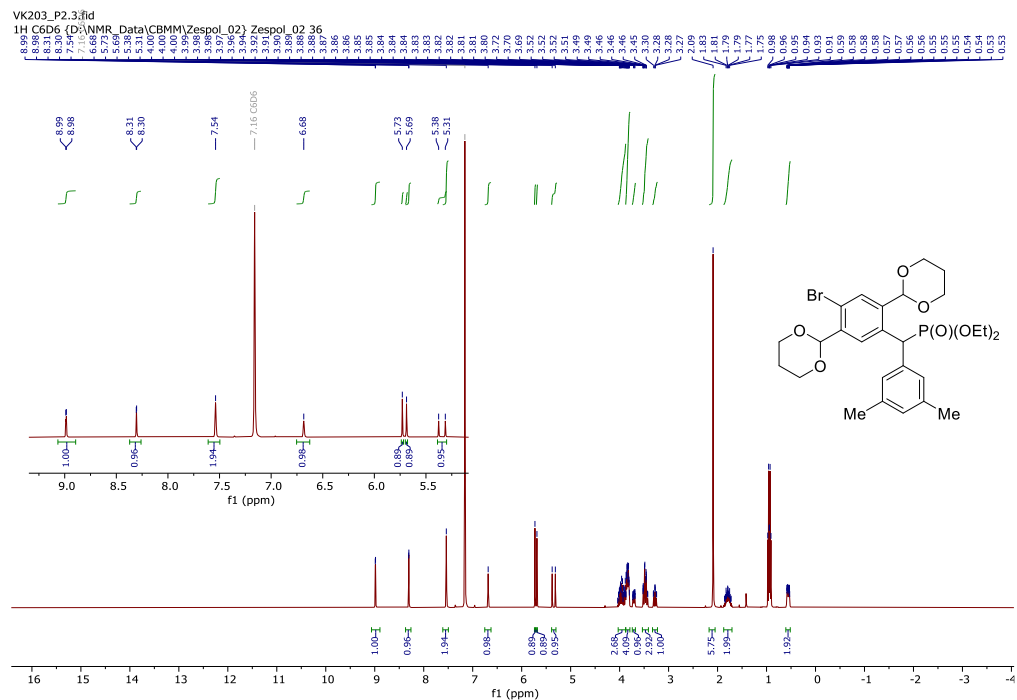
Figure S38. ^{1}H (400 MHz, C$_6$D$_6$) NMR spectrum of **4c**.

VK203_P2.5.fid
13C{1H} C6D6 {D:\NMR_Data\CBMM\Zespol_02} Zespol_02 36
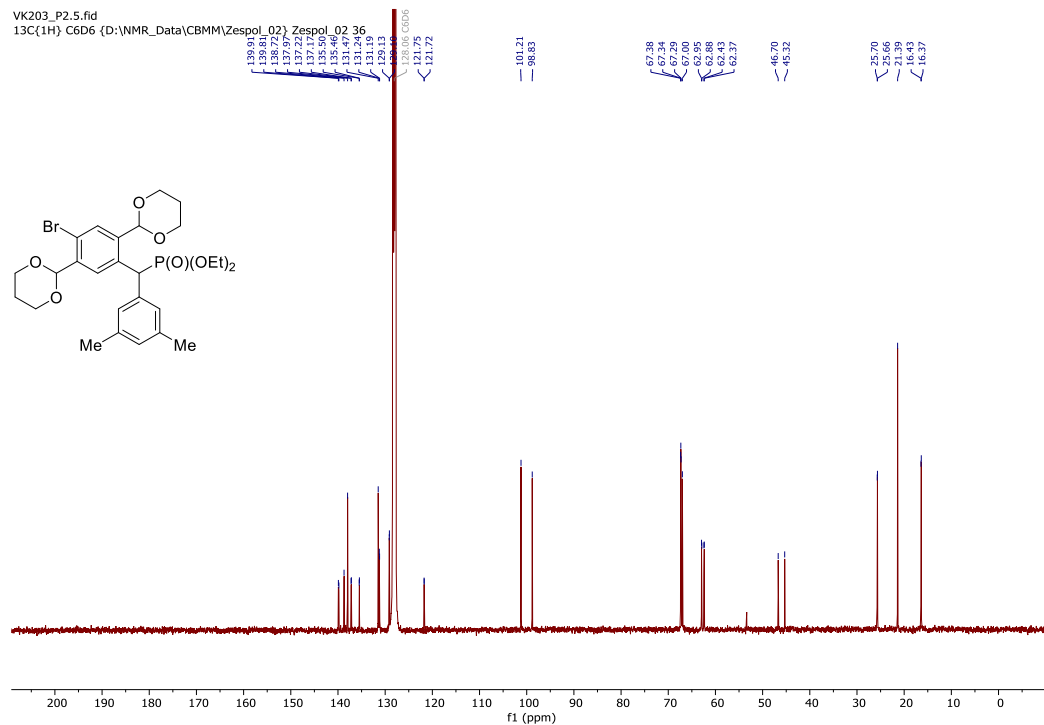
Figure S39. $^{13}C\{^{1}H\}$ (101 MHz, C$_6$D$_6$) NMR spectrum of **4c**.

VK207_P1.2.fid
31P{1H} C6D6 {D:\NMR_Data\CBMM\Zespol_02} Zespol_02 32
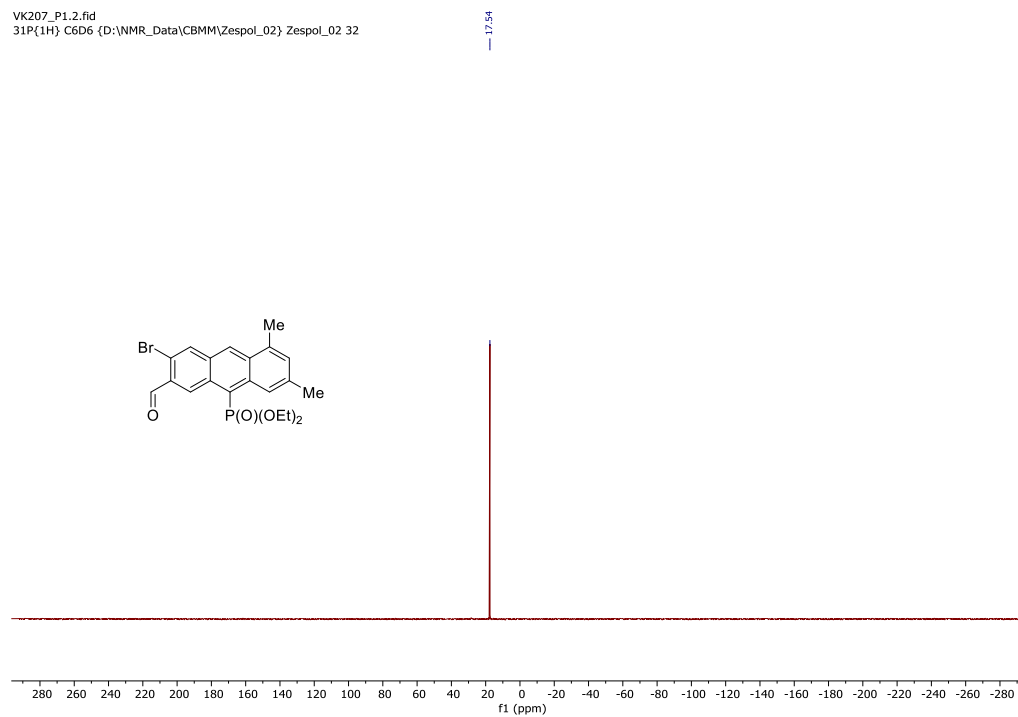
Figure S40. ^{31}P (162 MHz, C$_6$D$_6$) NMR spectrum of **2c**.

Figure S41. ^{1}H (400 MHz, C$_6$D$_6$) NMR spectrum of **2c**.

Figure S42. ^{13}C{^{1}H} (101 MHz, C$_6$D$_6$) NMR spectrum of **2c**.

Figure S43. ^{31}P (162 MHz, CD$_2$Cl$_2$) NMR spectrum of **4d**.

Figure S44. ^{1}H (400 MHz, CD$_2$Cl$_2$) NMR spectrum of **4d**.

Figure S45. $^{13}C\{^1H\}$ (101 MHz, CD$_2$Cl$_2$) NMR spectrum of **4d**.

Figure S46. ^{31}P (162 MHz, CD$_2$Cl$_2$) NMR spectrum of **2d**.
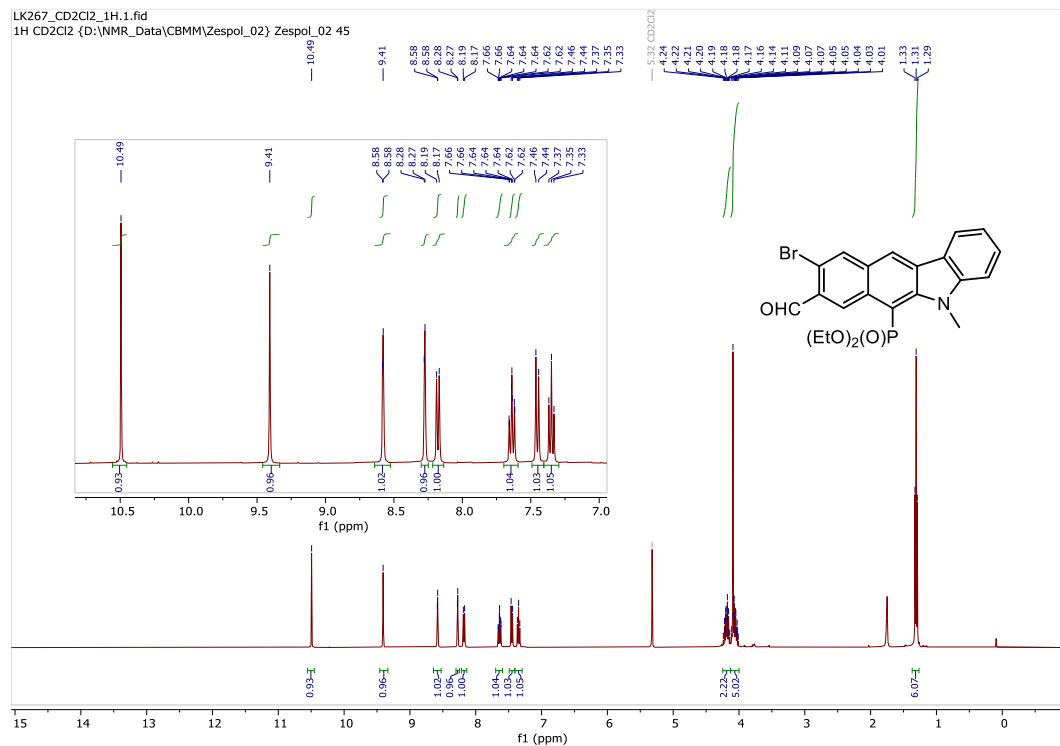
Figure S47. ^{1}H (400 MHz, CD$_2$Cl$_2$) NMR spectrum of **2d**.

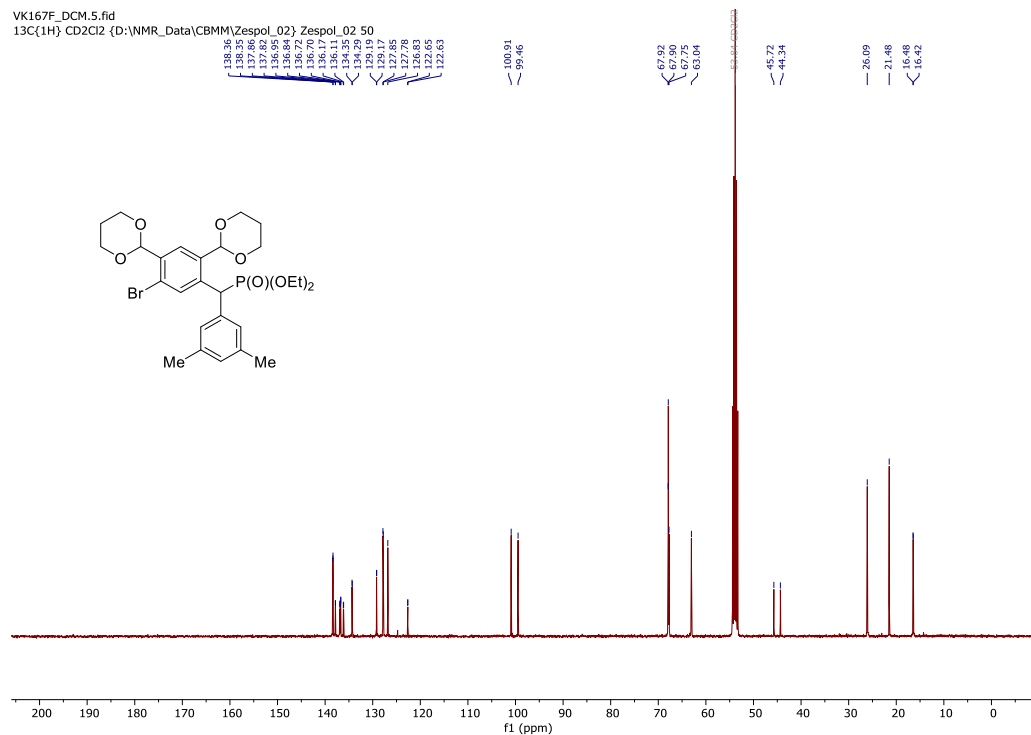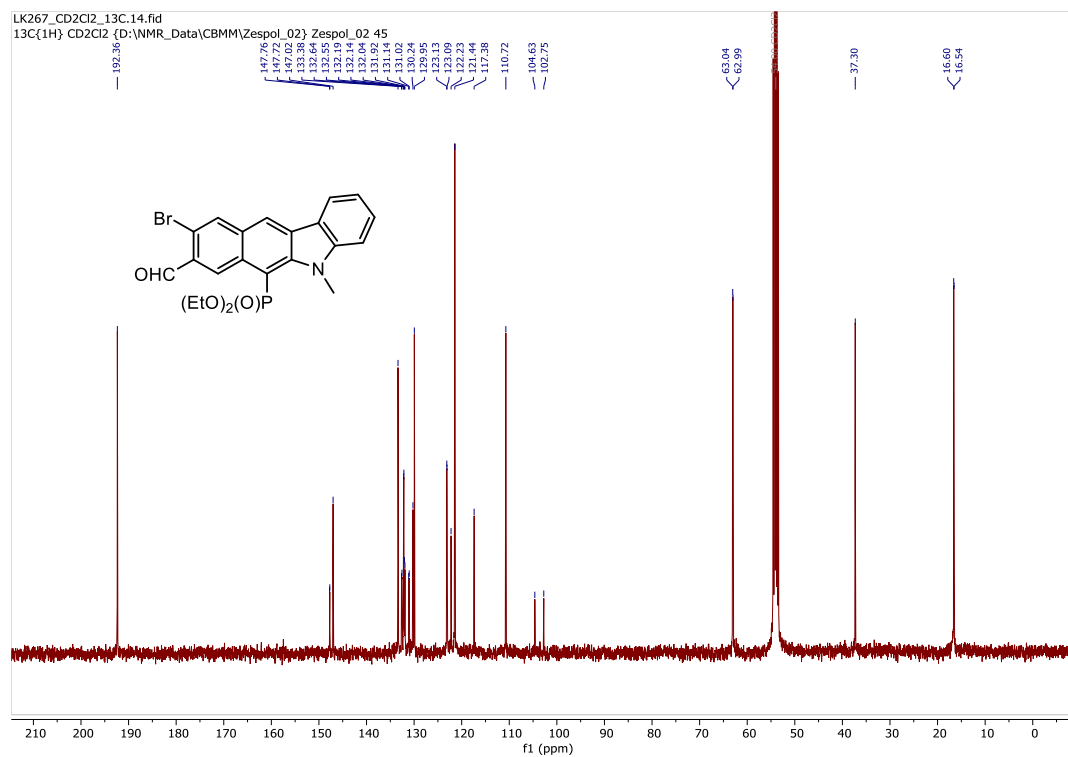**Figure S48.** ^{13}C{^{1}H} (101 MHz, CD$_2$Cl$_2$) NMR spectrum of **2d**.

3.8.4 Photophysical properties

Absorption and emission spectra for (hetero)acenes **1a-d** and **2a-d** were recorded on a Jasco V770 spectrometer in spectroscopic grade solvents (toluene, DCM, and MeOH) at concentrations 10^{-5} M. Results are shown in Figures S49-S53.
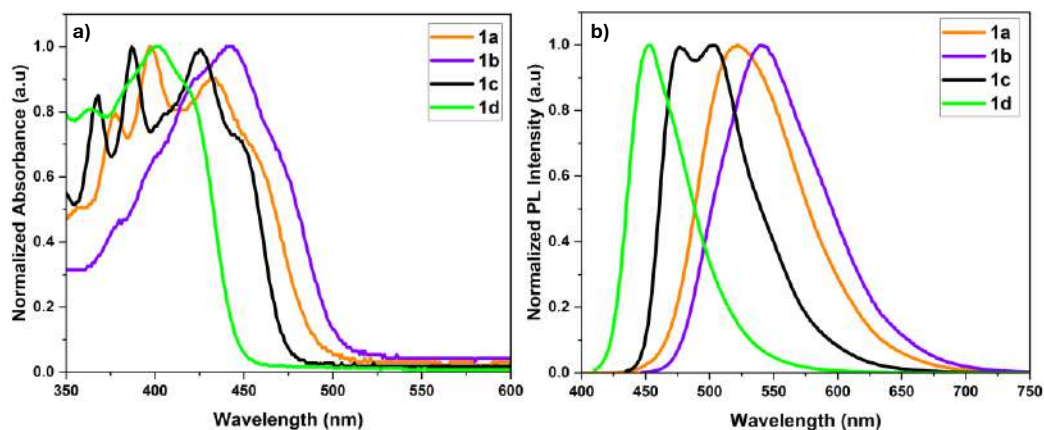
Figure S49. a), b) Normalized absorbance and emission spectra of isomeric (hetero)acenes **1a-d** in toluene solution (10^{-5} mol/L, toluene).
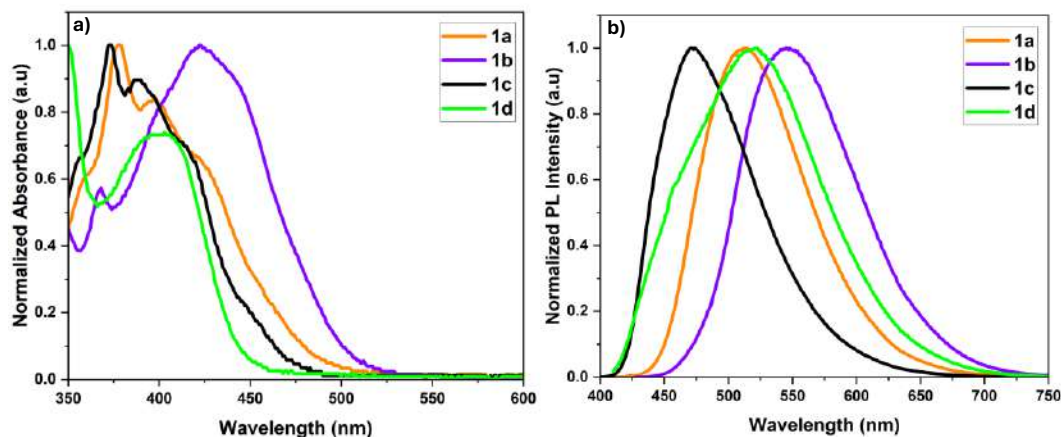
Figure S50. a), b) Normalized absorbance and emission spectra of isomeric (hetero)acenes **1a-d** in MeOH solution (10^{-5} mol/L, MeOH).
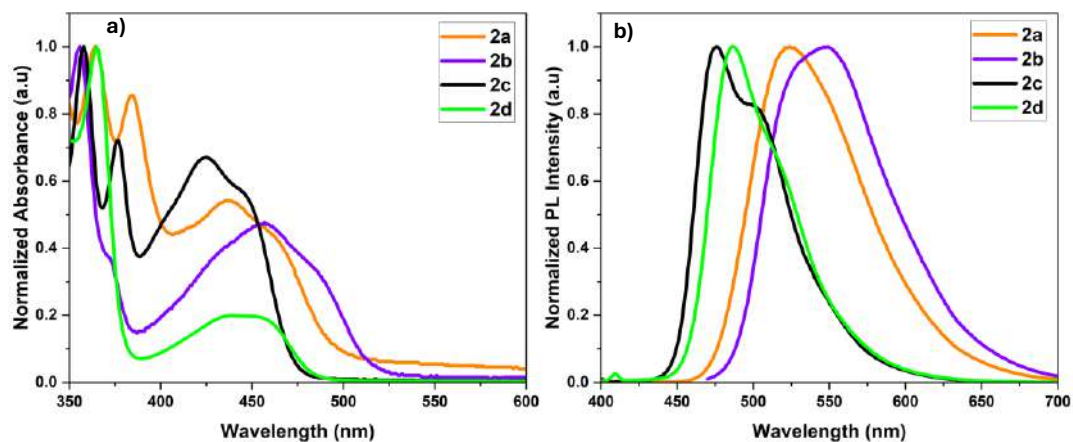
Figure S51. a), b) Normalized absorbance and emission spectra of isomeric (hetero)acenes **2a-d** in toluene solution (10^{-5} mol/L, toluene).
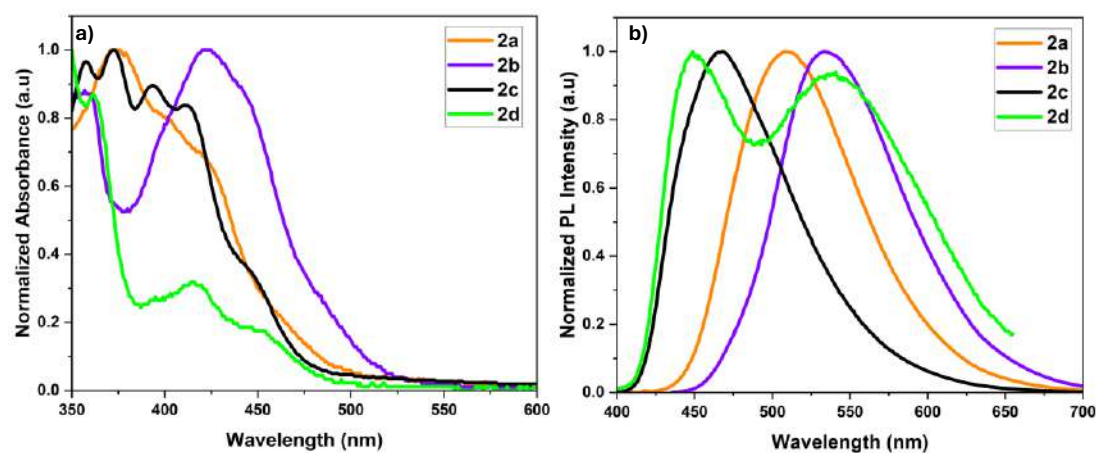
Figure S52. a), b) Normalized absorbance and emission spectra of isomeric (hetero)acenes **2a-d** in MeOH solution (10^{-5} mol/L, MeOH).

106
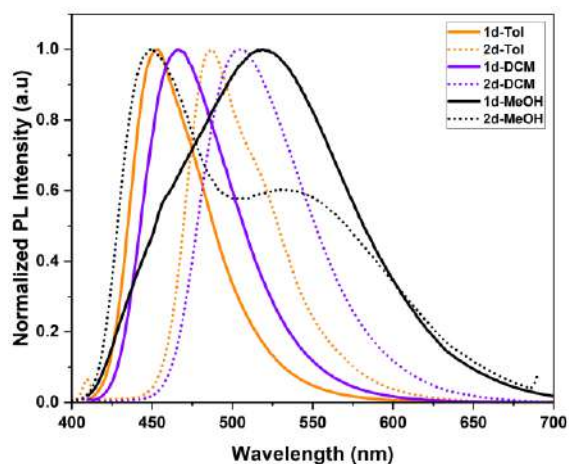
Figure S53. Normalized emission spectra of (hetero)acenes **1d** and **2d** in three solvents i.e., toluene, DCM, and MeOH.
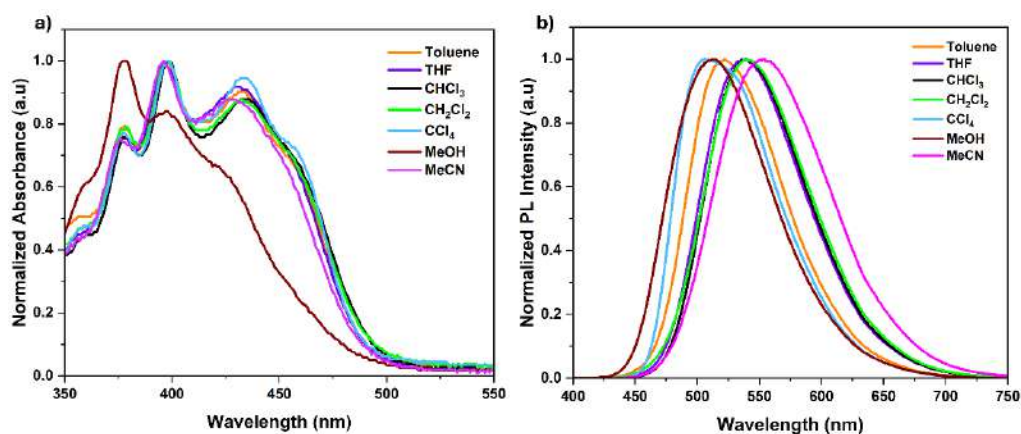
Figure S54. a), b) Normalized absorbance and emission spectra of **1a** of the best QY in seven solvents i.e., toluene, THF, CHCl₃, DCM, CCl₄, MeOH, and MeCN.

Table S1. Photophysical properties measured for **1a** in different solvents.

Property	Solvent						
	DCM	CHCl₃	CCl₄	MeOH	MeCN	THF	Toluene
Absorbance (Abs.) (nm)	432	434	433	397	429	432	433
Emission (PL) (nm)	541	540	508	512	553	538	522
Fluorescence QY (%)	64.7	49.9	85.6	46.1	26.4	43.3	93.3

3.8.5 Electrochemical properties

Electrochemical characterization of (hetero)acenes isomers **1a-d** and **2a-d** were conducted using a Metrohm Autolab PGSTAT128N potentiostat/galvanostat instrument. (Hetero)acenes were dissolved in dry, spectroscopic grade CH_2Cl_2 (concentration 0.5 mM) in the presence of [n-Bu_4N]$^+$[PF_6]$^-$ as an electrolyte (concentration 100 mM), and the resulting solution was degassed by purging with Ar gas for 20 minutes. A three-electrode electrochemical cell was used with a glassy carbon disk as the working electrode, Pt wire as the counter electrode, and Ag/AgCl wire as the reference electrode. All samples were measured versus Ag/AgCl with a scan rate of 50 mVs^{-1} (CV) or 5 mVs^{-1} (DPV) at 20 °C. The molecular frontier orbital levels were estimated from the electrochemical data by using the method described by Sun and Dalton[17] i.e, $E_{HOMO} = -(4.8+E_{1/2}$ Ox.); $E_{LUMO} = -(4.8+E_{1/2}$Red.); $E_g = E_{LUMO}-E_{HOMO}$. Cyclic Voltammetry (CV) and Differential Pulse Voltammetry (DPV) plots are shown in Figures S55-S62 and all the measured redox potentials and the calculated E_{HOMO} and E_{LUMO} energies and energy gaps E_g are given in Table S2.
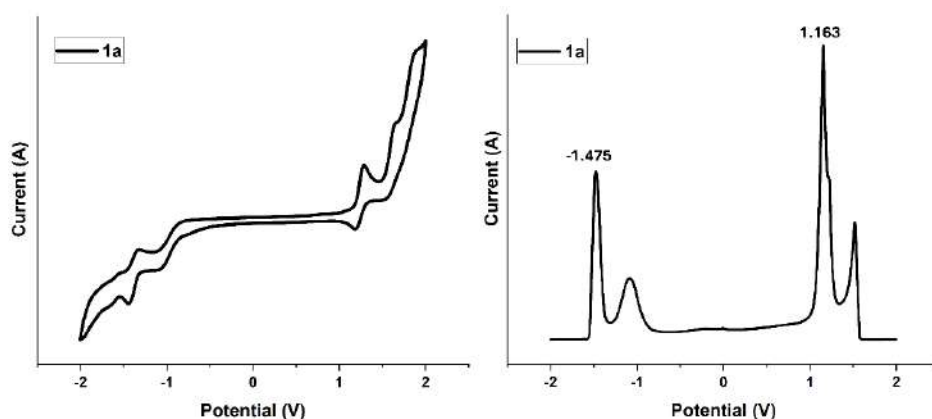
Figure S55. Cyclic and differential pulse voltammogram for the anthracene **1a** in CH_2Cl_2 solution.
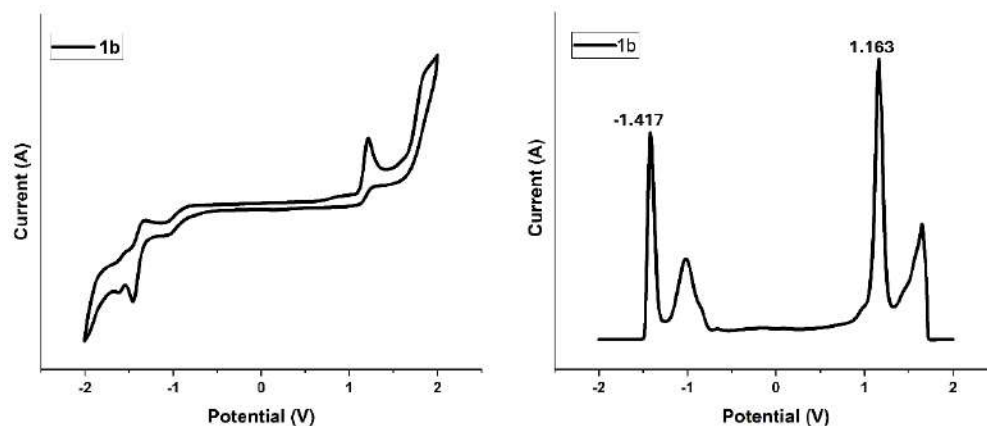
Figure S56. Cyclic and differential pulse voltammogram for the anthracene **1b** in CH_2Cl_2 solution.
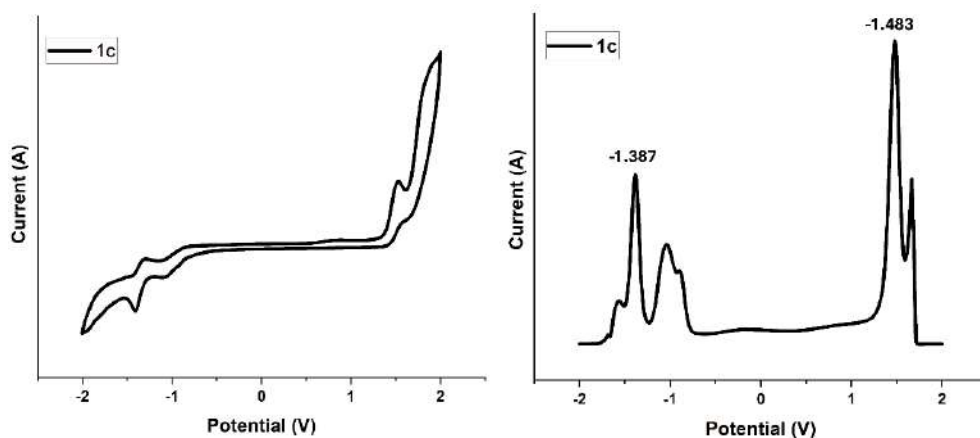
Figure S57. Cyclic and differential pulse voltammogram for the anthracene **1c** in CH$_2$Cl$_2$ solution.
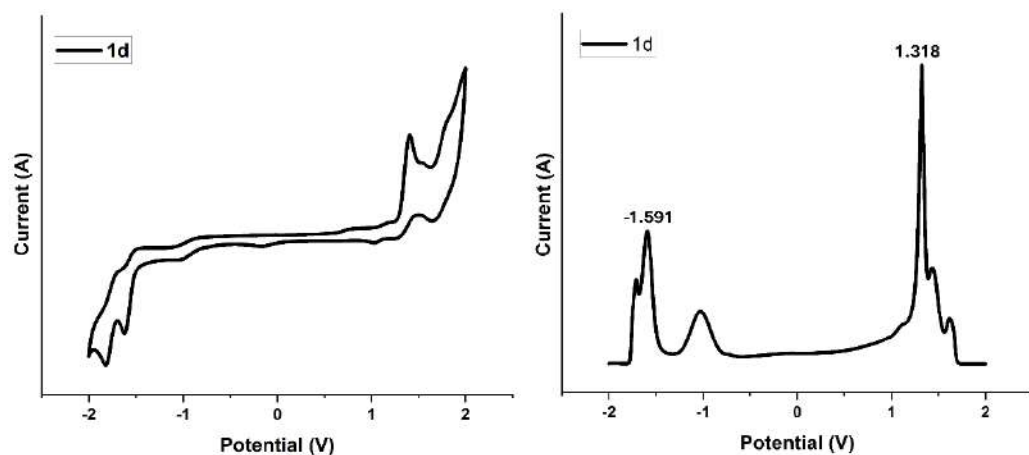
Figure
S58. Cyclic and differential pulse voltammogram for the (hetero)acene **1d** in CH$_2$Cl$_2$ solution.
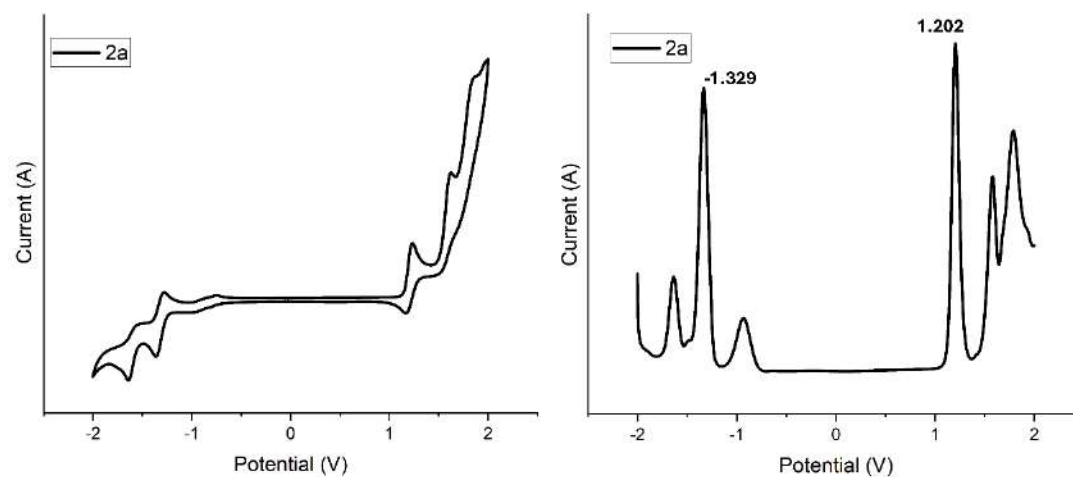
Figure S59. Cyclic and differential pulse voltammogram for the anthracene **2a** in CH_2Cl_2 solution.
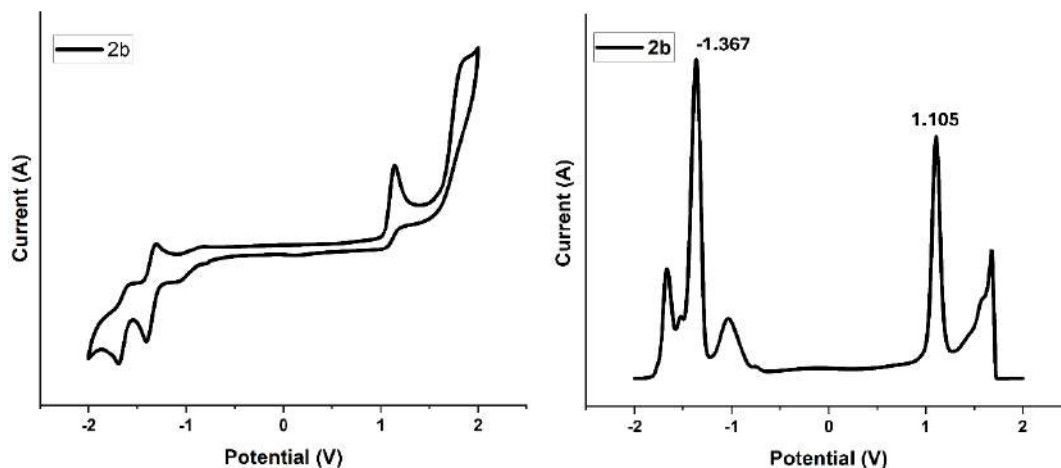
Figure S60. Cyclic and differential pulse voltammogram for the anthracene **2b** in CH_2Cl_2 solution.
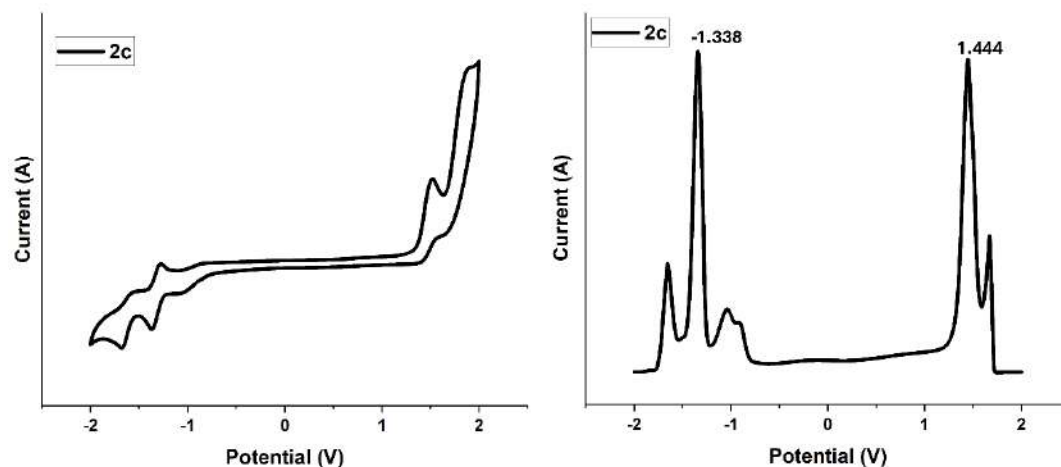
Figure S61. Cyclic and differential pulse voltammogram for the anthracene **2c** in CH_2Cl_2 solution.
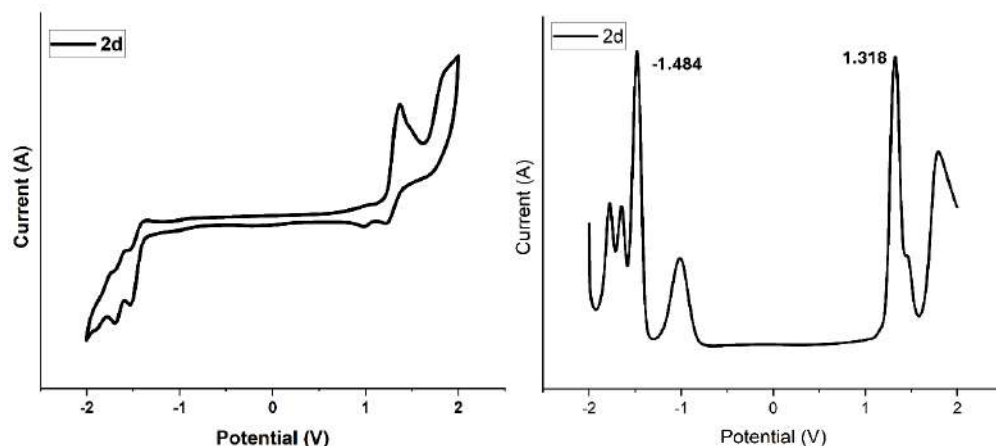
Figure S62. Cyclic and differential pulse voltammogram for the (hetero)acene **2d** in CH$_2$Cl$_2$ solution.

Table S2. Oxidation and reduction potentials (E_{ox}/E_{red}) from DPV for *ortho*-positional isomers **1a-d** and **2a-d** in DCM solution and E_{HOMO}, E_{LUMO} and E_g values estimated based on these data.

(Hetero)acene	E_{ox}/E_{red}	E_{HOMO} (eV)	E_{LUMO} (eV)	E_g (eV)
1a	1.16 / -1.47	-5.96	-3.33	2.63
1b	1.16 / -1.41	-5.96	-3.39	2.57
1c	1.48 / -1.38	-6.28	-3.42	2.86
1d	1.31 / -1.59	-6.11	-3.21	2.90
2a	1.20 / -1.32	-6.00	-3.48	2.52
2b	1.10 / -1.36	-5.90	-3.44	2.46
2c	1.44 / -1.33	-6.24	-3.47	2.77
2d	1.31 / -1.48	-6.11	-3.32	2.79

3.8.6 Computational studies

The molecular and electronic structures of **1a-d** and **2a-d** were calculated by the DFT method using the gradient corrected three-parameter hybrid functional (B3LYP) with the 6-31++G(d,p) basis set. Full geometry optimizations of compounds in the gas phase were performed using the GAUSSIAN 09 quantum chemistry package.[3] In order to check the structural optimizations, the calculated vibrational frequencies of the compounds were used (no imaginary frequencies). To visualize the shapes of frontier molecular orbitals (HOMO and LUMO), the Chemcraft program[4] was used. In order to determine the effect of molecular geometry, and especially intramolecular non-covalent interactions on significantly different fluorescence QYs of **1a/2a** and **1d/2d**, calculations in the framework of QTAIM (Quantum Theory of Atoms in Molecules)[5] and NCI (Non-Covalent Interactions) index[6] using Multiwfn 3.8 software[7-9], were employed. The QTAIM calculations enabled us to find the bond critical points (BCPs) of non-covalent interactions and to determine the properties of electron density at these points, such as the electron density at BCP (ρ_{BCP}), its Laplacian ($\nabla^2\rho_{BCP}$), the potential (V_{BCP}) and total (H_{BCP}) electron energy densities. The energies of hydrogen bonds (E_{HB} in kcal/mol) were calculated from the ρ_{BCP} values, according to the following equation: $E_{HB} = (\rho_{BCP}/2)\cdot627.61$, which was proposed by Emamian et al.[10]

For a deeper understanding of the very high QY of **1a** *versus* the very low QY of **1d**, the TD-DFT calculations in the gas phase were performed in combination with the IFCT (Inter-Fragment Charge Transfer) analysis using Multiwfn 3.8 software. This analysis allowed us to determine the percentage of local excitation (%LE) and charge transfer (%CT) in the electron excitation from the ground S0 state to the excited S1 state. Moreover, a so-called Charge Transfer Spectrum (CTS) was prepared for electron transition, which is a decomposition of the total UV-VIS spectrum into individual subspectra consisting of different IFCT terms corresponding to relevant molecular fragments.

To investigate the ability of chlorinated solvents to form specific non-covalent interactions with fluorophores, especially halogen bonds, an electrostatic potential (ESP) analysis was carried out on the molecular van der Waals surfaces of nonpolar CCl_4 and polar $CHCl_3$ as well as of **1a**, chosen as a representative of the compounds under study. The Multiwfn 3.8 program was used for this analysis as it enables a detailed examination of the ESP distribution as well as the identification and localization of ESP minima and maxima, which correspond to potential donors and acceptors involved in non-covalent interactions.
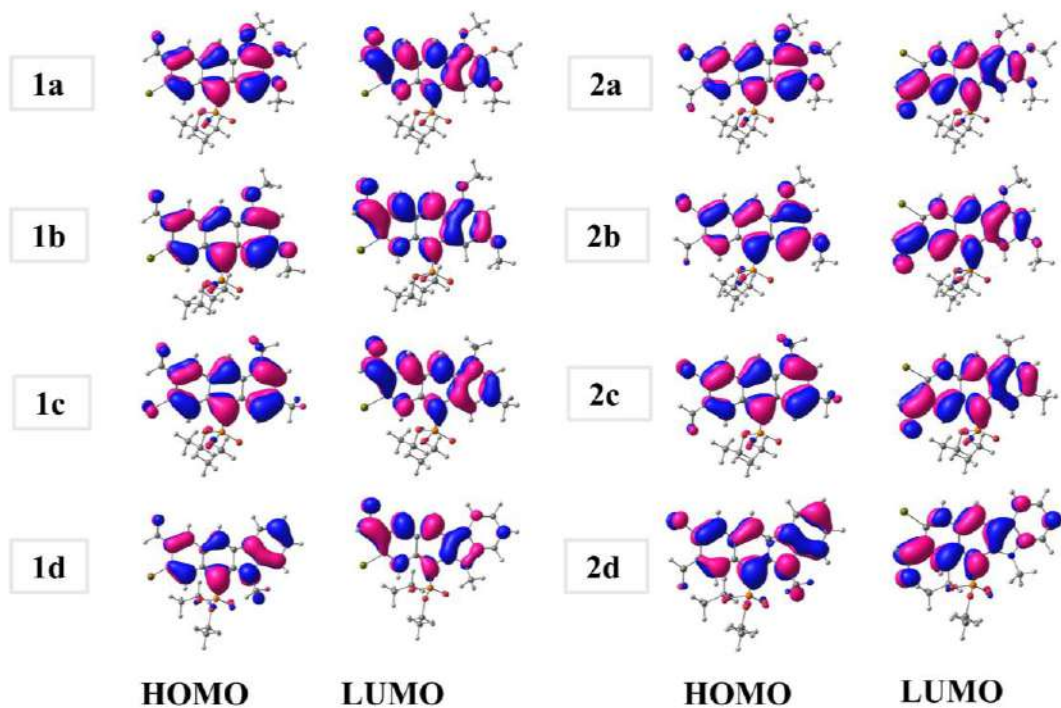
Figure S63. HOMO and LUMO orbitals calculated for (hetero)acenes **1a-d** and **2a-d** in the gas phase at the B3LYP/6-311++(d,p) level using the Gaussian 09 quantum chemistry package.

Table S3. E_{HOMO}, E_{LUMO}, and E_g values for (hetero)acenes **1a-d** and **2a-d** using the DFT method.

(Hetero)acene	E_{HOMO} [eV]	E_{LUMO} [eV]	E_g [eV]
1a	-5.74	-2.62	3.11
1b	-5.79	-2.64	3.15
1c	-6.00	-2.82	3.18
1d	-5.98	-2.47	3.51
2a	-5.68	-2.73	2.95
2b	-5.70	-2.76	2.95
2c	-5.95	-2.87	3.09
2d	-5.90	-269	3.21

Table S12. Topological parameters for intramolecular $(C-H)_{ar} \cdots P=O$ hydrogen bond in **1a/1b**.

Compound	ρ_{BCP}	$\nabla^2\rho_{BCP}$	G_{BCP}	V_{BCP}	H_{BCP}	K_{BCP}	E_{HB} [kcal/mol]
1a	0.0255	0.0988	0.0219	-0.0191	0.0028	-0.028	-4.95
1b	0.0255	0.0988	0.0219	-0.0192	0.0028	-0.028	-4.95
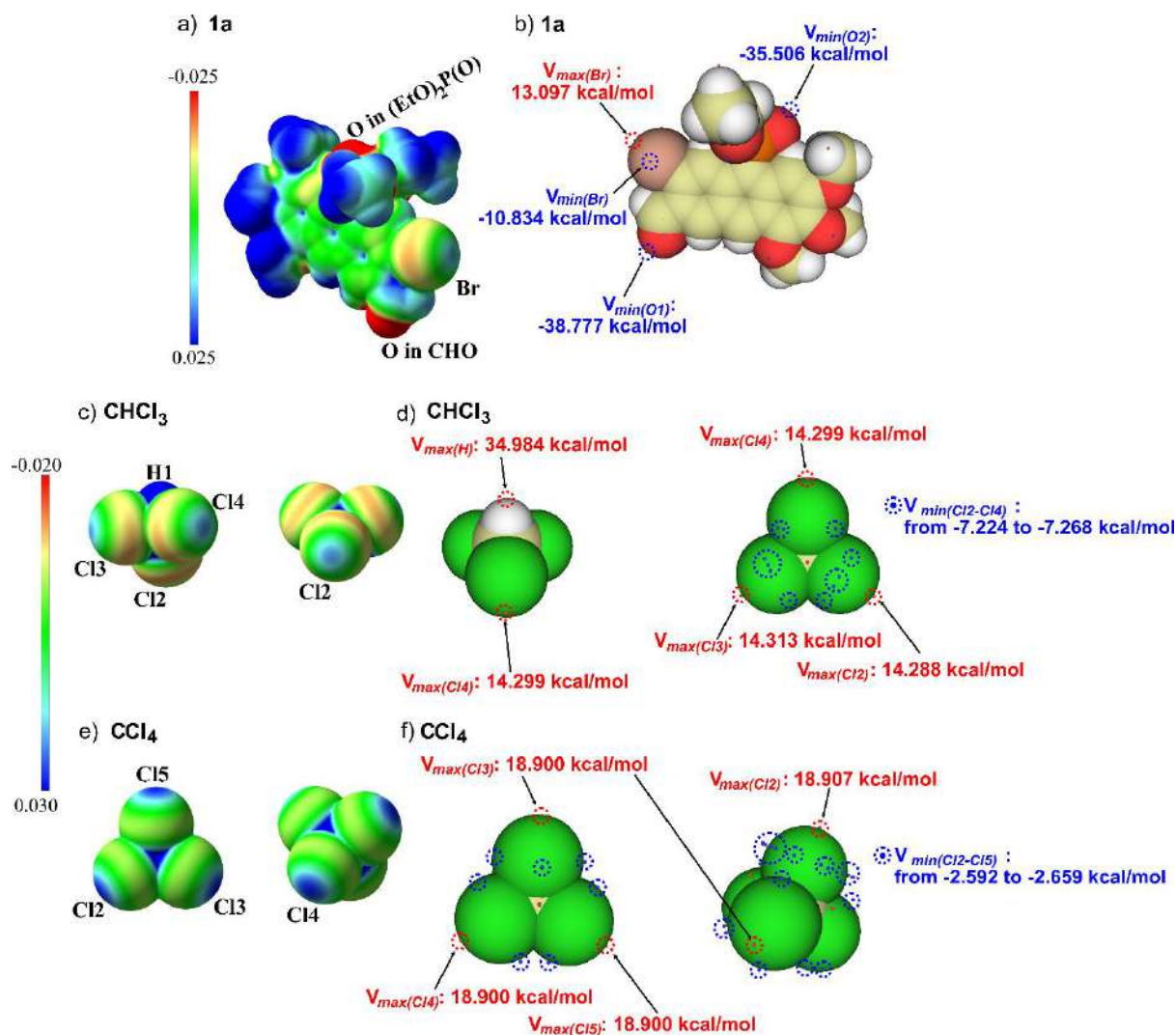
Figure S64. Surfaces of electrostatic potential (a, c, e) and its extrema for **1a** (b), CHCl$_3$ (d) and CCl$_4$ (f). The points corresponding to the values of largest V$_{max}$ (red) and V$_{min}$ (blue) are marked with dotted circles.
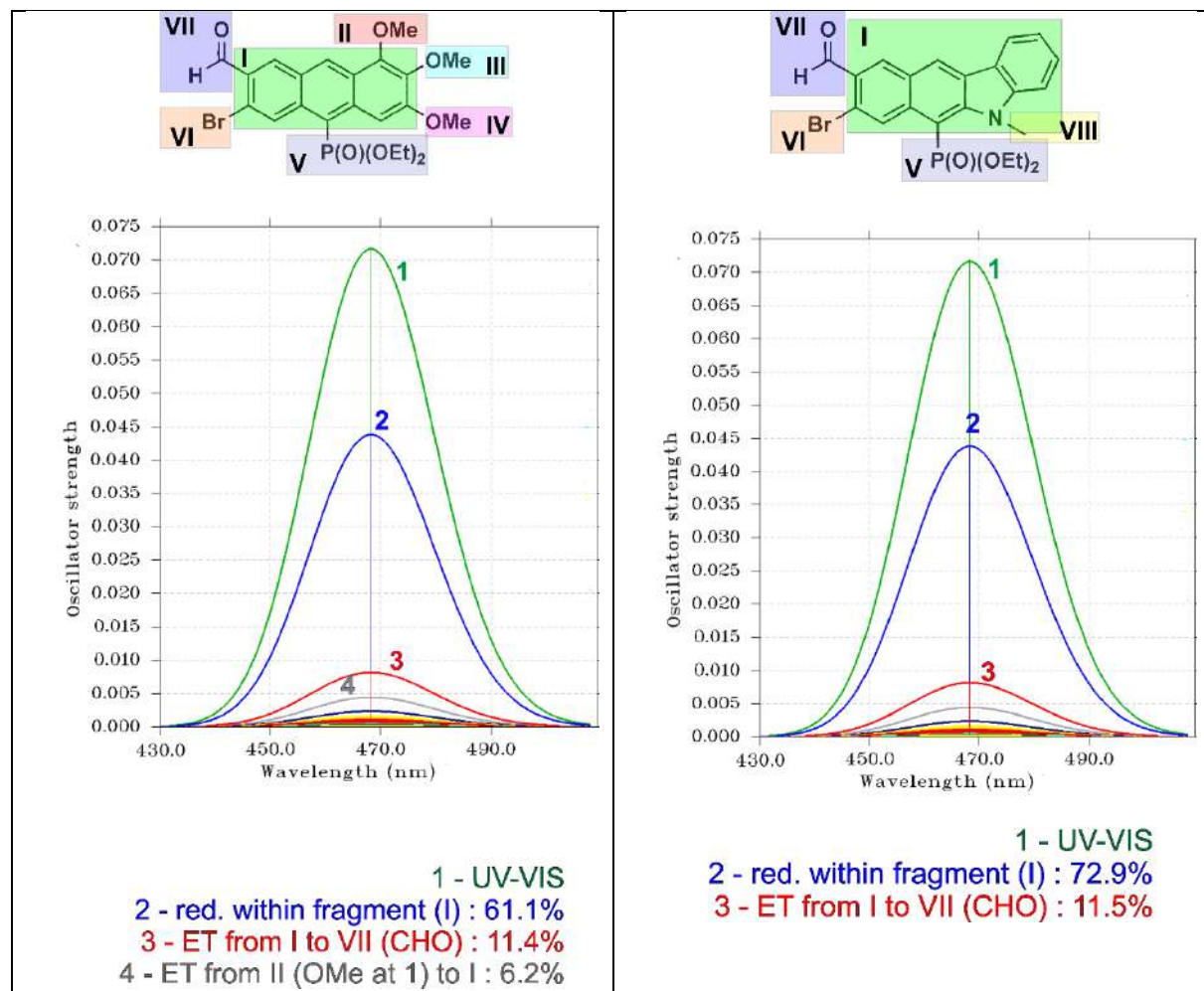
Figure S65. Charge transfer spectra showing the decomposition of the total UV-Vis spectra into individual sub-spectra contributed by different IFCT terms for S1 state of **1a** and **1d** The IFCT terms with contribution larger than 5% are shown.

3.8.7 CIE 1931 color space coordinates

Table S13. CIE 1931 color space chromaticity coordinates of **1a-d** and **2a-d** in three different solvents.

Anthracenes	Toluene		DCM		MeOH	
	x	y	x	y	x	y
1a	0.364	0.557	0.424	0.536	0.324	0.535
1b	0.419	0.544	0.474	0.511	0.440	0.525
1c	0.228	0.461	0.273	0.537	0.213	0.320
1d	0.198	0.193	0.137	0.232	0.395	0.490
2a	0.380	0.565	0.454	0.527	0.304	0.523
2b	0.427	0.551	0.488	0.503	0.405	0.542
2c	0.202	0.419	0.243	0.523	0.205	0.281
2d	0.243	0.243	0.389	0.514	0.487	0.493

3.8.8 Crystal Structures and Hirshfeld surface analysis

X-ray diffraction data for **1a** and **2a** were collected using an Oxford Diffraction Xcalibur Saphire 3 diffractometer with CuKα radiation. The structures were solved by direct methods and refined by full-matrix least-squares on F^2 with SHELXL-2019.[12] The non-hydrogen atoms were refined anisotropically. All aromatic H atoms and H atoms of methyl and methylene groups were positioned geometrically and constrained to ride on their parent atoms, with C–H distances of 0.93, 0.96 and 0.97 Å, respectively, and with $U_{iso}(H_{aromatic/methylene})$ and $U_{iso}(H_{methyl})$ values of 1.2 $U_{eq}(C_{aromatic/methylene})$. H atoms of formyl groups were located in difference-Fourier maps and refined with $U_{iso}(H) = 1.2 U_{eq}(C_{formyl})$. The ethoxy groups of **2a** were modeled as a two-component disorder with partial occupancies of 0.58(3)/0.42(3) (for C19 and C20). and 0.52(2)/0.48(2) (for C21 and C22). Details of data collections and structure refinements have been deposited with the Cambridge Crystallographic Data Centre as supplementary publication number: CCDC 2417579 (**1a**) and CCDC 2417580 (**2a**).[13]

In order to visualize and analyze the intermolecular interactions in the crystal structures of **1a** and **2a** (minor disorder components on the carbon ethoxy atoms of **2a** were exluded from the analysis), the CrystalExplorer 17 program,[14] was used. It has enabled us to construct the three dimensional (3D) Hirshfeld surfaces (HSs) of molecules in crystals,[15] which mapped with *dnorm* distance illustrate the interatomic contacts with distances equal to the sum of the van der Waals radii (represented as white) and with distances shorter (red) and longer (blue) than the values of this sum. To identify π···π interactions, the HS is mapped with shape index; these contacts are revealed on it in the form of pair of blue and red triangles. Moreover, the CrystalExplorer 17 was also used to obtain the fingerprint plots (FPs),[16] which are the two-dimensional (2D) representations of these surfaces, and are generated based on the *de* and *di* distances (*de* and *di* are the distances from the HS to the nearest atom outside and inside the surface,respectively).

a)

Crystal structure data for 1a: $C_{22}H_{24}O_7BrP$, M = 511.29, monoclinic, space group $P2_1/n$ (No. 14), a = 12.5677(3) Å, b = 8.3265(2) Å, c = 21.4441(4) Å, β = 91.703(2) °, Z = 4, T = 293(2) K, D_{calc} = 1.514 g·cm^{-3}, CuKα radiation, $2\theta_{max}$ = 135.930°, 32161 reflections collected, 4049 reflections unique and 3615 reflections with $I > 2\sigma(I)$. Final GooF = 1.067, R1 = 0.0474 for 3615 reflections and 288 parameters.
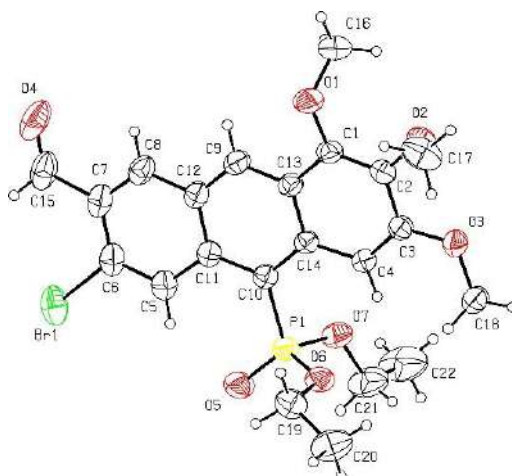
b)

Crystal structure data for 2a: $C_{22}H_{24}O_7BrP$, M = 511.29, monoclinic, space group $P2_1/n$ (No. 14), a = 12.5241(2)Å, b = 7.9430(1) Å, c = 22.7228(3)Å, β = 94.455(1) °, Z = 4, T = 293(2) K, D_{calc} = 1.507 g·cm^{-3}, CuKα radiation, $2\theta_{max}$ = 136.036, 33125 reflections collected, 4093 reflections unique and 3860 reflections with $I > 2\sigma(I)$. Final GooF = 1.059, R1 = 0.0391 for 3860 reflections and 330 parameters.
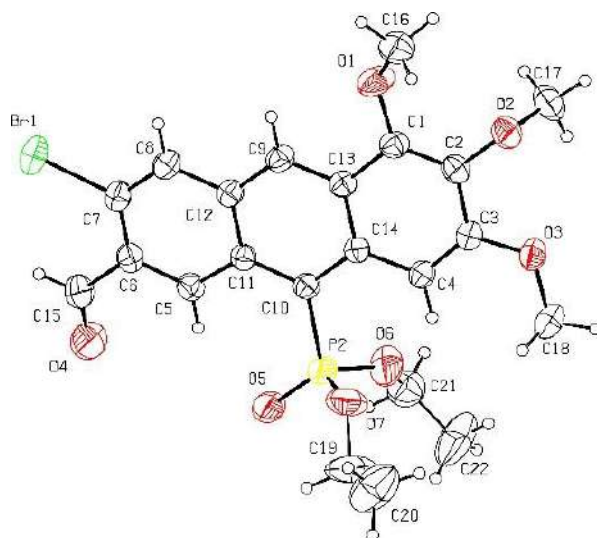
Figure S66. Crystal structure data for **1a** (a) and **2a** (b) and its molecular structures; displacement ellipsoids are drawn at the 30% probability level. Minor disorder components on the carbon atoms of the ethoxy groups of **2a** are not shown for clarity.

118
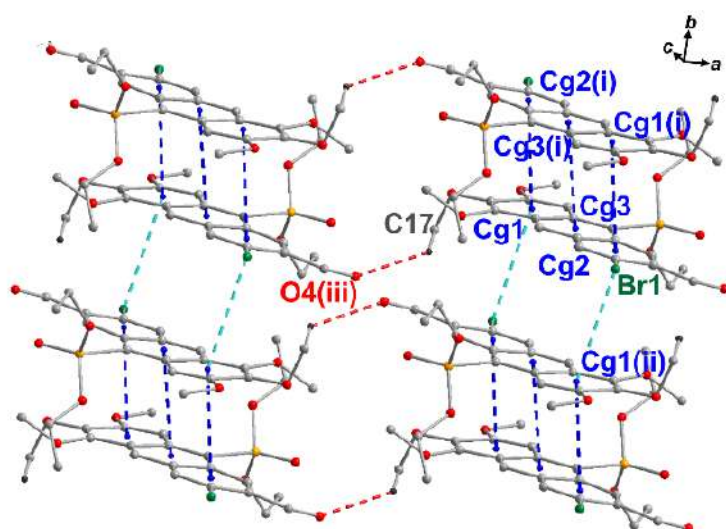
Figure S67. Crystal packing of **2a**, showing key intermolecular interactions (dashed lines), including C-H···O (red), π···π (blue) and halogen···π (magenta) and C-H···O interactions, respectively. All H-atoms not involved in hydrogen bonds and atoms of minor disorder component have been omitted for clarity. Symmetry codes are given in Table S14.

Table S14. Geometrical parameters of intermolecular interactions in the crystal structures of **1a** and **2a**.

1a				
WEAK HYDROGEN BONDS				
D-H···A	D-H (Å)	H···A (Å)	D···A (Å)	D-H···A (deg)
C18-H18C···O4[(i)]	0.96	2.59(3)	3.393(4)	141.4(2)
π···π INTERACTIONS				
π···π	Cg ···Cg (Å)	Dihedral angle α (deg)	Slippage distance S (Å)	
Cg1···Cg2[(i)]	3.732(2)	7.6(1)	0.539	
Cg2···Cg1[(i)]	3.732(2)	7.6(1)	0.792	
X-Y···π INTERACTION				
X-Y···Cg	X-Y (Å)	Y···Cg (Å)	X-Y···Cg(deg)	
C7=O4···Cg1[(ii)]	1.191(6)	3.859(4)	96(3)	
HALOGEN···HALOGEN INTERACTION				
X-Hal···Hal	X-Hal (Å)	Hal···Hal (Å)	X-Hal···Hal (deg)	
C6-Br1···Br1[(iii)]	1.890(4)	3.6308(7)	154.5(1)	
Cg are centroids of benzene rings. Symmetry codes: (i)1-x, -y, -z, (ii) 1-x, 1-y, -z, (iii) -x,1-y,-z				
2a				
WEAK HYDROGEN BONDS				
D-H···A	D-H (Å)	H···A (Å)	D···A (Å)	D-H···A (deg)
C17-H17C···O4[(iii)]	0.96	2.64	3.372(4)	129(2)
π···π INTERACTIONS				
π···π	Cg ···Cg (Å)	Dihedral angle α (deg)	Slippage distance S (Å)	
Cg1···Cg2[(i)]	3.774(1)	7.6(1)	0.956	
Cg2···Cg1[(i)]	3.774(1)	7.6(1)	1.280	

Cg3⋯Cg3[i]	3.720(1)	0.0(1)	1.188
X-Y⋯π INTERACTION			
X-Y⋯Cg	X-Y (Å)	Y⋯Cg (Å)	X-Y⋯Cg(deg)
C7-Br1⋯Cg1[ii]	1.894(2)	3.785(1)	106.97(8)
Cg are centroids of benzene rings. Symmetry codes: (i) 1-x, 1-y, -z, (ii) 1-x, -y, -z, (iii) -1+x, y, z			
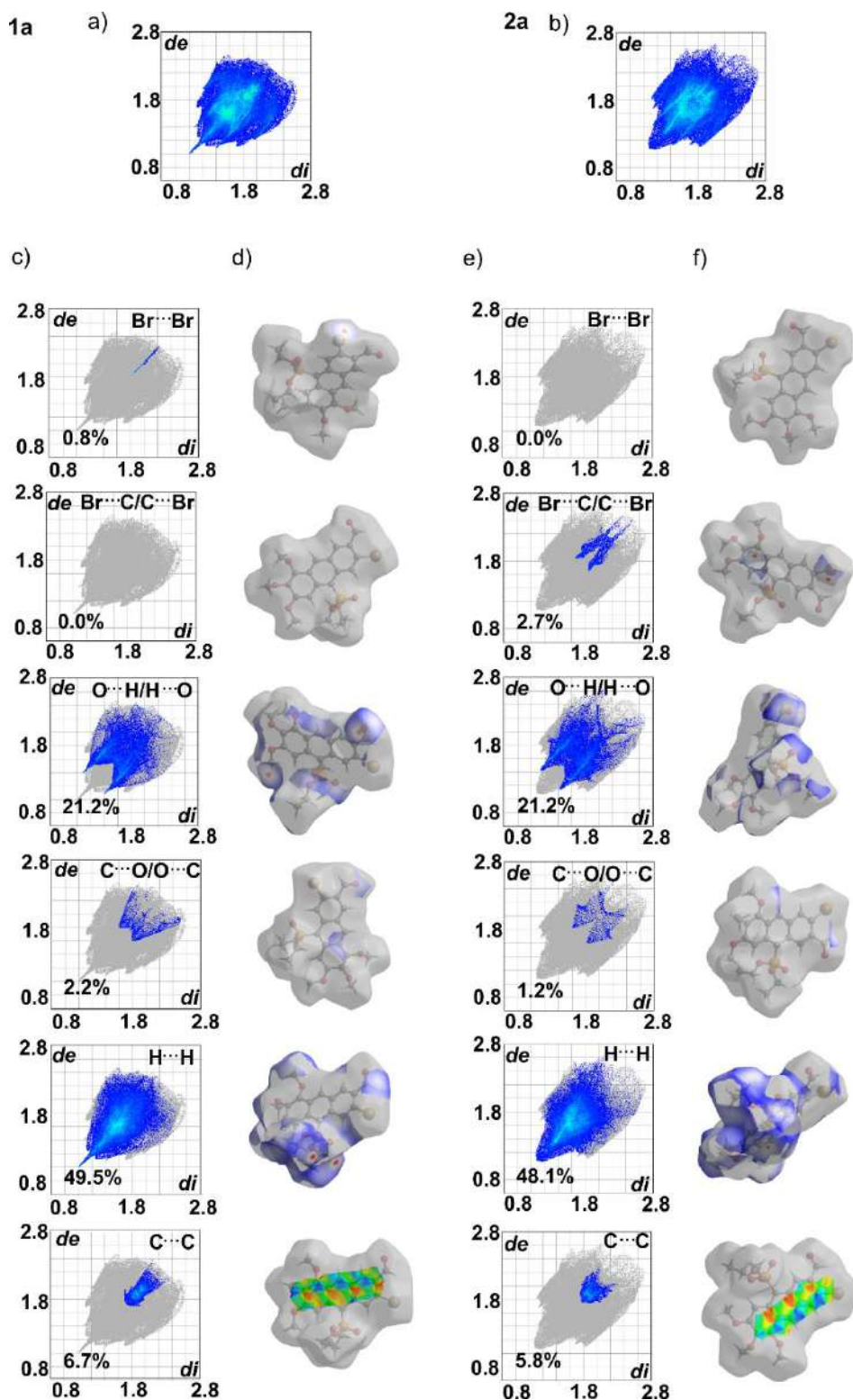
Figure S68. 3D-HSs of molecules **1a** and **1b** in crystals, mapped with d_{norm} distance, and in the case of C⋯C contacts wih the shape index (d, f) as well as 2D-FPs for all interatomic contact (a, b) and decomposed FPs for selected contacts (c, e).

3.8.9 References

1. Bodzioch, A.; Owsianik, K.; Skalik, J.; Kowalska, E.; Stasiak, A.; Różycka-Sokołowska, E.; Marciniak B.; Bałczewski; P. Efficient Synthesis of Bis(dibromomethyl)arenes as Important Precursors of Synthetically Useful Dialdehydes. *Synthesis* **2016**, *48*, 3509–3514.

2. Bałczewski, P.; Skalik, J.; Uznański, P.; Guziejewski, D.; Ciesielski, W. Use of isomeric, aromatic dialdehydes in the synthesis of photoactive, positional isomers of higher analogs of *o*-bromo(hetero)acenaldehydes. *RSC Adv*, **2015**, *5*, 24700–24704.

3. Frisch M. J.; Trucks G. W.; Schlegel H. B.; Scuseria G. E.; Robb M. A.; Cheeseman J. R.; Scalmani G.; Barone V.; Petersson G. A.; Nakatsuji H.; Li X.; Caricato M.; Marenich A.; Bloino J.; Janesko B. G.; Gomperts R.; Mennucci B.; Hratchian H. P.; Ortiz J. V.; Izmaylov A. F.; Sonnenberg J. L.; Williams-Young D.; Ding F.; Lipparini F.; Egidi F.; Goings J.; Peng B.; Petrone A.; Henderson T.; Ranasinghe D.; Zakrzewski V. G.; Gao J.; Rega N.; Zheng G.; Liang W.; Hada M.; Ehara M.; Toyota K.; Fukuda R.; Hasegawa J.; Ishida M.; Nakajima T.; Honda Y.; Kitao O.; Nakai H.; Vreven T.; Throssell K.; Montgomery J. A.; Peralta J. E.; Ogliaro F.; Bearpark M.; Heyd J. J.; Brothers E.; Kudin K. N.; Staroverov V. N.; Keith T.; Kobayashi R.; Normand J.; Raghavachari K.; Rendell A.; Burant J. C.; Iyengar S. S.; Tomasi J.; Cossi M.; Millam J. M.; Klene M.; Adamo C.; Cammi R.; Ochterski J. W.; Martin R. L.; Morokuma K.; Farkas O.; Foresman J. B.; Fox D. J. Gaussian 09, Revision A.02, Gaussian, Inc., Wallingford CT, **2016**.

4. Chemcraft - graphical software for visualization of quantum chemistry computations. https://www.chemcraftprog.com.

5. Bader, R. F. W. *Atoms in Molecules: A Quantum Theory*; Clarendon Press: Oxford, New York, **1990**.

6. Contreras-García, J.; Boto, R. A.; Izquierdo-Ruiz, F.; Reva, I.; Woller, T.; Alonso, M. A. A benchmark for the non‑covalent interaction (NCI) index or… is it really all in the geometry? *Theor. Chem. Acc.* **2016**, *135*, 242.

7. Lu, T.; Chen, F. Multiwfn: A multifunctional wavefunction analyzer. *J. Comput. Chem.* **2012**, *33*, 580-592.

8. Lu, T. A comprehensive electron wavefunction analysis toolbox for chemists, Multiwfn. *J. Chem. Phys.* **2024**, *161*, 082503.

9. Lu, T. Multiwfn Manual, version 3.8, **2024**. http://sobereva.com/multiwfn

10. Emamian, S.; Lu, T.; Kruse, H.; Emamian, H. Exploring Nature and Predicting Strength of Hydrogen Bonds: A Correlation Analysis Between Atoms-in-Molecules Descriptors, Binding Energies, and Energy Components of Symmetry-Adapted Perturbation Theory. *J. Comput. Chem*. **2019**, *40*, 2868–2881.

11. Humphrey, W.; Dalke, A.; Schulten, K. VMD: Visual molecular dynamics. *J. Mol. Graphics,* **1996**, *14*, 33-38.

12. Sheldrick, G. M. Crystal structure refinement with SHELXL. *Acta Crystallogr. C*, **2015**, *71*, 3-8.

13. Deposition numbers CCDC 2417579 (for **1a**) and CCDC 2417580 (for **1b**) contain the supplementary crystallographic data for this paper. These data are provided free of charge by the joint Cambridge Crystallographic Data Centre.

14. Spackman, P. R.; Turner, M. J.; McKinnon, J. J.; Wolff, S. K.; Grimwood, D. J.; Jayatilaka, D.; Spackman, M. A. CrystalExplorer: a program for Hirshfeld surface

analysis, visualization and qu-antitative analysis of molecular crystals. *J. Appl. Cryst., 2021, 54*, 1006–1011.

15. Spackman, M. A.; Jayatilaka, D. Hirshfeld surface analysis. *Cryst. Eng. Comm.*, **2009**, *11*, 19–32.

16. Spackman, M. A.; McKinnon, J. J. Fingerprinting intermolecular interactions in molecular crystals. *Cryst. Eng. Comm*. **2002**, *4*, 378–392.

17. Sun, S. S.; Dalton, L. R. *Introduction to Organic Electronic and Optoelectronic Materials and Devices*, CRC, Boca Raton, **2008**, Chapter 3.4.

3.9 Experimental section-III for post-synthetic functionalization of *ortho-positional isomers*

3.9.1 General Information

Tetrahydrofuran and toluene were dried using Solvent Purification System (MBraun SPS-800). Dry glassware was obtained by oven-drying and assembly under dry argon. For flash chromatography, chromatography system – Büchi Pure C-850 FlashPrep was used. The melting points were obtained with an electrothermal model IA9100 apparatus and are uncorrected. Mass spectra were obtained by using a SYNAPT G2-Si HDMS (Waters) instrument. NMR spectra were recorded with a Bruker AV 200 MHz, Bruker AVANCE Neo 400 MHz or Bruker AVANCE III 500 MHz using $CDCl_3$, C_6D_6, CD_2Cl_2, as the solvents as internal standards. The UV-Vis absorption spectra were recorded in 1 cm cuvettes on a Shimadzu spectrophotometer UV-2700. Emission spectra were obtained with the Horiba Jobin Yvon, Fluoromax 4 spectrofluorimeter. Electrochemical characterization were conducted using a Metrohm Autolab PGSTAT128N potentiostat/galvanostat instrument. The fluorescence quantum yields Φ of the obtained compounds were determined in three different solvents (toluene, DCM, and MeOH) on excitation at their absorption maximum using an integrating sphere (Horiba, Jobin Yvon, Quanta-φ F-3029 Integrating sphere).

Starting materials: Compounds **1a** and **2a** were prepared according to the reported procedure.[1]

3.9.2 Synthesis and characterization
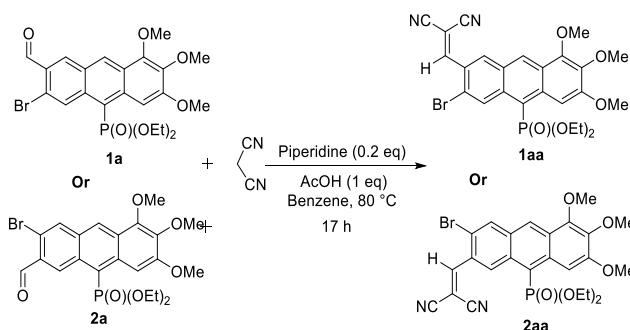
Scheme S1. Synthesis of anthracenes **1aa** and **2aa**.
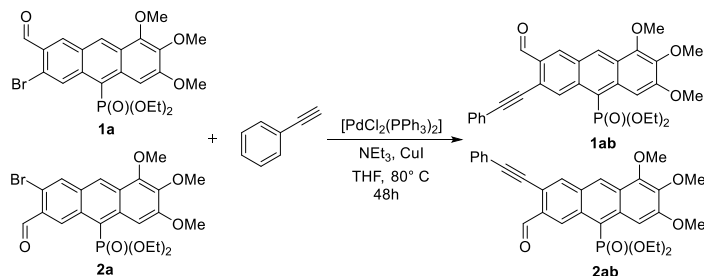
Scheme S2. Synthesis of anthracenes **1ab** and **2ab**.
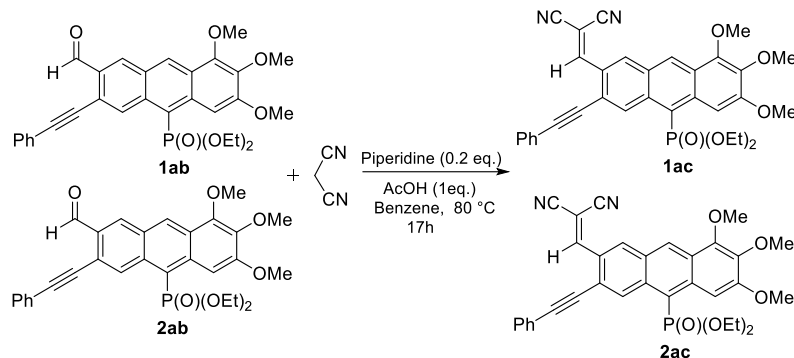
Scheme S3. Synthesis of anthracenes **1ac** and **2ac**.

General procedure for the Knoevenagel condensations:

To a solution of the anthracene containing aldehyde group (**1a**, **2a**, **1ab**, and **2ab**) (200 mg, 1.0 eq.) in benzene (10 mL), were successively added malononitrile (1.1 eq.), piperidine (0.2 eq.), and AcOH (1 eq.) at room temperature and heated at 80 °C for 17 h. Then, the crude product was concentrated in vacuo, and the residue was purified by column chromatography over silica gel eluting with hexane-EtOAc to give **1aa**, **1ac**, **2aa**, and **2ac.**

General procedure for the Sonogashira couplings:

A mixture of the bromoanthracene (**1a** or **2a**) (500 mg, 1 eq.), phenylacetylene (0.15 mL, 1.2 eq.), [Pd(PPh$_3$)$_2$Cl$_2$] (32 mg, 0.05 eq.) and CuI (15 mg, 0.1eq.) was dissolved in THF (15 mL)under argon. Then, triethylamine (0.5 mL, 3 eq.) was added *via* syringe. The mixture was stirred for 48 h at 70 °C. Then, the mixture was left to cool to room temperature and for the precipitate to form. The resulting precipitate was collected by filtration and was successively washed with ethyl acetate and water. The product was further purified by column chromatography with *n*-hexane-EtOAc to give **1ab** and **2ab**.

Diethyl (7-bromo-6-(2,2-dicyanovinyl)-2,3,4-trimethoxyanthr-9-yl)phosphonate (1aa):

R$_f$ = 0.70 (EtOAc), red solid, m.p.160-162 °C, 84 % yield; **^{1}H NMR** (400 MHz, C$_6$D$_6$) δ 10.05 (s,
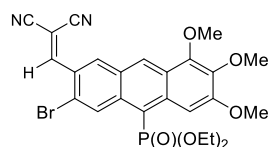
1H), 9.04 (s, 1H), 9.00 (d, *J* = 1.8 Hz, 1H), 8.46 (d, *J* = 2.1 Hz, 1H), 7.62 (s, 1H), 4.13 - 4.07 (m, 2H), 3.92 - 3.84 (m, 2H), 3.79 (s, 3H), 3.75 (s, 6H), 1.00 (t, *J* = 7.1 Hz, 6H); **^{31}P{^{1}H} NMR** (162 MHz, C$_6$D$_6$) δ 18.49; **^{13}C{^{1}H} NMR** (101 MHz, C$_6$D$_6$) δ 157.56 (s), 157.05 (s), 147.68 (d, *J$_{PC}$* = 2.3 Hz), 140.98 (s), 136.44 (d, *J$_{PC}$* = 13.3 Hz), 136.24 (d, *J$_{PC}$* = 10.7 Hz), 133.52 (s), 132.13 (d, *J$_{PC}$* = 3.7 Hz), 130.98 (d, *J$_{PC}$* = 3.5 Hz), 127.53 (s), 126.51 (s), 126.06 (d, *J$_{PC}$* = 15.0 Hz), 122.15

(s), 117.68 (d, J_{PC} = 178.2 Hz), 113.80 (s), 112.79 (s), 102.21 (d, J_{PC} = 3.8 Hz), 84.83 (s), 62.18 (d, J_{PC} = 5.1 Hz), 61.36 (s), 60.89 (s), 55.82 (s), 16.38 (d, J_{PC} = 6.2 Hz); **HRMS** (TOF MS ES+): Calc. for $C_{25}H_{25}O_4PBrN_2$ [M+H$^+$]: 559.0634; Found: 559.0628.

Diethyl (6-formyl-2,3,4-trimethoxy-7-(phenylethynyl)anthr-9-yl)phosphonate (1ab):
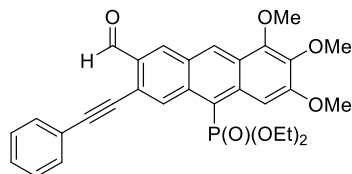
R_f = 0.74 (EtOAc), yellow solid, m.p.162-164 °C, 68 % yield; **^{1}H NMR** (400 MHz, C6D6) δ 10.87 (s, 1H), 10.07 (s, 1H), 9.28 (s, 1H), 8.95 (d, J = 2.2 Hz, 1H), 8.55 (d, J = 2.4 Hz, 1H), 7.44-7.41 (m, 2H), 7.00-6.97 (m, 3H), 4.16-4.06 (m, 2H), 3.95- 3.88 (m, 2H), 3.87 (s, 3H), 3.85, 3.85, 3.79 (s, 6H), 1.01 (t, J = 7.0 Hz, 6H); **^{31}P{^{1}H} NMR** (162 MHz, C_6D_6) δ 19.22; **^{13}C{^{1}H} NMR** (101 MHz, C_6D_6) δ 190.31 (s), 156.84 (s), 147.56 (d, J_{PC} = 2.3 Hz), 141.14 (s), 136.40 (d, J_{PC} = 12.7 Hz), 135.99 (d, J_{PC} = 10.2 Hz), 133.54 (d, J_{PC} = 3.9 Hz), 133.18 (s), 132.20 (s), 131.33 (d, J_{PC} = 3.6 Hz), 131.05 (s), 128.84 (s), 128.63 (s), 126.08 (d, J_{PC} = 15.4 Hz), 123.34 (s), 121.58 (s), 117.57 (d, J_{PC} = 176.8 Hz), 102.48 (d, J_{PC} = 3.8 Hz), 96.38 (s), 87.64 (s), 62.07 (d, J_{PC} = 4.8 Hz), 61.40 (s), 60.92 (s), 55.80 (s), 16.42 (d, J_{PC} = 6.2 Hz); **HRMS** (TOF MS ES+): Calc. for $C_{30}H_{30}O_7P$ [M+H$^+$]: 533.1729; Found: 533.1730.

Diethyl (6-(2,2-dicyanovinyl)-2,3,4-trimethoxy-7-(phenylethynyl)anthr-9-yl)phosphonate (1ac):
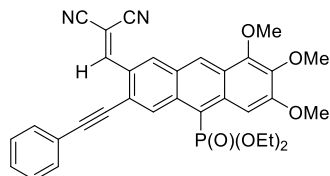
R_f = 0.78 (EtOAc), Red solid, m.p.197-199 °C, 80 % yield; **^{1}H NMR** (400 MHz, C_6D_6) δ 10.17 (s, 1H), 9.07 (d, J = 1.8 Hz, 1H), 9.05 (s, 1H), 8.80 (d, J = 2.3 Hz, 1H), 8.08 (s, 1H), 7.43- 7.41 (m, 2H), 6.99 (dd, J = 5.0, 1.9 Hz, 3H) , 4.18- 4.08 (m, 2H), 3.97- 3.87 (m, 2H), 3.80 (s, 3H), 3.76 (s, 6H), 1.02 (t, J = 7.0 Hz, 6H); **^{31}P{^{1}H} NMR** (162 MHz, C_6D_6) δ 18.83; **^{13}C{^{1}H} NMR** (101 MHz, C_6D_6) δ 157.28 (s), 156.34 (s), 147.70 (s), 141.12 (s), 136.37 (d, J_{PC} = 12.1 Hz), 135.48 (d, J_{PC} = 10.7 Hz), 133.00 (d, J_{PC} = 3.9 Hz), 132.59 (s), 132.03 (s), 131.02 (d, J_{PC} = 3.7 Hz), 129.30 (s), 128.87 (s), 128.59 (s), 126.86 (s), 126.31 (d, J_{PC} = 14.9 Hz), 122.61 (s), 121.97 (s), 117.81 (d, J_{PC} = 177.2 Hz), 114.34 (s), 113.31 (s), 102.37 (d, J_{PC} = 3.9 Hz), 97.38 (s), 87.44 (s), 83.71 (s), 62.19 (d, J_{PC} = 4.8 Hz), 61.37 (s), 60.92 (s), 55.79 (s), 16.43 (d, J_{PC} = 6.1 Hz); **HRMS** (TOF MS ES+): Calc. for $C_{33}H_{30}O_6PN_2$ [M+H$^+$]: 581.1841; Found: 581.1842.

Diethyl (6-bromo-7-(2,2-dicyanovinyl)-2,3,4-trimethoxyanthr-9-yl)phosphonate (2aa):
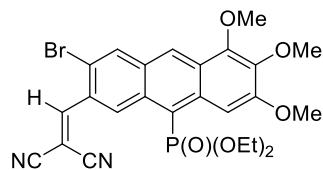
R_f = 0.60 (EtOAc), Red solid, m.p.173-175 °C, 80 % yield; ^{31}**P{**^{1}**H} NMR** (162 MHz, C$_6$D$_6$) δ 18.21; ^{1}**H NMR** (400 MHz, C$_6$D$_6$) δ 10.20 (s, 1H), 9.21 (s, 1H), 8.60 (s, 1H), 7.68 (d, J = 2.2 Hz, 1H), 7.61 (s, 1H), 4.32 - 4.22 (m, 2H), 4.15 - 4.05 (m, 2H), 3.87 (s, 3H), 3.80 (s, 3H), 3.76 (s, 3H), 1.10 (t, J = 7.0 Hz, 6H); ^{13}**C{**^{1}**H} NMR** (101 MHz, C$_6$D$_6$) δ 158.92 (s), 156.10 (s), 146.92 (d, J_{PC} = 2.3 Hz), 142.14 (s), 134.74 (d, J_{PC} = 11.9 Hz), 133.49 (s), 132.21 (d, J_{PC} = 10.5 Hz), 132.13 (d, J_{PC} = 4.2 Hz), 131.71 (d, J_{PC} = 14.1 Hz), 129.20 (s), 127.40 (d, J_{PC} = 15.2 Hz), 126.90 (d, J_{PC} = 3.6 Hz), 120.90 (d, J_{PC} = 177.9 Hz), 117.83 (s), 113.76 (s), 112.13 (s), 102.56 (d, J_{PC} = 4.0 Hz), 86.19 (s), 62.59 (d, J_{PC} = 5.3 Hz), 61.35 (s), 60.97 (s), 55.79 (s), 16.52 (d, J_{PC} = 5.8 Hz); **HRMS** (TOF MS ES+): Calc. for C$_{25}$H$_{25}$O$_4$PBrN$_2$ [M+H$^+$]: 559.0634; Found: 559.0627.

Diethyl (7-formyl-2,3,4-trimethoxy-6-(phenylethynyl)anthr-9-yl)phosphonate (2ab):
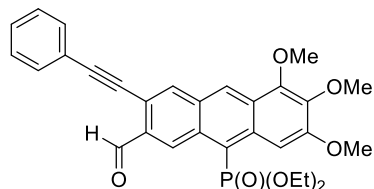
R_f = 0.54 (EtOAc), Orange solid, m.p.148-150 °C, 72 % yield; ^{31}**P{**^{1}**H} NMR** (162 MHz, C$_6$D$_6$) δ 18.62; ^{1}H NMR (400 MHz, C$_6$D$_6$) δ 10.94 (s, 1H), 10.14 (s, 1H), 9.57 (s, 1H), 8.84 (s, 1H), 8.02 (d, J = 2.3 Hz, 1H), 7.57 - 7.55 (m, 2H), 7.08 - 7.05 (m, 2H), 4.24 - 4.17 (m, 2H), 3.99 - 3.91 (m, 2H), 3.89 (s, 3H), 3.81 (s, 3H), 1.06 (t, J = 7.1 Hz, 6H); ^{13}**C{**^{1}**H} NMR** (101 MHz, CD$_2$Cl$_2$) δ 192.26 (s), 155.87 (s), 147.00 (s), 141.58 (s), 135.59 (s), 134.82 (d, J_{PC} = 11.6 Hz), 132.92 (s), 132.86 (d, J_{PC} = 11.3 Hz), 132.02 (s), 131.83 (d, J_{PC} = 4.0 Hz), 131.13 (d, J_{PC} = 14.6 Hz), 129.21 (s), 128.94 (s), 127.98 (d, J_{PC} = 3.8 Hz), 127.10 (d, J_{PC} = 15.1 Hz), 123.22 (s), 119.98 (d, J_{PC} = 177.9 Hz), 118.20 (s), 101.98 (d, J_{PC} = 4.3 Hz), 95.39 (s), 86.35 (s), 62.56 (d, J_{PC} = 5.1 Hz), 62.05 (s), 61.45 (s), 56.31 (s), 16.56 (d, J_{PC} = 6.6 Hz); **HRMS** (TOF MS ES+): Calc. for C$_{30}$H$_{30}$O$_7$P [M+H$^+$]: 533.1729; Found: 533.1732.

Diethyl (7-(2,2-dicyanovinyl)-2,3,4-trimethoxy-6-(phenylethynyl)anthr-9-yl)phosphonate (2ac):
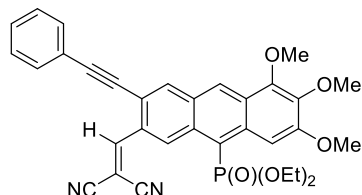
R_f = 0.76 (EtOAc), Red solid, m.p.209-211 °C, 82 % yield; ^{31}**P{^{1}H} NMR** (162 MHz, C_6D_6) δ 18.33; ^{1}**H NMR** (400 MHz, C_6D_6) δ 10.27 (s, 1H), 9.46 (s, 1H), 8.76 (d, J = 1.9 Hz, 1H), 8.05 (s, 1H), 7.86 (d, J = 2.3 Hz, 1H), 7.56 - 7.54 (m, 2H), 7.06 (dd, J = 5.3, 2.0 Hz, 3H), 4.39 - 4.29 (m, 2H), 4.23 - 4.13 (m, 2H), 3.88 (s, 3H), 3.80 (s, 3H), 3.78 (s, 3H), 1.15 (t, J = 7.0 Hz, 6H); ^{13}**C{^{1}H} NMR** (101 MHz, CD_2Cl_2) δ 159.71 (s), 156.00 (s), 146.92 (d, J = 2.2 Hz), 141.76 (s), 135.03 (s), 134.78 (d, J = 11.5 Hz), 132.77 (d, J = 10.5 Hz), 132.06 (s), 130.55 (d, J = 10.1 Hz), 130.48 (d, J = 4.1 Hz), 129.67 (s), 129.57 (s), 129.02 (s), 128.67 (s), 127.90 (d, J = 3.8 Hz), 127.25 (d, J = 15.0 Hz), 122.56 (s), 119.92 (d, J = 177.9 Hz), 118.47 (s), 114.50 (s), 112.55 (s), 102.18 (d, J = 4.3 Hz), 96.47 (s), 86.04 (s), 85.33 (s), 62.71 (d, J = 5.1 Hz), 62.05 (s), 61.47 (s), 56.33 (s), 16.59 (d, J = 6.2 Hz); **HRMS** (TOF MS ES+): Calc. for $C_{33}H_{30}O_6PN_2$ [M+H$^+$]: 581.1841; Found: 581.1838.

3.9.3 NMR spectra of anthracene derivatives
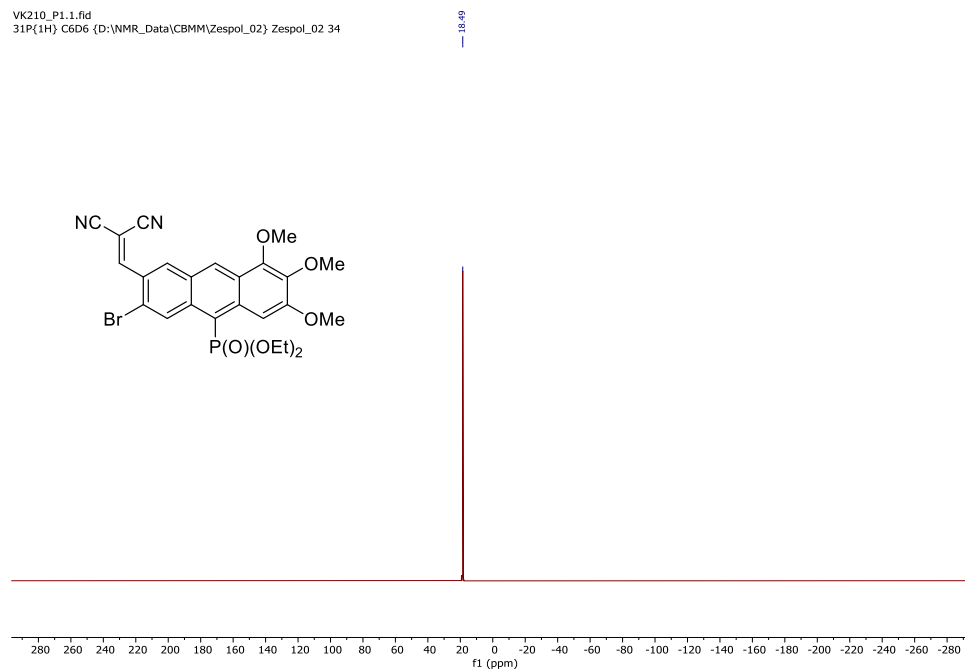
Figure S1. ^{31}P{^{1}H}-NMR (162 MHz, C_6D_6) spectrum of **1aa.**
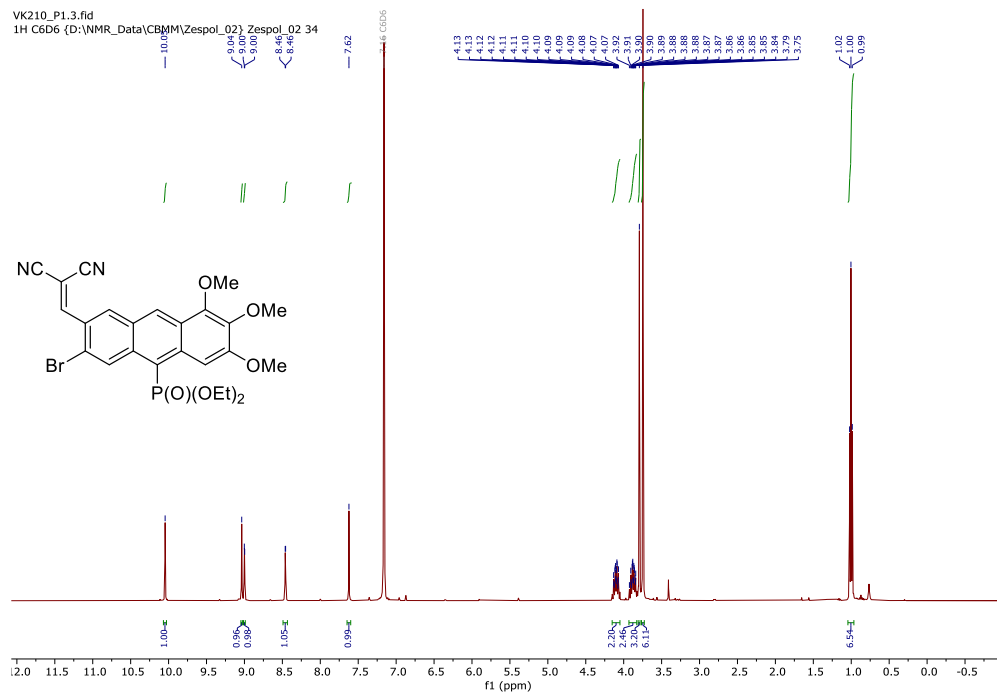
Figure S2. ^{1}H-NMR (400 MHz, C$_6$D$_6$) spectrum of **1aa.**

Figure S3. ^{13}C{^{1}H}-NMR (101 MHz, C$_6$D$_6$) spectrum of **1aa.**

VK231_P2.1.fid
31P{1H} C6D6 {D:\NMR_Data\CBMM\Zespol_02} Zespol_02 32

— 19.22
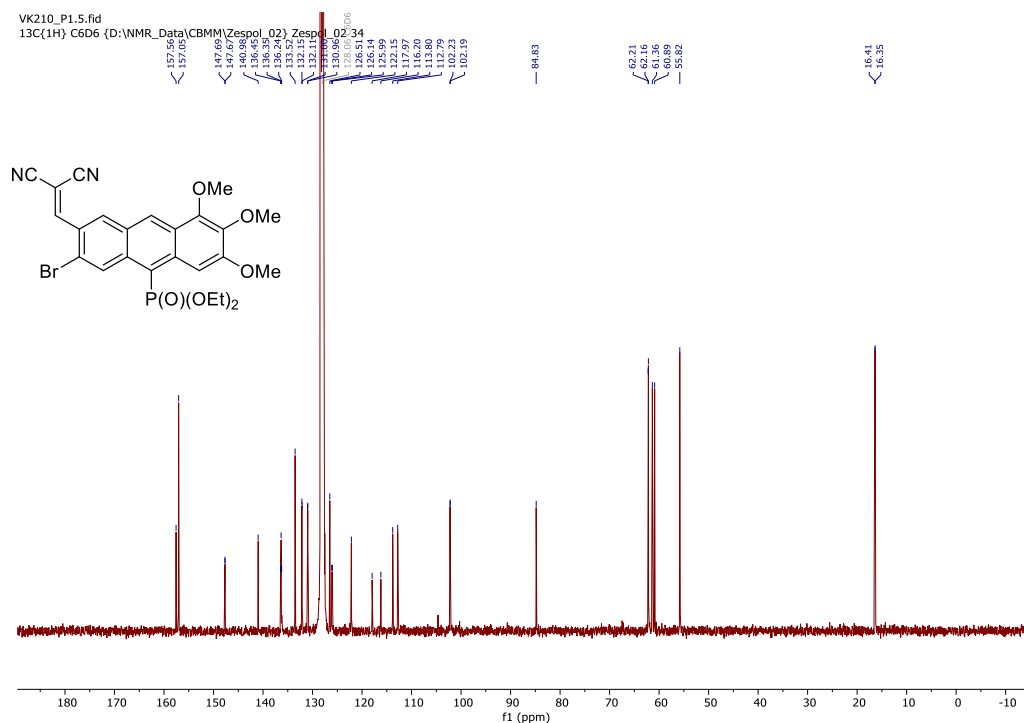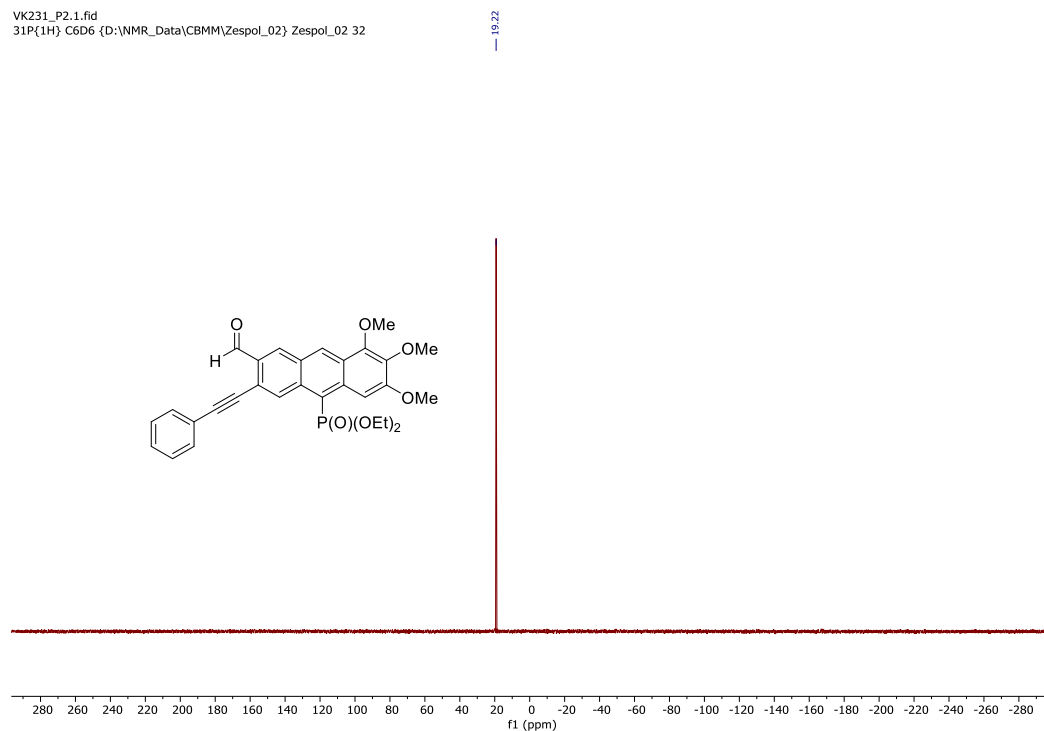
Figure S4. ^{31}P{^{1}H}-NMR (162 MHz, C$_6$D$_6$) spectrum of **1ab.**

VK231_P4.1.fid
1H C6D6 {D:\NMR_Data\CBMM\Zespol_02} Zespol_02 39
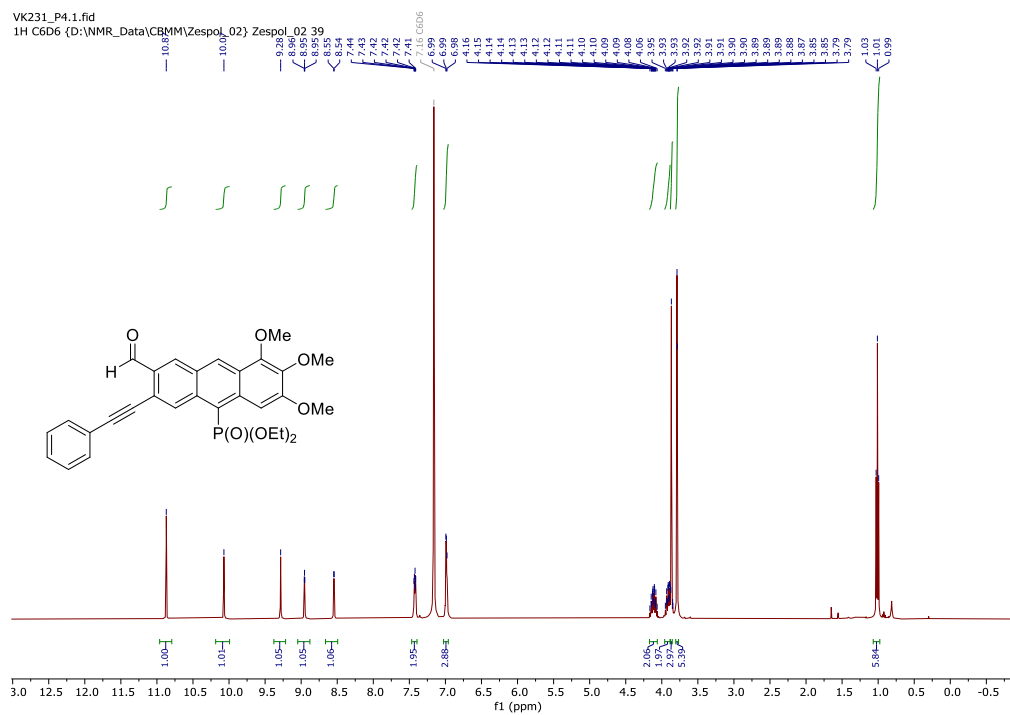
Figure S5. ^{1}H-NMR (400 MHz, C$_6$D$_6$) spectrum of **1ab.**
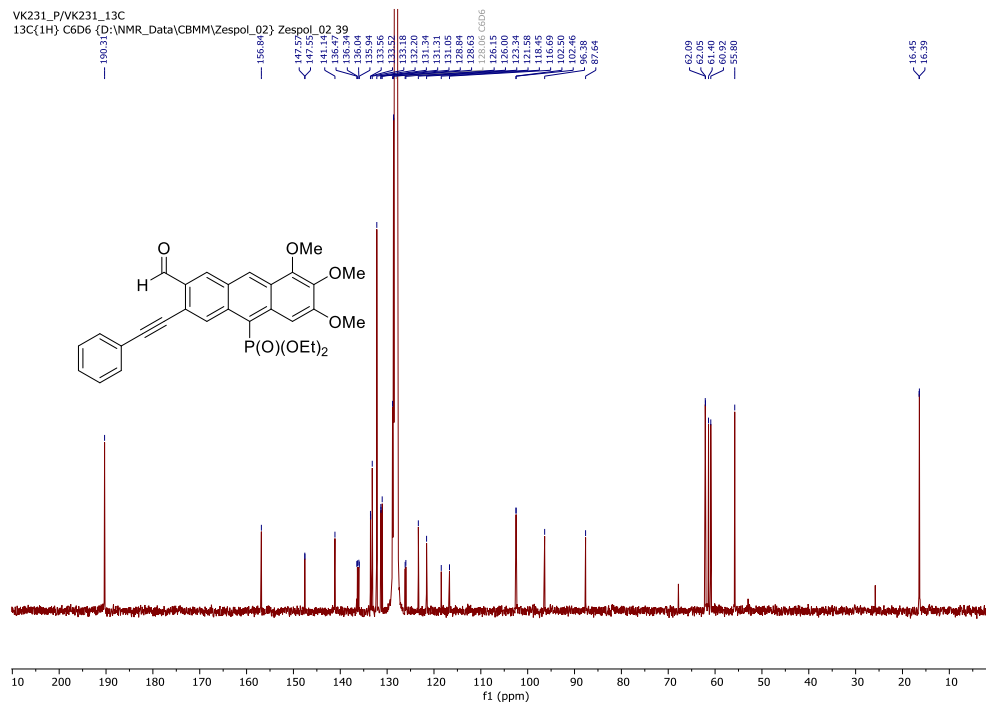
Figure S6. $^{13}C\{^1H\}$-NMR (101 MHz, C_6D_6) spectrum of **1ab.**
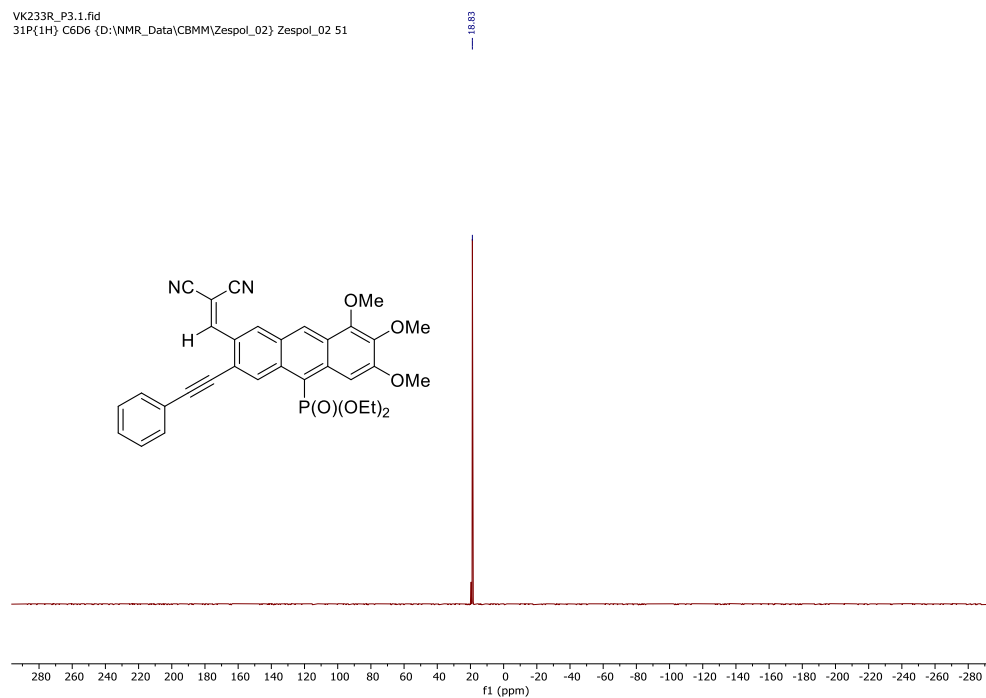
Figure S7. $^{31}P\{^1H\}$-NMR (162 MHz, C_6D_6) spectrum of **1ac.**

VK233R_P3.3.fid
1H C6D6 {D:\NMR_Data\CBMM\Zespol_02} Zespol_02_51

Figure S8. ^{1}H-NMR (400 MHz, C$_6$D$_6$) spectrum of **1ac.**

VK233R_P1_13C.1.fid
13C{1H} C6D6 {D:\NMR_Data\CBMM\Zespol_02} Zespol_02_60
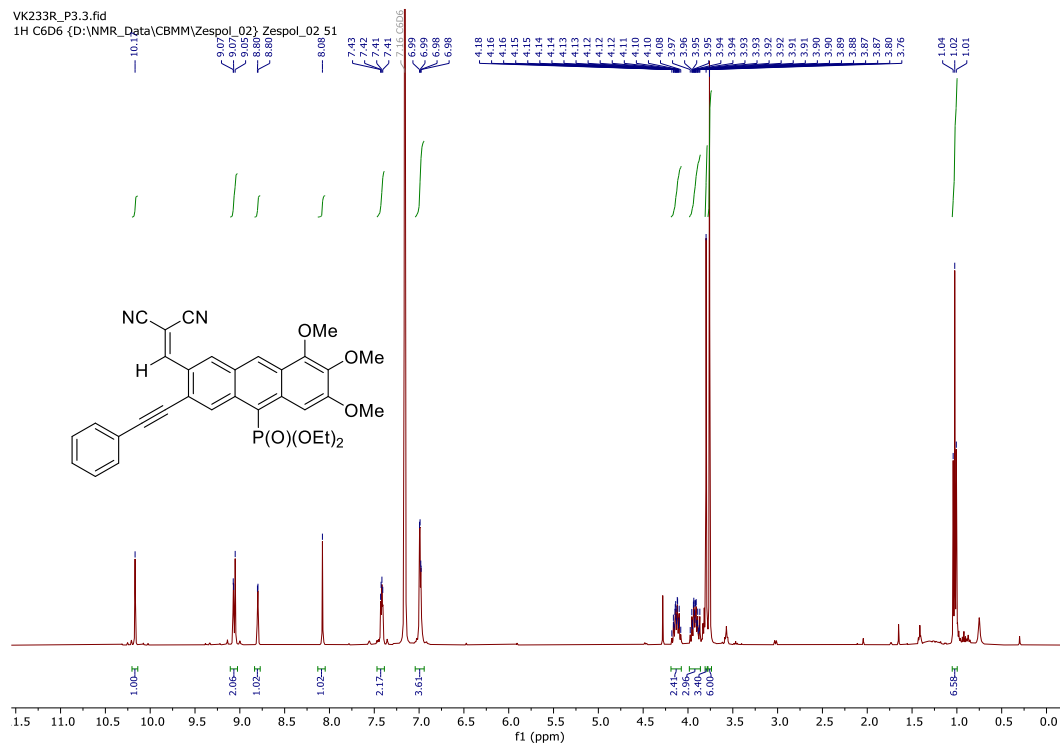
Figure S9. ^{13}C{^{1}H}-NMR (101 MHz, C$_6$D$_6$) spectrum of **1ac.**
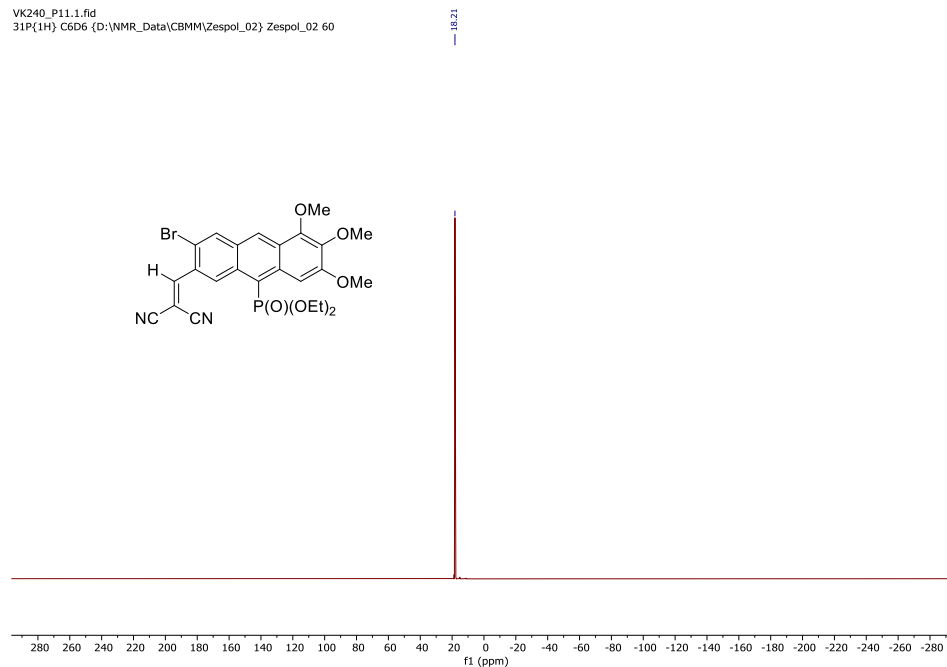
Figure S10. $^{31}P\{^1H\}$-NMR (162 MHz, C_6D_6) spectrum of **2aa.**
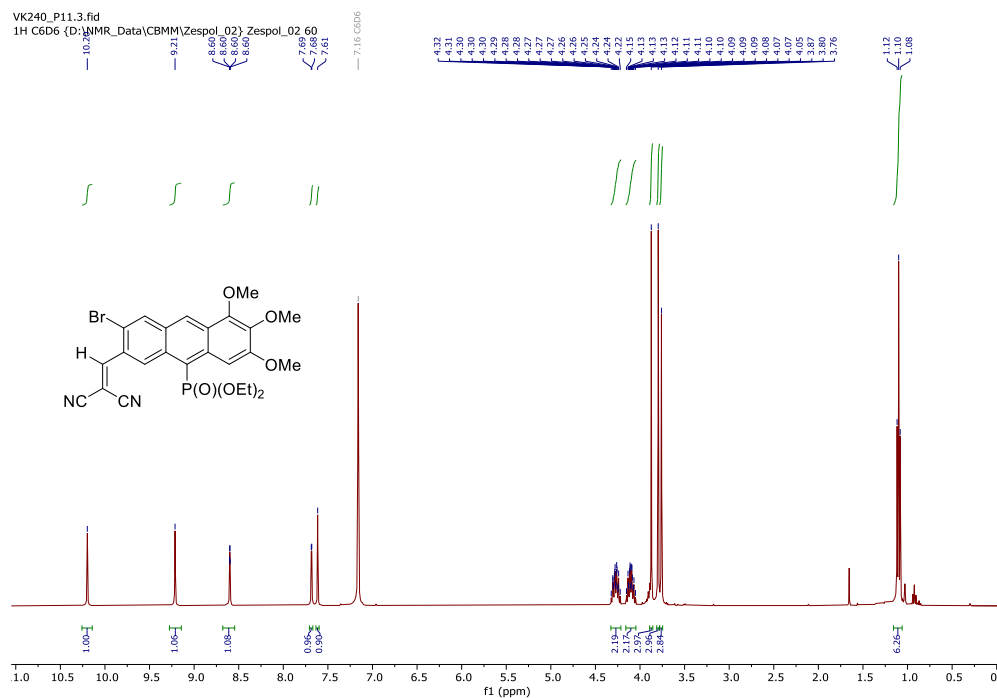
Figure S11. ^1H-NMR (400 MHz, C_6D_6) spectrum of **2aa.**

VK240P11_13C.1.fid
13C{1H} C6D6 {D:\NMR_Data\CBMM\Zespol_02} Zespol_02 45
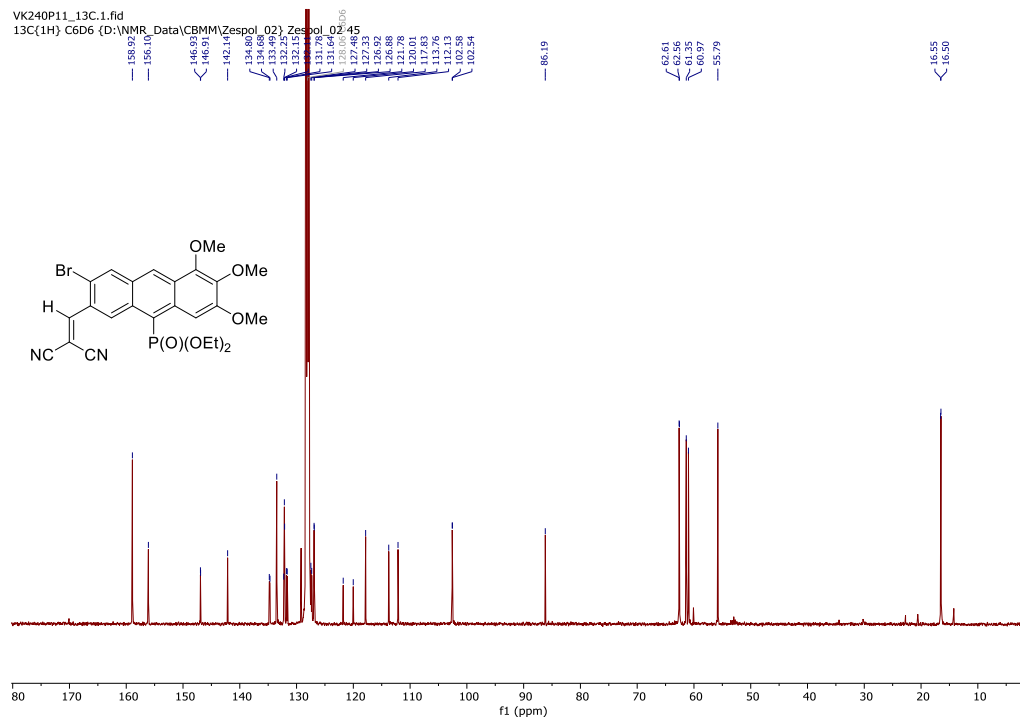
Figure S12. $^{13}C\{^1H\}$-NMR (101 MHz, C_6D_6) spectrum of **2aa.**

VK243P_16.1.fid
31P{1H} C6D6 {D:\NMR_Data\CBMM\Zespol_02} Zespol_02 53
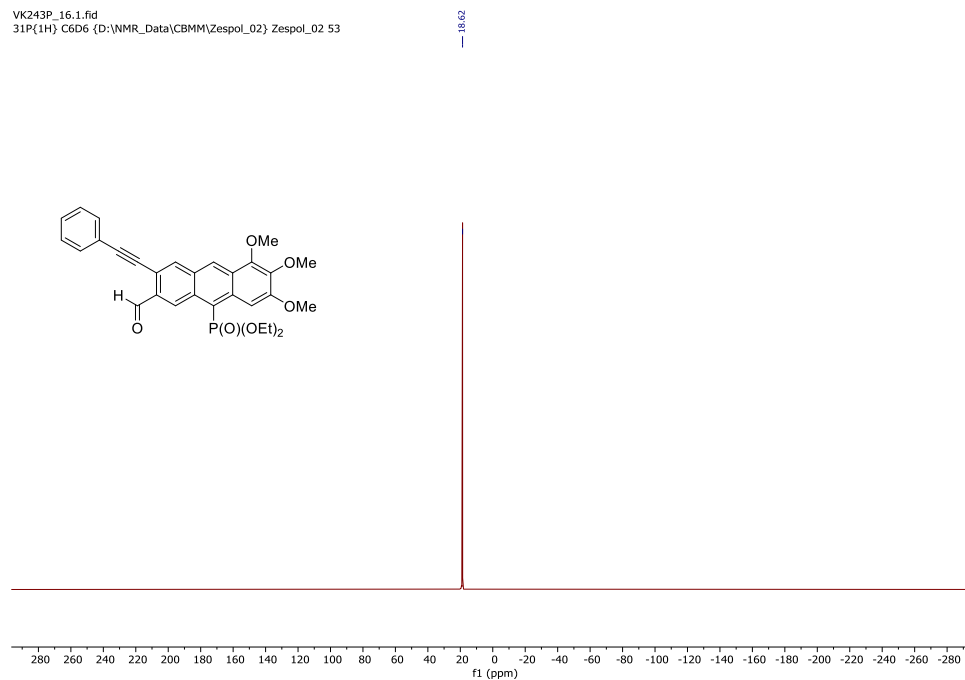
Figure S13. $^{31}P\{^1H\}$-NMR (162 MHz, C_6D_6) spectrum of **2ab.**
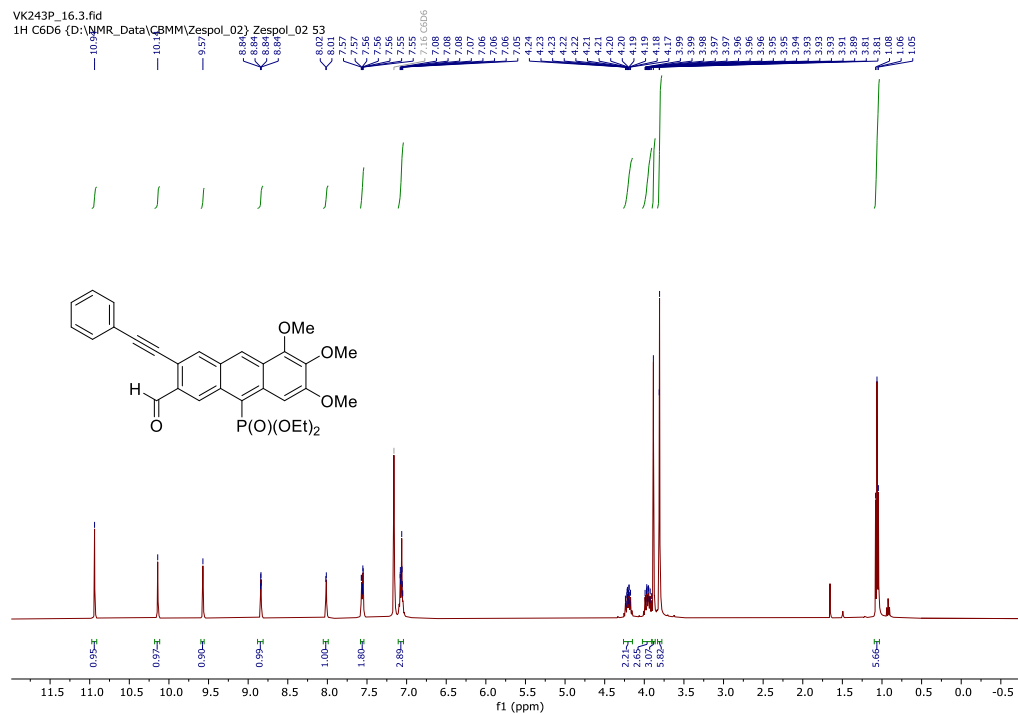
Figure S14. ^{1}H-NMR (400 MHz, C$_6$D$_6$) spectrum of **2ab.**
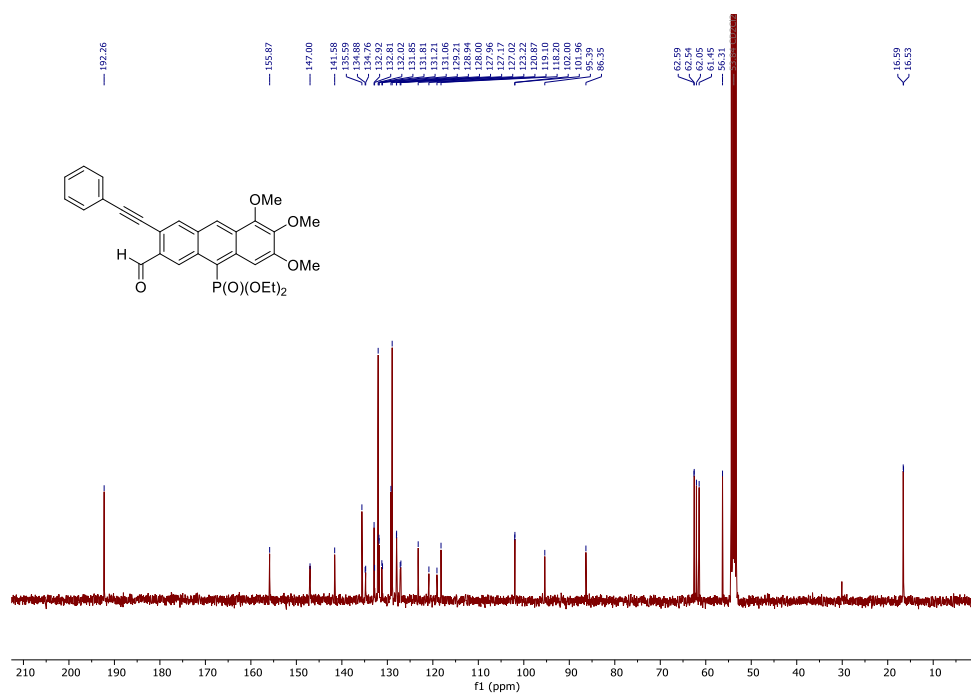
Figure S15. ^{13}C{^{1}H}-NMR (101 MHz, C$_6$D$_6$) spectrum of **2ab.**

VK247_P1.1.fid
31P{1H} C6D6 {D:\NMR_Data\CBMM\Zespol_02} Zespol_02 45

— 18.33
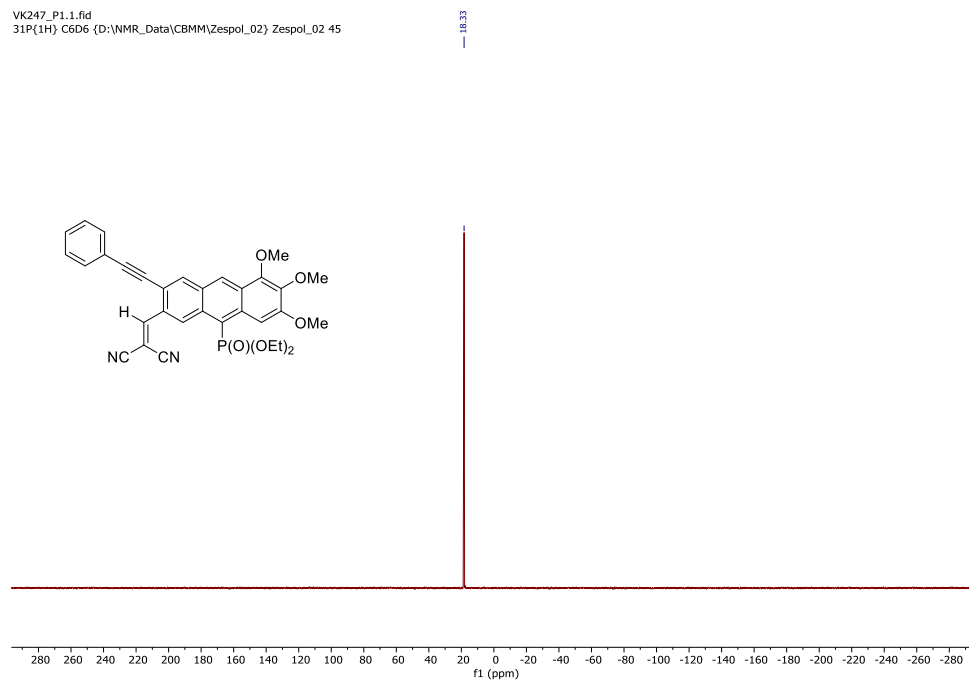
Figure S16. ^{31}P{^{1}H}-NMR (162 MHz, C$_6$D$_6$) spectrum of **2ac.**

VK247_P1.3.fid
1H C6D6 {D:\NMR_Data\CBMM\Zespol_02} Zespol_02 45
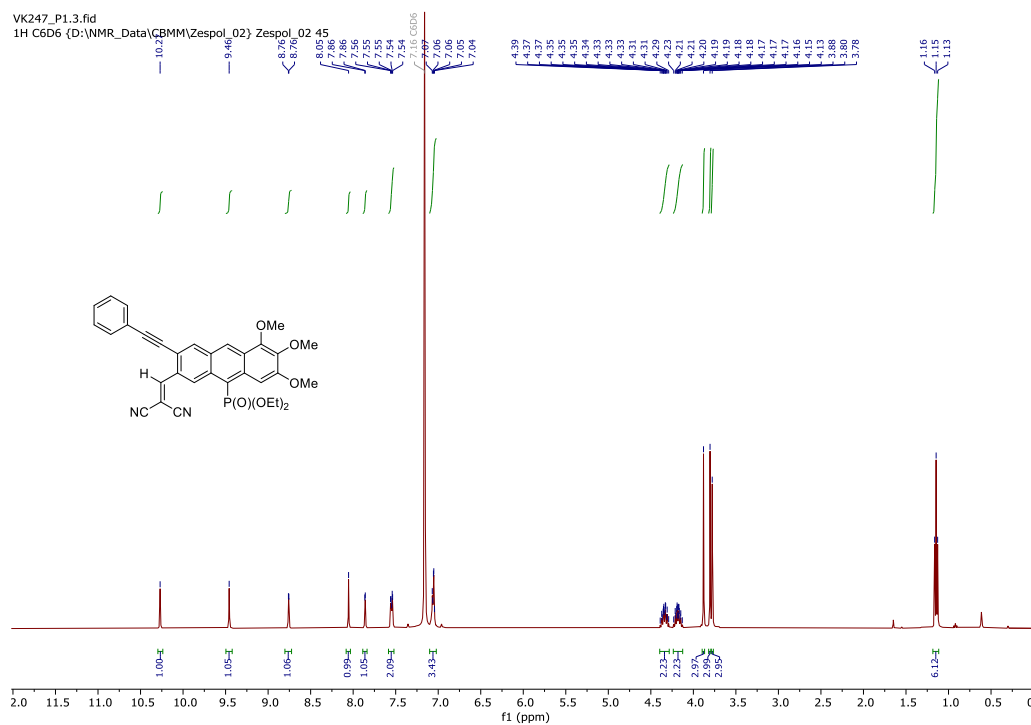
Figure S17. ^{1}H-NMR (400 MHz, C$_6$D$_6$) spectrum of **2ac.**
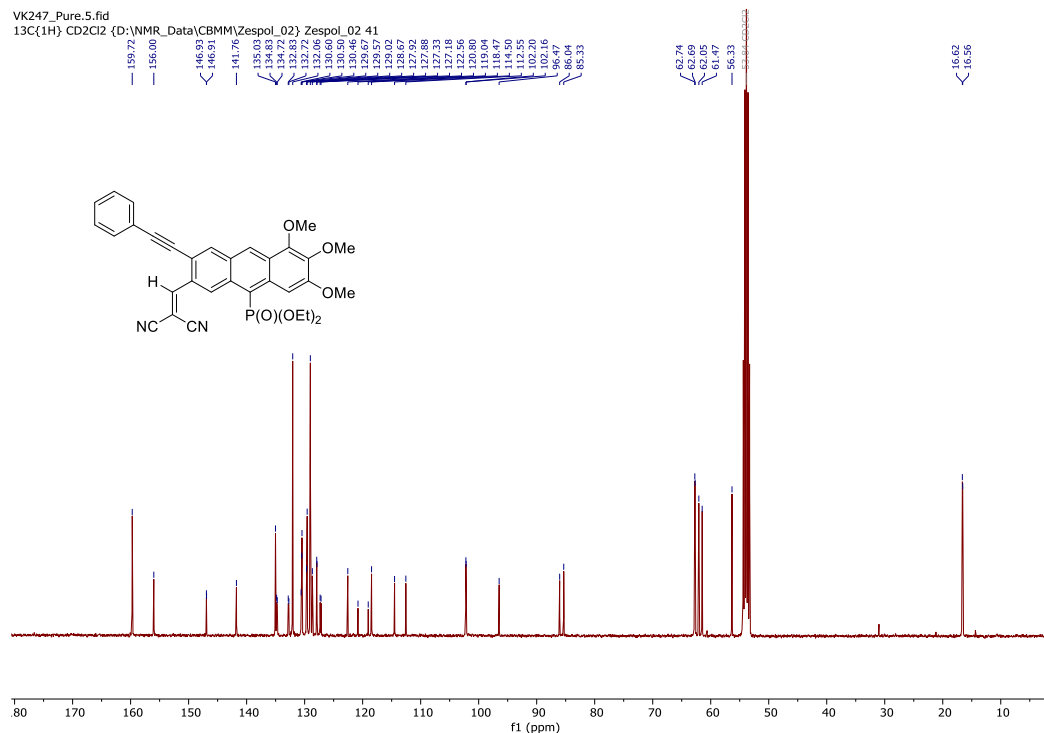
Figure S18. $^{13}C\{^1H\}$-NMR (101 MHz, C_6D_6) spectrum of **2ac.**

3.9.4 Photophysical properties

Absorption and emission spectra for *ortho*-positional isomers **1aa-ac** and **2aa-ac** were recorded on a Jasco V770 spectrometer in solvents of spectroscopic grade (toluene, DCM, and MeOH) at concentrations 10^{-5} mol/L. Results are shown in Figures S19-S21.
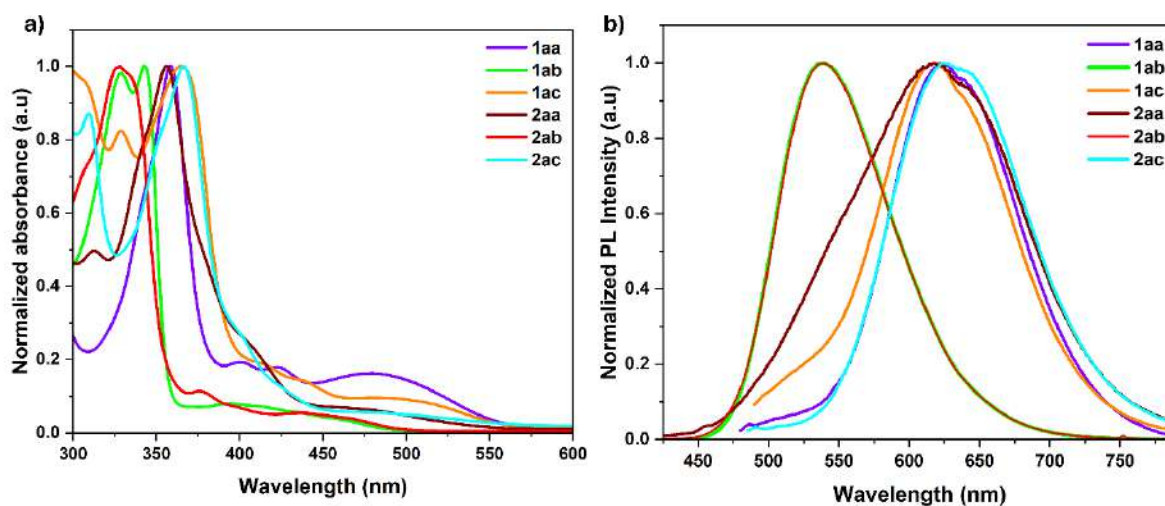
Figure S19. (a) Normalized absorbance and (b) emission spectra of **1aa-ac** and **2aa-ac** (10^{-5} mol/L, DCM).
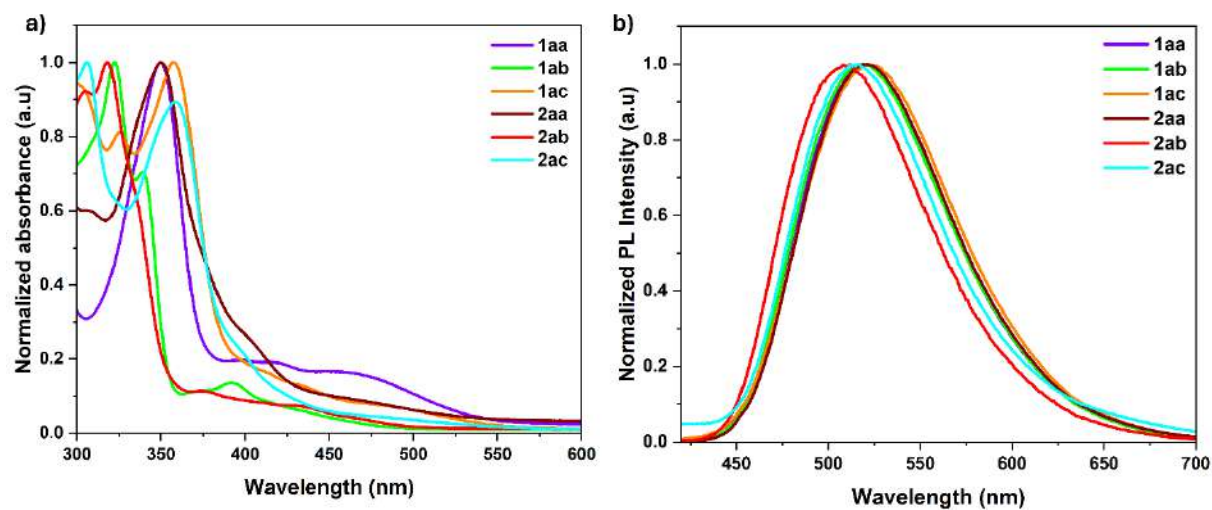
Figure S20. (a) Normalized absorbance and (b) emission spectra of **1aa-ac** and **2aa-ac** (10^{-5} mol/L, MeOH).
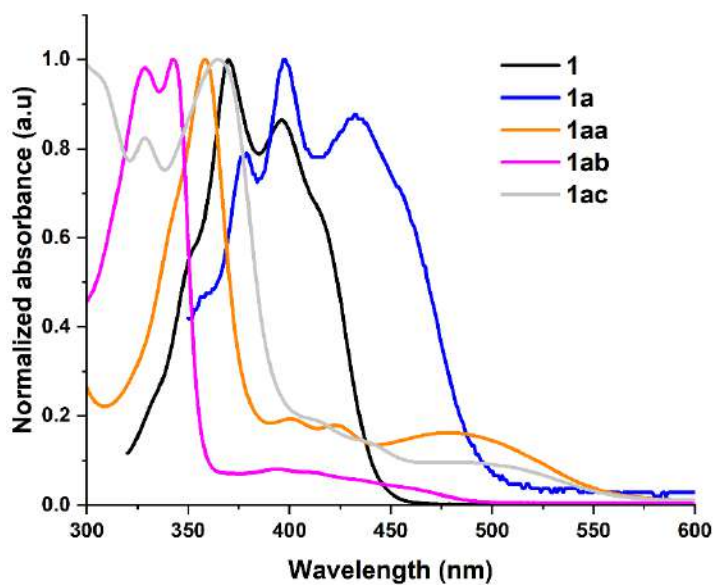
Figure S21. Normalized absorbance spectra of **1**, **1a**, and **1aa-ac** (10^{-5} mol/L, DCM).
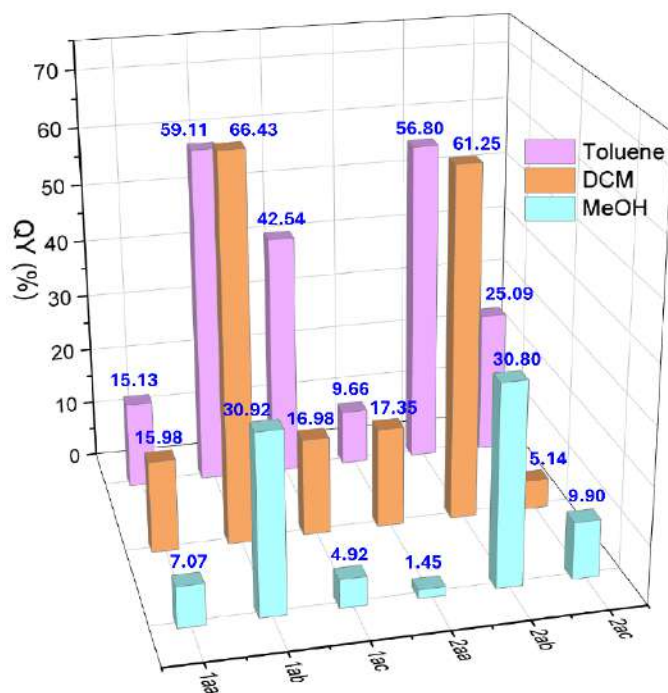
Figure S22. The absolute photoluminicence quantum yields (QY) of **1aa-ac** and **2aa-ac** in toluene (pink), DCM (orange), and MeOH (blue).

3.9.5 Electrochemical properties

Electrochemical characterization of *ortho*-positional isomers **1aa-ac** and **2aa-ac** were conducted using a Metrohm Autolab PGSTAT128N potentiostat/galvanostat instrument. All anthracene deriavtives were dissolved in dry, CH_2Cl_2 of spectroscopic grade (concentration 0.5 mM) in the presence of $[n\text{-}Bu_4N]^+[PF_6]^-$ as an electrolyte (concentration 100 mM), and the resulting solution was degassed by purging with Ar gas for 20 minutes. A three-electrode electrochemical cell was used with a glassy carbon disk as the working electrode, Pt wire as the counter electrode, and Ag/AgCl wire as the reference electrode. All samples were measured versus Ag/AgCl with a scan rate of 50 mVs^{-1} (CV) or 5 mVs^{-1} (DPV) at 20 °C. The molecular frontier orbital levels were estimated from the electrochemical data by using the method described by Sun and Dalton[2] i.e, $E_{HOMO} = -(4.8 + E_{1/2} Ox.)$; $E_{LUMO} = -(4.8 + E_{1/2}Red.)$; $E_g = E_{LUMO} - E_{HOMO}$. Cyclic voltammetry (CV) and differential pulse voltammetry (DPV) plots are shown in Figures S23 and S24 and all the measured redox potentials and the calculated E_{HOMO}, and E_{LUMO} energies, and energy gaps E_g are given in Table S1.
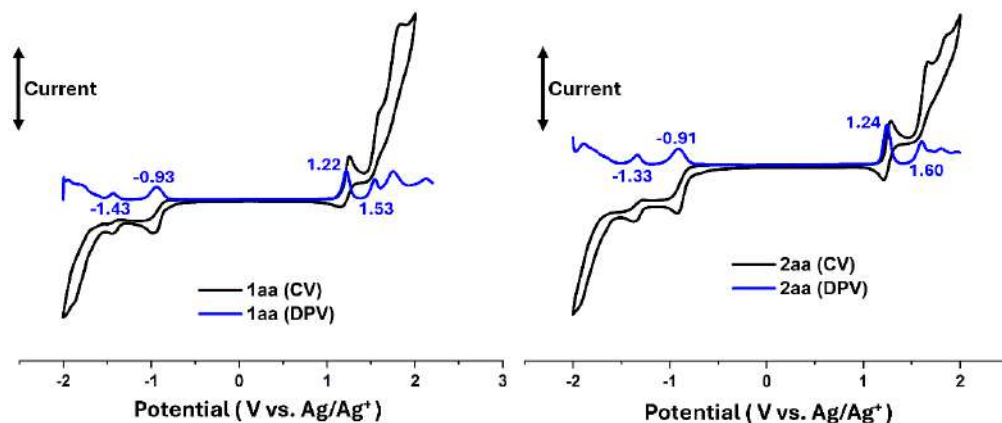
Figure S23. Cyclic and differential pulse voltammogram for *ortho*-positional isomers **1aa** and **2aa** in the CH$_2$Cl$_2$ solution.
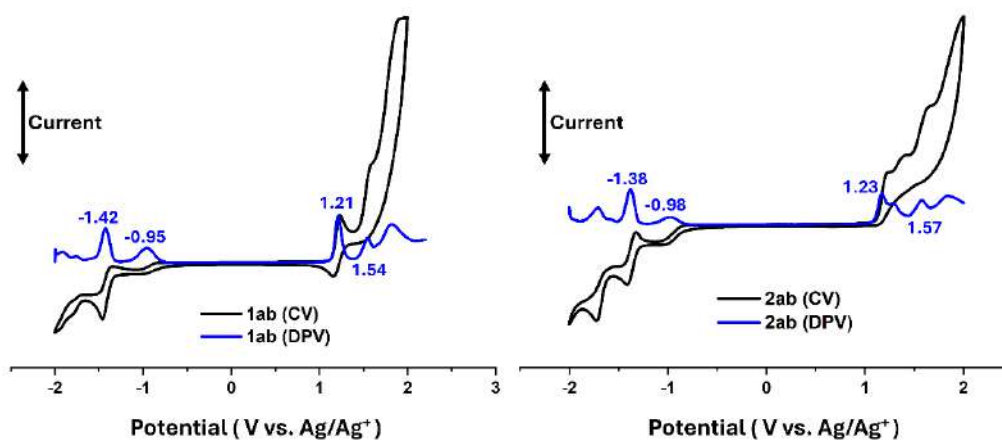
Figure S24. Cyclic and differential pulse voltammogram for *ortho*-positional isomers **1ab** and **2ab** in the CH$_2$Cl$_2$ (DCM) solution.

Table S1. Oxidation and reduction potentials (E$_{ox}$ /E$_{red}$) from DPV for *ortho*-positional isomers **1aa-ac** and **2aa-ac** in the DCM solution and E$_{HOMO}$, E$_{LUMO}$, and E$_g$ values estimated based on these data.

	$E_{Ox1,2}$	$E_{Red1,2,3}$	E_{HOMO} (eV)	E_{LUMO} (eV)	E_g (eV)
1aa	1.22, 1.53	-0.93, -1.43	-6.02	-3.38	2.64
1ab	1.21, 1.54	-0.95, -1.42	-6.01	-3.38	2.63
1ac	1.26, 1.61	-0.90, -1.39, -1.71	-6.06	-3.41	2.65
2aa	1.24, 1.60	-0.91, -1.33	-6.04	-3.47	2.57
2ab	1.23, 1.58	-0.98, -1.38	-6.05	-3.42	2.63
2ac	1.25, 1.58	-0.89, --1.34, -1.76	-6.05	-3.46	2.59

141

3.9.6 Computational studies

The molecular and electronic structures of **1aa-ac** and **2aa-ac** were calculated by the DFT method using the gradient corrected three-parameter hybrid functional (B3LYP) with the 6-31++G(d,p) basis set. Full geometry optimizations of compounds in the gas phase were performed using the GAUSSIAN09 quantum chemistry package.[3] In order to check structural optimizations, calculated vibrational frequencies of the compounds were used (no imaginary frequencies). To visualize the shapes of frontier molecular orbitals (HOMO and LUMO), the Chemcraft program[4] was used.
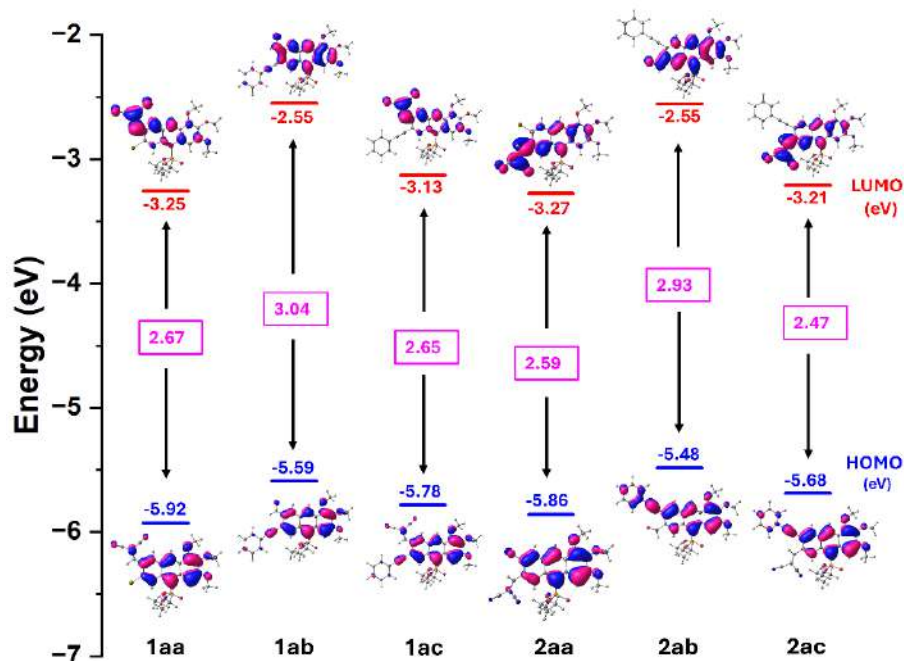
Figure S25. HOMO and LUMO orbitals calculated for *ortho*-positional isomers **1aa-ac** and **2aa-ac** in the gas phase at B3LYP/6-311++(d,p) level using Gaussian 09.

Table S2. HOMO, LUMO and E_g level for **1aa-ac** and **2aa-ac** calculated using the DFT method.

DFT Calculations data			
Nr.	E_{HOMO} [eV]	E_{LUMO} [eV]	E_g [eV]
1aa	-5.928	-3.257	2.671
1ab	-5.590	-2.552	3.038
1ac	-5.783	-3.130	2.653
2aa	-5.861	-3.277	2.584
2ab	-5.485	-2.558	2.927
2ac	-5.689	-3.211	2.478

3.9.7 CIE 1931 color space coordinates
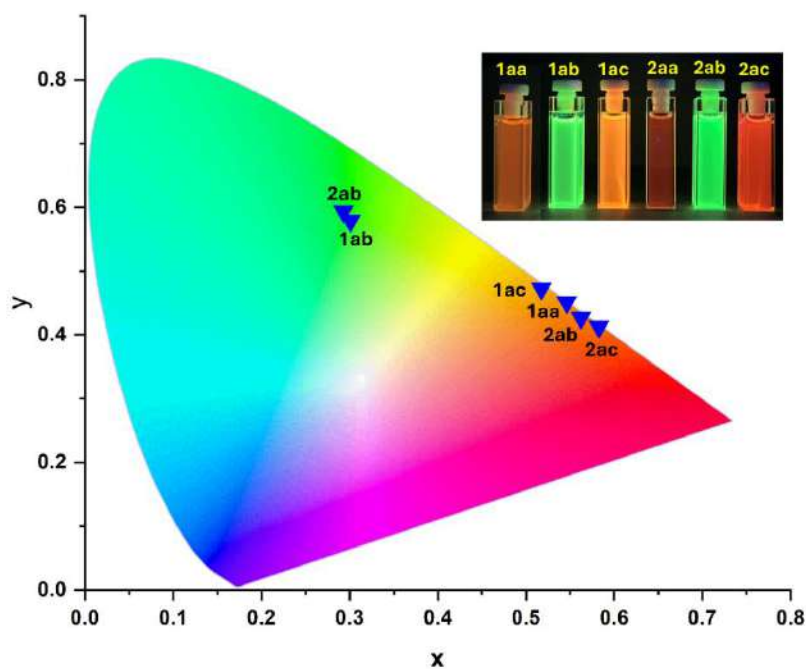
Figure S26. Commission Internationale de L'Eclairage (CIE) 1931 chromaticity coordinates for **1aa-ac** and **2aa-ac** in the toluene solution.
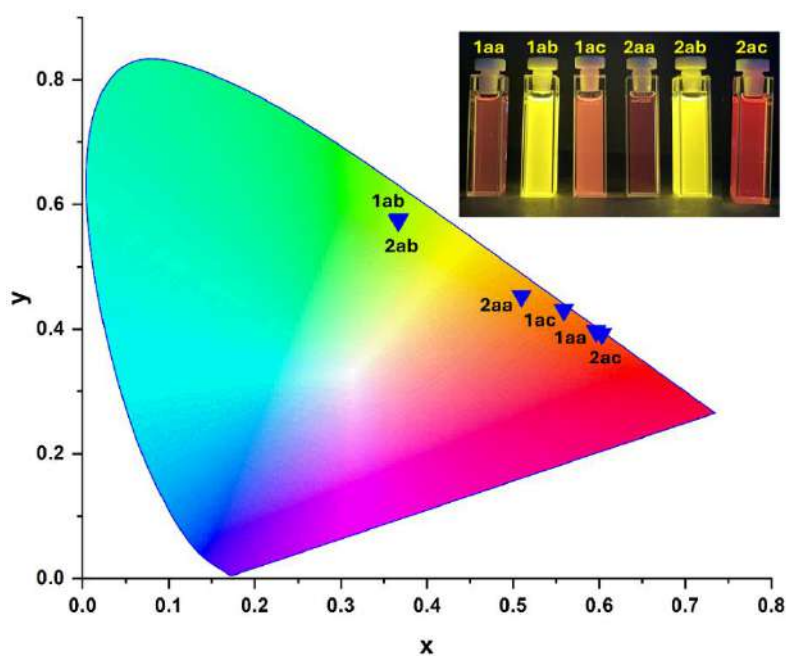
Figure S27. Commission Internationale de L'Eclairage (CIE) 1931 chromaticity coordinates for **1aa-ac** and **2aa-ac** in the DCM solution.
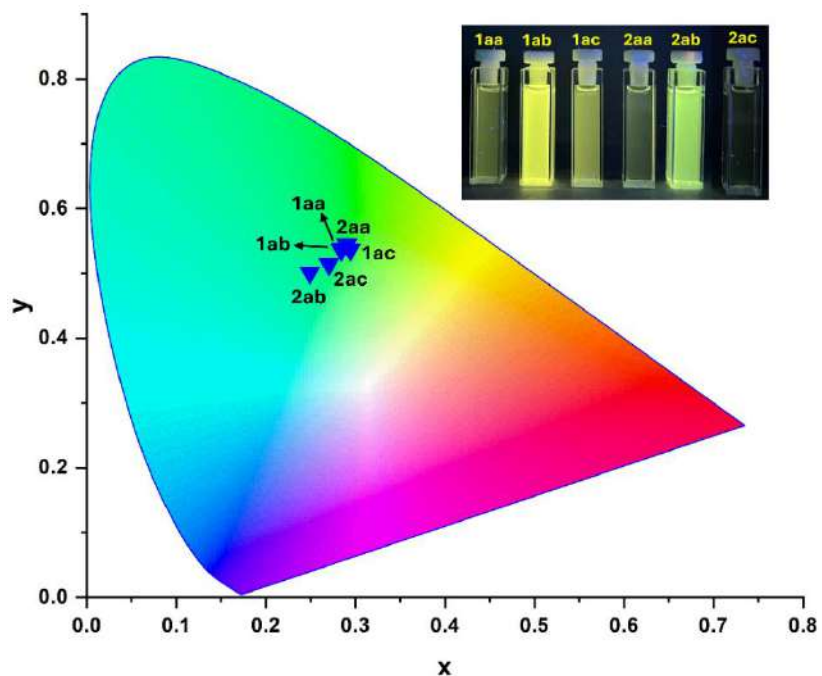
Figure S28. Commission Internationale de L'Eclairage (CIE) 1931 chromaticity coordinates for **1aa-ac** and **2aa-ac** in the MeOH solution.

Table S2. Commission Internationale de L'Eclairage (CIE) 1931 chromaticity coordinates for **1aa-ac** and **2aa-ac** in the toluene, DCM and MeOH solutions.

	Toluene		DCM		MeOH	
	X	Y	X	Y	X	Y
1aa	0.542	0.441	0.450	0.471	0.402	0.523
1ab	0.353	0.569	0.419	0.545	0.347	0.543
1ac	0.479	0.457	0.388	0.507	0.369	0.558
2aa	0.580	0.417	0.486	0.411	0.368	0.578
2ab	0.350	0.569	0.417	0.547	0.306	0.521
2ac	0.613	0.386	0.618	0.379	0.415	0.460

3.9.8 References

1. V. Vivek, M. Koprowski, E. Różycka-Sokołowska, Ł. Knopik, B. Dudziński, K. Owsianik, P. Bałczewski. *ortho*-Positional Isomers of Anthracenes and Carbazole Derivatives Containing Phosphonate Ester Group and Their Optical Properties. (under peer-review in Oraganic Letters, Section 3.4)

2. Sun, S. S.; Dalton, L. R. *Introduction to Organic Electronic and Optoelectronic Materials and Devices*, CRC, Boca Raton, **2008**, Chapter 3.4.

3. Frisch M. J.; Trucks G. W.; Schlegel H. B.; Scuseria G. E.; Robb M. A.; Cheeseman J. R.; Scalmani G.; Barone V.; Petersson G. A.; Nakatsuji H.; Li X.; Caricato M.; Marenich A.; Bloino J.; Janesko B. G.; Gomperts R.; Mennucci B.; Hratchian H. P.; Ortiz J. V.; Izmaylov A. F.; Sonnenberg J. L.; Williams-Young D.; Ding F.; Lipparini F.; Egidi F.; Goings J.; Peng B.; Petrone A.; Henderson T.; Ranasinghe D.; Zakrzewski V. G.; Gao J.; Rega N.; Zheng G.; Liang W.; Hada M.; Ehara M.; Toyota K.; Fukuda R.; Hasegawa J.; Ishida M.; Nakajima T.; Honda Y.; Kitao O.; Nakai H.; Vreven T.; Throssell K.; Montgomery J. A.; Peralta J. E.; Ogliaro F.; Bearpark M.; Heyd J. J.; Brothers E.; Kudin K. N.; Staroverov V. N.; Keith T.; Kobayashi R.; Normand J.; Raghavachari K.; Rendell A.; Burant J. C.; Iyengar S. S.; Tomasi J.; Cossi M.; Millam J. M.; Klene M.; Adamo C.; Cammi R.; Ochterski J. W.; Martin R. L.; Morokuma K.; Farkas O.; Foresman J. B.; Fox D. J. Gaussian 09, Revision A.02, Gaussian, Inc., Wallingford CT, **2016**.

4. Chemcraft - graphical software for visualization of quantum chemistry computations. https://www.chemcraftprog.com.

4. Publication constituting this Doctoral Dissertation

4.1 High-efficiency light emitters: 10-(diphenylphosphoryl)-anthracenes from one-pot synthesis including C–O–P to C–P(=O) rearrangement

4.2 Multiply substituted (hetero)acenes containing phosphonate group at the central unit as high-efficiency light emitters

4.3 *ortho*-Positional isomers of anthracenes and carbazole derivatives containing phosphonate ester group and their optical properties

Article

High-Efficiency Light Emitters: 10-(Diphenylphosphoryl)-anthracenes from One-Pot Synthesis Including C−O−P to C−P(=O) Rearrangement

Vivek Vivek, Marek Koprowski, Ewa Różycka-Sokołowska,* Marika Turek, Bogdan Dudziński, Krzysztof Owsianik, Łucja Knopik, and Piotr Bałczewski*

Read Online

ACCESS | Metrics & More | Article Recommendations | SI Supporting Information

ABSTRACT: We report a one-pot synthesis of 10-(diphenylphos-phoryl)-anthracenes, featuring a rare multisubstitution on flanking rings with donor−acceptor groups (F, Br, CN, CF$_3$, MeO, OCH$_2$O) in 24−60% yields. Catalyzed by TMSOTf, the process involves a phosphinite-to-phosphine oxide rearrangement and cyclization. These emitters exhibit excellent photoluminescence quantum yields of up to 95% in both solution and solid states. Postsynthetic anthracene functionalization as well as the optoelectronic effect of substituents, particularly the Ph$_2$P=O group, and the aggregation effect in solid on the photophysical properties, were also explored.
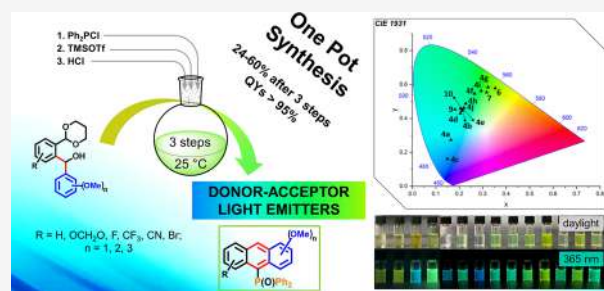
INTRODUCTION

Organic luminescent compounds have been the subject of current research due to their potential applications in organic light-emitting diodes (OLEDs),[1] organic field-effect transistors (OFETs),[2] sensors,[3] and lasers.[4] Many studies focus on organic-emitting materials based on fused aromatic hydrocarbons, such as anthracenes,[5−7] pyrenes,[8] benzimidazoles,[9] fluorenes,[10] fluoranthenes,[11] and carbazoles,[12] which are more stable than pentacenes or extended analogs. However, if appropriately substituted, they can exhibit reasonable stability and high fluorescence quantum yields and are therefore promising materials for organic electronic devices. Several reports have shown that anthracenes are useful for constructing efficient light-emitting materials.[13−15] However, unsubstituted or poorly substituted anthracenes are unsuitable for direct use because they tend toward π−π stacking and crystallization, which results in low quantum yields. An effective approach to terminate the π−π stacking involves chemical modification by substitution of the anthracene core.[16−19] Most of the known anthracenes are substituted at positions 9 and 10 only,[5b] since electron density mapping of the anthracene aromatic system shows that the highest electron density occurs just at these positions. There is a lack of synthetic methods for introducing substituents into other positions, such as the flanking rings of anthracene, to fully exploit the potential of this aromatic system.

Traditionally, 10-substituted or 9,10-disubstituted anthracenes by dipenylphosphoryl group (Ph$_2$P=O) are obtained from existing aromatic backbones by the reaction of chlorodiphenylphosphine with the corresponding lithioanthracenes obtained via the Br/Li exchange followed by

oxidation of the resulting P^{III} derivative with hydrogen peroxide.[20]

In this work, we present a one-pot, three-step synthesis of highly substituted anthracenes possessing the Ph$_2$P=O group at position 10 and other substituents of differentiated electron character on the flanking rings. The presence of the electron-withdrawing Ph$_2$P=O group lowers the energy levels of the neighboring π-electron system.[21,22] In addition, the Ph$_2$P=O group behaves as a Lewis basic site for complexing metals, cations, and protons through coordination, electrostatic, and hydrogen-bonding interactions.[23−25] In the field of materials, the Ph$_2$P=O group is used for constructing emitters, host matrices, and electron-transporting materials (ETMs) in OLEDs with excellent performance in all applications.[26−29]

Background. The Michaelis−Arbuzov rearrangement is one of the key reactions in organophosphorus chemistry for the formation of phosphonates, phosphinates, and phosphine oxides. Wiemer et al. have reported a modification of this reaction for the synthesis of phosphonates from benzylic and allylic alcohols using Lewis acids,[30,31] which has recently been modified by our group to synthesize diarylmethylphosphonates in excellent yields from diarylmethyl alcohols **1a−j** in the presence of ZnI$_2$.[30−32] However, analogous attempts to directly

synthesize diarylmethyl phosphine oxides **3a–j** using diarylmethanols **1a–j** and ethyl-diphenylphosphinite (EtO-PPh$_2$) instead of trialkyl phosphites, failed due to the rearrangement of the starting ethyl diphenylphosphinite (EtO-PPh$_2$) to ethyl diphenyl phosphine oxide (Et-P(O)Ph$_2$) under the influence of heat and Lewis acid (ZnI$_2$). Renard et al. have also shown a Lewis-acid-catalyzed rearrangement of phosphinites to phosphine oxides using trimethylsilyl triflate (TMSOTf) and BF$_3$·OEt$_2$.[33]

This inspired us to convert diarylmethyl alcohols **1a–j** to diarylmethyl phosphinites **2a–j** and then to rearrange the latter to diarylmethyl phosphine oxides **3a–j** with a catalytic amount of TMSOTf followed by cyclization to anthracenes **4a–j** (Scheme 1). This idea has been successfully realized as a one-

Scheme 1. Synthesis of Donor–Acceptor 10-(Diphenylphosphoryl)-anthracenes 4a–j
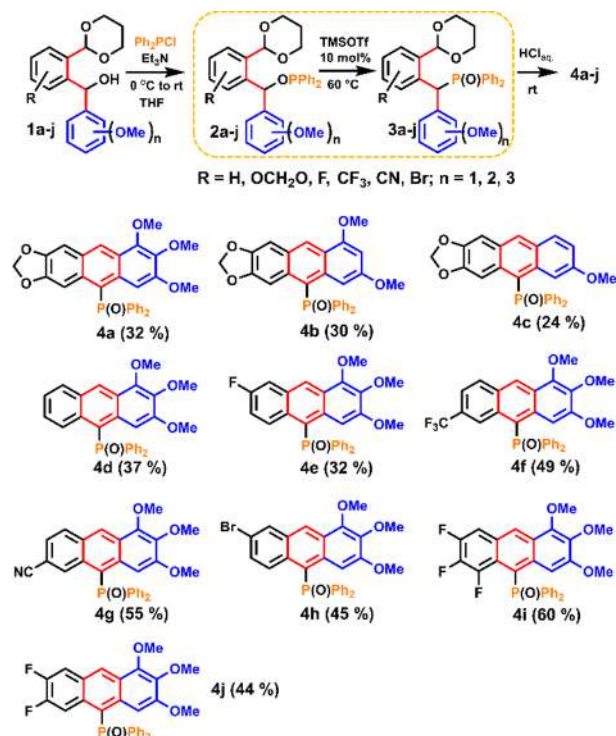
pot process without separating intermediate products **2a–j** and **3a–j**. All obtained anthracenes **4a–j** were fully characterized, and their potential in organic electronics as light emitters has been shown.

RESULTS AND DISCUSSION

Synthesis. The three-step, one-pot synthesis of multiply substituted anthracenes **4a–j** started from diarylmethyl alcohols **1a–j**, which were synthesized from 1-(1,3-dioxanyl)-2-bromo benzaldehydes according to our previous protocol.[19]

The alcohols **1a–j** were converted into phosphinites **2a–j** with triethylamine (NEt$_3$) and chlorodiphenylphosphine (PPh$_2$Cl) at room temperature, followed by the addition of TMSOTf (10 mol %) to rearrange the resulting phosphinites **2a–j** to phosphine oxides **3a–j** at 60 °C [C–O–P to C–P(═ O)] according to Scheme 1 (reaction mechanism, Scheme 1S, SI). Treatment of the latter with aqueous HCl (12 N) under mild conditions resulted in the formation of easily separable anthracenes **4a–j** in 24–60% yields after three steps, which

gave an average of 70–85% per step (reaction mechanism, Scheme 2S, SI).

A further modification of the anthracene moiety was carried out starting with P^{III} derivative **5** (Scheme 2). Thus, the in situ

Scheme 2. Syntheses of the Phosphine 5, the Phosphine Sulfide 6, the Phosphine Selenide 7, the Au^I Complex 8, and the Dephosphorylated Derivative 9
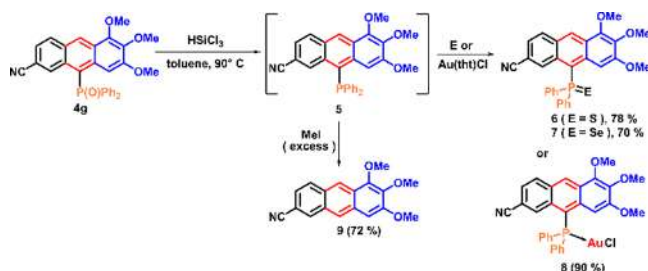
reductive deoxygenation of the phosphine oxide **4g** (δ_{31P} = 29.8 ppm, CD$_2$Cl$_2$) with trichlorosilane in toluene resulted in the formation of the phosphine **5** (δ_{31P} = −24.2 ppm, CD$_2$Cl$_2$), which was subsequently converted into the phosphine sulfide **6** in 78% yield (δ_{31P} = 33.9 ppm, CD$_2$Cl$_2$) and the phosphine selenide **7** in 70% yield (δ_{31P} = 25.2 ppm, CD$_2$Cl$_2$) by treatment of the former with elemental sulfur and selenium, respectively, in refluxing toluene. Treatment of the phosphine derivative **5** with chloro(tetrahydrothiophene)gold, [Au^I(tht)-Cl] at room temperature for 2h, resulted in the formation of the gold(I) complex **8** in 90% yield (δ_{31P} = 23.3 ppm, CD$_2$Cl$_2$) (Scheme 2).[34,35]

Compounds **5** and **8** were unstable in air and could be easily oxidized back to phosphine oxide **4g**. Furthermore, when **4g** was reduced to **5** with an excess of HSiCl$_3$ followed by treatment with an excess of iodomethane, unexpectedly, a dephosphorylated compound **9** was formed in 72% yield, instead of the expected phosphonium salt, as a result of the *ipso* attack of the Si–H bond, facilitated by the presence of the 6-CN group (reaction mechanism, Scheme S3, SI).

Postsynthesis functionalization of the anthracene backbone to further enhance π-conjugation was demonstrated by the synthesis of the 7-thienyl derivative **10** in 94% yield, using the Suzuki - Miyaura cross-coupling reaction of 7-Br-**4h** with 2-thienylboronic acid (Scheme 3).[36]

Scheme 3. Synthesis of the 7-Thienyl Derivative 10
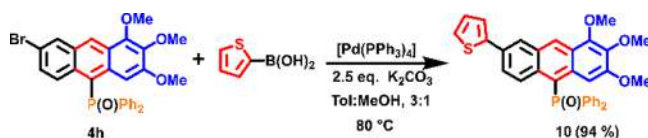
Crystal Structures. X-ray diffraction measurements for crystals of anthracenes **4b**, **4j**, and **9**, obtained from CH$_2$Cl$_2$ (DCM) solutions revealed that the anthracene **9** crystallized as solvent-free form (Figure S81 in SI) while **4b** and **4j** as DCM solvates, **4b·DCM** and **4j·DCM** (Figures S82–S83 in SI)). Crystal structure data are given in the Supporting Information, SI.

Photophysical Properties in Solution and Solid. The ultraviolet–visible (UV–vis) absorption, photoluminescent emission (PL), and quantum yield data of anthracenes **4a–j**, **6**, **7**, **9**, and **10** in three different solvents (toluene, DCM, and

Table 1. Photophysical Data for Anthracenes 4a−j, 6, 7, 9, and 10 in Different Solvents

	toluene				DCM				MeOH			
Nr	Abs.[a] $\lambda_{max.}$ (nm)	PL[b] $\lambda_{max.}$ (nm)	v^c (cm^{-1})	QY[d] (%)	Abs.[a] $\lambda_{max.}$ (nm)	PL[b] $\lambda_{max.}$ (nm)	v^c (cm^{-1})	QY[d] (%)	Abs.[a] $\lambda_{max.}$ (nm)	PL[b] $\lambda_{max.}$ (nm)	v^c (cm^{-1})	QY[d] (%)
4a	409	468	3082	60.5	409	476	3442	71.7	412	490	3863	51.4
4b	418	484	3262	69.9	421	499	3712	81.4	426	514	4018	63.9
4c	408	452	2385	44.7	408	460	2770	40.2	408	470	3233	31.8
4d	423	489	3190	66.6	422	498	3616	86.1	422	511	4127	60.7
4e	419	490	3458	69.9	420	500	3809	83.3	420	516	4429	58.4
4f	420	502	3889	71.4	421	514	4297	87.2	421	529	4849	56.7
4g	427	513	3926	82.5	432	527	4172	94.8	434	546	4726	34.4
4h	423	495	3438	72.1	424	505	3346	80.0	424	519	4317	64.8
4i	429	511	3740	64.4	430	521	4062	72.2	430	537	4633	37.7
4j	414	495	3952	72.7	413	503	4332	86.5	415	519	4828	57.6
6	447	513	4030	14.6	448	527	4389	15.8	446	538	4832	14.6
7	453	511	3420	1.9	456	524	3957	2.0	452	539	4543	2.1
9	411	451	5149	48.9	411	466	5938	71.7	406	471	6317	37.2
10	436	488	3604	46.0	439	499	4115	62.4	437	509	4392	64.5

[a]Abs. ($\lambda_{max.}$)—absorption maximum. [b]PL ($\lambda_{max.}$)—emission maximum. [c]Stokes shift, $(v) = 1/\lambda_{abs} - 1/\lambda_{em}$. [d]The absolute photoluminescence quantum yield (QY).
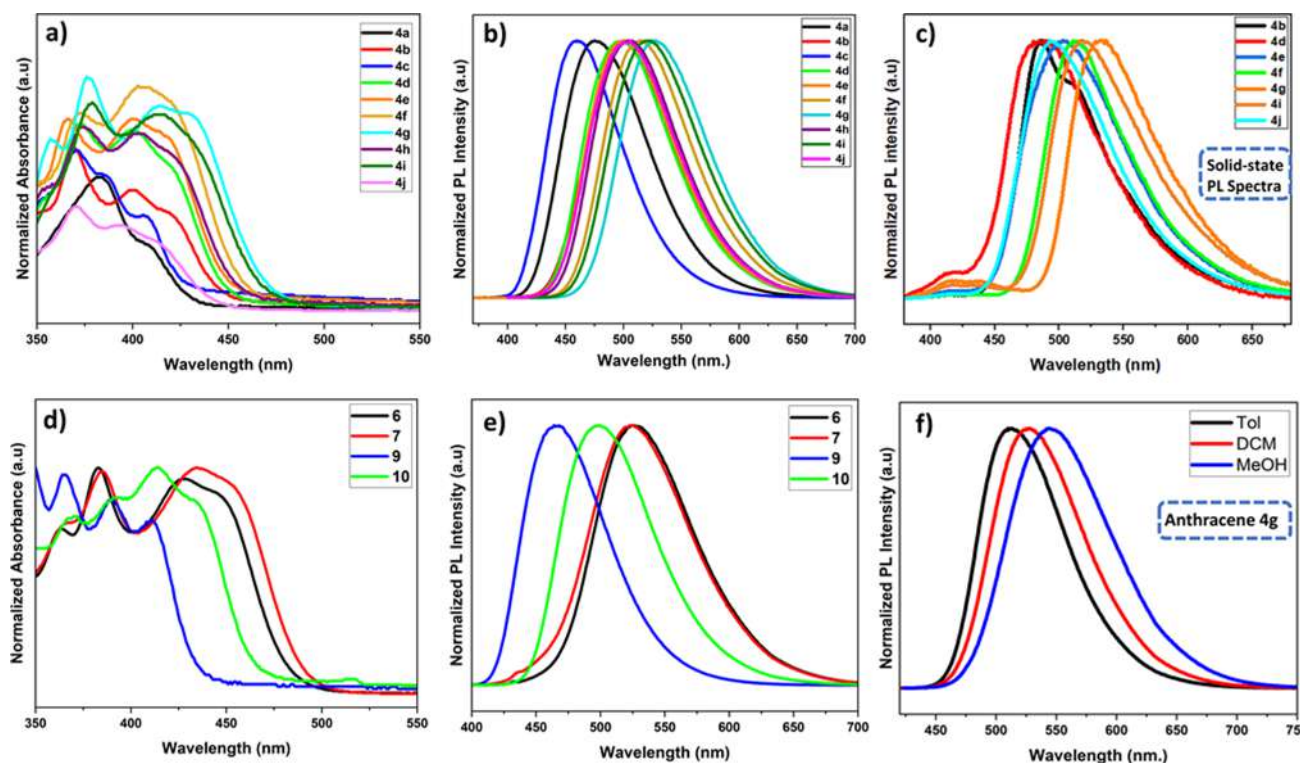
Figure 1. (a,b) Normalized absorption and emission spectra of anthracenes 4a−j (10^{-5} mol/L, DCM); (c) normalized emission spectra of selected anthracenes in solid-state; (d,e) normalized absorption and emission spectra of anthracenes 6, 7, 9, and 10 (10^{-5} mol/L, DCM); (f) normalized emission spectra of the anthracene 4g in three different solvents (10^{-5} mol/L).

methanol) are given in Table 1. As shown in Figure 1a, the absorption spectra of the substituted anthracenes 4a−j exhibited intense bands in the 360−430 nm range. The lower energy absorption was assigned to the S$_0$ → S$_1$ transition and had the typical $\pi \rightarrow \pi^*$ character, known for many anthracene derivatives.[37−40] The anthracenes 4a−j emitted blue to yellow-green light in a 450−550 nm range, in DCM solutions (Figure 1b).

The values of absorption maxima for anthracenes 4a (409 nm), 4b (418 nm), and 4c (408 nm) with electron-donating 1,2,3-tri-MeO, 1,3-di-MeO, and 3-MeO groups, respectively,

did not arrange themselves in a logical order depending on the number of MeO groups (Figure 1a). Similarly, no trend was observed in emission maxima of 4a−c (λ_{max} = 476, 499, and 460 nm, respectively) (Figure 1b). However, the absorption maxima of 4f (420 nm) and 4g (427 nm), containing electron-withdrawing 6-CF$_3$ and 6-CN groups, respectively, absorbed, as expected, lower than all three anthracenes 4a−c with electron-donating MeO groups (Figure 1a). The same trend was observed in emission wavelengths of 4f and 4g (λ_{max} = 514 and 527 nm, respectively) versus that of 4d (498 nm) (Figure 1b).
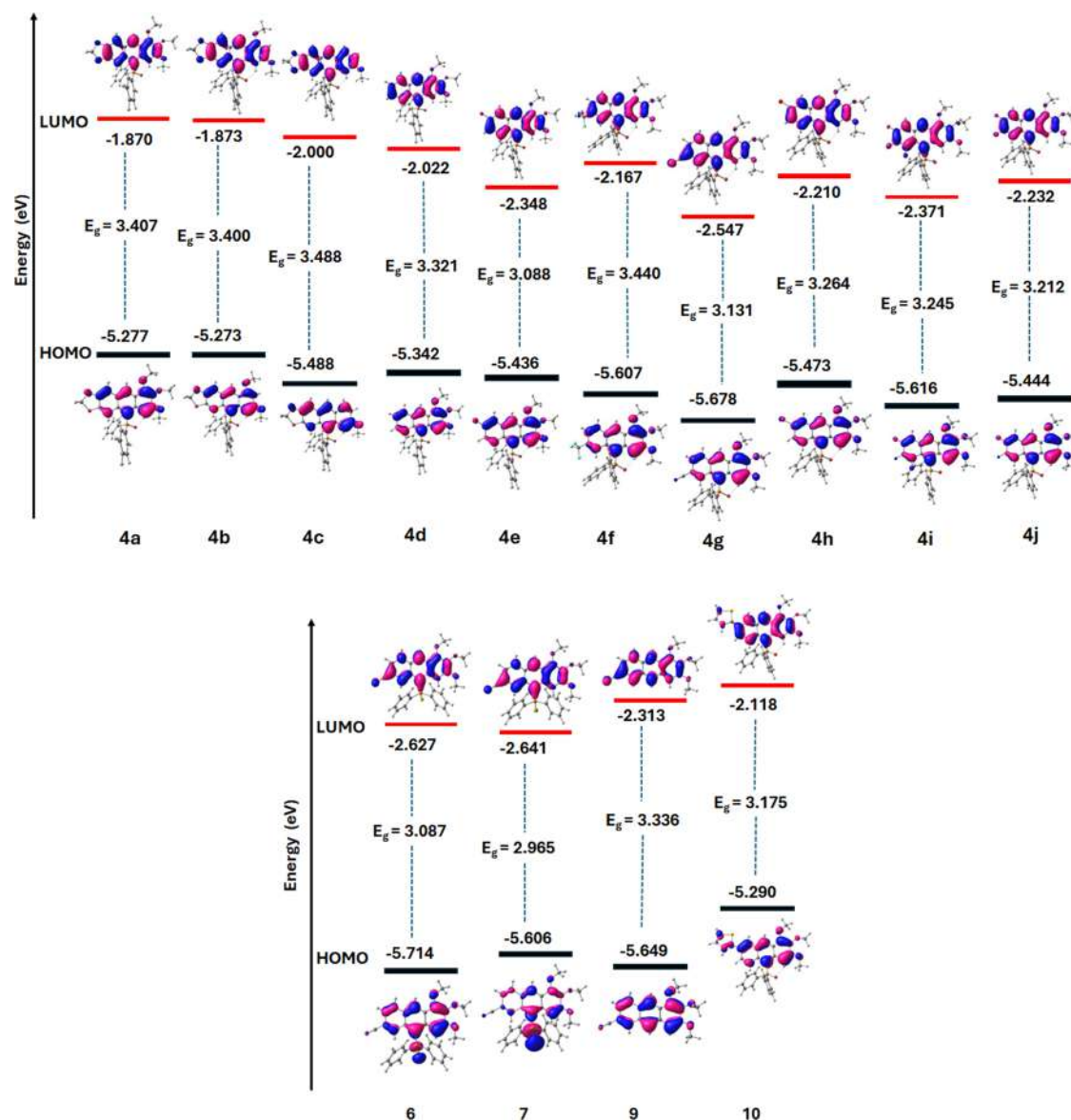
Figure 2. Molecular orbitals calculated for anthracenes **4a–j**, **6**, **7**, **9**, and **10** at DFTB3LYP/6-311++G(d,p).

The anthracenes **4e** (419 nm) and **4h** (423 nm) with halogen 7-F and 7-Br substituents showed redshifts compared to that of the unsubstituted anthracene **4d** (422 nm) on the left flanking ring (Figure 1a). This was also the case with the wavelengths of light emission (Figure 1b). The values of absorption maxima for the multiply substituted fluoro anthracenes **4e** (419 nm), **4j** (414 nm), and **4i** (429 nm) with one 7-F, two 6,7-di-F and three 5,6,7-tri-F electron-withdrawing groups on the left flanking ring, respectively, again did not form a clear order in relation to the number of fluorine groups, as in the case of emission maxima (Figure 1a,b). On the other hand, all three fluoro anthracenes **4e**, **4i**, and **4j** showed redshifts compared to the unsubstituted anthracene **4d** in both absorption and emission spectra due to enhancing the donor–acceptor character of the whole conjugated system.

The absorption maxima of nitrile-substituted anthracenes 6-CN-**4g**, 6-CN-**6**, and 6-CN-**7** with 10-Ph$_2$P=O (432 nm), 10-Ph$_2$P=S (448 nm), and 10-Ph$_2$P=Se (456 nm) groups on the anthracene backbone (Table 1), respectively, revealed all redshifts compared to the 10-unsubstituted anthracene **9** (411

nm) and a clear trend due to the increasing polarizability of P=O > P=S > P=Se bonds which made electron excitation easier (Figure 1d). Interestingly, the emission wavelengths of **4g**, **6**, and **7** showed practically no difference in toluene and DCM (Table 1, Figure 1e).

The anthracene **10** with 7-thienyl substituent, showed a higher absorption maximum (439 nm) than the starting 7-bromo anthracene **4h** (424 nm), as expected, due to the extension of the conjugate system (Figure 1d). In contrast, the latter (λ_{max} = 505 nm) emitted at a higher wavelength than anthracene **10** (λ_{max} = 498 nm) containing the 7-thienyl substituent (Figure 1e).

The emission properties of the anthracene derivatives were solvent-dependent.[5b] Most anthracenes showed redshifts in more polar solvents, such as methanol, compared to less polar toluene and DCM (Figure 1f, Table 1). A comparison of emission maxima of 10-unsubstituted anthracene **9** (466 nm) and the anthracene 6-CN-**4g** (527 nm) showed the largest red-shift of 61 nm, indicating a significant effect of the 10-Ph$_2$P=O group on the optical properties (Table 1).

The emission properties were also studied in the solid state (Figure 1c). The anthracenes **4e** (λ_{max} = 503 nm), **4f** (λ_{max} = 513 nm), and **4g** (λ_{max} = 533 nm) with electron-withdrawing 7-F, 6-CF$_3$, and 6-CN groups showed the largest redshifts compared to the unsubstituted **4d** (λ_{max} = 483 nm) on the left flanking ring (Table S1, see SI). Like in solution, the synthesized anthracenes showed no trends in the solid-state emission maxima.

Effect of Substituents on Quantum Yields (QYs) in Solution. The anthracenes **4a−4j** generally showed very good QYs with an average value of 78.3% for ten compounds, and the highest QY of 94.8% for the anthracene 7-CN-**4g** (all in DCM) (Table 1). The presence of many electron-donating groups (MeO, OCH$_2$O) with electron (+M) effect, as in **4a**, weakened the donor−acceptor character of the investigated anthracenes in comparison to anthracene **4d** and anthracenes **4e−4j** with electron-withdrawing substituents. This resulted in a reduction in QYs (**4a**: 71.7 versus **4d**: 86.1 and **4e−4j**: 72.2−94.8, all in DCM; Table 1). Moreover, in general, E_{LUMO}, E_{HOMO}, and E_g for **4d** and **4e−4j** were lower than those for **4a** (Figure 2, Table S17 in SI). High QYs observed in DCM, were strongly perturbed in MeOH due to the fluorescence quenching caused by the intermolecular P=O⋯H−O and, in the case of 7-CN-**4g**, additionally by C≡N⋯H−O hydrogen bonds.

Anthracenes **6** and especially **7** with Ph$_2$P=S and Ph$_2$P=Se groups, respectively, emitted much less efficiently than anthracenes **4a−4j** with the Ph$_2$P=O group despite favorable E_g and E_{LUMO} values for the former (**6**/3.087, −2.627 eV; **7**/2.965, −2.641 eV, respectively, versus, e.g., **4g**/3.131, −2.547 eV; Figure 2, Tables S17 and S18 in SI).

Analysis of the molecular geometries of **6**, **7**, and their oxygen analog **4g** revealed that, unlike the P=O group, the presence of P=S and P=Se groups caused butterfly bending of the anthracene plane (also observed in other anthracenes)[35] with the pronounced butterfly angle at the C9−C10 axis ($\omega_{P1/P2}$ is approximately 11° in **6** and **7** compared to 2° in **4g**) (Figure 3), thereby disturbing π-conjugation within the anthracene core. In compounds **6** and **7**, the dihedral angles between planes containing phosphine phenyls (P4 and P5 planes in Figure 3) and anthracene plane (i.e., $\omega_{P3/P5}$ and $\omega_{P4/P5}$), were notably larger than in **4g** (Figure 3). Additionally, the relative orientation between P4 and P5 planes in the

Ph$_2$P=S and Ph$_2$P=Se groups exhibited increased twisting compared to that in the Ph$_2$P=O group (Figure 3). In **6** and **7**, these planes are on the same side of the anthracene plane, while in **4g** they are on opposite sides of this plane.

Moreover, the P=O substituent in **4g** remained nearly coplanar with the anthracene plane, in contrast to the P=S and P=Se substituents in **6** and **7**, which were out of the plane. Both the differences in the situation of the P=X substituents relative to the anthracene plane and the butterfly bending causing a partial disturbance of π-conjugation, and additionally the heavy atom effect in the case of S and Se,[41] were the reason for the significant decrease in quantum yields to the level of 15 and 2%, respectively.

The fluorescence lifetimes of **4b**, **4d−4g**, **4i**, and **4j** were within the typical range of 15.3 ns for 1,3-di-MeO-**4b** to 23.3 ns for 7-CN-**4g** in the same solvent (Table S1 in SI). In the solid, the highest QY, exceeding 95% was shown by the anthracene 7-CF$_3$-**4f**, which again was the highest value in the group of anthracenes known in the literature (Table S1 in SI).

The remarkable effect of the Ph$_2$P=O group on the emission properties of the obtained anthracenes is related to its high electron-withdrawing power, which promotes the formation of strong donor−acceptor systems. The measure of this effect is the Hammett σ_p constant, calculated with ACD/Percepta[42] for Ph$_2$P=O (σ_p = 0.6) which corresponds to the high σ_p values of other powerful electron-withdrawing CN and CF$_3$ groups (σ_p = 0.66/0.51, respectively). Analysis of the σ_{ind} and σ_{res} components, which are positive, shows that inductive (-I) and resonance (-M) effects are both responsible for the electron-withdrawing character of the Ph$_2$P=X groups (X=O: $\sigma_{ind}/\sigma_{res}$ = 0.26/0.34; X=S: $\sigma_{ind}/\sigma_{res}$ = 0.28/0.22).

For the Ph$_2$P=O group, the resonance (-M) effect predominates over the inductive (-I) effect while the opposite is true for the Ph$_2$P=S group. Electron-donating MeO groups in the donor−acceptor systems show σ_p = −0.27 and $\sigma_{ind}/\sigma_{res}$ = 0.30/−0.58 which means that the (+M) effect almost doubles the (-I) effect. It is interesting that fluorine, as the most electronegative element, shows the lowest sigma σ_p = 0.06 value among electron-withdrawing groups, which is due to the small difference between the σ_{ind} = 0.54 and σ_{res} = −0.48 values. This indicates only a slight predominance of the -I effect over the + M effect and a relatively significant contribution of the resonance structure with the fluorine group to the resonance hybrid.

Color Space Studies. All anthracene phosphine oxides **4a−j** emit blue to yellow-green light in DCM solutions (Figure 4: **4a**, **4b**) Particularly striking is the rapid color change from blue-green (3xMeO), through green (2xMeO) toward again deep blue (1xMeO) for anthracenes **4a−c** differing only in the number of methoxy groups (Figure 4: **4b**). The CIE 1931 color space chromaticity coordinates of anthracenes **4a−j**, **6**, **7**, **9**, and **10** in DCM, toluene, and MeOH are provided in SI (Table S19).

Aggregation Effects on the Photophysical Properties of 4j and 4b in Solids. For most of the compounds (**4b**, **4d**, **4e**, and **4j**), we observed that the QY in the DCM solution was much higher (about 81−87%) than in the solid state (about 37−47%). This indicated that various intermolecular interactions operated in solid, which led to molecular aggregation causing emission quenching (ACQ: Aggregation-Caused Quenching).[43,44] The compound **4i** showed a dramatically low QY in the solid state (13.3%) with a much higher QY in the DCM (72.2%), indicating the strongest ACQ effect. The
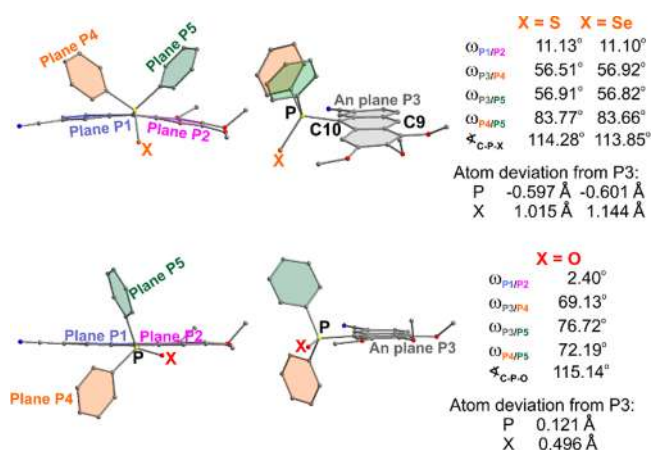
Figure 3. Molecular structures of anthracenes **6**, **7**, and **4g**, illustrating key geometric differences influencing the fluorescence QY.

	X = S	X = Se
$\omega_{P1/P2}$	11.13°	11.10°
$\omega_{P3/P4}$	56.51°	56.92°
$\omega_{P3/P5}$	56.91°	56.82°
$\omega_{P4/P5}$	83.77°	83.66°
∢$_{C-P-X}$	114.28°	113.85°

Atom deviation from P3:
P   -0.597 Å   -0.601 Å
X   1.015 Å   1.144 Å

	X = O
$\omega_{P1/P2}$	2.40°
$\omega_{P3/P4}$	69.13°
$\omega_{P3/P5}$	76.72°
$\omega_{P4/P5}$	72.19°
∢$_{C-P-O}$	115.14°

Atom deviation from P3:
P   0.121 Å
X   0.496 Å
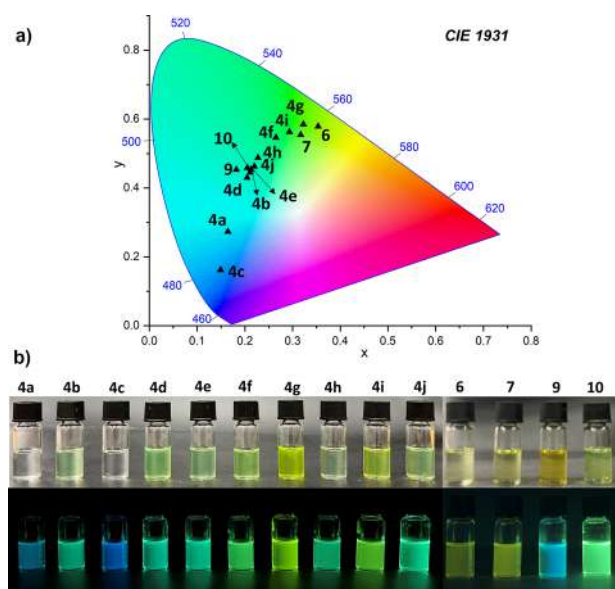
Figure 4. (a) Commission Internationale de L'Eclairage (CIE) 1931 chromaticity coordinates for anthracenes **4a−j** and **6−10** in DCM solutions; (b) photos of the anthracene **4a−j** and **6−10** samples in DCM solutions under daylight and UV (365 nm) light (bottom).

exceptions were **4f** and **4g**, which retained very high emissions in the solid state (>95 and 79.2%, respectively), suggesting an aggregation-induced emission (AIE) phenomenon[44,45] in which aggregation reduced nonemission relaxation pathways, increasing QY. To determine the effect of aggregation in the solid state on emission properties, and in particular the significantly lower QY, we analyzed intermolecular interactions, molecular packing, and the possibility of excimer formation in crystals **4j** and **4b** (both DCM solvated).

In the crystal structure of **4j·DCM**, three $\pi\cdots\pi$ interactions between anthracene units link molecules into the centrosymmetric dimer (Figure 5, Figure S85 and Table S2 in SI), showing a 49.9% area overlapping (AO) (Figure 5D), calculated using the phenomenological approach proposed by Curtis et al.[18] in combination with a simple model introduced by Janzen et al.[46] These $\pi\cdots\pi$ interactions are revealed on the three-dimensional, molecular Hirshfeld surface (HS) as three pairs of blue and red triangles and on the two-dimensional fingerprint plot (FP) as light blue points lying on the diagonal at around di = de = ~1.8 Å (Figure 5B), both obtained using CrystalExplorer.[47] The dimer is additionally stabilized by one weak C−H⋯O hydrogen bond and by two DCM molecules through two weak hydrogen bonds, i.e., $(C-H)_{DCM}\cdots O_{4j}$ and $(C-H)_{DCM}\cdots F_{4j}$ (Figures 5A and S85 in SI). Furthermore, the molecules of neighboring dimers are connected by a single $\pi\cdots\pi$ interaction (also revealed on HS and FP) and a (C−Cl)$_{DCM}\cdots\pi$ interaction linking them in a stack running parallel to the *a*-axis (Figures 5A,C and S85). A slight blue shift of 9 nm relative to the solution indicates that despite stacking arrangement in solid, the $\pi\cdots\pi$ interactions between molecules are too weak to fully develop the excimer state with a characteristic, strong red shift. A decrease in fluorescence QY from 86.5% in solution to 36.6% in the solid state (Table S1 in SI) indicates that aggregation leads to ACQ. In contrast to that of **4j·DCM**, the crystal structure of **4b·DCM** reveals a markedly different mode of aggregation. Here, two molecules are connected solely by a single C−H⋯O═P hydrogen bond to form a dimer (Figures 6A and S84), with no significant $\pi\cdots\pi$
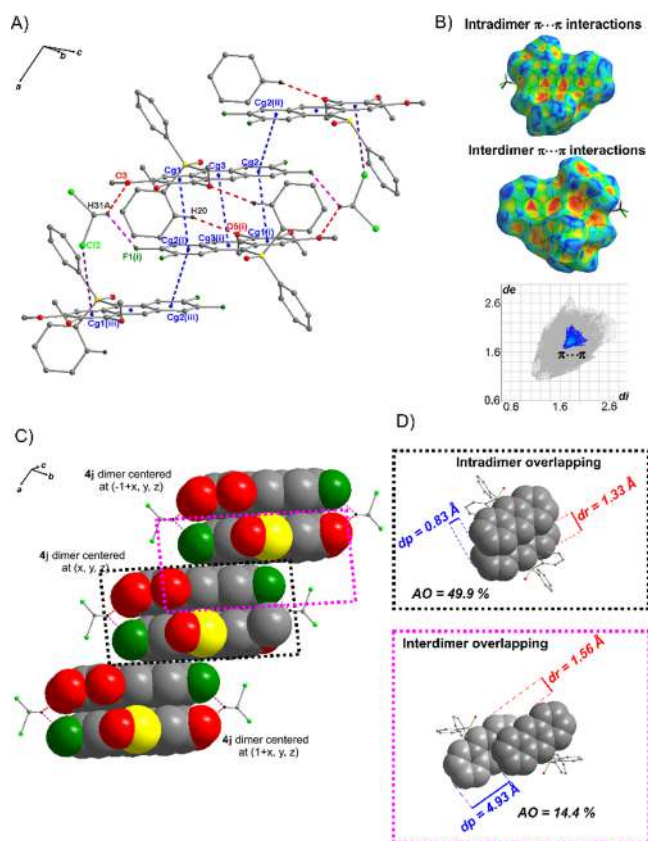
Figure 5. (A) Part of the crystal structure of **4j·DCM** showing key intermolecular interactions, including $\pi\cdots\pi$ interactions (blue dashed lines), hydrogen bonds (red and pink dashed lines), and C−Cl⋯π interaction (gray dashed line); the centroids of rings are denoted by small blue circles, and all H atoms not involved in the hydrogen bonds have been omitted for clarity. Symmetry codes (i)−(iii) are given in Table S2 in SI. (B) Molecular Hirshfeld surface mapped with shape index, and the corresponding fingerprint plot,[47] showing $\pi\cdots\pi$ interactions. (C) Arrangement of **4j** dimers in stack parallel to the *a* axis. (D) Quantification of intra- and interdimer $\pi−\pi$ overlapping, with associated AO and displacement pitch and roll parameters (dp and dr).[18]

interactions (Figure 6A,B). Each dimer is further linked to four neighboring dimers via DCM molecules through two weak $(C-H)_{DCM}\cdots O_{4b}$ and $(C-H)_{DCM}\cdots\pi_{4b}$ hydrogen bonds, leading to the formation of a layer parallel to the (101) plane (Figure 6A,C). The lack of $\pi−\pi$ stacking interactions in the crystal structure (Figure 6B), combined with the blue shift of the emission maximum (from 499 nm in DCM solution to 486 nm in the solid), indicated that the observed fluorescence is not due to an excimer excited state. The notable reduction in fluorescence QY in the solid state indicates that, similarly to **4j**, the molecular arrangement in **4b** leads to ACQ, where nonradiative relaxation pathways dominate, suppressing efficient emission.

Additionally, analysis of the molecular geometry of **4j** and **4b** in the dimers, identified in solid, showed that the anthracene plane in **4b** is more bent into a butterfly than in **4j** ($\omega_{P1/P2}$ angles are equal to ca. 7° and 2°, respectively), and the P═O substituent in **4j** is coplanar with this plane, in contrast to **4b** (deviations of P and O atoms from the plane are 0.096 and 0.025 Å, respectively, in **4j** versus 1.042 and 0.499 Å in **4b**). Moreover, we observed similar differences between molecules **4b** in monomer (from DFT calculations: $\omega_{P1/P2}$ is of ca. 3°,
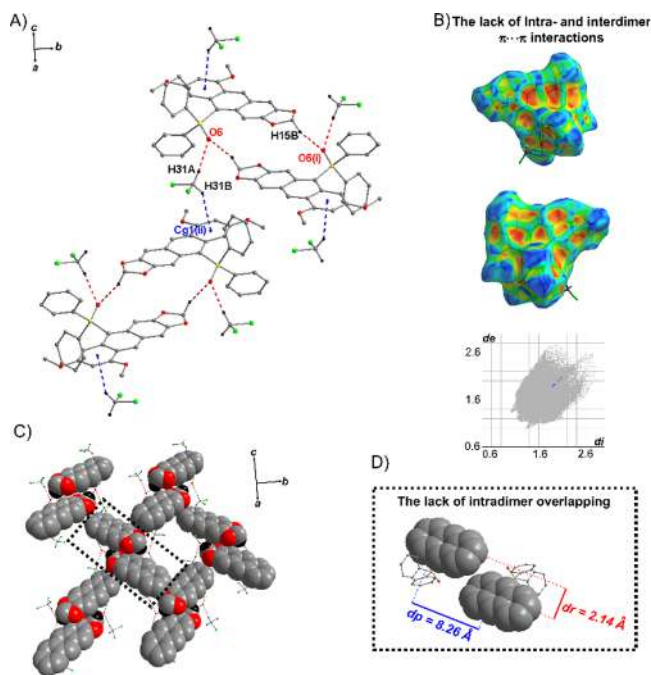
Figure 6. (A) Part of the crystal structure of **4b·DCM** showing key intermolecular interactions, including hydrogen bonds (red and pink dashed lines) and C−H···π interactions (blue dashed lines); the centroids of benzene rings are denoted by small blue spheres, and all H atoms not involved in the hydrogen bonds have been omitted for clarity. Symmetry codes (i)−(ii) are given in Table S2 in SI. (B) Molecular Hirshfeld surface mapped with the shape index and the corresponding fingerprint plot,[47] showing the lack of π···π interactions. (C) Arrangement of **4b** dimers in layer parallel to the (101) plane. (D) Dimer of **4b** formed by C−H···O hydrogen bond, with dp and dr parameters.[18]

deviations of P and O atoms from the plane are 0.200 and 0.583 Å) and dimer (in crystal). π···π Interactions linking **4j** molecules into dimers with AO = 49.9% result in planarity of anthracene, while the absence of these interactions in **4b** dimers results in a greater anthracene flexibility and susceptibility to interactions of a different type, resulting in anthracene plane bending.

CONCLUSIONS

In summary, a series of novel, multiply substituted 10-(diphenylphosphoryl)-anthracenes with electron-withdrawing 6-CN, 6-CF₃, 7-F, 6,7-di-F, and 5,6,7-tri-F substituents on one of the flanking anthracene ring and electron-donating substituents on the other one, in addition to the strong electron-withdrawing Ph₂P=O group on the middle anthracene ring, makes the obtained anthracenes very effective donor−acceptor emitters. To the best of our knowledge, these are the first multiply substituted compounds of this type in the literature. The QYs of the anthracene 6-CN-**4g** in the DCM solution and the anthracene 7-CF₃-**4f** in the solid state exceeding 95%, are the highest values in this group of compounds and 6 times higher than unsubstituted anthracene (15%, DCM). The analysis of crystal structures of **4j·DCM** and **4b·DCM** showed the crucial role of noncovalent interactions and molecular packing in modulating emission properties in solid, where fluorescence quenching by aggregation took place, without excimer formation. The 10-Ph₂P = X (X = O, S, Se) group attached to anthracene plays a key role in lowering the

LUMO levels of the investigated donor−acceptor aromatic systems and tuning their electron and optical properties. Comparative analysis of the molecular geometries of **6** and **7** with **4g** revealed that heavy atoms (S or Se) in this group caused structural changes (butterfly bending of the anthracene plane and the situation of the P=S and P=Se groups out of this plane) that disturbed π-conjugation, leading to a lower fluorescence QY. The presented results underscore the potential of multiply substituted anthracenes as tunable emitters for use in organic electronics. Further studies are underway to develop other phosphorus-based anthracene-emitting materials.

EXPERIMENTAL SECTION

General Information. Tetrahydrofuran and toluene were dried using a Solvent Purification System (MBraun SPS-800). Dry glassware was obtained by oven-drying and assembly under dry argon. For flash chromatography, a Chromatography System−Büchi Pure C-850 FlashPrep was used. The melting points were obtained with an Electrothermal Model IA9100 apparatus and are uncorrected. Mass spectra were obtained using a SYNAPT G2-Si HDMS (Waters) instrument. NMR spectra were recorded with a Bruker AV 200 MHz, Bruker AVANCE Neo 400 MHz, or Bruker AVANCE III 500 MHz using CDCl₃, C₆D₆, CD₂Cl₂, and CD₃CN, as internal standards. The UV−vis absorption spectra were recorded in 1 cm cuvettes on a Shimadzu UV-2700 spectrophotometer UV-2700. Emission spectra were obtained with a Horiba Jobin Yvon, Fluoromax 4 Plus spectrofluorometer. The fluorescence quantum yields Φ of the obtained compounds were determined in three different solvents (EtOH, cyclohexane, CH₂Cl₂) on excitation at their absorption maximum using an integrating sphere (Horiba, Jobin Yvon, Quanta-φ F-3029 Integrating sphere).

General Procedure for the Synthesis of 4a−j. In a 50 mL Schlenk tube, a solution of diaryl alcohols **1a−j** (200 mg, 1 equiv) in anhydrous THF (10 mL) at 0 °C, triethyl amine (1.1 equiv) was added, and the reaction mixture was stirred at room temperature for 1 h. After cooling, the mixture, again to 0 °C, chlorodiphenylphosphine (1.2 equiv) was added and stirred at room temperature for another 3 h. Then, a catalytic amount of TMSOTf (10 mol %) was added, and the crude mixture was stirred overnight in an oil bath at 60 °C. Once the intermediate was consumed (checked with ³¹P NMR), the aqueous solution of HCl (2 mL, 12 N) was added, and the crude mixture was stirred for 1 h. After evaporation of the solvent, the organic layer was dissolved in ethyl acetate and washed with water (5 × 2 mL), then with NaHCO₃ (5 mL) and extracted with ethyl acetate (10 mL). After drying over MgSO₄ and evaporation of the solvent, the product was purified by flash chromatography (hexane/EtOAc) to give pure anthracene compounds **4a−j**.

(7,8,9-Trimethoxyanthra[2,3-d][1,3]dioxol-5-yl)diphenyl phosphine oxide (4a). R_f = 0.43 (EtOAc), *n*-hexane:EtOAc (1:2), green solid, mp 202−204 °C, 81 mg, 32% yield: **¹H NMR** (400 MHz, CD₂Cl₂) δ 8.72 (s, 1H), 8.32 (s, 1H), 7.71−7.65 (m, 4H), 7.55−7.50 (m, 2H), 7.46−7.41 (m, 4H), 7.27 (s, 1H), 7.22 (s, 1H), 5.99 (s, 2H), 4.10 (s, 3H), 3.89 (s, 3H), 3.25 (s, 3H); **¹³C{¹H} NMR** (101 MHz, CD₂Cl₂) δ 152.9 (s), 148.9 (s), 146.7 (d, J_{PC} = 2.2 Hz), 146.6 (s), 139.1 (s), 136.2 (d, J_{PC} = 102.4 Hz), 134.4 (d, J_{PC} = 8.4 Hz), 131.6 (d, J_{PC} = 9.5 Hz), 131.4 (d, J_{PC} = 2.7 Hz), 131.3 (d, J_{PC} = 9.9 Hz), 128.8 (d, J_{PC} = 12.1 Hz), 128.3 (d, J_{PC} = 11.0 Hz), 126.4 (d, J_{PC} = 3.1 Hz), 123.1 (d, J_{PC} = 10.9 Hz), 117.2 (d, J_{PC} = 100.4 Hz), 103.5 (s), 102.5 (d, J_{PC} = 7.0 Hz), 102.0 (d, J_{PC} = 7.9 Hz), 101.5 (s), 61.5 (s), 60.8 (s), 55.3 (s); **³¹P NMR** (162 MHz, CD₂Cl₂) δ 30.54; **HRMS** (TOF MS ES+): calcd. for C₃₀H₂₆O₆P [M + H⁺] 513.1467, found 513.1462.

(7,9-Dimethoxyanthra[2,3-d][1,3]dioxol-5-yl)diphenyl phosphine oxide (4b). R_f = 0.50 (EtOAc), *n*-hexane:EtOAc (1:2), yellow crystals, mp 232−234 °C, 78 mg, 30% yield: **¹H NMR** (400 MHz, CD₂Cl₂) δ 8.84 (s, 1H), 8.46 (s, 1H), 7.72−7.66 (m, 4H), 7.53−7.49 (m, 2H), 7.45−7.40 (m, 4H), 7.25 (d, *J* = 1.7 Hz, 1H), 6.80 (s, 1H),

6.31 6.31 (d, J = 2.0 Hz, 1H), 5.99 (s, 2H), 3.99 (s, 3H), 3.18 (s, 3H); ^{13}C{^{1}H} NMR (101 MHz, CD$_2$Cl$_2$) δ 158.1 (s), 156.8 (d, J_{PC} = 2.2 Hz), 149.7 (s), 146.8 (s),136.7 (d, J_{PC} = 102.5 Hz), 135.9 (d, J_{PC} = 8.4 Hz), 135.4 (d, J_{PC} = 9.5 Hz), 131.7 (d, J_{PC} = 2.3 Hz), 131.6 (d, J_{PC} = 10.3 Hz), 129.1 (d, J_{PC} = 11.9 Hz), 128.1 (d, J_{PC} = 11.1 Hz), 127.4 (d, J_{PC} = 3.0 Hz), 120.8 (d, J_{PC} = 11.3 Hz), 117.2 (d, J_{PC} = 101.2 Hz), 104.3 (s), 102.9 (d, J_{PC} = 6.7 Hz), 101.9 (s), 98.1 (d, J_{PC} = 8.3 Hz), 96.6 (s), 56.1 (s), 55.3 (s). ^{31}P NMR (162 MHz, CD$_2$Cl$_2$) δ 30.56; **HRMS** (TOF MS ES+): calcd. for C$_{29}$H$_{24}$O$_5$P [M + H$^+$] 483.1361, found 483.1358.

(7-Methoxyanthra[2,3-d][1,3]dioxol-5-yl)diphenyl phosphine oxide (4c). R_f = 0.53 (EtOAc), n-hexane:EtOAc (1:2), green solid, mp 227−229 °C, 60 mg, 24% yield: ^{1}H NMR (400 MHz, CD$_2$Cl$_2$) δ 8.42 (d, J = 12.0 Hz, 2H), 7.83 (dd, J = 9.1, 1.9 Hz, 1H), 7.72−7.67 (m, 4H), 7.55−7.50 (m, 2H), 7.46−7.41 (m, 4H), 7.31 (d, J = 2.4 Hz, 1H), 7.23 (d, J = 1.7 Hz, 1H), 7.00 (dd, J = 9.1, 2.4 Hz, 1H), 6.00 (s, 2H), 3.22 (s, 3H); ^{13}C{^{1}H} NMR (101 MHz, CD$_2$Cl$_2$) δ 157.5 (s), 149.6 (s), 147.0 (s), 136.6 (d, J_{PC} = 102.5 Hz), 135.6 (d, J_{PC} = 8.5 Hz), 135 (d, J_{PC} = 8.8 Hz), 133 (d, J_{PC} = 3.1 Hz), 131.8 (d, J_{PC} = 2.8 Hz), 131.7 (d, J_{PC} = 9.9 Hz), 130.6 (s), 129.2 (d, J_{PC} = 12.2 Hz), 128.6 (d, J_{PC} = 11.3 Hz), 127.1 (d, J_{PC} = 10.8 Hz), 119.39 (s), 117.7 (d, J_{PC} = 100.1 Hz), 105 (d, J_{PC} = 7.8 Hz), 103.5 (s), 103 (d, J_{PC} = 6.8 Hz), 102 (s), 55.24 (s); ^{31}P NMR (162 MHz, CD$_2$Cl$_2$) δ 30.28; **HRMS** (TOF MS ES+): calcd. for C$_{28}$H$_{21}$O$_4$P [M + H$^+$] 453.1256, found 453.1256.

(2,3,4-Trimethoxyanthr-9-yl)diphenyl Phosphine Oxide (4d). R_f = 0.41 (EtOAc), n-hexane:EtOAc (1:2), yellow solid, mp 150−151 °C, 96 mg, 37% yield: ^{1}H NMR (400 MHz, CD$_2$Cl$_2$) δ 8.98 (d, J = 1.7 Hz, 1H), 8.62 (dt, J = 9.1, 1.0 Hz, 1H), 8.07 (dt, J = 8.4, 1.8 Hz, 1H), 7.73−7.67 (m, 4H), 7.61 (s, 1H), 7.54−7.49 (m, 4H), 7.46−7.40 (m, 2H), 7.39−7.36 (m, 1H), 7.27−7.23 (m, 1H), 4.15 (s, 3H), 3.94 (s, 3H), 3.39 (s, 3H); ^{13}C{^{1}H} NMR (101 MHz, CD$_2$Cl$_2$) δ 154 (s), 146.9 (s), 139.7 (s), 136.6 (d, J_{PC} = 102.5 Hz), 135.2 (d, J_{PC} = 8.5 Hz), 133.4 (d, J_{PC} = 9.0 Hz), 131.5 (d, J_{PC} = 2.9 Hz), 131.4 (d, J_{PC} = 9.8 Hz), 130.2 (d, J_{PC} = 10.9 Hz), 129.7 (s), 128.9 (d, J_{PC} = 11.9 Hz), 128.3 (d, J_{PC} = 3.2 Hz), 126.9 (d, J_{PC} = 7.0 Hz), 126.3 (s), 124.6 (d, J_{PC} = 11.1 Hz), 124.3 (s), 118.7 (d, J_{PC} = 100.1 Hz), 101.9 (d, J_{PC} = 7.5 Hz), 61.7 (s), 61.1 (s), 55.5 (s); ^{31}P NMR (162 MHz, CD$_2$Cl$_2$) δ 29.57; **HRMS** (TOF MS ES+): calcd. for C$_{29}$H$_{25}$O$_4$P [M + H$^+$] 469.1568, found 469.1569.

(6-Fluoro-2,3,4-trimethoxyanthr-9-yl)diphenyl Phosphine Oxide (4e). R_f = 0.46 (EtOAc), n-hexane:EtOAc (1:2), yellow solid, mp 154−156 °C, 78 mg, 32% yield: ^{1}H NMR (400 MHz, CD$_2$Cl$_2$) δ 8.97−8.91 (m, 2H), 7.71−7.66 (m, 5H), 7.56−7.51 (m, 2H), 7.47−7.42 (m, 4H), 7.36 (s, 1H), 7.15−7.10 (m, 1H), 4.14 (s, 3H), 3.93 (s, 3H), 3.31 (s, 3H); ^{13}C{^{1}H} NMR (101 MHz, CD$_2$Cl$_2$) δ 159.4 (d, J_{CF} = 247.4 Hz), 154.1 (s), 146.8 (s), 140.4 (s), 136.4 (d, J_{PC} = 102.8 Hz), 133.1 (d, J_{PC} = 8.3 Hz), 132.7 (d, J_{PC} = 8.7 Hz), 132 (d, J_{PC} = 2.8 Hz), 131.6 (d, J_{PC} = 10 Hz), 131.2 (dd, J_{PC} = 10.1, J_{CF} = 19.7 Hz), 130.2 (dd, J_{PC} = 7.5, J_{CF} = 15.2 Hz), 129.2 (d, J_{PC} = 12.1 Hz), 127.5 (dd, J = 6.7, 3.2 Hz), 125.6 (d, J_{PC} = 11 Hz), 119.9 (d, J_{PC} = 99.7 Hz), 117.7 (d, J_{CF} = 26.1 Hz), 111.4 (d, J_{CF} = 20.0 Hz), 102.3 (d, J_{PC} = 7.8 Hz), 61.9 (s), 61.3 (s), 55.8 (s); ^{31}P NMR (162 MHz, CD$_2$Cl$_2$) δ 29.87; ^{19}F NMR (376 MHz, CD$_2$Cl$_2$) δ −117.04; **HRMS** (TOF MS ES+): calcd. for C$_{29}$H$_{25}$O$_4$PF [M + H$^+$] 487.1472, found 487.1474.

(2,3,4-Trimethoxy-7-(trifluoromethyl)anthr-9-yl)diphenyl Phosphine Oxide (4f). R_f = 0.56 (EtOAc), n-hexane:EtOAc (1:2), green solid, mp 134−137 °C, 123 mg, 49% yield: ^{1}H NMR (400 MHz, CD$_2$Cl$_2$) δ 9.22 (s, 1H), 9.06 (s, 1H), 8.20 (d, J = 8.8 Hz, 1H), 7.80−7.68 (m, 4H), 7.63 (s, 1H), 7.80−7.68 (m, 4H), 4.17 (s, 3H), 3.97 (s, 3H), 3.44 (s, 3H); ^{13}C{^{1}H} NMR (101 MHz, CD$_2$Cl$_2$) δ: 154.8 (s), 147.1 (s), 140.7 (s), 136.2 (d, J_{PC} = 103.1 Hz), 134.1 (d, J_{PC} = 8.5 Hz), 133.8 (d, J_{PC} = 8.1 Hz), 132.1 (d, J_{PC} = 3.1 Hz), 131.6 (d, J_{PC} = 9.9 Hz), 131.3 (s), 130.9 (d, J_{PC} = 10.5 Hz), 129.3 (d, J_{PC} = 12.2 Hz), 128.5 (d, J_{PC} = 3.1 Hz), 127.5 (q, J_{CF} = 31.6 Hz), 126.3 (d, J_{PC} = 10.5 Hz), 125.3 (dq, J_{PC} = 5.3 Hz, J_{PC} = 5.3 Hz), 124.7 (q, J_{CF} = 271.8 Hz), 121.35 (d, J_{PC} = 98.3 Hz), 119.5 (q, J_{CF} = 3.0 Hz), 102.4 (d, J_{PC} = 7.9 Hz), 62 (s), 61.3 (s), 55.9 (s); ^{31}P NMR (162 MHz, CD$_2$Cl$_2$) δ 29.28; ^{19}F NMR (376 MHz, CD$_2$Cl$_2$) δ −63.00; **HRMS** (TOF MS ES+): calcd. for C$_{30}$H$_{25}$O$_4$PF$_3$ [M + H$^+$] 537.1442, found 537.1443.

9-(Diphenylphosphoryl)-5,6,7-trimethoxyanthra-2-carbonitrile (4g). R_f = 0.54 (EtOAc); n-hexane:EtOAc (1:2), yellow solid, mp 176−178 °C; 141 mg, 55% yield: ^{1}H NMR (400 MHz, CD$_2$Cl$_2$) δ 9.61 (s, 1H), 9.03 (s, 1H), 8.14 (dd, J = 8.8, 1.8 Hz, 1H), 7.75−7.70 (m, 4H), 7.59−7.54 (m, 2H), 7.50−7.45 (m, 5H), 7.30 (s, 1H), 4.15 (s, 3H), 3.95 (s, 3H), 3.33 (s, 3H); ^{13}C{^{1}H} NMR (101 MHz, CD$_2$Cl$_2$) δ 155 (s), 147.1 (s), 140.9 (s), 135.8 (d, J_{PC} = 103.4 Hz), 134.3 (s), 134.2 (d, J_{PC} = 5.6 Hz), 133.7 (d, J_{PC} = 8.7 Hz), 132.3 (d, J_{PC} = 3.2 Hz), 131.6 (d, J_{PC} = 10.0 Hz), 131.2 (s), 130.8 (d, J_{PC} = 10.2 Hz), 129.3 (d, J_{PC} = 12.2 Hz), 128.6 (d, J_{PC} = 3.1 Hz), 126.6 (d, J_{PC} = 10.6 Hz), 124.1 (s), 121.1 (d, J_{PC} = 97.2 Hz), 119.6 (s), 109.9 (s), 102.4 (d, J_{PC} = 7.9 Hz), 62 (s), 61.3 (s), 55.9 (s); ^{31}P NMR (162 MHz, CD$_2$Cl$_2$) δ 29.88; **HRMS** (TOF MS ES+): calcd. for C$_{30}$H$_{25}$O$_4$PN [M+H$^+$] 494.1531, found 494.1521.

(6-Bromo-2,3,4-trimethoxyanthr-9-yl)diphenyl Phosphine Oxide (4h). R_f = 0.45 (EtOAc), n-hexane:EtOAc (1:2), orange oil, 112 mg, 45% yield: ^{1}H NMR (400 MHz, CD$_2$Cl$_2$) δ 8.87−8.86 (m, 1H), 8.67 (d, J = 9.6 Hz, 1H), 8.22 (dd, J = 2.1, J = 2.1 Hz, 1H), 7.69−7.64 (m, 4H), 7.55−7.51 (m, 2H), 7.46−7.41 (m, 5H), 7.30 (dd, J = 9.6, 2.2 Hz, 1H), 4.12 (s, 3H), 3.92 (s, 3H), 3.33 (s, 3H); ^{13}C{^{1}H} NMR (101 MHz, CD$_2$Cl$_2$) δ 154.2 (s), 146.8 (s), 140.1 (s), 36.1 (d, J_{PC} = 102.8 Hz),133.6 (d, J_{PC} = 8.6 Hz), 133.2 (d, J_{PC} = 8.7 Hz), 131.7 (d, J_{PC} = 2.7 Hz), 131.4 (d, J_{PC} = 10.1 Hz), 131.2 (s), 131.1 (s), 129.4 (s), 128.9 (d, J_{PC} = 12.1 Hz), 128.8 (d, J_{PC} = 6.5 Hz),127.2 (d, J_{PC} = 3.1 Hz), 125.3 (d, J_{PC} = 10.6 Hz), 119.5 (d, J_{PC} = 99.4 Hz), 118.2 (s), 102 (d, J_{PC} = 7.5 Hz), 61.7 (s), 61.1 (s), 55.5 (s); ^{31}P NMR (162 MHz, CD$_2$Cl$_2$) δ 29.60; **HRMS** (TOF MS ES+): calcd. for C$_{29}$H$_{24}$O$_4$PBr [M + H$^+$] 547.0672, found 547.0670.

(1,2,3-Trifluoro-5,6,7-trimethoxyanthr-9-yl)diphenyl Phosphine Oxide (4i). R_f = 0.40 (EtOAc), n-hexane:EtOAc (1:2), yellow solid, mp 186−188 °C; 151 mg, 60% yield: ^{1}H NMR (400 MHz, C$_6$D$_6$) δ 8.70 (s, 1H), 8.11 (s, 1H), 7.71−7.66 (m, 4H), 6.96−6.89 (m, 7H), 3.92 (s, 3H), 3.71 (s, 3H), 3.25 (s, 3H); ^{13}C{^{1}H} NMR (101 MHz, C$_6$D$_6$) δ 155.1 (s), 149.1 (dd, J_{CF} = 251.2, 14.1 Hz), 146.9 (s), 146 (dd, J_{CF} = 251.03, 14.3 Hz), 140.4 (dd, J_{CF} = 251.8, 13.9 Hz), 141.1 (s), 138.2 (dd, J_{PC} = 105.9, 4.3 Hz), 135.6 (d, J_{PC} = 6.8 Hz), 130.9 (dd, J_{PC} = 9.5, 2.4 Hz), 130.7 (d, J_{PC} = 2.8 Hz), 129.3 (s), 128.4 (d, J_{PC} = 12.3 Hz), 127.1 (d, J_{PC} = 4.2 Hz), 126.1 (d, J_{PC} = 10.2 Hz), 124.1 (dd, J_{PC} = 12.1, 6.1 Hz), 119.2 (d, J_{PC} = 99.4 Hz), 109.4 (dd, J_{CF} = 16.6, 4.3 Hz), 103.5(d, J_{PC} = 8.0 Hz), 61.3 (s), 60.9 (s), 55.6 (s); ^{31}P NMR (162 MHz, C$_6$D$_6$) δ 26.95 (d, J_{PF} = 12.2 Hz); ^{19}F NMR (376 MHz, C$_6$D$_6$) δ −157.88 (ddd, J_{FF} = 19.6 Hz, J_{FF} = 17.5 Hz, J_{HF} = 7.5 Hz), −136.48 (ddd, J_{FF} = 19.6 Hz, J_{FF} = 5.5 Hz, J_{HF} = 10.0 Hz), −116.51 (ddd, J_{FF} = 17.5, J_{PF} = 12.2 Hz, J_{FF} = 5.5 Hz); ^{19}F{^{1}H} NMR (376 MHz, C$_6$D$_6$) δ −157.88 (dd, J_{FF} = 19.6 Hz, J_{FF} = 17.5 Hz), −136.48 (dd, J_{FF} = 19.6 Hz, J_{FF} = 5.5 Hz), −116.51 (ddd, J_{FF} = 17.5 Hz, J_{PF} = 12.2 Hz, J_{FF} = 5.5 Hz); **HRMS** (TOF MS ES+): calcd. for C$_{29}$H$_{22}$O$_4$PF$_3$ [M + H$^+$] 523.1288, found 523.1286.

(6,7-Difluoro-2,3,4-trimethoxyanthr-9-yl)diphenyl Phosphine Oxide (4j). R_f = 0.56 (EtOAc), n-hexane:EtOAc (1:2), green crystals, mp 176−178 °C; 112 mg, 44% yield: ^{1}H NMR (400 MHz, C$_6$D$_6$) δ 9.47 (dd, J = 15.2, 8.3 Hz, 1H), 8.80 (s, 1H), 7.93 (s, 1H), 7.78 (dd, J = 12.1, 7.6 Hz, 4H), 6.99−6.90 (m, 7H), 3.87 (s, 3H), 3.71 (s, 3H), 3.12 (s, 3H); ^{13}C{^{1}H} NMR (101 MHz, C$_6$D$_6$) δ 154.6 (s), 151.3 (dd, J_{CF} = 251.7, 17.1 Hz), 148.8 (dd, J_{CF} = 250.8, 16.9 Hz), 147.3 (s), 140.5 (s), 136.8 (d, J_{PC} = 102.5 Hz), 133.5 (d, J_{PC} = 8.5 Hz), 133.4 (s), 132.1 (s), 131.8 (d, J_{PC} = 9.8 Hz), 131.5 (d, J_{PC} = 2.8 Hz), 128.9 (d, J_{PC} = 12.0 Hz), 125.1 (d, J_{PC} = 9.8 Hz), 120.4 (d, J_{PC} = 2.8 Hz), 119.9 (dd, J_{PC} = 102.6, 6.8 Hz), 114.2 (d, J_{CF} = 16.1 Hz), 113.8 (dd, J_{CF} = 21.6, 6.1 Hz), 102.6 (d, J_{PC} = 7.5 Hz), 61.2 (s), 60.8 (s), 55.4 (s); ^{31}P NMR (162 MHz, C$_6$D$_6$) δ 28.83; ^{19}F NMR (376 MHz, C$_6$D$_6$) δ −137.45 (ddd, J_{FF} = 20.0, J_{HF} = 15.7, 9.6 Hz), −131.50 (ddd, J_{FF} = 21.0, J_{HF} = 15.1, 8.7 Hz); ^{19}F{^{1}H} NMR (376 MHz, C$_6$D$_6$) δ −137.45 (d, J_{FF} = 21.1 Hz), −131.50 (d, J_{FF} = 20.9 Hz); **HRMS** (TOF MS ES+): calcd. for C$_{29}$H$_{23}$O$_4$PF$_2$ [M+H$^+$] 505.1377, found 505.1380.

Procedure for the Synthesis of 5. In a Schlenk tube dried and filled with argon, **4g** (50 mg, 0.101 mmol) was dissolved in dry toluene (10 mL). Then, trichlorosilane (138 mg, 1.01 mmol) was added dropwise at room temperature and the mixture was stirred in

an oil bath at 90 °C for 2 h. The volatiles were removed under reduced pressure and the crude product was dissolved in DCM (10 mL) and filtered through the aluminum oxide layer. After evaporation of the solvent, the crude compound containing 27% silane was obtained as a yellow solid and was further used as such in the syntheses of **6–9**.

9-(Diphenylphosphanyl)-5,6,7-trimethoxyanthracene-2- carbonitrile (5). Yellow solid, mp 193–195 °C; ^{1}**H NMR** (400 MHz, C_6D_6) δ 9.83 (d, J = 7.1 Hz, 1H), 8.89 (s, 1H), 7.70 (d, J = 3.5 Hz, 1H), 7.47 (d, J = 8.6 Hz, 1H), 7.42–7.38 (m, 4H), 6.95–6.93 (m, 7H), 3.83 (s, 3H), 3.67 (s, 3H), 3.10 (s, 3H); ^{13}**C{^{1}H} NMR** (101 MHz, C_6D_6) δ 154.9 (s), 147.7 (s), 141.6 (s), 136.4 (d, J_{PC} = 22.1 Hz), 136.2 (d, J_{PC} = 14.1 Hz), 135.2 (d, J_{PC} = 5.1 Hz), 134.6 (d, J_{PC} = 36.09 Hz), 131.9 (d, J_{PC} = 18.4 Hz), 131.7 (s), 131.1 (s), 131.1 (d, J = 5.2 Hz), 128.9 (d, J_{PC} = 5.6 Hz), 127 (s),126.9 (s), 126.2 (s), 124.1 (s), 119.5 (s), 110.6 (s), 103.6 (d, J_{PC} = 15.3 Hz), 61.2 (s), 60.7 (s), 55.4 (s); ^{31}**P NMR** (162 MHz, CD_2Cl_2) δ −24.21.

Procedure for the Synthesis of 6 and 7. Compound **5** (50 mg, 0.105 mmol) was treated with sublimed sulfur (15 mg, 0.467 mmol) in toluene (7 mL) at reflux under an argon atmosphere. Once compound **5** was consumed (checked with TLC), the solvent was evaporated, and the crude mixture was separated using silica-gel flash chromatography with hexane/EtOAc as eluents (2:1 v/v) to afford **6** (40 mg) as an orange solid (78% from **4g**). When elemental selenium (33 mg, 0.418 mmol) was used instead of sulfur, **7** (39 mg) was obtained as an orange solid in 70% yield from **4g**.

9-(Diphenylphosphorothioyl)-5,6,7-trimethoxyanthracene-2-carbonitrile (6). R_f = 0.86 (EtOAc), *n*-hexane:EtOAc (1:1), orange solid, mp 156–158 °C: 40 mg, 78% yield; ^{1}**H NMR** (400 MHz, CD_2Cl_2) δ 8.94 (s, 1H), 8.20 (s, 1H), 8.11 (dd, J = 8.7, 2.0 Hz, 1H), 7.85–7.80 (m, 4H), 7.48–7.44 (m, 1H), 7.41–7.36 (m, 6H), 7.08 (s, 1H), 4.14 (s, 3H), 3.92 (s, 3H), 3.23 (s, 3H); ^{13}**C{^{1}H} NMR** (101 MHz, CD_2Cl_2) δ 154.7 (s), 147.2 (s), 141.2 (s), 136.9 (d, J_{PC} = 82.3 Hz), 133.5 (d, J_{PC} = 9.7 Hz), 132.5 (d, J_{PC} = 7.9 Hz), 131.5 (d, J_{PC} = 3.0 Hz), 131.3 (d, J_{PC} = 10.1 Hz), 130.9 (d, J_{PC} = 10.2 Hz), 129.2 (d, J_{PC} = 12.4 Hz), 127.9 (d, J_{PC} = 2.8 Hz), 127.4 (d, J_{PC} = 81.2 Hz), 127.1 (s), 126.9 (s), 123.9 (s), 122 (d, J_{PC} = 87.4 Hz), 119.1 (s), 109.1 (s), 102.9 (d, J_{PC} = 10.8 Hz), 62.1 (s), 61.4 (s), 55.9 (s); ^{31}**P NMR** (162 MHz, CD_2Cl_2) δ 33.92; **HRMS** (TOF MS ES+): calcd. for $C_{30}H_{25}O_3PNS$ [M+H$^+$] 510.1295, found 510.1296.

9-(Diphenylphosphoroselenoyl)-5,6,7-trimethoxyanthracene-2-carbonitrile (7). R_f = 0.83 (EtOAc); *n*-hexane:EtOAc (1:1), orange solid, mp 164–166 °C; 39 mg, 70% yield: ^{1}**H NMR** (400 MHz, C_6D_6) δ 8.79 (s, 1H), 8.45 (s, 1H), 7.95- 7.89 (m, 4H), 7.51 (s, 1H), 7.36 (dd, J = 8.6, 2.0 Hz, 1H), 6.85- 6.80 (m, 6H), 6.78 (d, J = 1.4 Hz, 1H), 3.87 (s, 3H), 3.68 (s, 3H), 3.01 (s, 3H); ^{13}**C{^{1}H} NMR** (101 MHz, C_6D_6) δ 154 (s), 146.8 (s), 140.9 (s), 135.2 (d, J_{PC} = 73.3 Hz), 133.1 (d, J_{PC} = 9.5 Hz), 132.1 (d, J_{PC} = 7.6 Hz), 131.6 (d, J_{PC} = 10.8 Hz), 130.7 (d, J_{PC} = 3.1 Hz), 130.5 (d, J_{PC} = 10.3 Hz), 130.3 (s), 128.6 (d, J_{PC} = 77.1 Hz), 128.5 (d, J_{PC} = 12.6 Hz), 126.8 (d, J_{PC} = 3.5 Hz), 126.6 (d, J_{PC} = 10.5 Hz), 123.4 (s), 121.2 (s), 118.4 (s), 109.1 (s), 103.4 (d, J_{PC} = 11.4 Hz), 61 (s), 60.5 (s), 55.1 (s); ^{31}**P NMR** (162 MHz, CD_2Cl_2) δ 25.25; (d,$^1J_{PSe}$ = 754 Hz); ^{77}**Se NMR** (76 MHz, CD_2Cl_2) δ −289.76 (d,$^1J_{PSe}$ = 738.9 Hz); ^{77}**Se NMR** (76 MHz, C_6D_6) δ −291.02 (d,$^1J_{PSe}$ = 754.5 Hz); **HRMS** (TOF MS ES+): calcd. for $C_{30}H_{25}O_3PNSe$ [M+H$^+$] 557.0660, found 557.0686.

Procedure for the Synthesis of the Gold(I) Complex 8. Compound **5** (20 mg) was dissolved in CH_2Cl_2 (5 mL) and treated with [Au(tht)Cl] (12 mg, 0.042 mmol) at room temperature under an argon atmosphere. The resulting mixture was stirred for 2 h. After 2 h, the volatiles were removed under vacuum. The crude mixture was redissolved in CH_2Cl_2 and filtered through the aluminum oxide layer, and the product was obtained as a yellow solid (25 mg, 90% from **4g**).

(8): yellow solid, 25 mg, 90% yield: ^{1}**H NMR** (400 MHz, CD_2Cl_2) δ 9.02 (s, 1H), 8.15 (dd, J = 8.7, 1.7 Hz, 1H), 8.06 (s, 1H), 7.71–7.65 (m, 4H), 7.60 (dd, J = 7.4, 2.0 Hz, 1H), 7.58–7.55 (m, 2H), 7.53–7.48 (m, 4H), 7.44 (dd, J = 8.6, 1.4 Hz, 1H), 4.17 (s, 3H), 3.97 (s, 3H), 3.62 (s, 3H); ^{13}**C{^{1}H} NMR** (101 MHz, CD_2Cl_2) δ 155.8 (s), 147.5 (s), 141.3 (s), 134.3 (d, J_{PC} = 10.6 Hz), 134.1 (d, J_{PC} = 14.2 Hz), 132.5 (d, J_{PC} = 2.7 Hz), 132.3 (d, J_{PC} = 10.5 Hz), 131.8 (s),

130.9 (d, J_{PC} = 8.3 Hz), 130.4 (d, J_{PC} = 60.3 Hz), 130.2 (d, J_{PC} = 12.1 Hz), 129.4 (d, J_{PC} = 12.2 Hz), 128.8 (d, J_{PC} = 2.9 Hz), 126.9 (d, J_{PC} = 8.9 Hz), 124.1 (s), 118.9 (s), 116.2 (d, J_{PC} = 58.4 Hz), 109.9 (s), 101.1 (d, J_{PC} = 18.6 Hz), 62.1 (s), 61.5 (s), 56.4 (s); ^{31}**P NMR** (162 MHz, CD_2Cl_2) δ 23.39; **HRMS** (TOF MS ES+): calcd. for $C_{30}H_{24}O_3PNAuCl$ [M$^+$] 709.0875, found 709.0888.

Procedure for the Synthesis of 9. Compound **5** (50 mg, 0.105 mmol) was treated with iodomethane (60 mg, 0.467 mmol) in toluene (7 mL) at reflux. Once compound **5** was consumed (checked with TLC), the solvent was evaporated, and the crude mixture was separated using silica-gel flash chromatography with hexane/EtOAc as eluents (2:1 v/v) to afford **9** (22 mg) as an orange solid (72% from **4g**).

5,6,7-Trimethoxyanthracene-2-carbonitrile (9). R_f = 0.87 (EtOAc); *n*-hexane:EtOAc (1:1), orange solid; mp 127–129 °C: 22 mg, 72% yield: ^{1}**H NMR** (400 MHz, C_6D_6) δ 8.60 (s, 1H), 7.87 (s, 1H), 7.73 (s, 1H), 7.45 (d, J = 8.7 Hz, 1H), 6.99 (dd, J = 8.6, 1.6 Hz, 1H), 6.66 (s, 1H), 3.86 (s, 3H), 3.79 (s, 3H), 3.43 (s, 3H); ^{13}**C{^{1}H} NMR** (101 MHz, C_6D_6) δ 154.6 (s), 147.6 (s), 142.3 (s), 134.7 (s), 130.6 (s), 130.4 (s), 130.2 (s), 129.9 (s), 126.7 (s), 125.6 (s), 124.1 (s), 121.2 (s), 119.6 (s), 109.4 (s), 101.2 (s), 61.1 (s), 60.9 (s), 55.3 (s); **HRMS** (TOF MS ES+): calcd. for $C_{18}H_{16}O_3N$ [M+H$^+$] 294.1116, found 294.1130.

Procedure for the Synthesis of 10. In a Schlenk tube, dried and filled with argon, **4h** (40 mg, 0.074 mmol), 2-thienylboronic acid (11 mg, 0.080 mmol), Pd(PPh$_3$)$_4$ (6 mg, 0.08 equiv) and K_2CO_3 (28 mg, 2.5 equiv) were dissolved in a toluene:MeOH (3:1 v/v) solution (4 mL). The reaction mixture was stirred in an oil bath at 80 °C for 36 h. Then, the solvent was removed in a vacuum, and the resulting solid was dissolved in EtOAc (10 mL) and washed with water (7 × 2 mL). After drying with $MgSO_4$, the solvent was removed, and the crude product was purified using flash silica chromatography with hexane: EtOAc (1:1 v/v) used as an eluent. Finally, product **10** was obtained as a green solid (37 mg) in a 94% yield.

(2,3,4-Trimethoxy-6-(thien-2-yl)anthr-9-yl)diphenyl Phosphine Oxide (10). R_f = 0.42 (EtOAc); *n*-hexane:EtOAc (1:2), yellow oil; 37 mg 94% yield: ^{1}**H NMR** (400 MHz, CD_2Cl_2) δ 8.96 (s, 1H), 8.64 (d, J = 9.3 Hz, 1H), 8.26 (s, 1H), 7.73–7.67 (m, 4H), 7.57 (s, 1H), 7.55–7.50 (m, 4H), 7.46–7.43 (m, 4H), 7.42 (dd, J = 3.0, 1.2 Hz, 1H), 7.35 (dd, J = 5.1, 1.1 Hz, 1H), 7.13 (dd, J = 5.1, 3.6 Hz, 1H), 4.15 (s, 3H), 3.93 (s, 3H), 3.38 (s, 3H); ^{13}**C{^{1}H} NMR** (101 MHz, C_6D_6) δ 154.7 (s), 147.5 (s), 144.1 (s), 140.7 (s), 137.6 (d, J_{PC} = 102.0 Hz), 134.7 (dd, J_{PC} = 8.7, 6.0 Hz), 134. Three (d, J_{PC} = 102.56 Hz), 132.4 (d, J_{PC} = 9.6 Hz), 131.9 (d, J_{PC} = 9.8 Hz), 131.5 (d, J_{PC} = 2.8 Hz), 131.2 (d, J_{PC} = 2.8 Hz), 130.8 (d, J_{PC} = 10.7 Hz), 130.4 (s),128.8 (d, J = 12.0 Hz), 128.6 (d, J = 4.9 Hz), 128.5 (d, J_{PC} = 10.9 Hz), 125.9 (d, J_{PC} = 10.9 Hz), 125.4 (s), 125.3 (d, J = 2.8 Hz), 124.1 (s), 120 (d, J_{PC} = 98.5 Hz), 103 (d, J_{PC} = 6.8 Hz), 61.3 (s), 60.8 (s), 55.5 (s); ^{31}**P NMR** (162 MHz, CD_2Cl_2) δ 29.57; **HRMS** (TOF MS ES+): calcd. for $C_{33}H_{28}O_4PS$ [M+H$^+$] 551.1444, found 551.1446.

■ ASSOCIATED CONTENT

Data Availability Statement

The data underlying this study are available in the published article and its Supporting Information (SI).

Ⓢ Supporting Information

The Supporting Information is available free of charge at https://pubs.acs.org/doi/10.1021/acs.joc.4c03139.

> General information, detailed experimental procedures, characterization data for compounds, NMR spectra, photophysical properties, crystal structure data, computational studies, and CIE 1931 color space coordinates data; and additional references 48–52 (PDF)

Accession Codes

Deposition Numbers 2378974–2378976 contain the supplementary crystallographic data for this paper. These data can be obtained free of charge via the joint Cambridge Crystallo-

graphic Data Centre (CCDC) and Fachinformationszentrum Karlsruhe Access Structures service.

■ AUTHOR INFORMATION

Corresponding Authors

Ewa Różycka-Sokołowska − *Institute of Chemistry, Faculty of Science and Technology, Jan Długosz University in Częstochowa, Częstochowa 42-201, Poland*; Email: e.sokolowska@ujd.edu.pl

Piotr Bałczewski − *Division of Organic Chemistry, Centre of Molecular and Macromolecular Studies, Polish Academy of Sciences, Łódź 90-363, Poland; Institute of Chemistry, Faculty of Science and Technology, Jan Długosz University in Częstochowa, Częstochowa 42-201, Poland*; ⊙ orcid.org/0000-0001-5981-551X; Email: piotr.balczewski@cbmm.lodz.pl

Authors

Vivek Vivek − *Division of Organic Chemistry, Centre of Molecular and Macromolecular Studies, Polish Academy of Sciences, Łódź 90-363, Poland; The Bio-Med-Chem Doctoral School of the University of Łódź and Łódź Institutes of the Polish Academy of Sciences, University of Łódź, Łódź 90-237, Poland*

Marek Koprowski − *Division of Organic Chemistry, Centre of Molecular and Macromolecular Studies, Polish Academy of Sciences, Łódź 90-363, Poland*

Marika Turek − *Institute of Chemistry, Faculty of Science and Technology, Jan Długosz University in Częstochowa, Częstochowa 42-201, Poland*

Bogdan Dudziński − *Division of Organic Chemistry, Centre of Molecular and Macromolecular Studies, Polish Academy of Sciences, Łódź 90-363, Poland*

Krzysztof Owsianik − *Division of Organic Chemistry, Centre of Molecular and Macromolecular Studies, Polish Academy of Sciences, Łódź 90-363, Poland*

Łucja Knopik − *Division of Organic Chemistry, Centre of Molecular and Macromolecular Studies, Polish Academy of Sciences, Łódź 90-363, Poland; The Bio-Med-Chem Doctoral School of the University of Łódź and Łódź Institutes of the Polish Academy of Sciences, University of Łódź, Łódź 90-237, Poland*

Complete contact information is available at:
https://pubs.acs.org/10.1021/acs.joc.4c03139

Author Contributions

V.V. and P.B. designed the overall research plan; P.B. received funding; V.V. carried out the synthesis of substituted anthracenes, while M.K. and K.O. conducted the photophysical experiments; E.R.-S. and M.T. performed the DFT calculations; E.R.-S. determined X-ray crystal structures and performed structural analysis; L.K. and B.D. synthesized the substrates. The manuscript was written with input from all authors. All authors have approved the final version of the manuscript.

Notes

The authors declare no competing financial interest.

■ ACKNOWLEDGMENTS

■ REFERENCES

(1) (a) Ostroverkhova, O. Organic Optoelectronics Materials: Mechanism and Applications. *Chem. Rev.* **2016**, *116*, 13279−13412. (b) Gather, M. C.; Köhnen, A.; Meerholz, K. White Organic Light-Emitting Diodes. *Adv. Mater.* **2011**, *23*, 233−248.

(2) Allard, S.; Forster, M.; Souharce, B.; Thiem, H.; Scherf, U. Organic Semiconductors for Solution-Processable Field-Effect Transistors (OFETs). *Angew. Chem., Int. Ed.* **2008**, *47*, 4070−4098.

(3) You, L.; Zha, D.; Anslyn, E. V. Recent Advances in Supramolecular Analytical Chemistry Using Optical Sensing. *Chem. Rev.* **2015**, *115*, 7840−7892.

(4) Kuehne, A. J. C.; Gather, M. C. Organic Lasers: Recent Developments on Materials, Device Geometries, and Fabrication Techniques. *Chem. Rev.* **2016**, *116*, 12823−12864.

(5) (a) Bahadur, S. K.; Thangaraji, V.; Yadav, N.; Nanda, G. P.; Das, S.; Gandeepan, P.; Colman, E. Z.; Rajamalli, P. High performance non-doped green organic light emitting diodes via delayed fluorescence. *J. Mater. Chem. C* **2021**, *9*, 15583−15590. (b) Murayama, N.; Jorolan, J. H.; Minoura, M.; Nakano, H.; Ikoma, T.; Matano, Y. 9-(Diphenylphosphoryl)-10-(phenylethynyl)anthracene Derivatives: Synthesis and Implications for the Substituent and Solvent Effects on the Light-Emitting Properties. *ChemPhotoChem.* **2022**, *6*, No. e202200100. (c) Schillmoller, T.; Ruth, P. N.; Herbst-Irmer, R.; Stalke, D. Three colour solid-state luminescence from positional isomers of facilely modified thiophosphoranyl anthracenes. *Chem. Commun.* **2020**, *56*, 7479−7482.

(6) Song, J. Y.; Park, S. N.; Lee, S. J.; Kim, Y. K.; Yoon, S. S. Novel fluorescent blue-emitting materials based on anthracene-fluorene hybrids with triphenylsilane group for organic light-emitting diodes. *Dyes Pigm.* **2015**, *114*, 40−46.

(7) Aydemir, M.; Haykir, G.; Battal, A.; Jankus, V.; Sugunan, S. K.; Dias, F. B.; Attar, H. A.; Turksoy, F.; Tavasli, M.; Monkman, A. P. High efficiency OLEDs based on anthracene derivatives: The impact of electron donating and withdrawing group on the performance of OLED. *Org. Electron.* **2016**, *30*, 149−157.

(8) Mallesham, G.; Swetha, C.; Niveditha, S.; Mohanty, M. E.; Babu, N. J.; Kumar, A.; Bhanuprakash, K.; Rao, V. J. Phosphine oxide functionalized pyrenes as efficient blue light emitting multifunctional materials for organic light emitting diodes. *J. Mater. Chem. C* **2015**, *3*, 1208−1224.

(9) Chen, D.; He, W. Z.; Liao, H. S.; Hu, Y. X.; Xie, D. D.; Wang, B. Y.; Chi, H. J.; Lv, Y. L.; Zhu, X.; Li, X. Benzimidazole/carbazole-based bipolar host materials for highly efficient green phosphorescent OLEDs with negligible efficiency roll-off. *Org. Electron.* **2023**, *113*, No. 106715.

(10) Li, C.; Zhang, M.; Chen, X.; Li, Q. Fluorinated 9,9'-spirobifluorene derivative as host material for highly efficient blue, fluorescent OLED. *Opt. Mater. Express* **2016**, *6*, 2545−2553.

(11) Kumar, S.; Kumar, D.; Patil, Y.; Patil, S. Fluoranthene derivatives as blue fluorescent materials for non-doped organic light-emitting diodes. *J. Mater. Chem. C* **2016**, *4*, 193−200.

(12) Yiu, T. C.; Gnanasekaran, P.; Chen, W. L.; Lin, W. H.; Lin, M. J.; Wang, D. Y.; Lu, C. W.; Chang, C. H.; Chang, Y. J. Multifaceted Sulfone−Carbazole-Based D−A−D Materials: A Blue Fluorescent Emitter as a Host for Phosphorescent OLEDs and Triplet−Triplet Annihilation Up-Conversion Electroluminescence. *ACS Appl. Mater. Interfaces* **2023**, *15*, 1748−1761.

(13) Wang, Y.; Liu, W.; Ye, S.; Zhang, Q.; Duan, Y.; Guo, R.; Wang, L. Molecular engineering of anthracene-based emitters for highly efficient nondoped deep-blue fluorescent OLEDs. *J. Mater. Chem. C* **2020**, *8*, 9678–9687.

(14) Li, W.; Chasing, P.; Nalaoh, P.; Chawanpunyawat, T.; Chantanop, N.; Sukpattanacharoen, C.; Kungwan, N.; Wongkaew, P.; Sudyoadsuk, T.; Promarak, V. Deep-blue high-efficiency triplet–triplet annihilation organic light-emitting diodes using hydroxyl-substituted tetraphenylimidazole-functionalized anthracene fluorescent emitters. *J. Mater. Chem. C* **2022**, *10*, 9968–9979.

(15) Wu, C. L.; Chang, C. H.; Chang, Y. T.; Chen, C. T.; Chen, C. T.; Su, C. J. High efficiency non-dopant blue organic light-emitting diodes based on anthracene-based fluorophores with molecular design of charge transport and red-shifted emission proof. *J. Mater. Chem. C* **2014**, *2*, 7188–7200.

(16) Zhang, Z.; Zhang, Y.; Yao, D.; Bi, H.; Javed, I.; Fan, Y.; Zhang, H.; Wang, Y. Anthracene-Arrangement-Dependent Emissions of Crystals of 9-Anthrylpyrazole Derivatives. *Cryst. Growth Des.* **2009**, *9*, 5069–5076.

(17) Zhao, J.; Chen, K.; Hou, Y.; Che, Y.; Liu, L.; Jia, D. Recent progress in heavy atom-free organic compounds showing unexpected intersystem crossing (ISC) ability. *Org. Biomol. Chem.* **2018**, *16*, 3692–3701.

(18) Curtis, M. D.; Cao, J.; Kampf, J. W. Solid-State Packing of Conjugated Oligomers: From π-Stacks to the Herringbone Structure. *J. Am. Chem. Soc.* **2004**, *126*, 4318–4328.

(19) (a) Bałczewski, P.; Kowalska, E.; Różycka-Sokołowska, E.; Skalik, J.; Owsianik, K.; Koprowski, M.; Marciniak, B.; Guziejewski, D.; Ciesielski, W. Mono-Aryl/Alkylthio-Substituted (Hetero)acenes of Exceptional Thermal and Photochemical Stability by the Thio-Friedel–Crafts/Bradsher Cyclization Reaction. *Chem.—Eur. J.* **2019**, *25*, 14148–14161. (b) Bałczewski, P.; Kowalska, E.; Skalik, J.; Koprowski, M.; Owsianik, K.; Różycka-Sokołowska, E. Ultrasound-assisted synthesis of RO- and RS-substituted (hetero)acenes via oxo- and thio-Friedel-Crafts/Bradsher reactions. *Ultrasonics—Sonochemistry* **2019**, *58*, 10464.

(20) Zhao, Y.; Duan, L.; Zhang, X.; Zhang, D.; Qiao, J.; Dong, G.; Wang, L.; Qiu, Y. White light emission from an exciplex based on a phosphine oxide type electron transport compound in a bilayer device structure. *RSC Adv.* **2013**, *3*, 21453–21460.

(21) Duan, K.; Wang, D.; Yang, M.; Liu, Z.; Wang, C.; Tsuboi, T.; Deng, C.; Zhang, Q. Weakly Conjugated Phosphine Oxide Hosts for Efficient Blue Thermally Activated Delayed Fluorescence Organic Light-Emitting Diodes. *ACS Appl. Mater. Interfaces* **2020**, *12*, 30591–30599.

(22) Goushi, K.; Adachi, C. Efficient organic light-emitting diodes through up-conversion from triplet to singlet excited states of exciplexes. *Appl. Phys. Lett.* **2012**, *101*, No. 023306.

(23) Baumgartner, T.; Reau, R. Organophosphorus π-Conjugated Materials. *Chem. Rev.* **2006**, *106*, 4681–4727.

(24) Bouit, P. A.; Escande, A.; Szűcs, R.; Szieberth, D.; Lescop, C.; Nyulászi, L.; Hissler, M.; Réau, R. Dibenzophosphapentaphenes: Exploiting P Chemistry for Gap Fine-Tuning and Coordination-Driven Assembly of Planar Polycyclic Aromatic Hydrocarbons. *J. Am. Chem. Soc.* **2012**, *134*, 6524–6527.

(25) Takeda, Y.; Nishida, T.; Minakata, S. 2,6-Diphospha-s-indacene-1,3,5,7(2H, 6H)-tetraone: A Phosphorus Analogue of Aromatic Diimides with the Minimal Core Exhibiting High Electron-Accepting Ability. *Chem.—Eur. J.* **2014**, *20*, 10266–10270.

(26) Jeon, S. O.; Lee, J. Y. Phosphine oxide derivatives for organic light emitting diodes. *J. Mater. Chem.* **2012**, *22*, 4233–4243.

(27) Yook, K. S.; Lee, J. Y. Small Molecule Host Materials for Solution Processed Phosphorescent Organic Light-Emitting Diodes. *Adv. Mater.* **2014**, *26*, 4218–4233.

(28) Zhang, J.; Ding, D.; Wei, Y.; Han, F.; Xu, H.; Huang, W. Multiphosphine-Oxide Hosts for Ultralow-Voltage-Driven True-Blue Thermally Activated Delayed Fluorescence Diodes with External Quantum Efficiency beyond 20%. *Adv. Mater.* **2016**, *28*, 479–485.

(29) Kan, W.; Zhu, L.; Wei, Y.; Ma, D.; Sun, M.; Wu, Z.; Huang, W.; Xu, H. Phosphine oxide-jointed electron transporters for the reduction of interfacial quenching in highly efficient blue PHOLEDs. *J. Mater. Chem. C* **2015**, *3*, 5430–5439.

(30) Barney, R. J.; Richardson, R. M.; Wiemer, D. F. Direct Conversion of Benzylic and Allylic Alcohols to Phosphonates. *J. Org. Chem.* **2011**, *76*, 2875–2879.

(31) Richardson, R. M.; Barney, R. J.; Wiemer, D. F. Synthesis of dialkyl and diaryl benzylphosphonates through a ZnI$_2$-mediated reaction. *Tetrahedron Lett.* **2012**, *53*, 6682–6684.

(32) Bałczewski, P.; Dudziński, B.; Koprowski, M.; Knopik, Ł.; Owsianik, K. Patent PL-245310, 21.06.2024.

(33) Renard, P. Y.; Vayron, P.; Leclerc, E.; Valleix, A.; Miokowski, C. Lewis Acid Catalyzed Room-Temperature Michaelis–Arbuzov Rearrangement. *Angew. Chem., Int. Ed.* **2003**, *42*, 2389–2392.

(34) Breshears, A. T.; Behrle, A. C.; Barnes, C. L.; Laber, C. H.; Baker, G. A.; Walensky, J. R. Synthesis, spectroscopy, electrochemistry, and coordination chemistry of substituted phosphine sulfides and selenides. *Polyhedron* **2015**, *100*, 333–343.

(35) Schillmöller, T.; Ruth, P. N.; Irmer, R. H.; Stalke, D. Analysis of Solid-State Luminescence Emission Amplification at Substituted Anthracenes by Host–Guest Complex Formation. *Chem.—Eur. J.* **2020**, *26*, 17390.

(36) Sarkar, B.; Prasad, E.; Gardas, R. L. Systematic photophysical, thermal and electrochemical analysis of a series of phenothiazine cored conjugated aromatic unit appended D−π−A based high-solid state luminescent materials: their applications in reversible mechanofluorochromic and volatile acid sensing. *Mater. Adv.* **2022**, *3*, 2871–2883.

(37) Jones, R. N. The Ultraviolet Absorption Spectra of Anthracene Derivatives. *Chem. Rev.* **1947**, *41*, 353–371.

(38) Banerjee, S.; Both, A. K.; Sarkar, M. Probing the Aggregation and Signaling Behavior of Some Twisted 9,9′-Bianthryl Derivatives: Observation of Aggregation-Induced. *Blue-Shifted Emission. ACS Omega* **2018**, *3*, 15709–15724.

(39) Chan, J. M. W.; Tischler, J. R.; Kooi, S. E.; Bulovic, V.; Swager, T. M. Synthesis of J-Aggregating Dibenz[a,j]anthracene-Based Macrocycles. *J. Am. Chem. Soc.* **2009**, *131*, 5659–5666.

(40) Aydemir, M.; Haykir, G.; Selvitopi, H.; Yildirim, O. C.; Arslan, M. E.; Abay, B.; Turksoy, F. Exploring the potential of anthracene derivatives as fluorescence emitters for biomedical applications. *J. Mater. Chem. B* **2023**, *11*, 4287–4295.

(41) Panda, S.; Panda, A.; Zade, S. S. Organoselenium compounds as fluorescent probes. *Coord. Chem. Rev.* **2015**, *300*, 86–100.

(42) *ACD/Percepta, Version 14.0.0*; Advanced Chemistry Development, Inc.: Toronto, ON, Canada, 2015.

(43) Birks, J. B. *Photophysics of Aromatic Molecules*; Wiley: New York, 1970.

(44) Mei, J.; Leung, N. L. C.; Kwok, R. T. K.; Lam, J. W. Y.; Tang, B. Z. Aggregation-Induced Emission: Together We Shine, United We Soar! *Chem. Rev.* **2015**, *115*, 11718–11940.

(45) Luo, J.; Xie, Z.; Lam, J. W. Y.; Cheng, L.; Chen, H.; Qiu, C.; Kwok, H. S.; Zhan, X.; Liu, Y.; Zhu, D.; Tang, B. Z. Aggregation-induced emission of 1-methyl-1,2,3,4,5-pentaphenylsilole. *Chem. Commun.* **2001**, 1740–1741.

(46) Janzen, D. E.; Burand, M. W.; Ewbank, P. C.; Pappenfus, T. M.; Higuchi, H.; da Silva, Filho D. A.; Young, V. G.; Bredas, J. L.; Mann, K. R. Preparation and characterization of p-stacking quinodimethane oligothiophenes. Predicting semiconductor behavior and band widths from crystal structures and molecular orbital calculations. *J. Am. Chem. Soc.* **2004**, *126*, 15295–15308.

(47) Spackman, P. R.; Turner, M. J.; McKinnon, J. J.; Wolff, S. K.; Grimwood, D. J.; Jayatilaka, D.; Spackman, M. A. *CrystalExplorer*: a program for Hirshfeld surface analysis, visualization and quantitative analysis of molecular crystals. *J. Appl. Crystallogr.* **2021**, *54*, 1006–1011.

GDCh

Research Article

Angewandte
International Edition *Chemie*
www.angewandte.org

Check for updates

Organic Materials

Multiply Substituted (Hetero)acenes Containing Phosphonate Group at the Central Unit as High-Efficiency Light Emitters

Marek Koprowski,* Łucja Knopik, Ewa Różycka-Sokołowska,* Bogdan Dudziński,
Vivek Vivek, Krzysztof Owsianik, and Piotr Bałczewski*

Abstract: A new variant of the Friedel–Crafts–Bradsher (F-C-B) reaction offers access to dialkoxyphosphoryl substituted (hetero)acenes, especially to previously unavailable three- to seven-substituted, tri- and tetracyclic compounds, and features high chemical yields up to 95%, excellent photoluminescence (PL) quantum yields (QYs) up to 87.7%, large Stokes shifts up to 7943 cm^{-1}, and very mild, room temperature reaction conditions. The $(RO)_2P(O)$ has a distinct effect on the photophysical properties of acenes, increasing QYs by more than twofold compared to identical acenes not substituted by this group. DFT and TD-DFT calculations, combined with electron-hole analysis, indicated that local excitation (LE) had the dominant contribution to the electron excitation mechanism, and charge transfer (CT) of about 30% provided the highest fluorescence QYs. The multiple substitutions of (hetero)acenes bearing phosphonate moieties and electron-diverse substituents combined with a lower number of fused aromatic rings appear to be ideal for optimal chemical stability and high PL. The new, synthetic tool will accelerate exploitation of bulky (hetero)acene emitters for optoelectronic applications.

Introduction

Phosphonates play an important role in biological,[1] pharmaceutical,[2–4] agricultural,[5] and material chemistry,[6] both as final products[1–6] and synthetic phosphoroorganic reagents.[7] Among aromatic phosphonates, in which quinquevalent and tetracoordinated (P^{IV}) phosphorus atoms are directly linked to the sp^2 carbon atom, only (dialkoxyphosphoryl)benzenes[8–13] and (dialkoxyphosphoryl)naphthalenes[11–16] have been thoroughly investigated. More complex systems, such as (dialkoxyphosphoryl)anthracenes[13–17] are still insufficiently studied, and their higher analogs with more than three fused aromatic rings as well as those with a high degree of electron-diverse substitution that determines their final properties are still unknown.

[*] Dr. M. Koprowski, Ł. Knopik, Dr. B. Dudziński, V. Vivek,
Dr. K. Owsianik, Prof. P. Bałczewski
Division of Organic Chemistry, Centre of Molecular and
Macromolecular Studies, Polish Academy of Sciences, Sienkiewicza
112, Łódź 90–363, Poland
E-mail: marek.koprowski@cbmm.lodz.pl
piotr.balczewski@cbmm.lodz.pl

Ł. Knopik, V. Vivek
The Bio-Med-Chem Doctoral School of the University of Łódź and
Łódź Institutes of the Polish Academy of Sciences, University of
Łódź, Matejki 21/23, Łódź 90–237, Poland

Dr. E. Różycka-Sokołowska, Prof. P. Bałczewski
Institute of Chemistry, Faculty of Science and Technology, Jan
Długosz University in Częstochowa, Armii Krajowej 13/15,
Częstochowa 42–201, Poland
E-mail: e.sokolowska@ujd.edu.pl

Additional supporting information can be found online in the
Supporting Information section

In this article, we present the use of a new variant of the Friedel–Crafts–Bradsher (F-C-B) reaction as a tool that enables the synthesis of multiply substituted (hetero)acenes **2a–k** and **2m–o**. They are distinguished by their good solubility, high chemical stability, highest photoluminescence (PL) quantum yields (QYs), high chemical yields, one of the highest Stokes shifts, significant redshifts relative to other acenes, enhanced donor–acceptor properties, and the lowest synthesis temperature ever used in F-C type reactions. Noteworthy in this synthetic concept is the possibility of introducing a large number of substituents of different electron character, especially electron-withdrawing substituents, such as CN, CF$_3$, and P(O)(OEt)$_2$, which was not possible until now but is important for the final properties. The electron-withdrawing power of the P(O)(OEt)$_2$ group is comparable to that of the CN and CF$_3$ groups (Hammett's constant σ_{para} = 0.56, 0.66, and 0.51, respectively). However, unlike the CN and CF$_3$ groups, the contribution of the induction effect for the P(O)(OEt)$_2$ group is significantly smaller (σ_{ind} = 0.32 vs. 0.57 and 0.40 for CN and CF$_3$, respectively), while the resonance effect for P(O)(OEt)$_2$ strongly dominates over the resonance effect for the CN and CF$_3$ groups (σ_{res} = 0.24 vs. 0.08 and 0.11 for CN and CF$_3$, respectively) (Table S31), which is important for strong light absorption and emission.

Results and Discussion

Synthesis

The new variant of the F-C-B reaction proceeds at room temperature, i.e., under much milder conditions than other reactions proceeding via the S$_E$Ar mechanism. These reactions typically require temperatures up to 180 °C or higher, which excludes the presence of sensitive substituents on

Scheme 1. Synthesis of 10-(dialkoxyphosphoryl)anthracenes **2a–i** and their heteroanalogs **2m**, **2n**, and **2o** from *o*-bromo aromatic aldehydes **3a–i** and **3o**.

Scheme 2. Structures of (dialkoxyphosphoryl)-acenes **2a–k** and their heterocyclic analogs **2m**, **2n**, and **2o** obtained from **1a–o** as well as 10-unsubstituted analogs **6** and **7**.

aromatic systems.[18] The F-C-B reaction involves the cyclization of [(*ortho*-acetalaryl)aryl]methylphosphonates **1a–k** in an aqueous solution of mineral acid (6N HCl$_{aq}$) and EtOH (for diethyl phosphonates) or MeOH (for dimethyl phosphonates) to provide anthracenes **2a–k** in up to 95% (R^{1}OH: R^1 = Me, Et; Schemes 1 and 2). Exceptionally, for the tetracyclic (hetero)acene **2n**, obtained in 92% yield from the phosphonate **1n**, acetonitrile was chosen as a solvent due to the poor solubility of the substrate in ethanol. Other heteroanalogs **2m** and **2o** were prepared from **1m** and **1o** in 44% and 70% yields, respectively (Scheme 1). The new reaction proceeds via the carbocation formed by protonation followed by ring opening of the acetal function rather than via the carbocation formed by protonation of the aldehyde group, as in the original Bradsher reaction. Consequently, the final aromatization step proceeds with the leaving of 1,3-propandiol and not water. The reaction via the acetal derived carbocation occurs distinctly faster than via the aldehyde derived one, as in the Bradsher's dehydration, although the latter may be a competing process (Figure S61).

Scheme 1 also shows that the F-C-B cyclization is a three-step process that, in the first step, involves a high-yield acetalization of *ortho*-bromo aromatic aldehydes **3a–i** with 1,3-propanediol using concentrated sulfuric acid, as an acidic catalyst, to give acetals **4a–i**. Then, the Br/Li exchange with *n*-BuLi at −78 °C and condensation of the resulting aryl lithiums with electron rich aromatic aldehydes leads to diarylmethanols **5a–i** in up to 88% yields. The use of sulfuric acid instead of *p*-toluenesulfonic acid, which has usually been used in acetalization reactions, resulted in a significant reduction of the reaction time and in an increase in yields of acetals **4a–i**. The final step, leading to **1a–i** in up to 70% yield, is the Lewis acid (ZnI$_2$) promoted Arbuzov-like reaction of diarylmethanols **5a–i** with trialkyl (R = Me, Et) phosphites. This reaction, used for benzyl and allyl alcohols by Wiemer
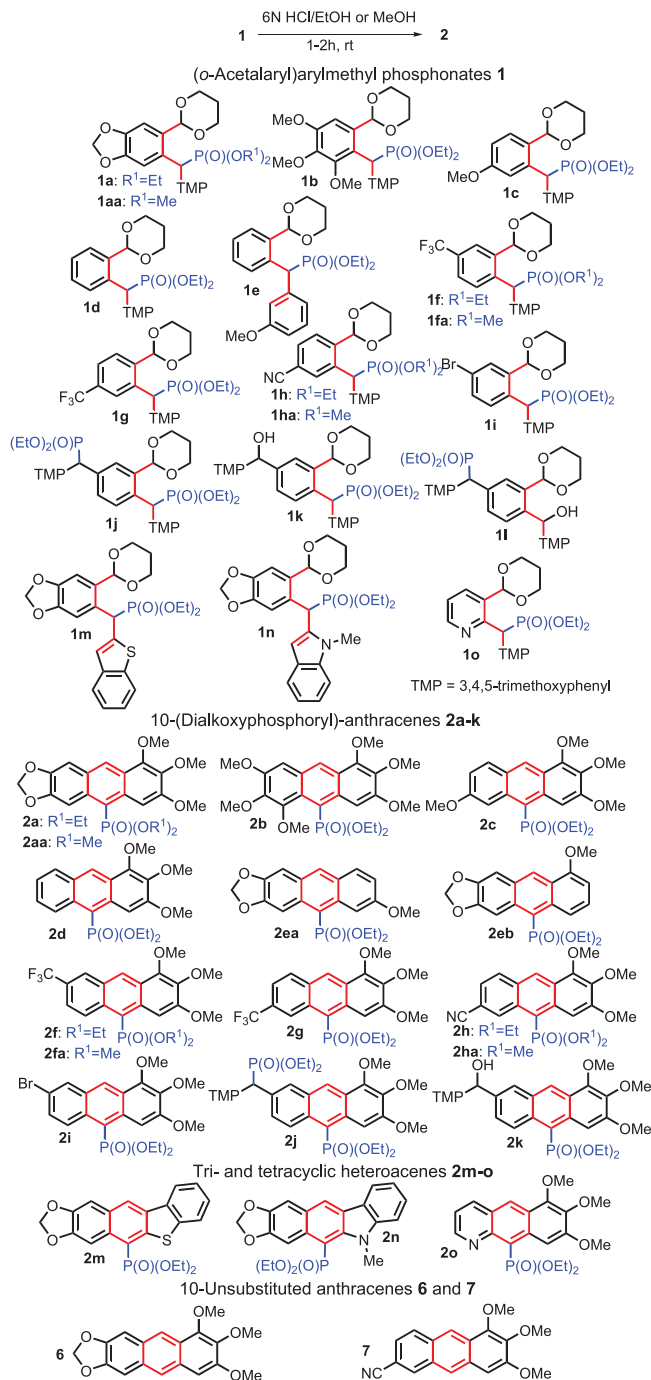
et al.[19,20] has been successfully extended here to sensitive substrates: (1) dibenzylic alcohols **5a–i** containing the Lewis acid labile acetal function on one of the aryl moieties, (2) bis(dibenzylic alcohol) **5j**, with the labile acetal function on the central aryl moiety, and (3) dimethyl phosphonates that in general are the least stable group of dialkyl phosphonates and have not been synthesized by this method, as well.

The Scheme 2 shows structures of starting [(*ortho*-acetalaryl)aryl]methylphosphonates **1a–o** as well as

Angew. Chem. Int. Ed. **2025**, *64*, e202508168 (2 of 8)

© 2025 Wiley-VCH GmbH
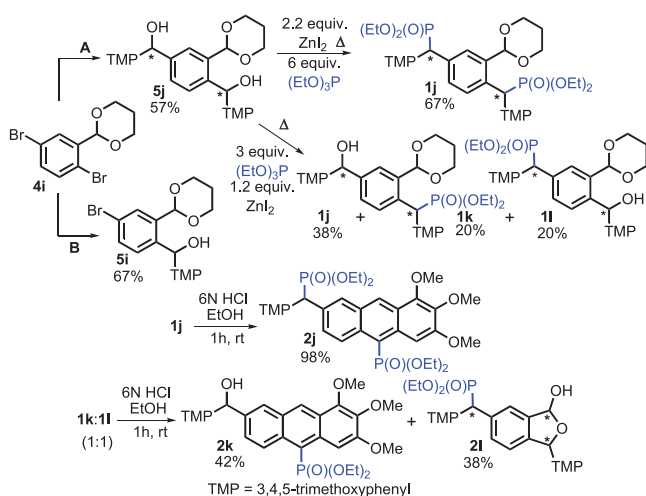
Scheme 3. Transformations of 2,5-dibromobenzaldehyde acetal **4i** to monophosphonates **1k/1l** and the bisphosphonate **1j**. The cyclization of **1j** to **2j** and the mixture of **1k/1l** to the anthracene **2k** and the lactol **2l**.

$(RO)_2P(O)$ substituted cyclization products **2a–o** and 10-unsubstituted analogs **6** and **7**. All cyclization reactions leading to the latter occurred in a short time, up to 2 h, at room temperature, in high 72%–98% yields. Also, dimethyl phosphonates **1aa**, **1fa**, and **1ha**, which are less stable under acidic conditions than diethyl phosphonates, were cyclized to anthracenes **2aa**, **2fa**, and **2ha** in high 84%–95% yields. Heterocyclic derivatives **2m–o**, with the ring sulfur and nitrogen atoms, were also obtained in good yields (**2n**, 92%; **2m**, 44%; **2o**, 70%).

In this study, we have extended the applicability of the Arbuzov-like reaction on bis(dibenzylic alcohols) starting from the bis(diarylmethanol) **5j**, which was obtained by dilithiation of 2,5-dibromobenzaldehyde acetal **4i** with an excess of *n*-BuLi (2.2 equiv.) followed by the reaction with 3,4,5-trimethoxybenzaldehyde (2.4 equiv., TMP-CHO) (procedure A). The diol **5j** was obtained as a 1:1 mixture of two diastereoisomers (¹H NMR), in 57% yield (Scheme 3). The use of stoichiometric amounts of *n*-BuLi (1.1 equiv.) and TMP-CHO (1.2 equiv.) (procedure B) gave the monoalcohol **5i** in 67% yield (Scheme 3).

The subsequent Arbuzov-like reaction of the diol **5j** with $(EtO)_3P$ (6 equiv.) in the presence of ZnI_2 (2.2 equiv.) in THF at 80 °C, after 18 h, afforded the bisphosphorylated product **1j** in 67% yield, as the inseparable mixture of two diastereoisomers in a 1:1 ratio (¹H NMR) (Scheme 3). Two phosphorus atoms in **1j** were coupled to each other with the long-range coupling constant $^7J_{PP} = 3.3$ Hz.

The Arbuzov-like reaction of the diol **5j** in the presence of lesser amounts of $(EtO)_3P$ (3 equiv.) and ZnI_2 (1.2 equiv.) than before gave three products: the bisphosphonate **1j** in 38% yield and the inseparable mixture of two regioisomeric monophosphonates **1k** and **1l** in 40% overall yield (Scheme 3). Regioisomeric monophosphonates **1k/1l** were formed in 20% yield each, as a mixture of diastereoisomers in a 1:1 ratio (³¹P NMR). The bisphosphonate **1j** was easily separable from the mixture of monophosphonates **1k** and **1l** with column chromatography over silica gel.

Treatment of the inseparable mixture **1k/1l** with mineral acid (6N HCl, EtOH) resulted in deprotection of the acetal function to give a mixture of two easily separable products, the anthracene **2k** and the lactol **2l** (Schemes 2 and 3).

The expected anthracene **2k** was obtained from **1k** in 42% yield. The lactol **2l**, obtained from **1l** in 38% yield, was the 1.8:1.4:1:1 mixture of four chromatographically inseparable diastereoisomers (³¹P and ¹H NMR).

Cyclization of the bisphosphonate **1j** led to the formation of the acene **2j** having two phosphonate groups, one at position 9 of the anthracene backbone and the other in the side chain (Scheme 2).

The next stage of this study involved measurements of optical properties. Table 1 presents the results of UV absorption maxima, PL maxima (λ_{max}), Stokes shifts, and QYs for ten acenes in three solvents of different polarity.

Stokes Shifts

The obtained donor–acceptor fluorophores generally showed high Stokes shift values, which are important for practical fluorescence applications because they allow separation of the excitation light from the emitted fluorescence, thereby reducing self-quenching that results from molecular self-absorption (Table 1). For anthracenes **2f**, isomeric **2g**, and **2h** with electron-withdrawing $(RO)_2P(O)$, CF_3, and CN substituents and three methoxy groups, the highest values of Stokes shift (6755 to 7492 cm⁻¹) were observed in polar solvents, such as DCM and EtOH. In non-polar cyclohexane, these values dropped to about 5700 cm⁻¹. Exceptionally high Stokes shifts values have been observed for **2o** with heteroaromatic benzo[*g*]quinoline ring up to 7943 cm⁻¹ (EtOH). Still high Stokes shifts up to 6775 cm⁻¹ (EtOH) have been recorded for **2d**, unsubstituted in one of the outer anthracene rings and electron-rich in the second outer ring. The anthracene **2a** bearing all electron-donating groups on both winged anthracene rings showed good Stokes shifts in all three solvents around 4900 cm⁻¹. The lowest shifts in all solvents have been observed for the poorly substituted **2m** with four fused rings, indicating the lack of efficient charge separation in ground and excited states.

Figure 1 shows changes in Stokes shifts of the selected anthracene **2h** in cyclohexane, DCM, and EtOH (see also Table 1). The absorption and emission spectra of the other anthracenes (**2a**, **2d**, **2ea**, **2eb**, **2f**, **2g**, **2h**, **2j**, **2k**, **2m**, **2n**, and **2o**) in these solvents are presented in the SI (Figures S1–S17) and for **6** and **7** in Table S3 and Figures S22–S29.

In the series of heteroacenes, exceptionally high Stokes shift values (up to 7943 cm⁻¹) were observed for the tricyclic arene **2o** with a benzo[*g*]quinoline ring in all solvents, while tetracyclic heteroacenes **2m** and **2n** with the ring sulfur and nitrogen atoms showed 3000 and 5000 cm⁻¹, respectively.

Photoluminescence Quantum Yields (QYs)

Anthracenes without ring heteroatoms showed QYs up to 87.7% with the highest values for **2f**, **2g**, **2h**, and **2j** in

Angew. Chem. Int. Ed. **2025**, 64, e202508168 (3 of 8)

© 2025 Wiley-VCH GmbH

Table 1: Absorption (Abs.) and PL maxima (λ_{max}), Stokes shifts, QYs in solution (cyclohexane, DCM, and EtOH) for **2a**, **2d**, **2ea**, **2eb**, **2f**, **2g**, **2h**, **2j**, **2k**, **2m**, **2n**, **2o**, **6**, and **7** (underlined values are the highest absorption maxima in lower parts of the spectra).

Nr	Abs. λ_{max} (nm)	PL λ_{max} (nm)	Stokes shift (cm^{-1})	QY (%)
	In Cyclohexane			
2a	378	466	4996	47.3
2d	369, 396	468	5733	64.9
2ea	365, 383, 403	433	4302	35.0
2eb	355, 371, 383, 404	420, 441	4278	51.3
2f	375, 398	475	5614	66.2
2g	350, 368, 401	471	5943	63.9
2h	338, 354, 374, 411	478	5818	67.4
2j	353, 372, 398	470	5605	70.3
2k	370, 394	470	5750	73.8
2m	345, 382	389	3279	8.2
2n	351, 384, 401	419	4624	39.1
2o	371, 406	493	6670	74.3
6	360, 380	389, 409	3328	20.7
7	328, 346, 365, 386, 409	423, 447	5261	49.8
	In DCM			
2a	381	467	4833	61.0
2d	370, 396	486	6451	67.3
2ea	368, 384, 404	444	4651	35.8
2eb	373	461	5118	76.8
2f	376, 398	504	6755	83.7
2g	370, 401	506	7264	78.2
2h	339, 356, 375, 411	519	7399	82.3
2j	372, 398	492	6557	87.7
2k	372, 395	488	6390	77.5
2m	350, 381	392	3061	8.7
2n	352, 384, 402	425	4880	33.6
2o	371, 402	516	7574	73.5
6	363, 381	398, 415	3452	29.1
7	331, 347, 365, 390, 410	466	7359	71.7
	In EtOH			
2a	380	468	4948	51.5
2d	369, 396	492	6775	63.6
2ea	368, 383, 403	446	4752	37.8
2eb	373	471	5578	63.4
2f	375, 399	509	7020	60.1
2g	369, 403	510	7492	60.2
2h	339, 354, 375, 413	527	7691	46.4
2j	372, 398	496	6721	74.2
2k	371, 395	492	6629	70.8
2m	350, 380	389	2865	9.8
2n	352, 384, 401	428	5045	41.5
2o	370, 400	524	7943	39.0
6	337, 360, 378	393, 410	3388	25.8
7	330, 346, 364, 388, 408	468	7534	45.9

Figure 1. Typical normalized absorption (solid line) and PL (dotted line) spectra for **2h** in cyclohexane, DCM, and EtOH (10^{-5} mol L^{-1}), illustrating a magnitude of the Stokes shift.
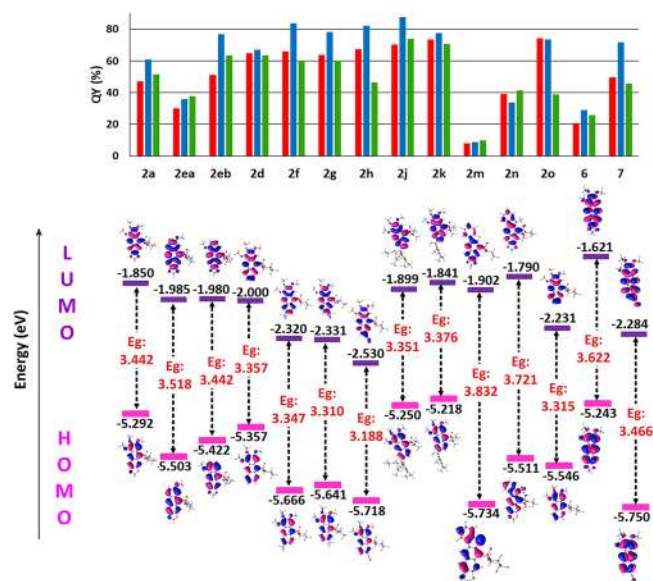
Figure 2. Graphs illustrating changes in fluorescence QY for the series of molecules **2a**, **2ea**, **2eb**, **2d**, **2f**, **2g**, **2h**, **2j**, **2k**, **2m**, and **2o** in solutions of cyclohexane (red), DCM (blue), and ethanol (green) and in the energy values of HOMO (E_{HOMO}), LUMO (E_{LUMO}), and band gap (E_G) optimized for these compounds at the DFT theory B3LYP/6–311++G(d,p), and also plots of the HOMO and LUMO orbitals.

DCM (see Table 1). A comparison of the HOMO and LUMO energy values (Figures 2 and S32), calculated by DFT/B3LYP/6–311++G(d,p) in the gas phase for **2f**, **2h**, and unsubstituted **2d** (Tables S6, S9, and S10, while Tables S5, S7, S11–S18 contain the results of DFT calculations for **2a**, **2ea**, **2eb**, **2g**, **2j**, **2k**, **2m**, **2n**, and **2o**) indicated that the introduction of electron-withdrawing substituents (CF$_3$ or CN) into **2d** reduced both energies by about 0.3 eV (HOMO for **2f–h** and LUMO for **2f**, **2g**) and, in the case of **2h**, by as much as about 0.5 eV (LUMO). This change was accompanied by an increase in QY, only when the polar aprotic solvent DCM

was used. For other solvents, no significant increase in QY was observed, and even its decrease for the solute-ethanol system, particularly pronounced in the case of **2h**, was noted (Table 1; Figures 2 and S32). A similar situation occurred when the molecule **2d** was modified by the exchange of the ring carbon/nitrogen atoms in **2o**. Here, decreasing the HOMO and LUMO energies by about 0.2 eV resulted in a minor increase in QY (DCM) and practically a twofold decrease when the solvent was changed to ethanol (Table 1; Figures 2 and S32). Compounds **2h** and **2o** contain nitrogen atoms,
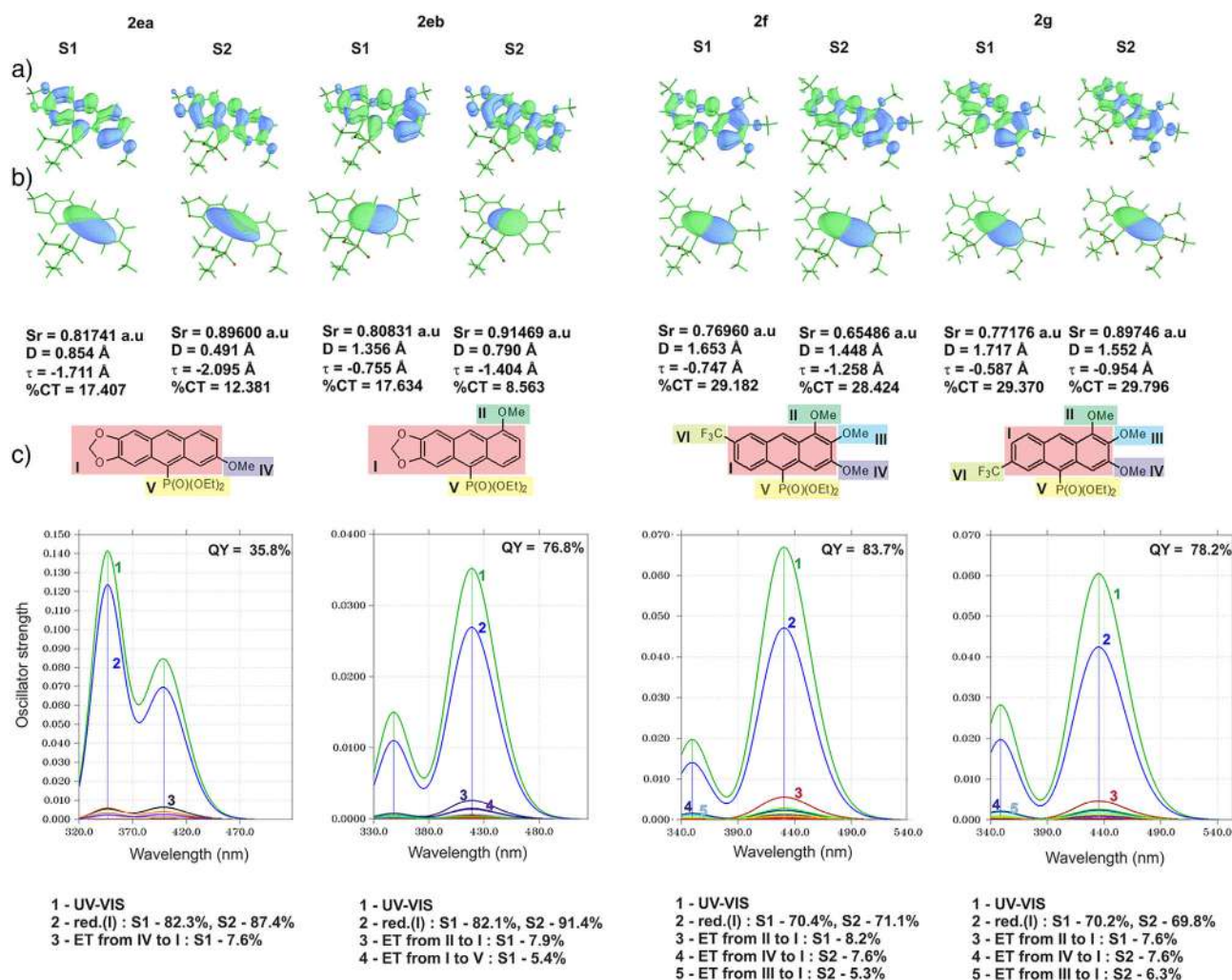
Figure 3. Graphical illustrations of a) hole (green) and electron (blue) distribution, b) Cele (green) and Chole (blue) maps, and c) CTS spectra showing the decomposition of the total UV–vis spectra into individual sub-spectra contributed by different IFCT terms such as electron redistribution (red.) within the fragment (I) and ETs between different fragments for the S1 and S2 excited states of isomeric pairs **2ea/2eb** and **2f/2g**.

which can be acceptors of hydrogen bonds; therefore, the fluorescence quenching was observed only in ethanol, i.e., a polar protic solvent with a high hydrogen bonding donor capability (Kamlet–Taft acidity parameter $\alpha = 0.83$, Table S25).

Hence, it can be assumed that the quenching was due to the formation of strong hydrogen bonds of the O—H···N type. In turn, bulky substituents in **2j** and **2k** had minor effects on HOMO/LUMO energies, which were comparable with those calculated for **2d** but significantly influenced QYs (Table 1; Figures 2, S32, and S33). In particular, **2j** showed a notable QY increase in DCM, where the bulky group might reduce non-radiative decay by restricting molecular motion.

Interestingly, the position of electron-donor 6-MeO/8-MeO substituents in isomeric anthracenes **2ea** and **2eb** contributed to the significant change in QYs (35.8 vs. 76.8%, in DCM, respectively) at comparable HOMO and LUMO energies (Table 1; Figures 2 and S32). To explain such a significant difference in QYs of the two isomers, the results of the hole-electron analysis[21] performed for their S1 and S2 excited states calculated by TD-DFT/B3LYP/6–311++G(d,p) (Tables S26) were compared (Figures 3, S36, and S37 while

Figures S34, S35, and S38–S47 contain the results of the hole-electron analysis for **2a**, **2d**, **2f–2h**, **2j**, **2k**, **2m**, **2n**, **2o**, **6**, and **7**). It was found that the hole and electron regions in regioisomers **2ea** and **2eb** were mainly located in the fused ring system, with the hole region located more on the right ring in **2eb** in contrast to **2ea** (Figure 3a). The S_r index characterizing the overlapping extent of the hole and electron and τ index being a measure of the separation degree of the hole and electron in the charge transfer (CT) direction indicated the local excitation (LE) mechanism in these two excited states of these isomers (Figure 3 and Table S27). However, in the case of **2eb**, the values of S_r index were slightly smaller, and the values of τ and D (charge-transfer length between centroids of hole and electron) were practically ca. 1.5–2 times higher for both states, compared to those calculated for **2ea** (Figure 3 and Table S27), indicating a greater charge separation and a more hybrid nature of electron excitation in the former isomer (i.e., LE with a greater contribution of CT). The results of the inter-fragment charge transfer (IFCT) analysis showed that the intrinsic electron CT percentage (%CT) for S1 states were comparable, but it was ca. 4% higher for the

Research Article

Angewandte
International Edition *Chemie*

S2 state in **2eb** compared to **2ea** (Figure 3; Table S27). In turn, the charge transfer spectra (CTS)[22] calculated for **2ea** and **2eb** (Figures 3C and S48) showed that in addition to the redistribution curve within the fragment I, they also included a curve related to inter-fragment electron transfers (ETs) from OMe groups, i.e., from the fragment II (in **2ea**) or IV (in **2eb**) to the fragment I (7.9% and 7.4%, respectively), and in the case of **2eb**, additionally a curve related to the transfer from the fragment I to the fragment V, i.e., to the P(O)(OEt)$_2$ group (5.4%) (Table S29). In the CTS spectra of these two regioisomers, the peaks corresponding to the S0→S1 and S0→S2 transitions differed significantly in the oscillator strength (f). For **2eb** with higher twice QY, the f value calculated for the S0→S1 transition (f$_{S1}$) was higher by ca. 40% than that for S0→S2, while in the case of **2ea**, the f value calculated for the S0→S2 transition (f$_{S2}$) was by ca. 60% higher compared to S0→S1 (Table S26). Expanding this observation to all analyzed compounds, a clear trend was observed between the f$_{S2}$/f$_{S1}$ ratio and the fluorescence QY. Namely, compounds with the f$_{S2}$/f$_{S1}$ values having close to 1 generally showed high QYs (Tables 1 and S26), while those with f$_{S2}$/f$_{S1}$ much greater than 1 showed significantly reduced QYs. For example, compounds with the f$_{S2}$/f$_{S1}$ values equal to 0.29 (**2d**) and 0.94 (**2j**) displayed QYs of 83.7% and 87.7%, respectively, while QYs of compounds with the f$_{S2}$/f$_{S1}$ values equal to 5.81 (**2m**) and 4.27 (**2n**) were only 9.8% and 41.5%, respectively. Moreover, the CTS spectra, calculated for **2m** and **2n**, were very similar and differed significantly from those calculated for **2d** and **2j** (Figures S48, S50, and S51). In the spectra of the former pair of compounds, the curves associated with electron redistribution within the fragment I lay close to the UV–vis curves, while in the spectra calculated for the latter pair, lay were clearly below. In contrast, the CTS spectra calculated for regioisomers **2f** and **2g** were very similar (unlike regioisomers **2ea** and **2eb**), each revealing for S0→S1 a single curve of ET (Figures 3C and S49). Thus, the electron-acceptor substituents 7-CF$_3$/6-CF$_3$ in these regioisomeric anthracenes brought almost no change in QYs.

To demonstrate the key effect of the electron-withdrawing phosphonate group on photophysical properties, we compared the absorption/PL maxima, Stokes shifts, and QYs of 10-(diethoxyphosphoryl)anthracenes **2a**/**2h** with their 10-unsubstituted analogs **6**/**7** (Scheme 2 and Figures S23–S31), showing a more than twofold increase in QYs for the pair **2a**/**6** (cyclohexane, DCM, and EtOH) and 1.15–1.32 for **2h**/**7** (cyclohexane, DCM). The effect of the phosphonate group for the latter was perturbed in EtOH by the fluorescence quenching in this solvent, caused by the intermolecular 6-CN···HOEt hydrogen bond. For both pairs, the increase in QY well correlated with a decrease of electron redistribution within the fragment I (S1: 73.8%/85.5% and S2: 78.2%/85.0% for **2a**/**6** and S1: 67.8%/76.5% and S2: 65.9%/73.5% for **2h**/**7**) (Table S28; Figures S48, S49, and S51), and an increase of %CT by ca. 7% (Table S27). In the group of heteroacenes, the compound **2n** with a ring nitrogen atom showed 4 times higher QYs depending on the solvent (up to 41.5% in EtOH) than its heteroanalog **2m** with the less electronegative ring sulfur atom (up to 9.8% in EtOH) (Table 1). This reflects almost twice the higher %CT (**2n**/**2m** = 13.594%/7.946% in
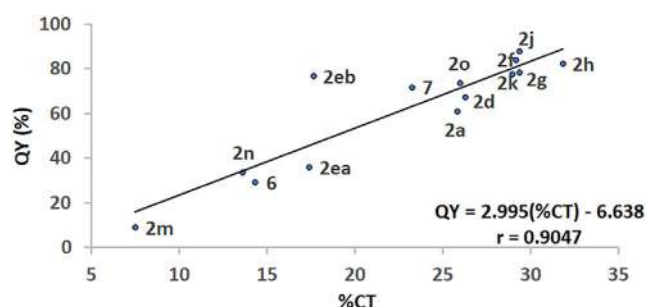

Figure 4. Dependence of fluorescence QY in DCM on the percentage of charge transport calculated by the IFCT method for compounds **2a**, **2d**, **2ea**, **2eb**, **2d**, **2f–2h**, **2j**, **2k**, **2m**, **2n**, **2o**, **6**, and **7**.

S1 and 7.941%/4.129% in S2) (Table S27). An analogue **2o** with the nitrogen atom replacing the C atom in the left ring of **2d** showed the excited states with higher %CT, which was reflected in a higher QYs in DCM and cyclohexane (Tables 1 and S27).

In a summary, the Sr, D, and τ index values (above 0.8, smaller than 2.0, and negative, respectively, for most of the (hetero)acenes, Table S27) indicated that S0→S1 and S0→S2 excitations were of the typical LE nature, but the IFCT analysis showed that CT was also involved in the electron excitation mechanism.

The effect of CT in electron excitation on QY of the tested compounds was demonstrated as a linear relationship: QY = f(%CT), with the best correlations found for DCM (r = 0.9047) (Figure 4) and cyclohexane (r = 0.9135), significantly higher than for ethanol (r = 0.7471) (Figure S52). The poorer correlation observed for ethanol can be attributed to its higher ability to quench fluorescence due to the formation of hydrogen bonds with the P(O)(OEt)$_2$ group in most of the compounds tested.

In order to gain a deeper understanding of the significant differences in QYs of the (hetero)acenes studied, the molecular geometries of **2f** and **2m**, treated as representatives of compounds with high and low QYs, respectively, were optimized in their S0, S1, and S2 states (TD-DFT/B3LYP, Tables S19–S24 and Figures S53–S58). Then, to clarify the strength and nature of possible non-covalent intramolecular interactions and their impact on the stabilization of molecules in these states, QTAIM and NCI calculations were carried out (Figure 5). All these calculations taken together, showed that the combination of the following factors (Table S30) could lead to much higher fluorescence QY of **2f** compared to **2m**, i.e.: (i) a smaller energy difference between S0→S1 (59.51 kcal mol^{-1} for **2f** vs. 72.27 kcal mol^{-1} for **2m**), (ii) a greater oscillator strength for the S1 state and significantly smaller for S2 (0.0671 and 0.0191 for **2f** vs. 0.0355 and 0.2019 for **2m**), (iii) the presence of intramolecular interactions in S0, S1, and S2 states (C−H$_{Ar}$···O=P hydrogen bonds with energies of −6.02, −6.98, and −6.62 kcal mol^{-1}, respectively, in **2f**, in contrast to weak non-covalent S···O=P interactions in **2m**), (iv) larger bond length changes during the S0→S1 transition (12 bonds constituting 35% of all bonds between non-hydrogen atoms in **2f**, compared to eight bonds, i.e., 25% of all bonds in **2m**) and (v) higher dipole moments
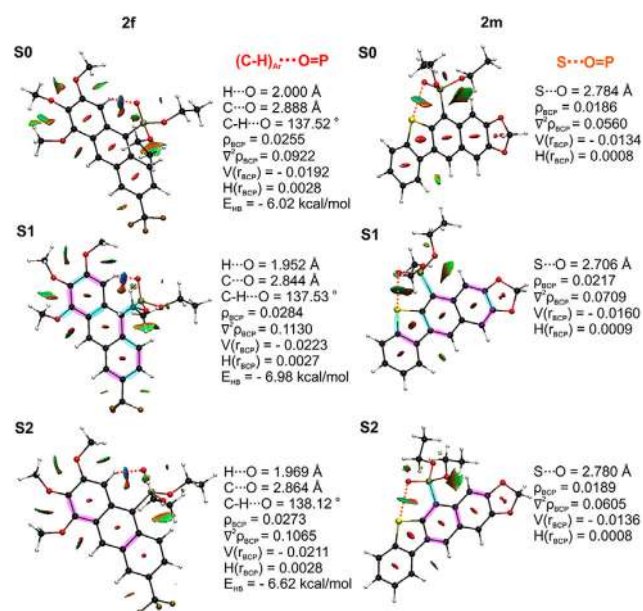
Figure 5. 3D-NCI plots with color-filled isosurfaces for **2f** and **2m** in the S0, S1, and S2 states, showing changes in bond lengths (larger than 0.02 Å) upon S0→S1 and S0→S2 electronic transitions (bonds that shorten are highlighted in blue lines, while those that elongate are marked in pink lines), and the geometrical parameters of non-covalent interactions (red and orange dashed lines) and the topological parameters calculated at their bond critical points (BCPs).

in S0, S1, and S2 states of **2f** (4.98 D in S0, 4.77 D in S1 and 5.62 D in S2 of **2f**, vs. 3.46 in S0, 3.72 in S1 and 3.76 in S2 of **2m**). Moreover, it was found that the strongest bands corresponded to S0→S1 (in **2f**) and S0→S2 (in **2m**) transitions, which originated from a single electron configuration HOMO→LUMO (97.4%) in **2f** and from the HOMO-1→LUMO (79.6%), HOMO→LUMO (3.2%), and HOMO→LUMO+1 (13.4%) electron configurations in **2m** (Figures S59 and S60).

The CIE 1931 Color Space

Depending on the chemical structure and the solvent used, (hetero)acenes **2** emit light from blue through green–blue to green. More polar solvents shift the emitted light toward longer wavelengths (Table 1). Figure 6 shows the results of chromaticity measurements (the CIE 1931 color coordinates) carried out for the tested fluorophores in DCM.[23]

The anthracene **2a** with all electron-donor substituents emits light mainly in the blue-wavelength range (in cyclohexane, DCM, and EtOH) (see SI Figures S18–S20). In contrast, the anthracene **2d** without substituents on one of the flanking rings emits blue light shifted toward longer green wavelengths. Anthracenes **2f**, **2g**, and **2h** with both electron-donor (MeO) and electron-acceptor (CF$_3$, (RO)$_2$P(O), or CN) groups emit light in the blue–green wavelength range depending on the solvent (see SI Figures S18–S20). Anthracenes **2j** and **2k**, differing in the presence of a phosphoryl or hydroxyl group at the benzylic position in the side chain, emit light of almost the same color (see SI Figure S21).
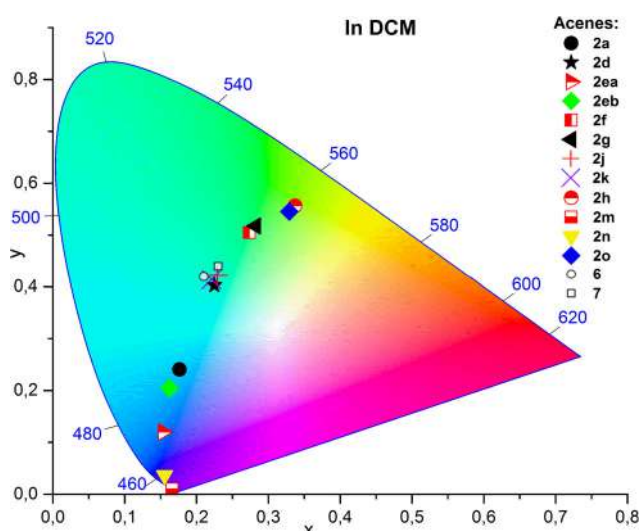
Figure 6. The CIE 1931 chromaticity coordinates for **2a**, **2d**, **2ea**, **2eb**, **2f**, **2g**, **2h**, **2j**, **2k**, **2m**, **2n**, **2o**, **6**, and **7** in the DCM solution (10^{-5} mol L^{-1}).

The heteroacene **2o** with a benzo[*g*]quinoline moiety emits light in the same blue–green wavelength range as the anthracene **2h**, having a strong electron withdrawing CN group. The low substituted tetracylic heteroacenes **2m** and **2n** emit in the deep blue part of the spectrum with no apparent solvent effect (see Figure 2 and Tables S1–S3; Figures S18–S20 in SI).

It can be concluded that in all solvents, there is a harmonic relationship between the electron character of substituents and the color of the emitted light. Thus, by controlling the number, position, and nature of substituents in the anthracene ring, the color of the light emitted by the (hetero)aromatic system can be easily tuned.

Conclusion

The presentation of the new variant of the F-C-B reaction, as useful synthetic tool in (hetero)organic chemistry, provides a valuable opportunity to initiate the development of new methods for the synthesis of promising, highly substituted acenes and heteroacenes, both linearly and angularly fused, equipped with electron and sterically diverse substituents, both achiral and chiral. Particularly important is the key role of the phosphonate group, which shapes the competitive photophysical properties and can even double the QY of a (hetero)acene compared to compounds without this group. The LE dominates in the tested compounds, but a hybrid excitation with a moderately significant CT enhances their QYs. The observed linear correlation between %CT and QY can be treated as a quantitative tool to design efficient fluorescent materials with tailored photophysical properties. We expect the presented approach will impact fields ranging from synthetic and material chemistry to molecular optoelectronics and will intensify the studies on the relationship between properties and the number, position, as well as electron nature of functional groups in highly substituted (hetero)acenes.

[1] R. Jojart, R. Laczko-Rigo, M. Klement, G. Kőhl, G. Kecskemeti, C. Özvegy-Laczka, E. Mernyak, *Bioorg. Chem. 112*, 104914.

[2] Y. Shi, Y. Wang, W. Meng, R. P. Brigance, D. E. Ryono, S. Bolton, H. Zhang, S. Chen, R. Smirk, S. Tao, J. A. Tino, K. N. Williams, R. Sulsky, L. Nielsen, B. Ellsworth, M. K. Y. Wong, J. H. Sun, L. W. Leith, D. Sun, D. R. Wu, A. Gupta, R. Rampulla, A. Mathur, B. C. Chen, A. Wang, H. G. Fuentes-Catanio, L. Kunselman, M. Cap, J. Zalaznick, X. Ma, et al., *J. Med. Chem.* **2022**, *65*, 4291–4317.

[3] A. Łupicka-Słowik, M. Psurski, R. Grzywa, M. Cuprych, J. Ciekot, W. Goldeman, E. Wojaczyńska, J. Wojaczyński, J. Oleksyszyn, M. Sieńczyk, *Invest. New Drugs* **2020**, *38*, 1350–1364.

[4] P. Finkbeiner, J. P. Hehn, C. Gnamm, *J. Med. Chem.* **2020**, *63*, 7081–7107.

[5] W. Wang, H. W. He, N. Zuo, H. F. He, H. Peng, X. S. Tan, *J. Agric. Food Chem.* **2012**, *60*, 7581–7587.

[6] J. Hopkins, K. Fidanovski, L. Travaglini, D. Ta, J. Hook, P. Wagner, K. Wagner, A. Lauto, C. Cazorla, D. Officer, D. Mawad, *Chem. Mater.* **2022**, *34*, 140–151.

[7] M. Z. K. Baig, D. Majhi, R. N. P. Tulichala, M. Sarkar, M. Chakravarty, *J. Mater. Chem. C* **2017**, *5*, 2380–2387.

[8] W. Xu, G. Hu, P. Xu, Y. Gao, Y. Yin, Y. Zhao, *Adv. Synth. Catal.* **2014**, *356*, 2948–2954.

[9] H. Luo, H. Liu, X. Chen, K. Wang, X. Luo, K. Wang, *Chem. Commun.* **2017**, *53*, 956–958.

[10] Y. L. Zhao, G. J. Wu, Y. Li, L. X. Gao, F. S. Han, *Chem. Eur. J.* **2012**, *18*, 9622–9627.

[11] R. Zhuang, J. Xu, Z. Cai, G. Tang, M. Fang, Y. Zhao, *Org. Lett.* **2011**, *13*, 2110–2113.

[12] D. Qiu, C. Lian, J. Mao, Y. Ding, Z. Liu, L. Wei, M. Fagnoni, S. Protti, *Adv. Synth.Catal.* **2019**, *361*, 5239–5244.

[13] M. Koohgard, M. Hosseini-Sarvari, *Org. Biomol. Chem.* **2021**, *19*, 5905–5911.

[14] J. C. Amicangelo, W. R. Leenstra, *Inorg. Chem.* **2005**, *44*, 2067–2073.

[15] Z. Shu, J. Zhou, J. Li, Y. Cheng, H. Liu, D. Wang, Y. Zhou, *J. Org. Chem.* **2020**, *85*, 12097–12107.

[16] D. French, J. G. Simmons, H. Everitt, S. H. Foulger, G. M. Gray, *ChemRxiv* **2020**, https://doi.org/10.26434/chemrxiv.12863873.v1.

[17] S. B. Nagode, R. Kant, N. Rastogi, *Org. Lett.* **2019**, *21*, 6249–6254.

[18] C. K. Bradsher, *Chem. Rev.* **1946**, *38*, 447–499.

[19] R. J. Barney, R. M. Richardson, D. F. Wiemer, *J. Org. Chem.* **2011**, *76*, 2875–2879.

[20] R. M. Richardson, R. J. Barney, D. F. Wiemer, *Tetrahedron Lett.* **2012**, *53*, 6682–6684.

[21] Z. Liu, T. Lu, Q. Chen, *Carbon* **2020**, *165*, 461–467.

[22] Z. Liu, X. Wang, T. Lu, Q. Chen, A. Yuan, X. Yan, *Carbon* **2022**, *187*, 78–85.

[23] "The C. I. E., colorimetric standards and their use," T. Smith, J. Guild, *Trans. Opt. Soc.* **1931**, *33*, 73–134. *The Measurement of Colour*, W. D. Wright, **1969**, Van Nostrand Reinhold Company. *Commission Internationale de L'éclairage (CIE) Colorimetry*, Publication Report No. 15.2, **1986**.

[24] E. Brown, J. P. Robin, R. Dhal, *Tetrahedron* **1982**, *38*, 2569–2579.

[25] P. Bałczewski, E. Kowalska, J. Skalik, M. Koprowski, K. Owsianik, E. Różycka-Sokołowska, *Ultrason. Sonochem.* **2019**, *58*, 104640.

[26] E. Kowalska, P. Bałczewski, *Ultrason. Sonochem.* **2017**, *34*, 743–753.

[27] M. J. Frisch, G. W. Trucks, H. B. Schlegel, G. E. Scuseria, M. A. Robb, J. R. Cheeseman, G. Scalmani, V. Barone, G. A. Petersson, H. Nakatsuji, X. Li, M. Caricato, A. Marenich, J. Bloino, B. G. Janesko, R. Gomperts, B. Mennucci, H. P. Hratchian, J. V. Ortiz, A. F. Izmaylov, J. L. Sonnenberg, D. Williams-Young, F. Ding, F. Lipparini, F. Egidi, J. Goings, B. Peng, A. Petrone, T. Henderson, D. Ranasinghe, et al., *Gaussian 09*, Revision A. 02, Gaussian, Inc., Wallingford CT **2016**.

[28] *Chemcraft – graphical software for visualization of quantum chemistry computations. Version 1.8, build 682* https://www.chemcraftprog.com.

[29] R. F. W. Bader, *Atoms in Molecules: A Quantum Theory*, Clarendon Press, Oxford, New York **1990**.

[30] J. Contreras-García, R. A. Boto, F. Izquierdo-Ruiz, I. Reva, T. Woller, M. A. Alonso, *Theor. Chem. Acc.* **2016**, *135*, 242.

[31] T. Lu, F. Chen, *J. Comput. Chem.* **2012**, *33*, 580–592.

[32] T. Lu, *J. Chem. Phys.* **2024**, *161*, 082503.

[33] T. Lu, Multiwfn Manual, version 3.8 http://sobereva.com/multiwfn, **2024**.

[34] E. Espinosa, E. Molins, C. Lecomte, *Chem. Phys. Lett.* **1998**, *285*, 170–173.

[35] W. Humphrey, A. Dalke, K. Schulten, *J. Mol. Graphics* **1996**, *14*, 33–38.

[36] M. J. Kamlet, J. L. Abboud, M. H. Abraham, R. W. Taft, *J. Org. Chem.* **1983**, *48*, 2877–2887.

[37] D. R. Lide, *CRC Handbook of Chemistry and Physics: A Ready – Reference of Chemical and Physical Data*, 85-th Ed., CRC Press, Boca Raton, FL **2004**.

[38] *ACD/Percepta, Version 14.0.0*, Advanced Chemistry Development, Inc., Toronto, ON, Canada **2015**.

ortho-Positional Isomers of Anthracenes and Carbazole Derivatives Containing Phosphonate Ester Group and Their Optical Properties

Vivek Vivek,[a,b] Marek Koprowski,*[a] Ewa Różycka-Sokołowska,*[c] Łucja Knopik,[a,b] Bogdan Dudziński,[a] Krzysztof Owsianik,[a] Piotr Bałczewski*[a,c]

[a] Division of Organic Chemistry, Centre of Molecular and Macromolecular Studies, Polish Academy of Sciences, Sienkiewicza 112, Łódź, 90-363, Poland.

[b] The Bio-Med-Chem Doctoral School of the University of Łódź and Łódź Institutes of the Polish Academy of Sciences, University of Łódź, Matejki 21/23, Łódź, 90-237, Poland.

[c] Institute of Chemistry, Faculty of Science and Technology, Jan Długosz University in Częstochowa, Armii Krajowej 13/15, Częstochowa, 42-201, Poland.

Supporting Information Placeholder
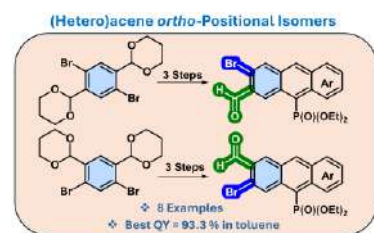
ABSTRACT: We report a synthesis of four pairs of *ortho*-positional isomers of anthracenes and carbazole derivatives, all with $(RO)_2P(O)$, *ortho*-Br and *ortho*-CHO groups *via* a three-step process involving the *phospho*-Friedel-Crafts-Bradsher cyclization. They were blue to yellow light emitters with the highest fluorescence quantum yield QY = 93.3% in toluene. Optical, electrochemical, and Density Functional Theory (DFT) studies revealed that the topology of *ortho* functional groups impacted electronic characteristics of the obtained pairs of isomers.

(Hetero)acenes, especially anthracenes, are of great interest in various sectors of material chemistry and related fields, with a particular focus on organic electronics.[1-4] Existing materials of this type are low substituted (hetero)acenes while multiply substituted ones are still scarce.[5-10] *ortho*-Positional isomers of (hetero)acenes are poorly recognized in the literature. Substitution with easily functionalizable formyl or bromine groups provides opportunity to synthesize more π-expanded derivatives.[11] Previous study indicates that formyl groups on the central and peripheral rings of the anthradithiophene core enhances its resistance to photooxidation.[12] Low degree of substitution also applies to literature phosphorus-substituted anthracenes.[13-15] Phosphonate ester group $(RO)_2P(O)$ on (hetero)acenes is important for optical and electronic properties of these compounds.[16]

In this project, we synthesized *ortho*-positional isomers of anthracenes and carbazole derivatives containing $(RO)_2P(O)$ group and diverse side-ring substituents, starting from isomeric *meta*- and *para* dibromo benzene diacetals **7** and **8**, in order to investigate the influence of the topology of formyl and Br groups on photophysical properties of the isomeric compounds (Scheme 1A).[17]

A synergistic combination of multiply substitution, *ortho*-positional isomerism, and presence of $(RO)_2P(O)$ group was expected to yield competitive emissive materials.

The title pairs of *ortho*-positional isomers **1a-d** and **2a-d** were synthesized in a three-step process starting from isomeric *meta*- and *para* derivatives **7** and **8**, respectively, to give isomeric diarylmethanols **5a-d** and **6a-d** in 30-60% yields (Scheme 1B). The next step involved a Lewis acid (ZnI_2) promoted Arbuzov-like reaction,[18] where **5a-d** and **6a-d** reacted with triethyl phosphite $(EtO)_3P$ to give pairs of isomeric diarylmethylphosphonates **3a-d** and **4a-d** in 30-52% yields, having acetal functions in *meta* and *para* positions. Finally, both series of phosphonates were cyclized with the *phospho*-Friedel-Crafts-Bradsher reaction using 6N HCl_{aq} in EtOH or acetonitrile (for **2a**) to give two groups of *ortho*-positional isomers **1a-d** and **2a-d** (Schemes 1B and 1C; Figures S1-S48 and S69-S84, SI).

The X-ray crystal structure analysis of the isomeric pairs **1a/2a** showed that they crystallized in the same space group $(P2_1/n)$ with similar unit cell dimensions (Figure S66, SI) and exhibited a similar overall crystal packing characterized by layers built up from ribbons of dimers (Figure 1 and
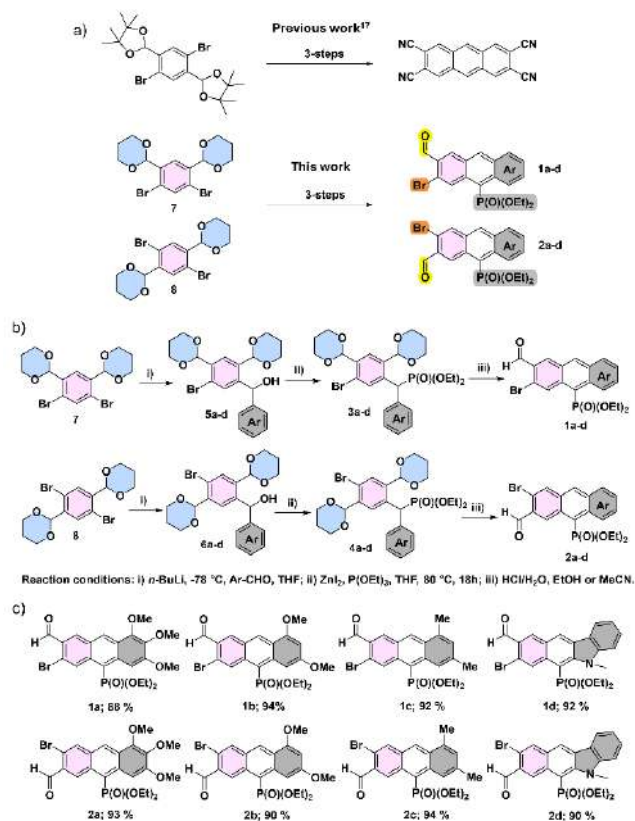
Scheme 1. (a) A synthetic strategy for *ortho*-positional isomers of anthracenes and carbazole derivatives with (EtO)$_2$P(O) group. (b) Synthesis routes for **1a-d** and **2a-d** from **7** and **8**. (c) Synthesized pairs of isomers **1a-d** and **2a-d**.

Figure S67, SI). Detailed analyses, including 3D Hirshfeld surfaces and 2D fingerprint plots (Figure S68, SI), revealed different types of weak intermolecular interactions forming ribbons of dimers (C-H···O, π···π and C=O···π in **1a** *versus* π···π and C-Br···π in **2a**) and between adjacent ribbons (Br···Br in **1a** *versus* C-H···O in **2a**). In summary, despite many similarities, the positional isomers **1a/2a** cannot be regarded as isostructural compounds.

Absorption and photoluminescence (PL) spectra, as well as QYs of **1a-d** and **2a-d**, were recorded in dichloromethane (DCM), toluene and methanol (Table 1 and Figures S49-S53, SI). The absorption spectra (DCM) for isomers **1a-d** were characterized by intense bands in the 400-443 nm range while noticeably less intense bands were recorded for the second series of **2a-d**, in a similar 425-454 nm range (Figures 2a and 2b). In the DCM solution, the differences in wavelengths of absorption maxima between **1a-1c** and **2a-2c** showed small values of only 2 (**1c/2c**), 3 (**1a/2a**) and 11 nm (**1b/2b**). Outside this trend, the four-ring isomers **1d** and **2d** remained with much higher values of 47 nm (Table 1). A similar trend was observed for the emission maxima in DCM (Table 1). *ortho*-Positional isomers **1b/2b** (557/564 nm) emitted at higher wavelengths compared to **1a/2a** (541/548 nm), **1c/2c** (503/495 nm) and **1d/2d** (467/506 nm), with the differences of 7-39 nm between emission maxima of two isomeric pairs. Anthracenes **1a-c** and **2a-c** showed higher emission maxima in DCM and lower values in methanol. In contrast, carbazole derivatives **1d** and **2d**

exhibited the highest emission maxima in methanol (520 and 538 nm) and the lowest values in toluene (453 and 487 nm) (Figure S53, SI). Anthracenes **1a-c** and **2a-c** showed good QYs across all solvents, with the highest value of 93.3% recorded for **1a** in toluene.

To assess the effect of solvent polarity on emission behavior, photophysical measurements for **1a** were conducted in MeCN, THF, CHCl$_3$, and CCl$_4$ (Table S1, Figure S54, SI). In contrast to non-polar toluene (λ_{em} = 522 nm, QY = 93.3%), polar aprotic solvents MeCN and THF induced red-shifted emission (553 and 538 nm) and significantly reduced QYs (26% and 43%, respectively). The TD-DFT calculations with IFCT (Inter-Fragment Charge Transfer) analysis showed a hybrid character of the S0→S1 electron excitation including local excitation (LE = 61.62%) with significance contribution of the CT component (38.38%), which is the only one that can be stabilized by the polar environment. This partial stabilization lowers the S1 energy, promotes non-radiative relaxation pathways, and accounts for bathochromic shift and QY decrease. Interestingly, in protic MeOH, a hypsochromic shift (λ_{em} = 512 nm) and moderate QY (46%) suggest that specific hydrogen bonds between MeOH and the (EtO)$_2$P(O) and/or CHO groups perturb the excited-state geometry (possibly *via* distorsion of functional groups or weakened π-conjugation), limit CT character, and favor LE-dominated emission, which is in line with literature.[19]

Among chlorinated solvents, a decrease in QY was observed from 85.6% in CCl$_4$ to 64.5% in DCM and 49.9% in CHCl$_3$, accompanied by a significant bathochromic shift in CHCl$_3$ and DCM (λ_{em} = 540 and 545 nm, respectively) compared to non-polar CCl$_4$ (λ_{em} = 508 nm) (Table S1, Figure S54, SI). This red-shift is consistent with stabilization of the CT component in more polar environment. In addition to solvent polarity, specific noncovalent interactions likely contribute to the observed emission changes. For example, polar CHCl$_3$ can act as a hydrogen bond donor *via* its acidic C–H group (electrostatic potential on H atom, V$_{max(H)}$ = +34.9 kcal/mol, Figure S64, SI) and participate in halogen bonding through σ-holes on Cl atoms (V$_{max(Cl2-Cl4)}$ = +14.3 kcal/mol). These interactions may involve the oxygen atoms of the CH(O1) and (EtO)$_2$P=(O2) groups or the Br atom in **1a** (V$_{min(O1)}$ =
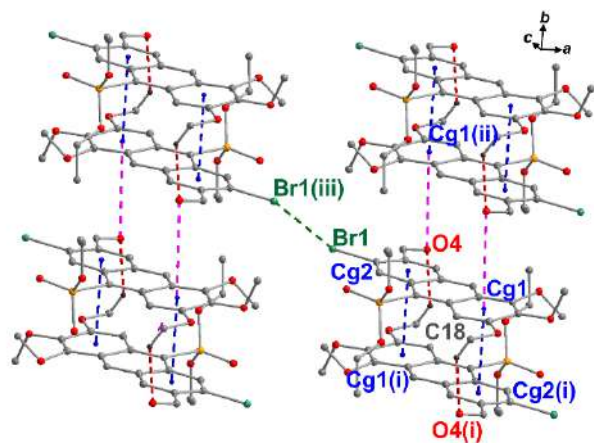

Figure 1. Crystal packing of **1a**, showing key intermolecular interactions (dashed lines: red C-H···O, blue π···π, pink C=O···π and green Br···Br). Symmetry codes (i)-(iii) are given in Table S14 in SI. For **2a**, see Figure S67, SI.
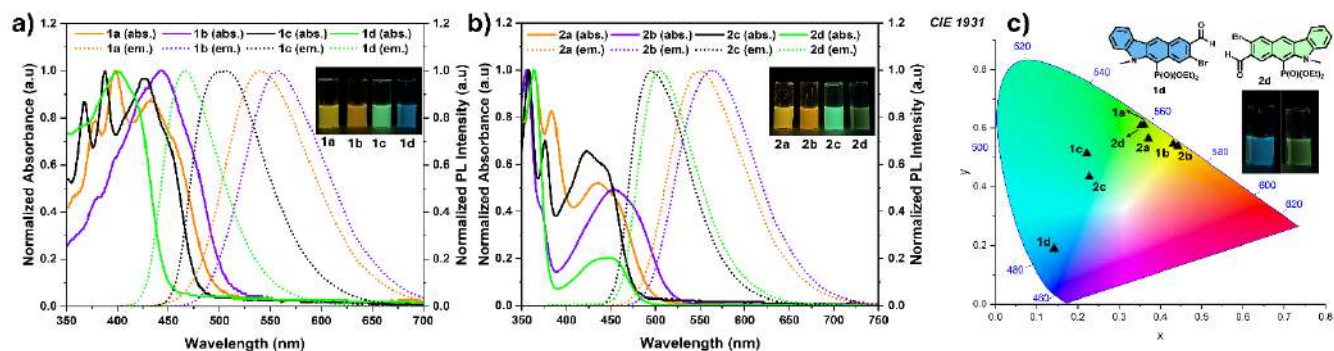
Figure 2. (a, b) Normalized absorbance and emission spectra of **1a-d** and **2a-d** (10^{-5} mol/L, DCM) and (c) Commission Internationale de L'Eclairage (CIE) 1931 chromaticity coordinates for **1a-d** and **2a-d** in DCM solutions.

Table 1. Photophysical data for *ortho*-positional isomers 1a-d and 2a-d in different solvents.

	Toluene				DCM				MeOH			
	Abs.[a]	PL[b]	υ[c]	QY[d]	Abs.[a]	PL[b]	υ[c]	QY[d]	Abs.[a]	PL[b]	υ[c]	QY[d]
	(nm)	(nm)	(cm⁻¹)	(%)	(nm)	(nm)	(cm⁻¹)	(%)	(nm)	(nm)	(cm⁻¹)	(%)
1a	433	522	3938	93.3	432	541	4664	64.7	397	512	6924	46.1
1b	422	541	5212	70.9	443	557	4620	59.5	422	546	5382	29.3
1c	425	502	3609	47.0	427	503	3538	73.6	388	473	4632	56.0
1d	401	453	2862	4.1	400	467	3587	5.5	400	520	5769	4.3
2a	438	524	3747	67.9	435	548	4740	37.8	375	510	7059	43.4
2b	458	547	3552	46.9	454	564	4295	21.1	422	534	4970	33.5
2c	425	475	2476	18.0	425	495	3327	43.3	412	467	2858	66.9
2d	447	487	1837	1.2	447	506	2608	0.9	416	538	5451	2.2

[a] Abs. ($\lambda_{max.}$) - absorption maximum; [b] PL ($\lambda_{max.}$) - emission maximum; [c] Stokes shift, $\upsilon = 1/\lambda_{abs}-1/\lambda_{em}$; [d] the absolute QY.

-38.8 kcal/mol, $V_{min(O2)}$ = -35.5 kcal/mol and $V_{max(Br)}$ = +13.1 kcal/mol, $V_{min(Br)}$ = -10.8 kcal/mol), which can promote non-radiative deactivation. In contrast, four spatially equivalent σ-holes on Cl atoms of CCl_4 ($V_{max(Cl2-Cl5)}$ = *ca.*+18.9 kcal/mol, Figure S64, SI), result in low directionality of potential interactions. This symmetry and lack of H atom means that CCl_4 does not form directional halogen or hydrogen bonds, unlike polar and unsymmetrical $CHCl_3$.

Unexpectedly, poorly substituted carbazole derivatives **1d** and **2d** exhibited the lowest QYs (1-5%) in all three solvents. Analysis of their calculated molecular geometries in comparison with **1a** and **2a** (B3LYP/6-311++G(d,p), Tables S4, S7, S8 and S11, SI) showed that, in contrast to the practically planar anthracenes, a clear bending of the plane of fused-ring systems in carbazoles derivatives **1d** and **2d** was observed. The bending angle ($\omega_{P1/P2}$) (Figure 3a), was approximately 7.5° in **1d** and **2d** compared to only 1.2° in **1a** and **2a**. Moreover, the P=O substituent in **1d** and **2d** was lying out of the P1 and P2 planes, unlike **1a** and **2a** where it remained nearly coplanar, favoring the intramolecular (C-H)$_{ar}$···O=P hydrogen bond, forming S(6) ring. This hydrogen bond was identified by QTAIM topological analysis[20] (Table S12, SI) and revealed by NCI calculations[21] as a blue disc-shaped isosurface (Figure 3a). In **1d** and **2d**, the out-of-plane orientation of P=O prevented formation of this interaction, and only weak van der Waals (VdW) contact (C-

H)$_{Me}$···O=P (green isosurface), was possible. This orientation and bending of the aromatic plane, which caused a partial disturbance of π-conjugation, could be the reason for the significant drop in QYs of **1d** and **2d**.

The cyclic voltammetry (CV) and differential pulse voltammetry (DPV) measurements for **1a-d** and **2a-d** (Figures S55-S62, SI) showed, that the redox processes were mostly irreversible, indicating the chemical instability of the (hetero)acenes under electrochemical conditions. Therefore, the energies of HOMO (E_{HOMO}) and LUMO (E_{LUMO}) obtained by the commonly used method of Sun and Dalton,[22] as well as band gap (E_g), should be considered only as estimates (Table S2, SI). Hence, to determine the E_{HOMO}, E_{LUMO} and E_g values, we used the DFT calculations (Tables S4-S11 and Table S3, SI).

Generally, isomers **2a–2d** showed higher (less negative) E_{HOMO}, indicating a slightly stronger electron donating character, and lower E_{LUMO} and E_g compared to **1a–1d**. These energies, and especially E_{LUMO} were affected by the nature and position of substituents. A comparison of the E_{HOMO}, E_{LUMO} and E_g values for the most efficient anthracene emitters **1a** and **2a** with those calculated for the analogous anthracene, unsubstituted on the left ring (E_{HOMO} = -5.36 eV, E_{LUMO} = -2.00 eV, E_g = 3.36 eV),[23] showed that the introduction of Br and CHO groups resulted in a significant reduction of these energies, and especially of E_{LUMO} by about 0.6 eV (**1a**) and

0.7 eV (**2a**), i.e. by about 30%. The **1d** and **2d** isomers were distinguished by the highest LUMO levels and, consequently, the largest HOMO-LUMO gaps (E_g = 3.51 and 3.21 eV for **1d** and **2d**, respectively, *versus* 3.10-3.18 eV for **1a-1c** and 2.95-3.08 eV for **2a-2c**). This correlated with their clearly different ring structures and molecular distortions (especially bending of the fused-ring plane, Figure 3a) in **1d** and **2d**. The HOMO and LUMO isosurfaces were localized predominantly on the fused ring core for all compounds, and the LUMO was also extended onto the CHO substituent (Figure 3b). Although the Hammett constant indicates strong electron-withdrawing (EWG) nature of the $(EtO)_2P(O)$ group (σ_p = 0.56, $\sigma_{ind}/\sigma_{res}$ = 0.32/0.24; ACD/Percepta[24]), its acceptor properties were reduced in both anthracenes and carbazole derivatives. In anthracenes, this could be due to the intramolecular $(C-H)_{ar}\cdots O=P$ hydrogen bond, while in carbazoles, it could be the result of a pronounced bending of the π-system and the location of the P=O substituent out of the plane of the π-system (Figure 3a), which disrupted the π-conjugation between the $(EtO)_2P(O)$ group and the aromatic core. As a result, the LUMO isosurfaces were not localized on this group, and the CHO group effectively took over the role of the main electron acceptor (Figure 3b and Figure S63, SI), despite its weaker EWG character based on the Hammett constant (σ_p = 0.42, $\sigma_{ind}/\sigma_{res}$ = 0.27/0.15[24]). The pronounced acceptor character of the CHO substituent in the excited state and its predominance over the $(EtO)_2P(O)$ group were strongly supported by the IFCT and CTS (Charge Transfer Spectrum) analyses performed for the S1 state of **1a** and **1d**. This enabled to identify a significant electron transfer from the aromatic core (fragment I, Figure S65, SI) toward the CHO group (fragment VII), accounting for 11.4% and 11.5% of the total electron excitation, respectively. In contrast, a contribution associated with electron transfer from the fragment I to $(EtO)_2P(O)$ group (fragment V) was approximately 2%.

The isomers of both series **1a-d** and **2a-d** emitted blue to yellow light in the 467-564 nm range (DCM). Despite the difference involving position of formyl and bromo groups as the only structural alteration, a rapid color change was observed between **1d**, which emitted blue light, and its positional isomer **2d** which emitted green light (Figure 1c). The CIE 1931 color space chromaticity coordinates[25] of **1a-1d** and **2a-d** in DCM, toluene, and MeOH are provided in Table S13 (SI).

In conclusion, four isomeric pairs of substituted anthracenes and carbazole derivatives with *ortho*-formyl and *ortho*-Br substituents, as well as $(RO)_2P(O)$ group have been synthesized. The highest fluorescence QY was 93.3% (for **1a**) in toluene, exceeding those for anthracene and its literature derivatives. The bending of the fused-ring plane and the out-of-plane orientation of the P=O group in the carbazole derivatives directly correlated with their significantly reduced QYs. The emission and fluorescence QY of anthracenes depended on the solvent polarity and specific noncovalent interactions (hydrogen and halogen bonds), as revealed by combined photophysical and computational data analysis for the representative **1a**. This research introduces a new family of isomeric materials with tunable optical and electronic properties.
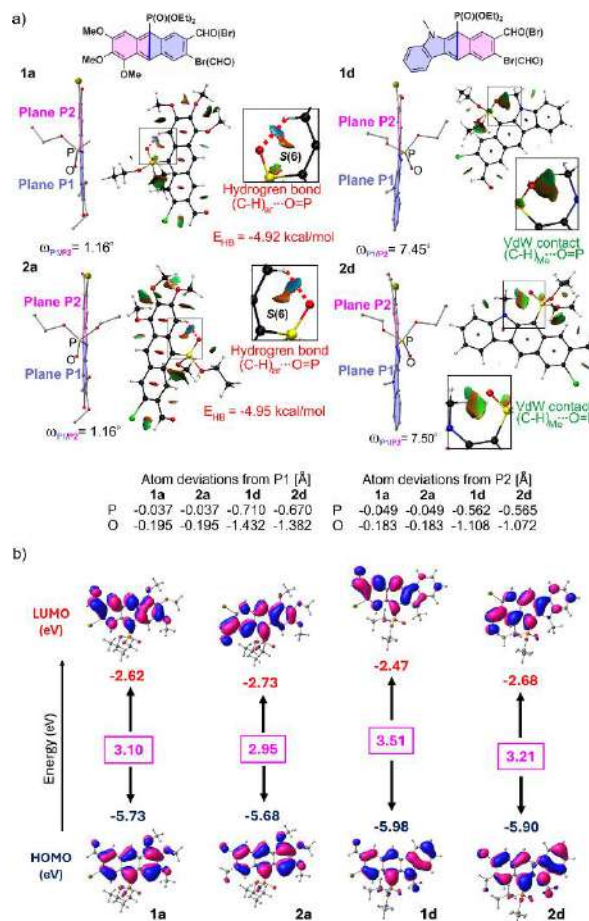
Figure 3. (a) Molecular structures of **1a/2a** and **1d/2d**, and 3D-NCI plots with color-filled isosurfaces, illustrating key differences in molecular geometries and non-covalent intramolecular interactions. (b) Molecular orbitals calculated for these isomers by DFT at B3LYP/6-311++G(d,p).

ASSOCIATED CONTENT

Data Availability Statements

The data underlying this study are available in the published article and its Supporting Information.

Supporting Information

General information, detailed experimental procedures, characterization data for compounds, NMR spectra, photophysical properties, crystal structure data, computational studies, and CIE 1931 color space coordinates data are available in the SI.

The Supporting Information is available free of charge on the ACS Publications website.

Corresponding Authors

*E-mails: piotr.balczewski@cbmm.lodz.pl; e.sokolowska@ujd.edu.pl; marek.koprowski@cbmm.lodz.pl

Author Contributions

P. B. designed the overall research plan. P.B. received funding. V. V., L. K. and B. D. carried out the synthesis of substituted anthracenes and carbazole derivatives, while M. K., K. O. and V. V. conducted the photophysical and CV experiments, and E. R.-S. performed the quantum-chemical calculations and X-ray crystal structure analysis. The manuscript was written with input from

all authors. All authors have approved the final version of the manuscript.

REFERENCES

1. Ostroverkhova, O. Organic Optoelectronic Materials: Mechanisms and Applications. *Chem. Rev.* **2016**, *116*, 13279–13412.

2. Baumgartner, T.; Réau, R. Organophosphorus π-Conjugated Materials. *Chem. Rev.* **2006**, *106*, *11*, 4681–4727.

3. a) Vivek, V.; Koprowski, M.; Różycka-Sokołowska, E.; Turek, M.; Dudziński, B.; Owsianik, K.; Knopik, Ł.; Bałczewski, P. High-Efficiency Light Emitters: 10-(Diphenylphosphoryl)-anthracenes from One-Pot Synthesis Including C–O–P to C–P(=O) Rearrangement. *J. Org. Chem.* **2025**, *90(13)*, 4580–4590. b) Sharma, N.; Wong, M. Y.; Hall, D.; Spuling, E.; Tenopala-Carmona, F.; Privitera, A.; Copley, G.; Cordes, D. B.; Slawin, A. M. Z.; Murawski, C.; Gather, M. C.; Beljonne, D.; Olivier, Y.; Samuel, I. D. W.; Zysman-Colman, E. Exciton efficiency beyond the spin statistical limit in organic light emitting diodes based on anthracene derivatives. *J. Mater. Chem. C* **2020**, *8*, 3773–3783.

4. Wu, C. L.; Chang, C. H.; Chang, Y. T.; Chen, C. T.; Chen, C. T.; Su, C. J. High efficiency non-dopant blue organic light-emitting diodes based on anthracene-based fluorophores with molecular design of charge transport and red-shifted emission proof. *J. Mater. Chem. C* **2014**, *2*, 7188–7200.

5. Gray, V.; Dzebo, D.; Lundin, A.; Alborzpour, J.; Abrahamsson, M.; Albinsson, B.; Moth-Poulsen, K. Photophysical Characterization of the 9,10-Disubstituted Anthracene Chromophore and Its Applications in Triplet–Triplet Annihilation Photon Upconversion. *J. Mater. Chem. C* **2015**, *3*, 11111–11121.

6. Bałczewski, P.; Kowalska, E.; Różycka-Sokołowska, E.; Skalik, J.; Owsianik, K.; Koprowski, M.; Marciniak, B.; Guziejewski, D.; Ciesielski, W. Mono-Aryl/Alkylthio-Substituted (Hetero)acenes of Exceptional Thermal and Photochemical Stability by the Thio-Friedel–Crafts/Bradsher Cyclization Reaction. *Chem. Eur. J.* **2019**, *25*, 14148–14161.

7. Zambianchi, M.; Benvenuti, E.; Bettini, C.; Zanardi, C.; Seeber, R.; Gentili, D.; Cavallini, M.; Muccini, M.; Biondo, V.; Soldano, C.; Generali, G.; Toffanin, S.; Melucci, M. Anthracene-Based Molecular Emitters for Non-Doped Deep-Blue Organic Light Emitting Transistors. *J. Mater. Chem. C* **2016**, *4*, 9411–9417.

8. Guo, R.; Ye, S.; Wang, Y.; Duan, Y.; Di, K.; Wang, L. Exploiting Asymmetric Anthracene-Based Multifunctional Materials Based on a "Bulky Peripheral Modification" Strategy for Constructing Simplified Efficient Deep-Blue Fluorescent OLEDs. *J. Mater. Chem. C* **2021**, *9*, 13392–13401.

9. Biswas, S.; Bhaumik, S. K.; Manikandan, R.; Jelinek, R. High-Performance Functionalized Anthracene Organic Supercapacitors. *RSC Appl. Interfaces* **2024**, *1*, 920–927.

10. Philippe, C.; Bui, A. T.; Batsongo-Boulingui, S.; Pokladek, Z.; Matczyszyn, K.; Mongin, O.; Lemiegre, L.; Paul, F.; Hamlin, T. A.; Trolez, Y. 1,1,4,4-Tetracyanobutadiene-Functionalized Anthracenes: Regioselectivity of Cycloadditions in the Synthesis of Small Near-IR Dyes. *Org. Lett.* **2021**, *23*, 2007–2012.

11. Qiu, F.; Dong, Y.; Liu, J.; Sun, Y.; Geng, H.; Zhang, H.; Zhu, D.; Shi, X.; Liu, J.; Zhang, J.; Ai, S.; Jiang, L. Asymmetric organic semiconductors for high performance single crystalline field-effect transistors with low activation energy. *J. Mater. Chem. C* **2020**, *8*, 6006–6012.

12. Balandier, J. Y.; Sebaihi, N.; Boudard, P.; Lemaur, V.; Quist, F.; Niebel, C.; Stas, S.; Tylleman, B.; Lazzaroni, R.; Cornil, J.; Geerts, Y. H. Anthradithiophene Derivatives Substituted at the 2,8-Positions by Formyl and Triphenylamine Units: Synthesis, Optical, and Electrochemical Properties. *Eur. J. Org. Chem.* **2011**, 3131–3136.

13. Schillmöller, T.; Ruth, P. N.; Herbst-Irmer, R.; Stalke, D. Three colour solid-state luminescence from positional isomers of facilely modified thiophosphoranyl anthracenes. *Chem. Commun.* **2020**, *56*, 7479–7482.

14. Iida, P.; Belyaev, A.; Su, B. K.; Liu, Z. Y.; Saarinen, J. J.; Hashim, I. I.; Steffen, A.; Chou, P. T.; Romero-Nieto, C.; Koshevoy, I. O. From Terminal to Spiro-Phosphonium Acceptors, Remarkable Moieties to Develop Polyaromatic NIR Dyes. *Chem. Eur. J.* **2023**, *29*, e202301073.

15. Murayama, N.; Jorolan, J. H.; Minoura, M.; Nakano, H.; Ikoma, T.; Matano, Y. 9-(Diphenylphosphoryl)-10-(phenylethynyl)anthracene Derivatives: Synthesis and Implications for the Substituent and Solvent Effects on the Light-Emitting Properties. *ChemPhotoChem* **2022**, *6*, e202200100.

16. Roscales, S.; Csáky, A. G. Metal-Free Aminophosphonation: Eco-Friendly Synthesis and Photophysical Properties of Fluorescent 3-(Aminoimidazo[1,2-a]Pyridin-2-yl)Phosphonates. *Angew. Chem. Int. Ed.* **2024**, *63*, e202412300.

17. Meindl, B.; Pfennigbauer, K.; Stöger, B.; Heeney, M.; Glöcklhofer, F. Double Ring-Closing Approach for the Synthesis of 2,3,6,7-Substituted Anthracene Derivatives. *J. Org. Chem.* **2020**, *85*, 8240–8244.

18. Bałczewski, P.; Dudziński, B.; Koprowski, M.; Knopik, Ł.; Owsianik, K. Condensed Aromatic Hydrocarbons Substituted with Organophosphorus Groups. Patent PL-245310, **2024**.

19. Song, P., Ma, F.-C. Effects of Hydrogen Bonding on Tuning Photochemistry: Concerted Hydrogen-Bond Strengthening and Weakening. *International Reviews in Physical Chemistry,* **2013**, *32*, 589–609.

20. Bader, R. F. W. Atoms in Molecules: A Quantum Theory; Clarendon Press: Oxford, New York, **1990**.

21. Contreras-García, J.; Boto, R. A.; Izquierdo-Ruiz, F.; Reva, I.; Woller, T.; Alonso, M. A. A benchmark for the non-covalent interaction (NCI) index or... is it really all in the geometry? *Theor. Chem. Acc.* **2016**, *135*, 242.

22. Sun, S. S.; Dalton, L. R. in Introduction to Organic Electronic and Optoelectronic Materials and Devices, Ch.3.4., CRC Press/Taylor & Francis: Boca Raton, Florida, USA, 2008.

23. Koprowski, M, Knopik, Ł., Różycka-Sokołowska, E; Dudziński, B., Vivek, V., Owsianik, K., Bałczewski, P. Multiply Substituted (Hetero)acenes Containing Phosphonate Group at the Central Unit as High-Efficiency Light Emitters. *Angew. Chem. Int. Ed.* **2025**, e202508168.

24. *ACD/Percepta, Version 14.0.0*; Advanced Chemistry Development, Inc.: Toronto, ON, Canada, **2015**.

25. "The C.I.E. colorimetric standards and their use". T. Smith, J Guild, *Trans. Opt. Soc.* **1931**, *33*, 73-134. *The Measurement of Colour*, W. D. Wright, **1969**, Van Nostrand Reinhold Company. Commission Internationale de L'éclairage (CIE), *Colorimetry*, Publication Report No. 15.2, **1986**.

5. Declaration of co-authors

Prof. dr hab. Eng. Piotr Bałczewski   Łódź, 01.09.2025

Centre of Molecular and Macromolecular Studies

Polish Academy of Sciences

90-363 Łódź, Sienkiewicza 112

E-mail: piotr.balczewski@cbmm.lodz.pl

Declarations

I hereby declare that in the following publications:

1. V. Vivek, M. Koprowski, E. Różycka-Sokołowska, M. Turek, B. Dudziński, K. Owsianik, Ł. Knopik, P. Bałczewski, High-Efficiency Light Emitters: 10-(Diphenylphosphoryl)anthracenes from One-Pot Synthesis Including C–O–P to C–P(=O) Rearrangement, *J. Org. Chem.* **2025**, *90* (13), 4580-4590.

2. M. Koprowski, Ł. Knopik, E. Różycka-Sokołowska, B. Dudziński, V. Vivek, K. Owsianik, P. Bałczewski, Multiply Substituted (Hetero)acenes Containing Phosphonate Group at the Central Unit as High-Efficiency Light Emitters, *Angew. Chem. Int. Ed.* **2025**, e202508168.

My contribution included:

For position 1:

Co-designing the overall research plan, co-writing manuscript, research supervision, receiving funding;

For position 2:

Co-designing the overall research plan, co-writing manuscript, research supervision, receiving funding.

Signature Not Verified

Dokument podpisany przez Piotr Bałczewski
Data: 2025.09.01 23:59:30 CEST

Name and signature

dr Ewa Różycka-Sokołowska

Institute of Chemistry,
Faculty of Science and Technology,
Jan Długosz University in Częstochowa, Częstochowa, Poland
Email: e.sokolowska@ujd.edu.pl
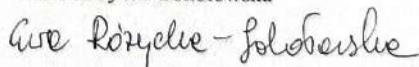
Czestochowa, 27.08.2025

Declarations

I hereby declare that in the preparation of publications:

1. V. Vivek, M. Koprowski, E. Różycka-Sokołowska, M. Turek, B. Dudziński, K. Owsianik, Ł. Knopik, P. Bałczewski, High-Efficiency Light Emitters: 10-(Diphenylphosphoryl)-anthracenes from One-Pot Synthesis Including C–O–P to C–P(=O) Rearrangement, *Journal of Organic Chemistry,* **2025**, *90* (13), 4580-4590.

2. M. Koprowski, Ł. Knopik, E. Różycka-Sokołowska, B. Dudziński, V. Vivek, K. Owsianik, P. Bałczewski, Multiply Substituted (Hetero)acenes Containing Phosphonate Group at the Central Unit as High-Efficiency Light Emitters, *Angew. Chem. Int. Ed.* **2025**, e202508168.

My contribution included:

- performing DFT calculations (publications 1 and 2), as well as TD-DFT calculations, hole-electron analysis, and QTAIM topological analysis (publication 2),

- analyzing and interpreting the obtained calculation results (publications 1 and 2),

- determining crystal structures and analyzing crystal packing and intermolecular interactions (publication 1),

- writing sections of manuscripts on computational and crystallographic studies.

Ewa Różycka-Sokołowska

Ewa Różycka-Sokołowska

Name and signature

Dr Marek Koprowski

Centre of Molecular and Macromolecular Studies

Polish Academy of Sciences

Sienkiewicza 112

90-363 Łódź

E-mail: marek.koprowski@cbmm.lodz.pl

Łódź, 21.08.2025

Declarations

I hereby declare that in the following publications:

1. V. Vivek, M. Koprowski, E. Różycka-Sokołowska, M. Turek, B. Dudziński, K. Owsianik, Ł. Knopik, P. Bałczewski, High-Efficiency Light Emitters: 10-(Diphenylphosphoryl)-anthracenes from One-Pot Synthesis Including C–O–P to C–P(=O) Rearrangement, *J. Org. Chem.* **2025**, *90* (13), 4580-4590.

2. M. Koprowski, Ł. Knopik, E. Różycka-Sokołowska, B. Dudziński, V. Vivek, K. Owsianik, P. Bałczewski, Multiply Substituted (Hetero)acenes Containing Phosphonate Group at the Central Unit as High-Efficiency Light Emitters, *Angew. Chem. Int. Ed.* **2025**, e202508168.

My contribution included:

For position 1:

Measurements of photophysical properties of some anthracenes. Formatting the manuscript, preparation to submission, submission to the journal and proofreading.

For position 2:

Participation in the development of research methodology. Synthesis of approximately one-third of substrates, intermediates, and anthracenes. Measurements of photophysical properties most of anthracenes. Analysis of the results and processing of experimental data. Writing and formatting the manuscript, submission to the journal, and proofreading.

Name and signature

Dr Bogdan Dudziński   Łódź, 29.08.2025 r.

Centre of Molecular and Macromolecular Studies,

Łódź, Sienkiewicza 112
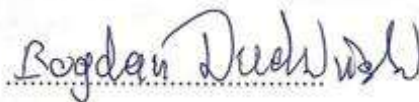
E-mail: bogdan.dudzinski@cbmm.lodz.pl

Declarations

I hereby declare that in the preparation of publications:

1. V. Vivek, M. Koprowski, E. Różycka-Sokołowska, M. Turek, B. Dudziński, K. Owsianik, Ł. Knopik, P. Bałczewski, High-Efficiency Light Emitters: 10-(Diphenylphosphoryl)-anthracenes from One-Pot Synthesis Including C–O–P to C–P(=O) Rearrangement, *Journal of Organic Chemistry*, **2025**, *90* (13), 4580-4590.

2. M. Koprowski, Ł. Knopik, E. Różycka-Sokołowska, B. Dudziński, V. Vivek, K. Owsianik, P. Bałczewski, Multiply Substituted (Hetero)acenes Containing Phosphonate Group at the Central Unit as High-Efficiency Light Emitters, *Angew. Chem. Int. Ed.* **2025**, e202508168.

My contribution was to synthesize a few starting materials in *Journal of Organic Chemistry*, **2025**, *90* (13), 4580-4590.

I synthesized some of the final products described in *Angew. Chem. Int. Ed.* 2025, e202508168, and assisted in the research and analysis of the final manuscript.

Name and signature

MSc Łucja Knopik

Łódź, 31.08.2025

Centre of Molecular and Macromolecular Studies, Polish Academy of Sciences

Sienkiewicza 112, 90-363 Łódź

E-mail: lucja.knopik@cbmm.lodz.pl

Declaration

I hereby declare that in the following publications:

1. V. Vivek, M. Koprowski, E. Różycka-Sokołowska, M. Turek, B. Dudziński, K. Owsianik, Ł. Knopik, P. Bałczewski, High-Efficiency Light Emitters: 10-(Diphenylphosphoryl)-anthracenes from One-Pot Synthesis Including C–O–P to C–P(=O) Rearrangement, *Journal of Organic Chemistry,* **2025**, *90* (13), 4580-4590.

2. M. Koprowski, Ł. Knopik, E. Różycka-Sokołowska, B. Dudziński, V. Vivek, K. Owsianik, P. Bałczewski, Multiply Substituted (Hetero)acenes Containing Phosphonate Group at the Central Unit as High-Efficiency Light Emitters, *Angew. Chem. Int. Ed.* **2025**, e202508168.

My contribution included:

For position 1:

Synthesizing some diarylmethanols as starting materials.

For position 2:

1) Synthesis of about one third of substrates, intermediates and anthracenes,
2) Participation in measurements of the photo-optical properties of the anthracenes and participation in writing of the manuscript.

Łucja Knopik

....

Name and signature

Dr Krzysztof Owsianik

Centre of Molecular and Macromolecular Studies

Poslish Academy of Sciences

Sienkiewicza 112

90-363 Łódź

e-mail: krzysztof.owsianik@cbmm.lodz.pl

Łódź, 01.09.2025

Declarations

I hereby declare that in the preparation of publications:

1. V. Vivek, M. Koprowski, E. Różycka-Sokołowska, M. Turek, B. Dudziński, K. Owsianik, Ł. Knopik, P. Bałczewski, High-Efficiency Light Emitters: 10-(Diphenylphosphoryl)-anthracenes from One-Pot Synthesis Including C–O–P to C–P(=O) Rearrangement, *Journal of Organic Chemistry,* **2025**, *90* (13), 4580-4590.

2. M. Koprowski, Ł. Knopik, E. Różycka-Sokołowska, B. Dudziński, V. Vivek, K. Owsianik, P. Bałczewski, Multiply Substituted (Hetero)acenes Containing Phosphonate Group at the Central Unit as High-Efficiency Light Emitters, *Angew. Chem. Int. Ed.* **2025**, e202508168.

My contribution included:

For position 1:

Measurements of photophysical properties of some anthracenes. Supporting the process of formatting the manuscript and preparation to submission.

For position 2:

Measurements of photophysical properties of some anthracenes. Supporting the process of formatting the manuscript and preparation to submission.

Name and signature

dr Marika Turek
Institute of Chemistry,
Faculty of Science and Technology,
Jan Długosz University in Częstochowa, Częstochowa, Poland
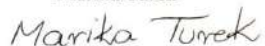Email: m.turek@ujd.edu.pl

Częstochowa, 29.08.2025

Declarations

I hereby declare that in the preparation of publication:

1. V. Vivek, M. Koprowski, E. Różycka-Sokołowska, M. Turek, B. Dudziński, K. Owsianik, Ł. Knopik, P. Bałczewski, High-Efficiency Light Emitters: 10-(Diphenylphosphoryl)-anthracenes from One-Pot Synthesis Including C–O–P to C–P(=O) Rearrangement, *Journal of Organic Chemistry*, **2025**, *90* (13), 4580-4590.

My contribution included taking part in performing DFT calculations and preparing figures for the computational section.

Marika Turek

Marika Turek

Name and signature

6. Curriculum Vitae

Mr. VIVEK

📍 Bio-Med-Chem Doctoral School of the University of Lodz and Lodz Institute of the Polish Academy of Sciences

📱 +48-696747486

✈ vivek.ch@cbmm.lodz.pl

Date of Birth: 31st October 1995

Nationality: Indian

Languages: English, Hindi

Academic Qualifications

Ph.D. Chemistry (2021- Present)	Bio-Med-Chem Doctoral School of the University of Lodz and Lodz Institute of the Polish Academy of Sciences, Lodz, Poland. **Supervisor**: Prof. Dr. Piotr Bałczewski
M.Sc. Chemistry (2017-19)	Discipline of Chemistry, Indian Institute of Technology, Indore, India. (CGPA: 7.2) **Supervisor**: Prof. Dr. Rajneesh Misra
B.Sc. (Honors) Chemistry (2016)	Deshbandhu College, University of Delhi. (First Division: CGPA: 6.8)
Higher Secondary School (2013)	Arya Vidya Mandir, Ballabgarh, CBSE Board. (Outstanding, CGPA: 7.5)
Senior Secondary School (2011)	Vivekanand Public School, Ballabgarh, HBSE Board. (Outstanding, CGPA: 8.5)

Teaching Experience

Faculty of Chemistry (2020-21)	Allen Career Institute, Kota, India.

Publications, Patents, and Poster/Oral Presentations

Publications/Patents:

1. **V. Vivek**, M. Koprowski, E. R. Sokołowska*, M. Turek, B. Dudziński, K. Owsianik, L. Knopik, P. Bałczewski*, High-Efficiency Light Emitters: 10-(Diphenylphosphoryl)-anthracenes from One-Pot Synthesis including C-O-P to C-P(=O) Rearrangement. *J.*

Org. Chem. **2025**, *90*, 13, 4580–4590.

2. M. Koprowski*, Ł. Knopik, E. R. Sokołowska*, B. Dudziński, **V. Vivek**, K. Owsianik, P. Bałczewski*, Multiply Substituted (Hetero)acenes Containing Phosphonate Group at the Central Unit as High-Efficiency Light Emitters, *Angew. Chem. Int. Ed.* **2025**, e202508168.

3. Y. Rout, **V. Vivek**, R. Misra*, Synthesis and Characterization of Isoindigo-Based Push–Pull Chromophore, *J. Org. Chem.* **2020**, *85* (7), 4611-4618.

4. K. Owsianik, E. R. Sokołowska, M. Koprowski, M. Turek, L. Knopik, **V. Vivek**, B. Dudziński, P. Bałczewski*, The First Example of the Friedel–Crafts Cyclization Leading to (10-Hydroxy-9,10-dihydroanthr-9-yl)phosphonium Salts without the Expected Bradsher Dehydration, *Int. J. Mol. Sci.* **2024**, *25*(3), 1741.

5. M. Koprowski, K. Owsianik, L. Knopik, **V. Vivek**, A. Romaniuk, E. R. Sokołowska, P. Bałczewski*, Comprehensive Review on Synthesis, Properties, and Applications of Phosphorus (PIII, PIV, PV) Substituted Acenes with More Than Two Fused Benzene Rings. *Molecules,* **2022**, *27*(19), 6611.

6. **V. Vivek**, M. Koprowski, K. Owsianik, E. R. Sokołowska, P. Bałczewski, 10-Phosphinoxylanthracenes - method of production and application (Patent Application submitted) **P.445384**.

7. **V. Vivek**, M. Koprowski*, E. R. Sokołowska*, Ł. Knopik, B. Dudziński, K. Owsianik, P. Bałczewski*, *ortho*-Positional Isomers of Anthracene and Carbazole Derivatives Containing Phosphonate Ester Group and Their Optical Properties (Under peer-review in the Organic Letters).

8. **V. Vivek**, M. Koprowski, E. R. Sokołowska, K. Owsianik, P. Bałczewski*, Synthesis and Optical Properties of 10-(Diphenylphosphoryl)-7-(phenylethynyl) anthracene Derivatives. (Manuscript under preparation)

9. **V. Vivek**, M. Koprowski, E. R. Sokołowska, K. Owsianik, P. Bałczewski*, Post-functionalization on *ortho*-Positional Isomers. (Manuscript under preparation)

Poster/Oral presentations:

1. 22nd European Symposium on Organic Chemistry, July 9-13, 2023, Ghent, Belgium. (Poster: Highly Substituted 10-PhosphinoxylAnthracenes via the P-O-C TO P(=O)-C Rearrangement)

2. 65th Scientific Meeting of the Polish Chemical Society, September 18-22, 2023, Torun, Poland. (Poster: Highly Substituted 10-PhosphinoxylAnthracenes via the P-O-C TO P(=O)-C Rearrangement)

3. XXIV International Symposium on "*Advances in Chemistry of Hetero-organic Compounds,* November 24, 2023, Lodz, Poland. (Poster: Highly Substituted 10-Phosphinoyl Anthracenes *via* the P-O-C to P(=O)-C Rearrangement and the phospho-Friedel-Crafts-Bradsher Reaction)

4. XXV International Symposium on "*Advances in Chemistry of Hetero-organic Compounds,* November 21-22, 2024, Lodz, Poland.
(Poster: High-Performance Light Emitters Achieved through Multiple Substitutions in 10-(Diphenylphosphoryl)-Anthracenes)
5. 11th Doctoral Symposium on Chemistry, May 16-17, 2024, Lodz, Poland. (Oral presentation title: Highly Substituted 9-Diphenyphosphoryl Anthracenes Derivatives *via* the C-O-P to C-P(=O) Rearrangement)

Experimental and instrumentation techniques learnt: Synthesis of novel organic conjugated compounds and characterization using NMR spectroscopy, mass spectrometry, and elemental analysis. Further techniques involve UV-Vis, PL spectroscopy, cyclic voltammetry, schlenk, and glove box techniques.

Awards and Achievements

- Secured the **STER-NAWA Incentive scholarship** for best performing international student.
- Secured funding from **Narodowe Centrum Nauki (NCN) OPUS 17** - The *phospho-*Friedel-Crafts/Bradsher reaction – a new member of a heteroatom family.
- Secured **AIR-534 rank in IIT-JAM** (Joint Admission Test for M.Sc.) 2017.
- Secured **87th rank in the Joint CSIR-UGC** Junior Research Fellowship & Eligibility for Lectureship (NET) Examination organized by CSIR, India in June 2018.
- Recipient of **Merit-Cum-Means Scholarship (MCM)** in Indian Institute of Technology, Indore, India, 2018-19 for supporting my master studies.
- Awarded with a medal and certificate in the "**CONTECH-15**" hosted by the Tata Institute of Fundamental Research, Mumbai.